Book of abstracts

PHOTONICA 2025

X International School and Conference on Photonics

25 - 29 August 2025

Belgrade, Serbia

Editors

Mihailo Rabasović, Uroš Ralević, Marina Lekić, Aleksandar Krmpot
Institute of Physics Belgrade, Serbia

Belgrade, 2025

ABSTRACTS OF TUTORIAL, KEYNOTE, INVITED LECTURES, PROGRESS REPORTS AND CONTRIBUTED PAPERS

of

X International School and Conference on Photonics
PHOTONICA 2025

25 - 29 August 2025

Belgrade, Serbia

Editors
Mihailo Rabasović, Uroš Ralević, Marina Lekić, Aleksandar Krmpot

Technical assistance
Stanko Nikolić and Marta Bukumira

ISBN 978-86-82441-72-4

Publisher
Institute of Physics Belgrade
Pregrevica 118
11080 Belgrade, Serbia

Printed by
Serbian Academy of Sciences and Arts, Knez Mihailova 35, Belgrade

Number of copies 30

CIP - Каталогизација у публикацији
Народна библиотека Србије, Београд
535(048)
621.37/.39:535(048)
621.37/.39:535]:61(048)
66.017/.018(048)
INTERNATIONAL School and Conference on Photonic (10 ; 2025 ; Beograd)
Book of abstracts / X International School and Conference on Photonics PHOTONICA 2025, 25 - 29 August 2025 Belgrade, Serbia ; editors Mihailo Rabasović ... [et al.]. - Belgrade: Institute of Physics, 2025 (Belgrade: SASA). - VIII, 175 str. : ilustr. ; 25 cm
Tiraž 30. - Bibliografija uz većinu apstrakata. - Registar.
ISBN 978-86-82441-72-4
1. Rabasović, Mihailo, 1977- [urednik]
a) Оптика -- Апстракти b) Оптички материјали -- Апстракти v) Оптоелектроника -- Апстракти g) Оптоелектроника -- Биомедицина -- Апстракти d) Телекомуникације -- Апстракти
COBISS.SR-ID 173823497

Book of abstracts X International School and Conference on Photonics © 2025 by Mihailo Rabasović, Uroš Ralević, Marina Lekić, Aleksandar Krmpot is licensed under CC BY-NC-ND 4.0

PHOTONICA 2025 (X International School and Conference on Photonics - www.photonica.ac.rs) is organized by Institute of Physics Belgrade, University of Belgrade (www.ipb.ac.rs), Serbian Academy of Sciences and Arts (www.sanu.ac.rs), and Optical Society of Serbia (www.ods.org.rs).

Institute of Physics Belgrade

Serbian Academy of Sciences and Arts

Other institution that helped the organization of this event are: Vinča Institute of Nuclear Sciences, University of Belgrade (www.vinca.rs), Faculty of Electrical Engineering, University of Belgrade (www.etf.bg.ac.rs), Institute of Chemistry, Technology and Metallurgy, University of Belgrade (www.ihtm.bg.ac.rs), Faculty of Technical Sciences, University of Novi Sad (www.ftn.uns.ac.rs), Faculty of Physics, University of Belgrade (www.ff.bg.ac.rs), and Faculty of Biology, University of Belgrade (www.bio.bg.ac.rs).

PHOTONICA 2025 is organized under auspices and with support of the Ministry of Science, Technological Development and Innovation, Serbia (https://nitra.gov.rs/en/).

The support of the sponsors of PHOTONICA 2025 is gratefully acknowledged:

Ministry of Education, Science and Technological Development of the Republic of Serbia

OPTICA

LRM d.o.o. Ljubljana / Slovenija

ANSAR-ANALITIKA ANALYTICAL EQUIPMENT

TEVUS Lab science

KRUG INTERNATIONAL LTD.

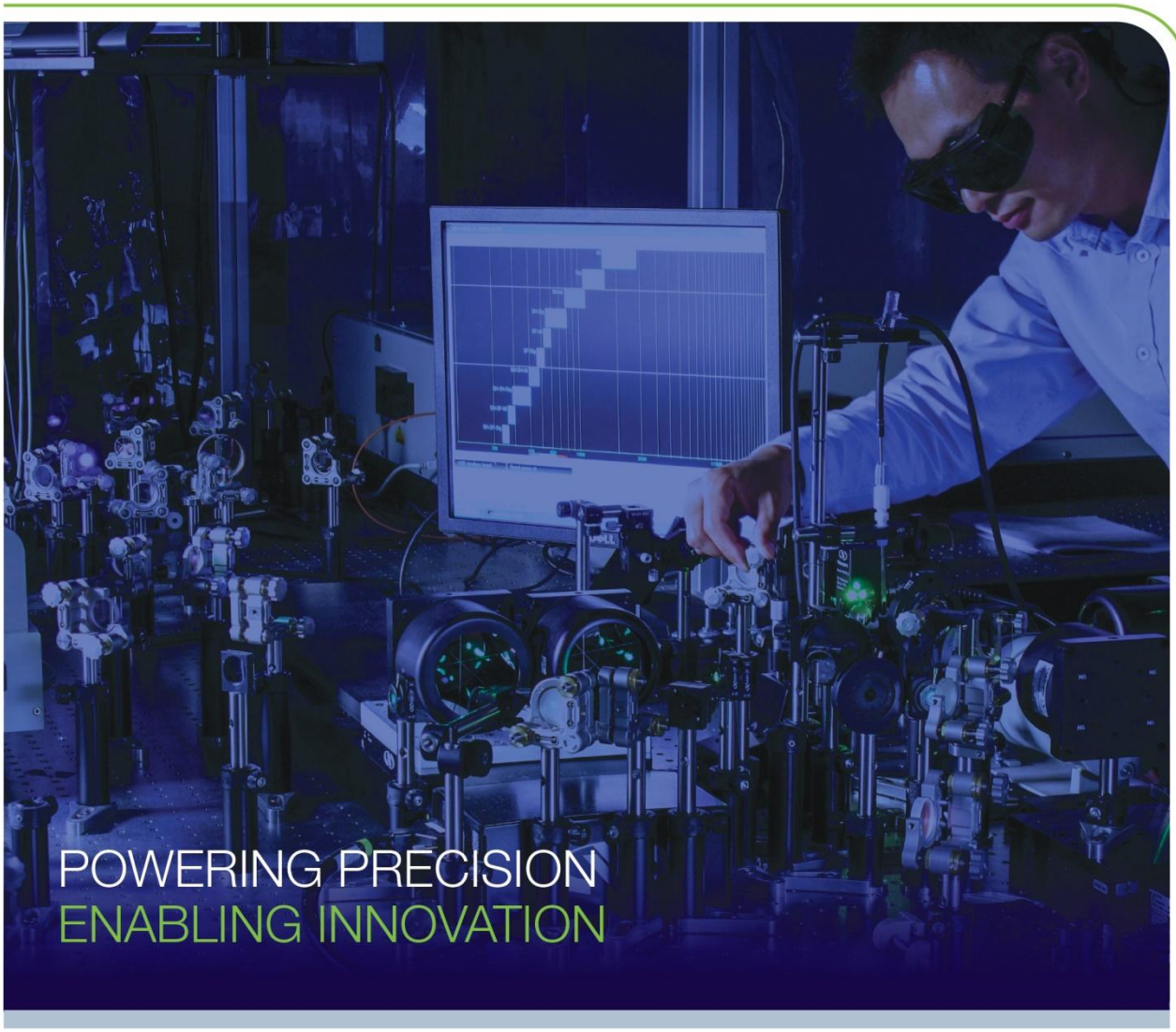

ADVANCED PHOTONICS

Discover the synergy of **Spectra-Physics®, Ophir®**, and **Newport™** - world-class brands united under **MKS Photonics Solutions**.

From semiconductor manufacturing, life and health science, research, and specialty industrial applications, we deliver end-to-end photonics innovation that enhances productivity, accuracy, and discovery.

Our portfolio includes:

- Laser Systems
- Vibration Isolation
- Optical Components
- Laser Power Measurement

Visit **www.mks.com** to explore how we're pushing the boundaries of light-based technologies.

mks | Newport | Ophir | Spectra-Physics

Committees

Scientific Committee and Review Board

- Aleksandar Krmpot, Photonics center, Institute of Physics Belgrade, University of Belgrade, Serbia
- Aleksandra Maluckov, VINČA Institute of Nuclear Science, University of Belgrade, Serbia
- Bojan Resan, School of Engineering, FHNW University of Applied Sciences and Arts, Northwestern Switzerland
- Boris Malomed, Department of Physical Electronics, School of Electrical Engineering, Tel Aviv University, Israel
- Branislav Jelenković, Photonics center, Institute of Physics Belgrade, University of Belgrade, Serbia
- Carsten Ronning, Institute of Solid State Physics, Friedrich-Schiller-Universität Jena, Germany
- Concita Sibilia, Department of Basic and Applied Sciences for Engineering, Sapienza University of Rome, Italy
- Darko Zibar, Department of Photonics Engineering, Technical University of Denmark, Denmark
- Dmitry Budker, Johannes Gutenberg University Mainz, Germany, Germany
- Dragan Inđin, Institute of Microwaves and Photonics, School of Electronic and Electrical Engineering, University of Leeds, United Kingdom
- Edik Rafailov, Aston Institute of Photonic Technologies, School of Engineering and Applied Science, Aston University, United Kingdom
- Francesco Cataliotti, European Laboratory for Non-Linear Spectroscopy, University of Florence, Italy
- Giannis Zacharakis, Institute of Electronic Structure and Laser, Foundation for Research and Technology – Hellas, Greece
- Goran Isić, Institute of Physics Belgrade, University of Belgrade, Serbia
- Goran Mašanović, Optoelectronics Research Centre (ORC), Zepler Institute, Faculty of Engineering and Physical Sciences, University of Southampton, United Kingdom
- Ivana Vasić, Institute of Physics Belgrade, University of Belgrade, Serbia
- Jasna Crnjanski, School of Electrical Engineering, University of Belgrade, Serbia
- Jelena Radovanović, School of Electrical Engineering, University of Belgrade, Serbia
- Jelena Stašić, VINČA Institute of Nuclear Science, University of Belgrade, Serbia
- Jerker Widengren, Department of Applied Physics, Royal Institute of Technology, Stockholm, Sweden
- Jovan Bajić, Faculty of Technical Sciences, University of Novi Sad, Serbia
- Ljupčo Hadžievski, VINČA Institute of Nuclear Science, University of Belgrade, Serbia
- Luca Antonelli, Department of Physics, York Plasma Institute, University of York, United Kingdom
- Marco Canepari, Laboratoire Interdisciplinaire de Physique, Université Grenoble Alpes, France
- Marko Krstić, School of Electrical Engineering, University of Belgrade, Serbia
- Marko Spasenović, Institute of Chemistry, Technology, and Metallurgy, University of Belgrade, Serbia
- Milan Kovačević, Department of Physics, Faculty of Science, University of Kragujevac, Serbia

- Milena Milošević, The Centre for Laser Microscopy, Faculty of Biology, University of Belgrade, Serbia
- Milivoj Belić, Texas A&M University at Qatar, Qatar
- Mirjana Novaković, VINČA Institute of Nuclear Science, University of Belgrade, Serbia
- Nikola Stojanović, Deutsches Elektronen-Synchrotron DESY, Hamburg, Germany
- Nikola Vuković, School of Electrical Engineering, University of Belgrade, Serbia
- Nikos Pleros, Department of Informatics (CSD), Aristotle University of Thessaloniki, Greece
- Pavle Andjus, The Centre for Laser Microscopy, Faculty of Biology, University of Belgrade, Serbia
- Petra Beličev, VINČA Institute of Nuclear Science, University of Belgrade, Serbia
- Sergei Turitsyn, School of Engineering and Applied Science, Aston University, United Kingdom
- Vladan Pavlović, Department of Physics, University of Niš, Serbia
- Vladan Vuletić, MIT, United States of America
- Vladana Vukojević, Center for Molecular Medicine, Department of Clinical Neuroscience, Karolinska Institute, Stockholm, Sweden
- Zoran Grujić, Photonics center, Institute of Physics Belgrade, University of Belgrade, Serbia

Organizing Committee

- Marina Lekić, Institute of Physics Belgrade (Chair)
- Aleksandar Krmpot, Institute of Physics Belgrade (Co-Chair)
- Uroš Ralević, Institute of Physics Belgrade (Co-Chair)
- Dušica Vukčević Stojiljković, Institute of Physics Belgrade (Secretary)
- Stanko Nikolić, Institute of Physics Belgrade (Webmaster)
- Mihailo Rabasović, Institute of Physics Belgrade
- Marija Ćurčić, Institute of Physics Belgrade
- Marta Bukumira, Institute of Physics Belgrade
- Miljana Piljević, Institute of Physics Belgrade
- Milica Ćurčić, Institute of Physics Belgrade
- Branka Hadžić, Institute of Physics Belgrade
- Aleksandra Kocić, Institute of Physics Belgrade
- Bojana Bokić, Institute of Physics Belgrade

Technical Organizer

Lufthansa City Center
Panacomp Wonderland
Travel

http://www.panacomp.net/
Tel: +381 21 466 075
Tel: +381 21 466 076
Tel: +381 21 466 077

Dear Colleagues, friends of photonics,

We are honored by your participation at our PHOTONICA 2025 and your contribution to the tradition of this even. It is our pleasure to host you in Belgrade and in Serbia. Welcome to the world of photonics.

The International School and Conference on Photonics- PHOTONICA, is a biennial event held in Belgrade since 2007. The first meeting in the series was called ISCOM (International School and Conference on Optics and Optical Materials), but it was later renamed to PHOTONICA to reflect more clearly the aims of the event as a forum for education of young scientists, exchanging new knowledge and ideas, and fostering collaboration between scientists working within emerging areas of photonic science and technology. A particular educational feature of the program is to enable students and young researchers to benefit from the event, by providing introductory lectures preceding most recent results in many topics covered by the regular talks. In other words, tutorial and keynote speakers will give lectures specifically designed for students and scientists starting in this field. Apart from the oral presentations PHOTONICA hosts vibrant poster sessions. A significant number of best posters will be selected and the authors will have opportunity to present their work through short oral presentations – contributed talks.

The wish of the organizers is to provide a platform for discussing new developments and concepts within various disciplines of photonics, by bringing together researchers from academia, government and industrial laboratories for scientific interaction, the showcasing of new results in the relevant fields and debate on future trends.

PHOTONICA 2025 will host four joint events: PhoBioS COST Action “Light and biological surface interaction for sensing applications”, BioQantSense workshop “Laser microscopy - classical and quantum”, SensSmart workshop “Multimodal Sensor Systems and Artificial Intelligence in Service of Cardiovascular Diagnostics” and “Advanced nanosystems for photoconversion”, Aerosol4solar and NIMPHA research projects. In addition, the representatives of the companies related to photonics will have significant role at the event by presenting the new trends in research and development sector. Following the official program, the participants will also have plenty of opportunities to mix and network outside of the lecture theatre with planned free time and social events.

This book contains 142 abstracts of all presentations at the X International School and Conference on Photonics, PHOTONICA 2025. Authors from all around the world, from all the continents, will present their work at this event. There will be 5 tutorial and 5 keynote lectures to the benefits of students and early-stage researches. The most recent results in various research fields of photonics will be presented through 16 invited lectures and 9 progress reports of early-stage researchers. Within the poster sessions and a number of contributed talks, authors will present 107 presentations on their new results in a cozy atmosphere of the building of Serbian Academy of Science and Arts.

Belgrade, August 2025

Editors

Conference Topics

1. Quantum optics and ultracold systems
2. Nonlinear optics
3. Optical materials
4. Biophotonics
5. Devices and components
6. Optical communications
7. Laser spectroscopy and metrology
8. Ultrafast optical phenomena
9. Laser - material interaction
10. Optical metamaterials and plasmonics
11. Machine learning in photonics
12. Other topics in photonics

Joint Events

PhoBioS COST Action - "Light and biological surface interaction for sensing applications”

BioQantSense Workshop - "Laser microscopy - classical and quantum"

SensSmart workshop - “Multimodal Sensor Systems and Artificial Intelligence in Service of Cardiovascular Diagnostics”

“Advanced nanosystems for photoconversion”, Aerosol4solar and NIMPHA research projects

Table of Contents

Tutorial Lectures..... 12

T.1 Tissue optical clearing as an innovative means for optical imaging and phototherapy from UV to terahertz.....13

T.2 Advancing the next generation of photonic systems using machine learning.....14

T.3 Lighting up superconductivity.....15

T.4 3D Printing at the nanoscale using MultiPhoton Lithography.....16

T.5 Integrated Quantum Photonics: Physics, technology, applications.....17

Keynote Lectures..... 18

K.1 Bose mixtures : magnetic and condensation phenomena 19

K.2 Perovskite Photovoltaics: Addressing Stability Challenges for Real-World Applications.....20

K.3 Seeing is believing: the modern approach to intracellular biochemistry 21

K.4 Manipulation of photoinduced reaction dynamics with strong laser fields.....22

K.5 Super-resolved imaging of obscured objects.....23

Invited Lectures..... 24

I.1 Electromagnetic Induction Imaging with Atomic Magnetometers: Coming of Age.....25

I.2 SiN PICs and PPICs for Photonic Neural Networks, High-Speed Transmitters, and Sensors 26

I.3 Twisted Light in Scattering Medium: From Optical Angular Momentum to Biomedical Diagnostics 27

I.4 Serial 2-photon imaging of the kidney reveals the dynamics of kidney fibrosis after acute injury 28

I.5 On the optical properties of laser-generated plasmonic nanoalloys and their use for the assessment of biodegradable nanomedicines 29

I.6 Bright and Quantum: Toward Intense and Non-Gaussian Quantum Light 30

I.7 Direct photosensitizer-free laser treatment of cancers 31

I.8 Quantum Cascade Lasers and Their Applications in Gas Sensing and Biomedical Fields 32

I.9 Overview of photon Bose-Einstein condensates 33

I.10 Sustainable Surface Engineering of Stainless Steel: Antimicrobial and Antiviral Functionalization via Femtosecond Laser Processing and Magnetron Deposition of Cu and Ag 34

I.11 Selected biomedical applications in Light sheet microscopy 35

I.12 Potential of 5-ALA in Neurosurgery – Fluorescence and Photodynamic Therapy 36

I.13 Neutral atom quantum computing at QuEra Computing 37

I.14 Tomography and Verification of Large-Scale Quantum Systems: Scalable Methods for Photonic Platforms 38

I.15 Nonlinear disordered photonics for cryptography and optical isolation 39

Progress Reports 40

P.1 Label-free characterization of red blood cells using advanced optical techniques 41

P.2 Multiphoton Live-Cell Metabolic Imaging and Femtosecond Laser Nanosurgery of Filamentous Fungi 42

P.3 Comparative Study of Ion Channels in Filamentous Fungi Following the Novel Development of Laser Nanosurgery for Cell Wall Removal 43

P.4 Analog Quantum Simulation and Digital Quantum Computation with Ultracold Atoms in Optical Lattices 44

P.5 Propagation and Stability of Compact Localized Modes in 2D Photonic Flat-band Lattices 45

P.6 Real-time imaging using *Morpho didius* wing scales as biophotonic microcantilever pixels 46

P.7 Illuminating the Brain: Pipedream or Impending Reality for Minimally Invasive Neurostimulation? 47

P.8 Electron-plasmon Scattering in Doped Graphene 48

P.9 AFM analysis of astrocyte membrane remodeling induced by immunoglobulin G from patients with amyotrophic lateral sclerosis 49

1. Quantum optics and ultracold systems 51

QO.1 Exploring the Phase Diagram of Quantum Many-Body Scars with Programmable Rydberg Atom Arrays 52

QO.2 Acoustic Control of Quantum Emission: Toward Time-Bin Encoded Single-Photon Sources 53

QO.3 Characterization of the Tunable Mid Infrared Photon Pair Source realized in the nonlinear $AgGaS_2$ medium 54

QO.4 Weighted Hartree-Fock-Bogoliubov method for interacting fermions 55

QO.5 Effect of dielectric environment on electronic and optical properties of spherical core/shell quantum dot: comparison of two models 56

QO.6 Collective dynamics of dipolar quantum droplets 57

2. Nonlinear optics 58

NO.1 Solutions to variants of the resonant nonlinear Schrödinger equation using the Jacobi elliptic function expansion method 59

NO.2 Various rogue wave clusters of the higher-order nonlinear Schrödinger equation 60

NO.3 Edge modes in nonlinear zig-zag modulated waveguide arrays with zero average modulation 61

NO.4 Deterministic aperiodic lattices generation with Weber beams 62

NO.5 Excitation of self-induced surface states in parabolic geometry 63

NO.6 Counterpropagating Peregrine-like soliton 64

NO.7 The nonlinear Talbot effect of counterpropagating rogue waves 65

NO.8 Nonlinear Optical Properties of Poly-Lactic Acid (PLA) for Photonic Applications 66

NO.9 Nonlinear Optical Properties of Borosilicate Glasses with Silver Nanoparticles for Photonic Applications 67

3. Optical materials 68

OM.1 Semiconductor-driven tunable nanostructured metamaterial with epsilon-near-zero transition layer 69

OM.2 Morphological transformation of (In,Ga)N nanoshells grown around pencil-like GaN nanowires 70

OM.3 Impact of Growth Pressure on the Physical Properties of Two-Step Grown Sb_2Se_3 Absorbers for Thin Film Solar Cell Applications 71

OM.4 Fiber optic sensors enhanced by diamond structures for biomedical and environmental sensing 72

OM.5 Plasma, UV Radiation and Ozone for Microplastics Degradation: Optical Characterization of Polystyrene, Polyethylene and Polypropylene Degradation using FTIR and Raman Spectroscopy 73

OM.6 First-Principles Investigation of the Optical Properties of Layered Phyllosilicates 74

OM.7 Strain-Induced Corrugation and Its Impact on Electronic and Optical Properties of hBN-GaS, -GaSe, and -InS heterostructures 75

OM.8 An exploration of the electromagnetic boundary conditions for two-dimensional materials with out-of-plane polarization 76

OM.9 Rapid vs. Conventional Annealing: Impact on Optical Losses in TiN Thin Films 77

OM.10 Temperature tunable biopolymer photonic structure 78

4. Biophotonics 79

B.1 Thermal Damage Modeling of CO2 Fractional Laser Induced Skin Micro-Tunnels 80

B.2 Novel Phosphorene-based Photodetector for biomarker analysis at UV range 81

B.3 Fiber Optic Based Sensors For Viral Biomarkers Detection 82

B.4 Tissue optics for low invasive diagnostics 83

B.5 Near-infrared Light-Driven Nanomotors: Toward Ballistic Transport of Medicaments Across the Cell Membrane 84

B.6 X-ray assisted photodynamic therapy for pancreatic cancer 85

B.7 Towards NIR and MIR quantum microscopy of biosamples with undetected photons 86

B.8 Nonlinear Laser Scanning Microscopy for noninvasive imaging of cells labeled by up-converting $NaY_{0.65}Gd_{0.15}F_4:Yb_{0.18}Er_{0.2}$ nanoparticles 87

B.9 The Subtle Interplay of Microfluidics and Optics in Nature 88

B.10 Parallel Factor Analysis of Essential Oils via Fluorescence Spectroscopy 89

B.11 Optimizing Optical Coherence Tomography for Tooth Lesions Diagnosis Through Optical Clearing Agents 90

B.12 Photonic Biosensors for Discriminating Sepsis, UTI, and Bladder Cancer via Biofunctionalized Optical Probes 91

B.13 Multimodal optical imaging and label-free sensing on-chip for monitoring intracellular and extracellular cellular processes 92

B.14 Prospects for heart failure diagnostics using photoplethysmography 93

B.15 A reflective holographic setup for simultaneous micro- and macro-scale imaging of biological samples 94

B.16 Performance Evaluation of Galvanometric Mirrors for Fast Scanning in Multimodal Laser Microscopy 95

5. Devices and components 96

DC.1 Fluorescent proteins as perspective elements of optoelectronic devices 97

DC.2 TERA-MIR Photonic Functionalities and Applications 98

DC.3 Cross waveguide design for color-centers in diamond 99

DC.4 Optimized AR Facet Coatings for 4.6 µm QCLs in Directed Infrared Countermeasures 100

DC.5 Etching-Based Mesa Formation for Quantum Cascade Laser Waveguides 101

DC.6 Single-Frequency DFB Laser based on High-Yb-doped photosensitive fiber 102

DC.7 Design and Fabrication of Thin Film for All Solid-State Lithium-Ion Batteries 103

DC.8 Electromagnetic Shielding Performance of Transparent ZTO/Ag/ZTO Multilayer Electrodes Deposited on Polymer Substrates 104

DC.9 Effect of pulse energy on the formation of Laser-Induced Periodic Surface Structure on Nb/Ti multilayer thin films 105

DC.10 Magnetron Sputtered Grown $LiCoO_2$ and Li7La3Zr2O12 Thin Film Layers for All-Solid-State Lithium-ion Batteries 106

DC.11 Laser-Induced Graphene and MXene on Biocompatible Polymer Substrates as Physical Sensors 107

DC.12 All optical fiber whispering gallery mode resonator 108

DC.13 Multifractal analysis of heart dynamics after running with PPG sensor 109

DC.14 Modelling of Terahertz Quantum Cascade Laser Self-Mixing Dynamics 110

DC.15 Wavelength demultiplexers based on coupled waveguide arrays with nonuniform lengths 111

DC.16 Method of registration of the different times of optical signals in multichannel laser systems 112

DC.17 Transition from normal to inverted band structure type in HgTe/CdTe nanowires 113

DC.18 Next-Generation Load Sensing: FBG Sensors vs. Classic Strain Gauge Approach 114

DC.19 High-power gold vapor laser operating in ultraviolet and deep ultraviolet spectral ranges 115

DC.20 High-power ultraviolet laser system based on frequency-converted copper vapor laser 116

6. Optical communications 117

OC.1 Data transmission rate estimates for OAM-carrying waves generated by various discrete EM radiating sources 118

OC.2 Reconfigurable NAND/NOR/S-R latch all-optical circuit based on a dual injection-locked Fabry-Pérot laser 119

OC.3 Design and first tests of the optical setup for experiments with the free-space OAM waves 120

OC.4 Simulation and adaptation of DPS and DQPS QKD protocols for practical implementation and coexistence within PON architecture 121

7. Laser spectroscopy and metrology 122

LS.1 A calibration method for laser interferometric instrument complexes based on stimulated Mandelstam-Brillouin scattering effect 123

LS.2 Wood Phantoms as Reference Material for Machine Learning Optical Spectroscopy of Construction Wood 124

LS.3 Raman spectroscopy as a predictive tool for Laser-Induced Graphene from wooden biomass 125

LS.4 Synthesis of Bimetallic Germanium-Copper Oxide Nanoparticles by Pulsed Laser Ablation in Liquids: Potential Application for LIBS Signal Enhancement 126

8. Ultrafast optical phenomena 127

UO.1 Controllable Splitting and Coherently Recombining Intense Femtosecond Pulses Using Structured Light 128

UO.2 Laser Polarization Control of High Harmonics in Centrosymmetric and Non-Centrosymmetric Semiconductors 129

9. Laser - material interaction 130

LM.1 Terahertz wave generation from laser-irradiated near-critical-density plasmas 131

LM.2 Enhancement of LIBS Signal via NELIBS and LIPSS for Biomedical Applications 132

LM.3 Ultrafast laser–tissue interaction modeled via two-electron-temperature and free-carrier dynamics 133

LM.4 Surface Modification for bioactivity improvement of Polyetheretherketone (PEEK) via Femtosecond Laser Microprocessing 134

LM.5 Comparison of laser-induced graphene on different types of synthesized crosslinked polyimides 135

LM.6 Grated target reflectivity evolution during laser prepulse irradiation 136

LM.7 Solid targets heating during laser prepulse 137

LM.8 Laser-Induced Nanostructuring and Surface Phonon Behavior in ZnO/MnO Nanocomposites 138

LM.9 Surface Modification of Wide Bandgap Semiconductor GaN Using Femtosecond Laser Induced Periodic Surface Structuring (LIPSS) 139

LM.10 Effects of high heat flux obtained by pulsed laser irradiation on PM 316L alloy 140

10. Optical metamaterials and plasmonics 141

OMP.1 Graphene Based Plasmon-Induced Terahertz Metamaterial for High-Performance Multispectral Detecting 142

OMP.2 Studying electronic properties and plasmonic reactivity of (functionalized) nanoparticles by x-ray aerosol photoelectron spectroscopy (XAPS).....143

OMP.3 Electron energy loss function in a graphene-hBN-graphene heterostructure 144

OMP.4 Monitoring Adsorption and Reduction Kinetics in a Plasmonic Microreactor Using Methylene Blue as a Model System 145

OMP.5 Influence of the GaN phonon excitations on the EELS spectra of a hole-doped graphene-GaN-graphene system.....146

11. Machine learning in photonics..... 147

MLP.1 Computational capacity of LA-VCSEL devices with complex resonator shapes.....148

MLP.2 Optical reservoir computing with controlled complexity 149

MLP.3 The interference effects in injection-locking-based reservoir computing: a case study of a Fabry-Perot laser diode under optical injection 150

MLP.4 Inverse Design for Femtosecond-Laser Photonic Surfaces with Direct Gradient Optimization 151

MLP.5 Principal Component Analysis for Photoacoustic Experiment Optimization: Evaluating Correlation vs. Covariance Approaches 152

MLP.6 Fiber optic interferometer sensor for condition surfaces monitoring.....153

MLP.7 Hardware matrix multiplication through silicon photonics 154

MLP.8 Reconfigurable all-optical sigmoid-like activator based on a Fabry-Pérot laser diode with multi-wavelength output capacity 155

MLP.9 Coupled phase-intensity bistability in Fabry-Pérot lasers under optical injection 156

MLP.10 End-to-end deep learning reconstruction of simulated off-axis holograms 157

12. Other topics in photonics 158

OP.1 Optomechanics of nanoparticles in a hybrid anapole state 159

OP.2 Electronic transport in semiconductors: from textbook knowledge to modern problems 160

OP.3 Nanophotonic light control for omnidirectional broadband absorption of the solar radiation for thin film solar cells 161

OP.4 Topologically Protected Modes in Diamond-like Photonic Ribbons 162

OP.5 Morphological changes and cell viability of GL261 and SMA-560 mouse glioma cells affected by direct infrared light illumination 163

OP.6 Efficacy of Multiple-Antenna Microwave Ablation in the Treatment of Liver Tumors 164

OP.7 The comparative analysis of electromagnetic shielding efficiency of graphene oxide composites with different silver nanostructures 165

OP.8 The impact of SRH recombination on the current-voltage characteristic of organic and perovskite solar cells 166

OP.9 Structural characterization of Nb_2CT_z MXene for energy storage application 167

OP.10 Self-consistent approach to quantum dynamics of photoinduced electronic excitations in molecular aggregates 168

OP.11 Single Shot Two-Dimensional Polarization Mapping of Birefringent Elements and Devices 169

OP.12 Polaron properties within the Peierls model using unitary-transform approach 170

Index 171

Tutorial Lectures

Tissue optical clearing as an innovative means for optical imaging and phototherapy from UV to terahertz

V. V. Tuchin
Institute of Physics and Science Medical Center, Saratov State University
Institute of Precision Mechanics and Control, FRS "Saratov Scientific Centre of the Russian Academy of Sciences"
Laboratory of Laser Molecular Imaging and Machine Learning, Tomsk State University, Russia
email: tuchinvv@mail.ru

Tissue optical clearing (TOC) is based on temporary and reversible suppression of light scattering in tissues and organs using biocompatible immersion optical clearing agents (OCAs) [1-3]. Delivery of the appropriate OCA to living tissue ensures its temporal transparency over a wide spectral range from deep UV to THz, thereby providing higher image depth and contrast for optical techniques and better precision of phototherapy and laser surgery.

The tutorial summarizes the fundamentals and latest advances in the development of the TOC method for solving problems of intravital optical imaging, diagnostics and therapy. TOC can significantly improve advanced multimodal spectroscopy/imaging and phototherapy technologies. The combination of optical techniques with US, CT and MRI is possible through use of commercial coupling or contrast agents. The TOC method provides additional molecular diffusion markers for monitoring *diabetes mellitus* complications and cancer detection, as well as gives important data for optimal cryopreservation of organs.

This work was supported by RSF grant № 24-44-00082.

REFERENCES:
[1] L. Oliveira and V.V. Tuchin, *The Optical Clearing Method: A New Tool for Clinical Practice and Biomedical Engineering*, Basel: Springer Nature Switzerland AG, 2019.
[2] V.V. Tuchin, D. Zhu, E.A. Genina (Eds.), *Handbook of Tissue Optical Clearing: New Prospects in Optical Imaging*, CRC Press, Boca Raton, FL, 2022.
[3] D. Zhu, V.V. Tuchin, Tissue optical clearing imaging from *ex vivo* toward *in vivo*, *BME Front.* **5**, 0058 (2024).

Advancing the next generation of photonic systems using machine learning

D. Zibar
DTU Electro, Technical University of Denmark, Ørsteds plads, Building 343, DK-2800, Kgs. Lyngby
e-mail: dazi@dtu.dk

The 2024 Nobel Prize in Physics underscores the growing influence of machine learning in diverse areas of physical science. In the field of photonics, machine learning is proving invaluable for tasks such as optimizing and designing fiber-optical communication systems, optical amplifiers, noise characterization of frequency combs, inverse design of photonic components, and quantum-noise-limited signal detection. In this talk, I will review notable applications of machine learning in photonics and explore future directions in this emerging field. Specifically, I will highlight its role in phase noise characterization of optical frequency combs, end-to-end learning for fiber-optic communication, and realization of programmable ultra-wideband Raman amplifiers. Lastly, I will introduce an exciting new application of machine learning: controlling nonlinear interactions in highly nonlinear waveguides.

Lighting up superconductivity

E. Demler
Institute for Theoretical Physics, ETH Zurich, Switzerland
e-mail: demlere@phys.ethz.ch

This talk will review new insights into high temperature superconductors revealed by novel optical probes with an emphasis on the theoretical models necessary for interpreting experimental results. We will start by discussing recent experiments in the pseudogap phase of the YBCO cuprates that have been interpreted as the light induced Meissner effect. We will approach this phenomenon from the perspective of nonlinear dynamics of the sine-Gordon model triggered by the strong terahertz pump pulse. This interpretation suggests that these experiments reveal strong superconducting correlations in the pseudogap state but do not require photoinduced superconductivity. I will argue that other experimentally observed features of the photoexcited transient state in YBCO can be explained from the perspective of a Floquet material. I will present a general theoretical framework for understanding Floquet materials, in which the pump-induced oscillations of a collective mode lead to the parametric generation of excitation pairs. This can result in features such as photo-induced edges in reflectivity, enhancement of reflectivity, and even light amplification.

3D Printing at the nanoscale using MultiPhoton Lithography

M. Farsari
FORTH/IESL, Heraklion, Greece
e-mail: mfarsari@iesl.forth.gr

Multiphoton Lithography (MPL) is an advanced laser-based additive manufacturing technique that enables the fabrication of highly complex three-dimensional micro- and nano-structures with resolutions down to just a few tens of nanometers[1]. By employing nonlinear multiphoton absorption, MPL offers unique capabilities that remain unmatched by any other 3D printing method currently available.

This exceptional resolution and design freedom make MPL a powerful tool for directly transforming computer-designed models into fully functional 3D devices with sub-micrometric precision. Over the past years, MPL has been applied to a wide range of materials, enabling the realization of micro-optical elements, electromagnetic and mechanical metamaterials, biomedical scaffolds, photocatalytic systems, and more.

In this tutorial, we will provide a comprehensive introduction to the principles and practical applications of Multiphoton Lithography, with a focus on practical examples that illustrate its unique potential. The session will begin with an overview of the nonlinear absorption mechanism that underpins MPL, the process parameters that determine resolution and fabrication speed, the workflow from computer-aided design (CAD) to printed structures. Special focus will be given to the materials used.

The tutorial will then explore in detail three case studies that showcase the versatility of MPL:

- **Micro-optical elements**, such as free-form lenses, diffractive optical elements, and waveguides for advanced photonic applications.
- **Electromagnetic and mechanical metamaterials**, demonstrating how MPL enables the creation of architected structures with tailored electromagnetic responses or unusual mechanical behaviours, such as electromagnetically induced transparency or auxeticity.
- **Scaffolds for tissue engineering**, highlighting how MPL can fabricate precisely controlled 3D architectures that support cell growth and guide tissue regeneration at the microscale.

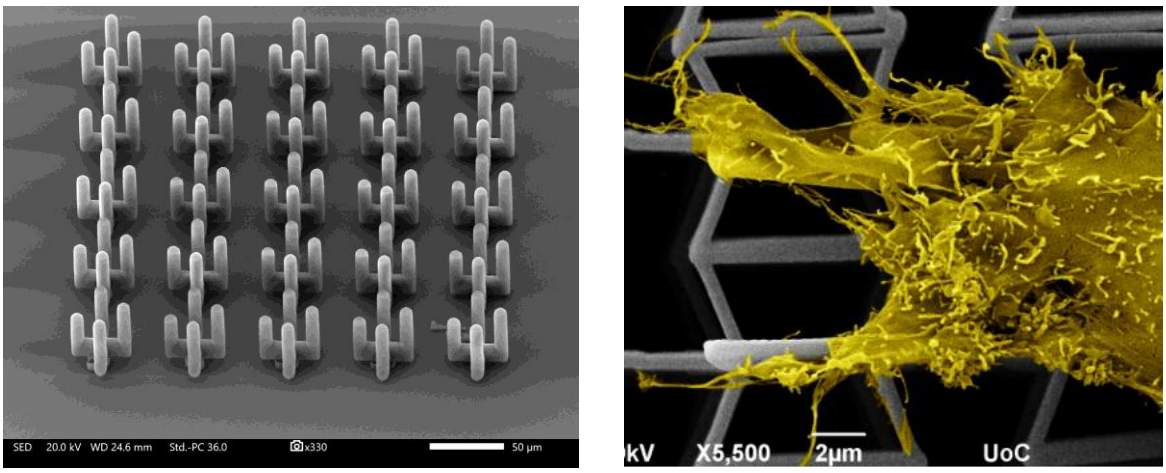

(a) (b)

Figure 1. (a) A THz metamaterial (b) SEM image of cells growing on an auxetic material

REFERENCES

[1] Zyla, G. & Farsari, M. *Laser & Photonics Reviews* **18**, 2301312, (2024).

ORCID: MF 0000-0003-2435-4156

Integrated Quantum Photonics: Physics, technology, applications

E. Kapon
Institute of Physics EPFL, Lausanne, Switzerland
e-mail: eli.kapon@epfl.ch

One of the emerging platforms for quantum technologies, integrated quantum photonics combines quantum light emitters with sub-wavelength photonic confinement and guidance to create and manipulate quantum states of light *on-chip*. Applications include efficient sources of single photons for secure quantum communications. This tutorial will review the physics and technology behind these systems, organized in two parts.

The first part will introduce the concepts of quantum confinement leading to the realization of semiconductor quantum dots (QDs) as emitters of quantum light, and of photonic crystals (PhCs) that make possible photonic confinement and guidance at sub-wavelength dimensions. The particular technology of pyramidal QDs, with its essential feature of producing QDs with site-control at the ~10nm scale, will be presented. The design and fabrication of PhC cavities and waveguides made on the same semiconductor substrates as the pyramidal QDs will be reviewed. The optical properties of the resulting QDs and PhCs will be illustrated and interpreted [1].

The second part will describe the fabrication and properties of the integrated structures, consisting of site-controlled QDs properly positioned within PhC cavities and waveguides. New features of light-matter interaction brought about by the modification of the photonic environment introduced by the PhCs will be evidenced and explained [2]. Examples of integrated structures employed for enhancing single photon emission, for single photon multiplexing and for single photon routing will be discussed [3].

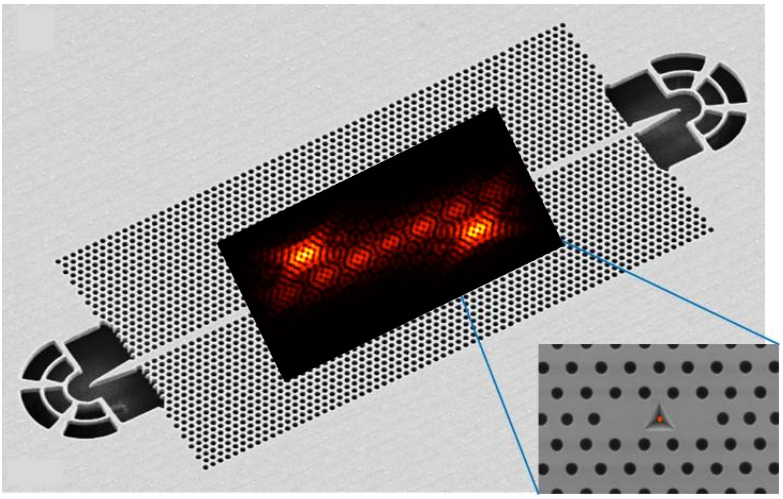

Figure 1. An example of an integrated quantum photonic structure.

REFERENCES

[1] M. Calic, et al., *Scientific Reports* **7**, 4100 (2017).
[2] A. Lyasota, et al., *Phys. Rev. X* **12**, 021042 (2022).
[3] Y. Yu, et al., *Optica* **8**, 1605 (2021).

Keynote Lectures

Bose mixtures : magnetic and condensation phenomena

S. Giorgini
Pitaevskii BEC Center CNR-INO, and Dipartimento di Fisica, Università di Trento, I-38123 Povo, Trento, Italy

Bose mixtures are one of the most active research directions in the field of ultracold atoms. They are realized with a two-component bosonic gas, either two atomic species or two hyperfine states of the same atomic species, where both components are brought to quantum degeneracy below the Bose-Einstein transition temperature. Atoms of different components can attract or repel each other realizing attractive or repulsive mixtures.

The ground state of such mixtures is fairly well understood using the standard Gross-Pitaevskii description: repulsive mixtures can undergo a phase separation transition from miscible to immiscible states which shares many analogies with the magnetic transition in spin ½ ferromagnets. Attractive mixtures, instead, can enter a regime where colapse is prevented by beyond mean-field correlations and self bound quantum droplets are formed. Experiments have clearly evidenced both the magnetic and the quantum condensation features exhibited by Bose mixtures as a function of the interspecies coupling.

At finite temperature, though, the situation is less well understood. Perturbative approaches based on Bogoliubov theory at finite temperature predict instabilities of the mixed phase driven by temperature in repulsive mixtures or fail completely when one tries to apply them to attractive mixtures in the regime where droplets are formed at zero temperature. At present no reliable simple theoretical picture can describe the magnetic behavior nor the gas to liquid condensation transition in quantum mixtures at finite temperature.

I will review recent works on the study of both repulsive and attractive Bose mixtures at finite temperature using exact path-integral quantum Monte-Carlo numerical methods. For repulsive mixtures in the quantum degenerate regime we rule out predictions of perturbative theories and find a first-order ferromagnetic transition as a function of the interspecies coupling constant. For attractive mixtures we investigate the gas to liquid transition and the region where the two phases coexist and droplets appear in equilibrium. A similar behavior is observed both in 3D and 2D geometries. In particular, the transition to the superfluid state occurs in a discontinuous way as the density jumps from the gas to the liquid phase. Furthermore, in 3D, the line of first-order transition terminates at a tricritical point and in 2D a relevant role in the gas-liquid transition is played by the quantum scale anomaly. The experimental relevance of these findings is also discussed.

REFERENCES

[1] Phase separation in binary Bose mixtures at finite temperature, G. Spada, L. Parisi, G. Pascual, N. G. Parker, T. P. Billam, S. Pilati, J. Boronat and S. Giorgini, SciPost Phys. **15**, 171 (2023).
[2] Attractive solution of binary Bose mixtures: liquid-vapour coexistence and critical point, G. Spada, S. Pilati and S. Giorgini, Phys. Rev. Lett. **131**, 173404 (2023).
[3] Quantum droplets in two-dimensional Bose mixtures at finite temperature, G. Spada, S. Pilati and S. Giorgini, Phys. Rev. Lett. **133**, 083401 (2024).

Perovskite Photovoltaics: Addressing Stability Challenges for Real-World Applications

E. Kymakis
Dept. of Electrical & Computer Engineering, Hellenic Mediterranean University, Heraklion, Crete, Greece
e-mail: kymakis@hmu.gr

Perovskite photovoltaics (PePVs) represent a rapidly advancing solar technology, having achieved power conversion efficiencies (PCEs) exceeding 26%, now competitive with traditional silicon solar cells. Their versatility makes them suitable for a broad range of applications, from low-power devices to large-scale solar farms. However, a critical hurdle to their widespread adoption remains: maintaining high efficiency and long-term stability in large-area panels under real-world environmental conditions.

PePVs exhibit sensitivity to ambient factors such as humidity, elevated temperatures, and prolonged light exposure, which significantly impact their long-term performance. Experimental observations reveal substantial degradation during summer months, primarily attributed to extended exposure to high temperatures and intense solar irradiance, often leading to lamination instability. Interestingly, this degradation demonstrates partial reversibility upon dark storage, with observed changes in the light soaking phenomenon (LSP) and improvements in electrical parameters [1]. The recovery duration is directly linked to the severity of prior degradation, with initial recovery occurring within daily dark cycles, but requiring more extended periods as degradation progresses.

This presentation will provide an in-depth exploration of the long-term performance of perovskite modules and panels deployed in outdoor environments. A key focus will be elucidating the origins of various degradation factors, distinguishing between intrinsic issues within the perovskite active layer and extrinsic challenges like lamination failure [2]. We will detail the measurement protocols employed to investigate the effects of dark storage and light soaking on panel performance and their subsequent partial recovery. Furthermore, the presentation will address the critical impact of voltage mismatch on the degradation rate of PePVs, identifying optimal connection configurations to ensure efficient long-term operation and successful upscaling. The pivotal role of lamination in preventing the ingress of external factors such as moisture and oxygen, thereby enhancing stability, will also be discussed. Continued research into the outdoor ageing process is essential to differentiate various recovery scenarios and ultimately guarantee long-term stability.

In summary, this presentation will offer comprehensive insights into the significant advancements and persistent challenges in the commercialization of perovskite photovoltaics. It will underscore the imperative for sustainable production, enhanced reliability, and robust recycling and remanufacturing strategies to firmly establish PePVs as a leading sustainable energy source in the global market.

REFERENCES

[1] Spiliarotis E., Viskadouros G., Rogdakis K., Pescetelli s., Agresti A., Tzoganakis N., Di Carlo A., Kymakis E., *EES Solar.* 2025.
[2] Pescetelli, S., Agresti, A., Viskadouros, et al., *Nature Energy* 2022, 7, 597–607

ORCID: E.K. 0000-0003-0257-1192

Seeing is believing: the modern approach to intracellular biochemistry

R. Bizzarri
Department of Surgical, Medical, Molecular Pathology, and Critical Care Medicine, University of Pisa, via Roma 55, 56126 Pisa, Italy
NEST, Istituto Nanoscienze-CNR and Scuola Normale Superiore, piazza San Silvestro 12, 56127 Pisa, Italy
e-mail: ranieri.bizzarri@unipi.it

The late biophysicist Mario Ageno (1915-1992), former Enrico Fermi's student, once stated that "Life is a coherent molecular system ruled by a program". The intrinsic coherency of life explicates in a complex interplay between temporal and spatial scales. Thus, an intriguing approach to biophysics targets the spatiotemporal description of cellular processes such as protein-protein or protein-DNA interactions, taking into account diffusion as well as molecular binding. This approach greatly relies upon the exquisite sensitivity of fluorescence microscopy combined with its high spatial and temporal resolution when applied to biological specimens.

In the first part of the talk, I will show how different techniques based on scanning fluorescence microscopy can be combined together to highlight the subtle interplay between protein dynamics and protein signaling/binding on cell membrane and between intracellular compartments.

Yet, the arsenal of fluorescent biosensors tailored to functional imaging of cells and theranostic applications is rapidly growing and benefits from recent developments in imaging techniques. In this context, I shall show how the rational tuning of the excited-state physicochemical properties may confer peculiar sensing and actuating capabilities to otherwise insensitive fluorescent dyes. For instance, rational design of the chemical structure transforms organic dyes into efficient biosensors of dielectric and viscosity properties with confocal spatial resolution at intracellular level. These biosensors were effectively applied to image physicochemical properties of intracellular organelles, shedding light on cell drug delivery mechanisms and chromatin compaction upon nuclear lamina misassembly in the Hutchinson-Guilford progeria syndrome, and membrane rigidification/fluidization upon ion-channel activation. Similarly, a single mutation in the primary sequence of otherwise photochemically-stable popular fluorescent protein variants relieves their intrinsic photoswitchable behaviour. Notably, photoswitchable (photochromic) fluorescent proteins (FPs) have become an invaluable tool for the optical labeling and tracking of living cells, organelles and intracellular molecules in a spatio-temporal manner. I shall describe their application to highlight the spatial organization of epigenetic modulators with relevant role in tumorigenesis.

Manipulation of photoinduced reaction dynamics with strong laser fields

L. Bañares
Departamento de Química Física and Center for Ultrafast Lasers, Facultad de Ciencias Químicas, Universidad Complutense de Madrid, 28040 Madrid, Spain
Instituto Madrileño de Estudios Avanzados en Nanociencia, IMDEA Nanoscience, C/ Faraday 9, 28049 Madrid, Spain
e-mail: lbanares@ucm.es

With current technology, ultrafast laser radiation can easily achieve electric fields that are intense enough to induce changes or even dramatically modify the behavior of molecules. Thus, a strong external laser field can be regarded as an additional reagent in molecular processes such as chemical reactions, and one that may be used to steer the reaction towards desired targets. In recent experiments, we have studied ultrafast molecular photodissociation processes taking place under the influence of strong laser fields. We have shown that it is possible to modify observables such as quantum yields, lifetimes, translational energies, or spatial distributions of the ejected fragments (i.e. the reaction stereodynamics) with strong picosecond or femtosecond near-infrared pulses. The control is achieved by opening new strong-field-induced reaction channels, or by creating light-induced conical intersections and modulating the potentials around them by light-induced potentials. These control scenarios and the outlook for future work will be the subject of the conference.

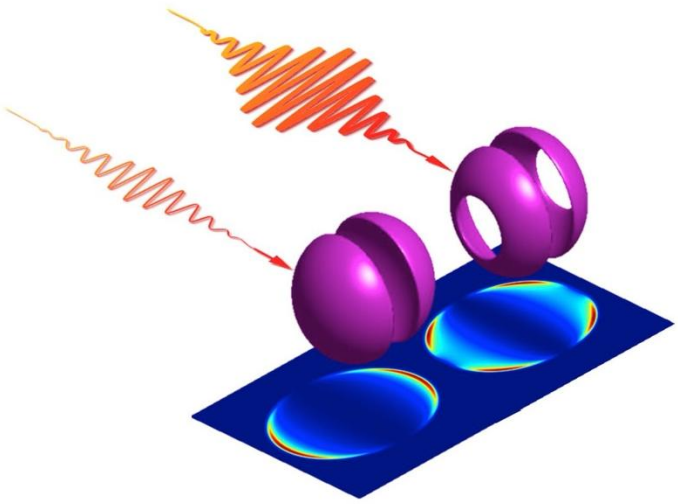

Figure 1. Effect of strong laser fields on stereodynamics of photodissociation reactions.

REFERENCES
[1] I. R. Solá, J. González-Vázquez, R. de Nalda, L. Bañares, Phys. Chem. Chem. Phys. 17, 13183 (2015).
[2] M. E. Corrales, G. Balerdi, V. Loriot, R. de Nalda, L. Bañares, Faraday Discuss. 163, 447 (2013).
[3] M. E. Corrales, J. Gonzá lez-Vázquez, G. Balerdi, I. R. Solá, R. de Nalda, L. Bañares, Nature Chem. 6, 785 (2014).
[4] M. E. Corrales, R. de Nalda, L. Bañares, Nature Comm. 8, 1345 (2017).
[5] I. M. Casasús, L. Bañares, et al. work in progress (2025).

ORCID: L. B. 0000-0002-0777-2375

Super-resolved imaging of obscured objects

E. Israeli, S. Elkabetz, A. Sanjeev, R. S. Rafeeka, G. Chen and Z. Zalevsky
Faculty of Engineering, Bar-Ilan University, Ramat-Gan 52900, Israel
e-mail: zeev.zalevksy@biu.ac.il

In this presentation we will present several schemes allowing us to perform high resolution imaging of obscured objects positioned behind scattering medium.

The first concept involves usage of time multiplexing super resolving technique that does not require a-priori knowledge on the projected encoding mask. The concept includes illuminating the object positioned behind scattering medium, through the scattering medium. This generates illumination of the object with speckle patterns. The patterns themselves are not a-priori known but the same projected pattern can be preserved and shifted by using the memory effect of the scattering medium. By properly capturing larger number of low-resolution images encoded with the projected time-shifting speckle patterns, a high-resolution image can be reconstructed after applying proper decoding algorithm.

Then, we discuss two schemes allowing 3D-position tunable focusing through and behind scattering medium. By scanning the object (that is positioned behind the scattering medium) with the position tunable focus one can perform its imaging. In the proposed schemes both the illumination module and the detection module are on the same side of the inspected object. In addition to that, the imaging process is a real time fast converging operation. The physics behind this concept involves either the assumption that the illuminating wavefront travels forward and backwards through the same scattering medium, or it uses temporal modulation (usage of pulsed light) of the spatial distribution of the illuminating beam to obtain the desired focusing.

Al the presented techniques allow reference-free, non-invasive imaging through scattering medium and since our illumination system and the detection system are on the same side of the object, it does not require the direct access behind the medium nor using feedback from there. Thus, the presented concepts might be providing high added value utility for biological and medical non-invasive imaging based diagnostic tool.

Keywords: Scattering medium, speckle patterns projection, time multiplexing super-resolution.

Invited Lectures

Electromagnetic Induction Imaging with Atomic Magnetometers: Coming of Age

F. Renzoni
Department of Physics & Astronomy, University College London, London (UK)
e-mail: f.renzoni@ucl.ac.uk

Electromagnetic induction imaging (EMI) is a well-established imaging technique, developed over several decades. It has been widely used to assess cracks in metallic structures and to detect and localise buried metallic objects. In its standard configuration, EMI's remit of application is severely restricted by the poor sensitivity of the sensing coil at low frequency. This prevents the exploration of interesting applications where low-frequency operation and/or extreme sensitivity is required, such as through-barrier imaging or imaging of human organs. The demonstration in 2014 of the use of an atomic magnetometer (AM) as sensor for EMI completely changed this scenario, and opened up new perspectives for EMI, as atomic magnetometers maintain their extreme sensitivity at low frequency. This talk discusses challenges and opportunities of EMI-AM in many sectors, from medicine to security and industrial monitoring.

REFERENCES

[1] C. Deans, L. Marmugi, S. Hussain, F. Renzoni, Electromagnetic Induction Imaging with a Radio-Frequency Atomic Magnetometer, Appl. Phys. Lett. 108, 103503 (2016).
[2] C. Deans, L.D. Griffin, L. Marmugi, and F. Renzoni, Machine learning based localization and classification with atomic magnetometers, Phys. Rev. Lett. 120, 033204 (2018).
[3] H. Yao, B. Maddox, and F. Renzoni, High-sensitivity operation of an unshielded single cell radio-frequency atomic magnetometer, Opt. Express 30, 42015 (2022).
[4]B. Maddox, C. Deans, H. Yao, Y. Cohen and F. Renzoni, Rapid Electromagnetic Induction Imaging with an Optically Raster-Scanned Atomic Magnetometer, IEEE Trans. Instr. Meas. 72, 4503105 (2023).
[5]B. Maddox, and F. Renzoni, Two-photon Electromagnetic Induction Imaging with an Atomic Magnetometer, Appl. Phys. Lett. 122, 144001 (2023).

ORCID: 0000-0002-4286-5323

SiN PICs and PPICs for Photonic Neural Networks, High-Speed Transmitters, and Sensors

K. Vyrsokinos[1,2], T. Chrisostomidis[1,2], D. Chatzitheocharis[2, 3], L. Damakoudi[1,2], P. Zdoupas[1,2], E. Chatzianagnostou[1] and D. Spasopoulos[1]
[1]*Center for Interdisciplinary Research, Aristotle University of Thessaloniki, Greece*
[2]*School of Physics, Aristotle University of Thessaloniki, Greece*
[3]*Now with OneTouch-Technologies, Ghent, Belgium*
e-mail: kv@auth.gr

Silicon Nitride (SiN) has emerged over the past years as the prominent material for fabricating Photonic Integrated Circuits (PICs), offering key advantages such as low cost, low propagation loss and improved coupling to single-mode fibers. A key strength of SiN lies though in its versatility to co-integrate various materials on the same chip enabling tailored properties for specific functionalities.

In this context, a SiN platform co-integrated with $BaTiO_3$ (BTO) demonstrated the capability to deliver ultra-efficient Phase Shifters (PSs), achieving a measured efficiency of 2.52 V·mm with a corresponding Pockels coefficient reaching up to 783 pm/V [1], while the propagation losses for the hybrid PSs were measured at 0.54 dB/mm. For a Mach–Zehnder Interferometer (MZI) employing these PSs, the power consumption during switching from ON to OFF states was found to be as low as 120 nW, delivering an extinction ratio between ON and OFF states up to 20 dB, with rise/fall times as low as 20 ns, limited by the electrical driving circuitry. These results establish the BTO/SiN platform as a compelling solution for large-scale photonic neural networks weighting a large number of input signals at ultra fast speed.

For high-speed transmitter applications, SiN contrary to silicon, is inherent incompatible with high-speed modulation. By co-integrating BTO and confining the optical field within ultra-dense slot waveguides using CMOS plasmonics, it is feasible to fabricate extremely compact modulator arrays capable of operating beyond 100 Gbaud, compatible with co-packaged optics. By altering the modulator configuration from simple MZM to Mach Zehnder In a Ring (MZIR) it is possible to reduce also the required voltage by 30% for Cu based plasmonics, while maintaining >100 Gbaud performance [2]. Experimental validation demonstrated 92 Gbps operation with a 3.5 Vpp driving voltage and only 10 μm-long plasmonic PSs in a MZIR device.

Plasmonics also enable high-sensitivity sensing by leveraging the strong interaction between the surrounding medium and surface plasmons propagating along the waveguide. A novel bimodal interferometer layout, achieved by folding the interferometer arms on a top and bottom propagating modes, demonstrated record-breaking sensitivities of up to 11,000 nm/RIU, setting a new benchmark for Plasmonic-Photonic Integrated Circuits (PPICs) in both performance and footprint [3].

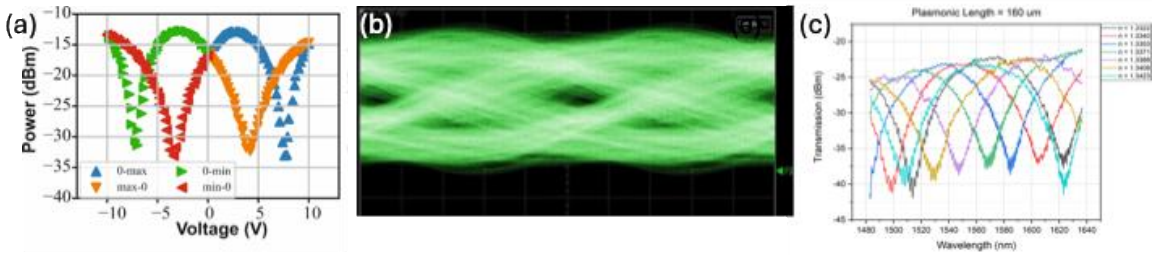

Figure 1. (a) Response of MZM with BTO PS featuring 2.52Vmm efficiency, (b) Eye diagrm of MZIR with BTO plasmonic phase shifters at 92Gbps, (c) Response of plasmonic Bimodal interfereomter with 11K nm/RIU sensitivity under different surrounding water based solutions.

REFERENCES

[1] T. Chrisostomidis et. al., “Ultra-Efficient Si3N4 MZIs with BaTiO3 as Weight Elements for Neuromorphic Photonics”, IEEE/OSA J. Lightw. Techn. 43, 09 (2025).

[2] D Chatzitheocharis et. al., “Si3N4-plasmonic ferroelectric MZIR modulator for 112-Gbaud PAM-4 transmission in the O-band”, OSA OpEx, 31, 19, (2023).

[3] P. Zdoupas and K. Vyrsokinos, “Low Loss Single Arm Bimodal/Trimodal Gold-Si_3N_4 Plasmo Photonic Sensor”, A44, ECIO 2025

ORCID: K.V. 0000-0003-3987-930X

Twisted Light in Scattering Medium: From Optical Angular Momentum to Biomedical Diagnostics

I. Meglinski
Aston Institute of Photonic Technologies, College of Engineering & Physical Sciences, Aston University, Birmingham, UK
e-mail: i.meglinski@aston.ac.uk

Structured light carrying orbital angular momentum (OAM), also known as twisted light, offers new capabilities for probing biological tissues with enhanced phase sensitivity and spatial resolution [1]. When propagating through tissue-like scattering media, OAM beams preserve their helical phase structure despite multiple scattering events [1,2]. This phenomenon, known as phase memory, enables retrieval of subtle refractive index variations that are typically lost in conventional optical-based imaging modalities.

In this lecture, we explore the propagation of structured light carrying OAM through complex scattering media such as biological tissues. We begin by introducing the fundamental concepts of spin and orbital angular momentum of light, discussing their physical origins, conservation laws, and interaction with matter. Emphasis is placed on how OAM modes, such as Laguerre–Gaussian beams, retain phase information even after passing through highly turbid, tissue-like environments.

Building on this theoretical foundation, we are going to discuss a Mach–Zehnder-based interferometric system developed for generating and probing OAM beams and show how OAM phase memory can be harnessed for non-invasive sensing of microstructural tissue changes (Fig.1). Our experimental studies, supported by custom Monte Carlo simulations, reveal that the twist of light is up to three orders of magnitude more sensitive to refractive index variations than conventional phase measurements, offering a powerful new avenue for early-stage diagnostics of cancer, diabetes-induced tissue changes, and retinal degeneration.

The talk will conclude with a discussion on the translational potential of OAM-based optical technologies in histology and clinical imaging [3], and how they may be further enhanced through AI-powered reconstruction and quantum photonics integration. A tutorial-style introduction at the beginning of the talk will provide essential background for early-stage researchers in photonics, optics, and biomedical imaging.

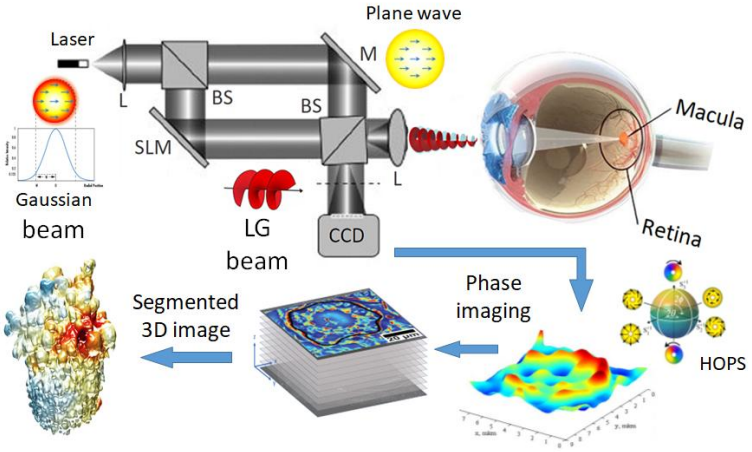

Figure 1. Schematic of a Mach–Zehnder interferometer illustrating how twisted light carrying OAM can be exploited for AI-driven non-invasive optical diagnostics of early tissue abnormalities.

REFERENCES
[1] I. Meglinski, *et al.*, *Light Sci. Appl.* 13, 214 (2024).
[2] F. Khanom, *et al.*, *Sci. Rep*. 14, 20662 (2024).
[3] I. Meglinski, *et al.*, *Optics and Photonics News*, 35(12), 43 (2024).

ORCID: IM: 0000-0002-7613-8191

Serial 2-photon imaging of the kidney reveals the dynamics of kidney fibrosis after acute injury

A. M. Kristensen[1], L. Bordoni[1,2], M. B. Nielsen[3,4], H. Kidmose[1], D. Sardella[1], K. E. Shipman[5], N. V. Krogstrup[4], J. Størling[6], H. Birn[1,3,4], R. Enger[2,7], I. M. Schiessl[1]
[1]*Department of Biomedicine, Aarhus University, Aarhus, Denmark*
[2]*Letten Centre, Department of Molecular Medicine, Institute of Basic Medical Sciences, University of Oslo, Oslo, Norway*
[3]*Department of Clinical Medicine, Aarhus University, Aarhus, Denmark*
[4]*Department of Renal Medicine, Aarhus University Hospital, Aarhus, Denmark*
[5]*School of Medicine, University of Pittsburgh, Pittsburgh, USA*
[6]*Steno Diabetes Center Copenhagen, Copenhagen, Denmark*
[7]*Department of Neurosurgery, Oslo University Hospital Rikshospitalet, Oslo Norway*
e-mail: ina.maria.schiessl@biomed.au.dk

Intravital Multiphoton Microscopy (MPM) is a powerful imaging modality for the investigation of renal pathophysiology in mice [1]. It uniquely allows to assess renal function and morphology at the same time and in the living animal. Following the implementation of an Abdominal Imaging Window (AIW) [2], it is possible to assess the same kidney regions by MPM serially for up to several weeks and to obtain longitudinal information regarding cellular behavior and changes in tissue structure.

Fibrosis is believed to play a key role in chronic kidney disease (CKD) onset and progression [3]. To halt CKD, inhibition of fibrosis has been explored both experimentally and in clinical trials. However, evidence for direct harmful effects of fibrosis is limited, as its close association with tissue injury hampers distinguishing between correlation and causation.
To investigate if fibrosis accelerates kidney injury through deterioration of injury-adjacent uninjured nephrons, we applied serial in vivo microscopy of transgenic mouse kidneys in two models of focal injury and used genetic lineage tracing to track renal fibroblasts at the interphase of injured and uninjured tissue over time. We demonstrate that fibroblast recruitment occurs reversibly, locally restricted, and injury-dependent.

Here, we use serial in vivo MPM to decipher tubular and interstitial remodeling processes after AKI over time and demonstrate important insights into the mechanisms of AKI-CKD transition.

REFERENCES
[1] I.M. Schiessl, and H. Castrop, Deep insights: intravital imaging with two photonmicroscopy. Pflugers Arch 468 (2016) 1505-16
[2] D. Sardella, A.M. Kristensen, L. Bordoni, H. Kidmose, A. Shahrokhtash, D.S. Sutherland, S. Frische, and I.M. Schiessl, Serial intravital 2-photon microscopy and analysis of the kidney using upright microscopes. Frontiers in Physiology 14 (2023)
[3] J. Majo, B.M. Klinkhammer, P. Boor, and D. Tiniakos, Pathology and natural history of organ fibrosis. Curr Opin Pharmacol 49 (2019) 82-89

ORCID: A.M.K. 0000-0002-7066-6989, L.B. 0000-0002-2428-0874, M.B.N. 0000-0003-3587-6638, D.S. 0000-0002-7648-1408, K.E.S. 0000-0002-1152-8359, N.V.K. 0000-0001-7144-730X, J.S. 0000-0002-7529-4264, H.B. 0000-0003-3715-7266, R.E. 0000-0001-9418-7117, I.M.S. 0000-0003-1613-2000

On the optical properties of laser-generated plasmonic nanoalloys and their use for the assessment of biodegradable nanomedicines

V. Amendola
Department of Chemical Sciences, University of Padova - Padova, Italy
e-mail: vincenzo.amendola@unipd.it

Compared to traditional plasmonic materials like gold and silver, their alloys exhibit a range of unique and enhanced properties, positioning them at the intersection of nanophotonics and various other disciplines, including catalysis and magnetism.[1] Less known, some nanoalloys of Au or Ag hold significant promise for cancer theranostics, offering multiple functionalities: they can be tracked in vivo using conventional imaging techniques such as magnetic resonance imaging (MRI) or X-ray computed tomography (CT) while also exerting therapeutic effects, such as enhancing radiotherapy.[2-4] Notably, certain nanoalloys of Au or Ag with carefully tuned compositions have demonstrated their ability to meet also a critical requirement like biodegradability, which is essential for minimizing the risks associated with the long-term persistence of nanomaterials in the body.[2-4] However, despite this immense potential, the synthesis of nanoalloys with the ideal theranostic characteristics is challenging due to the natural immiscibility of Au and Ag with other functional and biocompatible elements like iron or boron. Therefore, it is crucial to rapidly and reliably monitor synthesis outcomes to optimize fabrication protocols, which are possible only by laser ablation in liquid. Additionally, identifying biodegradable nanoalloy compositions requires extensive experimentation, as it necessitates tracking their structural evolution over time and under various incubation conditions.

Fortunately, the plasmonic absorption band of these alloys is highly composition-dependent, enabling real-time monitoring of their structure. Here, we present several examples demonstrating how the optical properties of these plasmonic nanoalloys can be leveraged to design and assess an emerging class of advanced inorganic nanomedicines for cancer theranostics.[6]

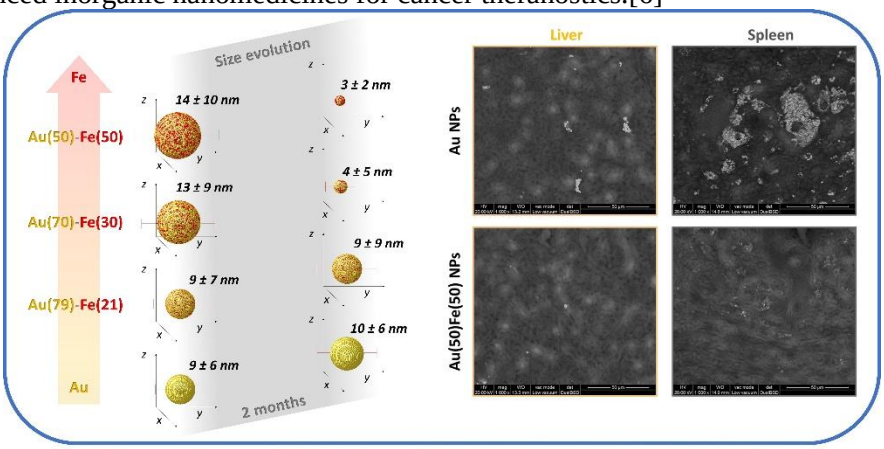

Figure 1. Left: Schematic depiction of the composition-dependent size transformation of Au-Fe nanoalloys, where an iron content above 30 at% corresponded to a size reduction below 10 nm after two months in the physiological environment. Right: The self-degradation and facilitated clearance of the Au-Fe nanoalloys was confirmed in murine models by environmental scanning electron microscopy images of their livers and spleens two months after administration. The animals treated with Au nanoparticles still show large agglomerates of gold, that are absent in the animals treated with Au-Fe nanoalloys.

REFERENCES

[1] Coviello, V., Forrer, D. and Amendola, V., ChemPhysChem 23, e202200136 (2022).
[2] Torresan, V., et al., ACS Nano 14, 12840–12853 (2020).
[3] Amendola, et al.., J. Colloid Interface Sci. 596, 332–341 (2021).
[4] Scaramuzza, S., et al., Adv. Funct. Mater. 33, 2303366 (2023).
[5] This research was funded by AIRC under the MFAG 2021-ID. 25681 project-P.I. A.V.

ORCID: A.V. 0000-0002-9937-7005

Bright and Quantum: Toward Intense and Non-Gaussian Quantum Light

C. A. Hermann
Departamento de Física, Facultad de Ciencias Físicas y Matemáticas, Universidad de Chile
e-mail: carla.hermann@uchile.cl

Non-Gaussian quantum states of light are related to quantum enhancements in quantum metrology, quantum computation, and quantum error correction. However, generating such states—and especially characterizing their nonclassical properties—remains an active challenge, particularly in the high-photon-number regime where full state reconstruction becomes impractical.

In this talk, I will present our theoretical work on how to generate a specific family of non-Gaussian states: the generalized coherent states (GCS), which arise from the nonlinear evolution of coherent light [PRR2023]. These states retain a classical Poissonian photon-number distribution while exhibiting non-Gaussian features in their Wigner representation. While this generation mechanism is well understood, identifying experimental observables that can reveal the nonclassical features of such states—without relying on complete quantum tomography—remains a key challenge.

I will discuss current strategies for addressing this problem, including the use of intensity-field correlation functions and displacement-based diagnostics of non-Gaussianity through differential current measurements. As a complementary perspective, I will briefly mention the entanglement potential upon beam splitter interaction, which—while theoretically informative—requires full state reconstruction and is thus less practical in the intense-light regime.

Direct photosensitizer-free laser treatment of cancers

E. U. Rafailov
Optoelectronics and Biomedical Photonics Group Aston Institute of Photonic Technologies, Aston University, Birmingham, B4 7ET, UK
e-mail: e.rafailov@aston.ac.uk

Recent advances in near-infrared laser technology have opened new avenues for the development of compact photonic platforms and novel approaches to disease diagnostics and therapy. Photodynamic therapy (PDT), a long-standing method for cancer treatment, typically relies on photosensitisers (PS) to convert visible light (440–650 nm) into reactive oxygen species (ROS), including singlet oxygen ($^1O_2$). In our work, we demonstrate a fundamentally different approach: the direct excitation of molecular oxygen into $^1O_2$ using 1267 nm laser irradiation, without the need for photosensitisers.

We present extensive experimental data on photosensitiser-free ROS generation using 1267 nm laser light in both normal and cancerous cells, as well as in animal models of glioblastoma. Our findings reveal selective oxidative effects and apoptosis induction in cancer cells, driven by $^1O_2$ production. Notably, in a rat glioblastoma model, a four-week treatment with a quantum-dot-based 1267 nm laser diode significantly inhibited tumor growth and increased survival rates from 34% to 64%.

Additionally, we report new results demonstrating the effective destruction of melanoma cells in a 3D human skin model using the same laser wavelength. These findings position 1267 nm photosensitiser-free laser therapy as a promising, non-invasive or minimally invasive treatment strategy for superficial cancers, particularly glioblastoma and melanoma.

Quantum Cascade Lasers and Their Applications in Gas Sensing and Biomedical Fields

L. Ozyuzer
Department of Physics, Izmir Institute of Technology, Urla, Izmir, Turkiye
Teknoma Technological Materials Industrial and Trading Inc., Urla, Izmir, Turkiye.
e-mail:ozyuzer@iyte.edu.tr

Quantum Cascade Lasers (QCLs) are semiconductor lasers that operate in the mid- and long-wave infrared (IR) and terahertz regions [1], enabling a broad spectrum of applications such as industrial gas detection, standoff explosive detection, infrared imaging, health monitoring, and advanced spectroscopy [2-3]. QCLs are compact, portable, capable of room-temperature operation, and deliver high optical power in both pulsed and continuous wave modes. Their ability across the 3–13 μm wavelength range coincides with the principal absorption bands of many atmospheric gases (e.g., CO_2, CO, NO, NO_2, SO_2, NH_3, CH_4) and biological species making them highly effective for sensitive and selective gas sensing. In this study, three distinct laser systems are being developed for: (i) greenhouse gas detection, (ii) biosensing spectroscopy of urea in blood, and (iii) directional infrared countermeasures (DIRCM). The active region of laser was designed by the Nextnano program for three wavelenghts. The superlattice structures were grown by using the MOCVD method on InP (100). The active region structure consisted of a periodically layered InGaAs/InAlAs quantum wells. The fabrication of quantum cascade lasers began with the formation of mesa structures on InP wafers using conventional lithography and chemical etching techniques. To ensure electrical insulation between the mesa top, its sidewalls, and the substrate, a thin film of SiO_2 was applied as a passivation layer, which was critical for stable laser operation. To enhance electrical contact and facilitate heat dissipation during laser emission, a thick gold layer was added to the laser bars, serving as heat sinks. Due to the high operating voltages and large threshold currents, significant heat was generated in the QCL's active region. These devices were typically cooled from the bottom of the substrate; thus, reducing the distance between the active core and the substrate base was essential for efficient thermal management. Accordingly, the QCL substrates were thinned. After thinning, the bottom of the substrate was coated with a thin titanium (Ti) layer as a buffer, followed by approximately 200 nm of Au. The progress of the ongoing project about the fabrication steps, the characterization and the characteristics of QCL chips will be discussed in detail.

Acknowledgment: This research is partially supported by TUBITAK (Scientific and Technical Research Council of Turkey) project number 22AG014, with collaboration ASELSAN A.Ş., Cumhuriyet University, Atatürk University, ASELSAN Hassas Optik A.Ş, TEKNOMA Teknolojik Mlz. Ltd. Şti., ELEKTRAL Elektromekanik A.Ş., Dokuz Eylül University and Karadeniz Technical University. We would like to thank the Research and Application Center for Quantum Technologies (RACQUT) of IZTECH for the experimental facilities.

REFERENCES:

[1] L. Ozyuzer, A. E Koshelev et al., Emission of coherent THz radiation from superconductors, Science **318**, 1291 (2007).
[2] M. Hitaka, T. Dougakiuchi, A. Ito, K. Fujita, Edamura T., Stacked quantum cascade laser and detector structure for a monolithic mid-infrared sensing device, Appl. Phys. Lett. **115**, 161102 (2019).
[3] S. Rouhi, M. Ozdemir, M. Ekmekcioglu, S. Yigen, Y. Demirhan, A. Szerling, & L. Ozyuzer, In-situ thin film copper–copper thermocompression bonding for quantum cascade lasers. Journal of Materials Science: Materials in Electronics **32**, 15605-15614 (2021).

Overview of photon Bose-Einstein condensates

A. Pelster
Physics Department and Research Center OPTIMAS, RPTU Kaiserslautern-Landau, Germany
e-mail: axel.pelster@rptu.de

The talk provides an overview of current theoretical challenges for describing a photon Bose-Einstein condensate (BEC), which represents a modern prime example for an open dissipative quantum many-body system. In the original experimental platform of dye-filled microcavities [1] the technique of direct laser writing [2] allows to microstructure potentials with different geometries on the mirror surfaces. In this way soon lattices of coupled photon condensates containing hundreds of individual sites are realizable, which are expected to have spiral vortices [3]. We show that their shape can be approximately determined analytically with a projection optimization method, which extends the variational optimization method for BECs of closed systems to open-dissipative condensates [4]. Furthermore, quite recently photon BECs have also been observed in vertical cavity surface-emitting lasers (VCSELs) [5–7]. Here frequent photon absorption and emission processes occur due to the creation and annihiliation of excitons in the semiconductor device, yielding a thermalization of photons. But it was found experimentally that the extracted spectral temperatures are significantly lower than those of the device, which warrants a theoretical explanation.

REFERENCES

[1] J. Klaers, J. Schmitt, F. Vewinger and M. Weitz, Nature 468, 545 (2010).
[2] J. Schulz, J. Noh, W. A. Benalcazar, G. Bahl, and G. von Freymann, Nature Comm. 13, 6597 (2022).
[3] V. N. Gladilin and M. Wouters, Phys. Rev. Lett. 125, 215301 (2020).
[4] J. Krauß, M.A.G. dos Santos Filho, F.E.A. dos Santos, and A. Pelster, arXiv:2311.10027 (2023)
[5] R. C. Schofield, M. Fu, E. Clarke, I. Farrer, A. Trapalis, H. S. Dhar, R. Mukherjee, J. Heffernan, F. Mintert, R. A. Nyman, and R. F. Oulton, Nature Photonics 18, 1083 (2024).
[6] M. Pieczarka, M. G ̨ebski, A. N. Piasecka, J. A. Lott, A. Pelster, M. Wasiak, and T. Czyszanowski, Nature Photonics 18, 1090 (2024).
[7] A. Fainstein and G. Usaj, Nature Photonics 18, 999 (2024).

ORCID: A.P. 0000-0002-5215-0348

Sustainable Surface Engineering of Stainless Steel: Antimicrobial and Antiviral Functionalization via Femtosecond Laser Processing and Magnetron Deposition of Cu and Ag

A.Daskalova[1], L. Angelova[1], A. Ivask[2], H. Kaur[2], M. Sikiric[3], T. Car[3], A. Shalaan[4], L. di Silvio[4], S. Neil[4], Z. Zhang[5], A. Stamboulis[5]
[1]*Institute of Electronics, Bulgarian Academy of Sciences, 72, Tzarigradsko Chaussee Blvd.1784 Sofia*
[2]*Institute of Molecular and Cell biology, U Tartu Riia 23-301, Tartu, Estonia*
[3]*Ruđer Bošković Institute, Bijenička c. 54, 10 000 Zagreb, Croatia*
[4]*Faculty of Dentistry, Guys Hospital SE1, 9RT London,UK*
[5]*School of Metallurgy and Materials, University of Birmingham, Edgbaston B15 2TT, UK*
e-mail: albdaskalova@gmail.com

Stainless steel (SS) is the most widely used material in healthcare and public infrastructure. Known cleaning methods via diverse chemicals could not be very effective and long lasting, thus leading to non continuous protection against diverse pathogens. This research is directed towards avoidance of SS surface contamination, and reducing microbial and viral transmission in high contact zones. A hybrid surface modification by employing femtosecond laser processing and magnetron sputtering, leading to formation of laser induced periodic surface structures (LIPSS) on SS surface followed by deposition of silver (Ag) and copper (Cu) thin films is presented in this study.

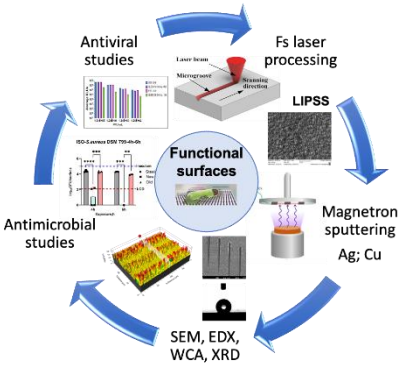

Figure 1. Schematic cycle of functional SS surfaces creation via femtosecond laser processing and magnetron sputtering.

The tests performed with *S. Aureus* demonstrated that the created LIPSS surfaces posses impoved antimicrobial properties. By additionally applying Ag and Cu thin films, it is possible to enhance the antimicrobial and antiviral efficacy of the SS surface. Femtosecond laser modification creates nanometric LIPSS structures, thus improving the surface area, wettability, and adhesion properties for deposition of thin metallic Cu and Ag layers. The sustainability of the applied coatings, was checked by nano scratched test, which showed a good adhesion properties of Cu and Ag thin films. Viral inactivation was detected on LIPSS sputtered with Cu layer. The combination between surface morphology and addition of antimicrobial metal agents was examined via SEM, EDX, WCA, and XRD and biological tests were done according to ISO-standard antimicrobial assays and antiviral activity tests. This synergetic approach is promising towards creation of effective antimicrobial, antiviral materials surfaces that meet sustainability criteria and are suitable for application in high-risk environments.

Acknowledgments: This work was funded by the European Union: Horizon Europe program under the Grant Agreement № 101057961, „Surface transfer of pathogens" (STOP). The research was carried out with the help of infrastructure purchased under the National Roadmap for Scientific Infrastructure (ELI-ERIC-BG), project D01-351.

REFERENCES

[1] Y. Meng, H. Wen, T. Yuan, Z. Ya, S. Qiang, Z. Bing, Sci China Tech Sci 65, (2022)

ORCID: A.D. 0000-0003-1131-6900, L.A. 0000-0002-1702-862X, A.I.0000-0003-3451-7211, M.S. 0000-0001-6230-5190, L.S. 0000-0003-2554-2052, S. N. 0000-0003-3306-5831, Z.Z. 0000-0002-0083-7025, A. S. 0000-0002-8366-590X

Selected biomedical applications in Light sheet microscopy

P. Loza-Alvarez
ICFO - Institut de Ciencies Fotoniques, The Barcelona Institute of Science and Technology, Castelldefels (Barcelona) 08860, Spain"
e-mail: Pablo.Loza@icfo.eu

In Light sheet fluorescence microscopy (LSFM), a sheet of excitation light is produced onto the sample plane. The generated fluorescence is then collected using a microscope objective placed orthogonal to the excitation light sheet plane. LSFM allows for a highly efficient excitation and collection of the generated signal. Altogether, such scheme minimises light dose onto the sample and results in a decreased photobleaching, reducing thus phototoxic effects [1].

LSFM has been put forward as an interesting candidate for fast volumetric imaging of biological samples. Here, I will present our efforts for achieving fast 3D imaging for high through put applications based a fluidic system based on the use of a FEP tube and a syringe pump [2, 3]. During the second part, I will present a LSFM microscope for fast volumetric imaging based on the use of an electrically tunable lens (ETL) [3,4]. This system is used to image the spontaneous Ca^{2+}activity, as reported by GCaMP fluorescence. Finally, I will present the use of wavefront coding (WFC) combined with machine learning in a light sheet fluorescence microscopy (LSFM) system to visualize the 3D dynamics of sperm flagellar motion [5].

REFERENCES

[1] O. E. Olarte, et al., *Adv. Opt. Photon*. 10, 111 (2018)
[2] M. Bernardello et al., *Scientific Reports* 12(1), (2022)
[3] E. J. Gualda, et al. *Biomedical Optics Express* 16, 2020 (2025)
[4] O. E. Olarte, et al; *Optica* 2, 702 (2015)
[5] J. Licea-Rodriguez, et al. *EPJ Web of Conferences*. Vol. 309. EDP Sciences, 2024.

ORCID: https://orcid.org/0000-0002-3129-1213

Potential of 5-ALA in Neurosurgery – Fluorescence and Photodynamic Therapy

R. Sroka[1,2], M. Aumiller[1,2], N. Thon[3], H. Stepp[1,2] and A. Rühm[1,2]
[1]*Laser-Forschungslabor, LIFE-Zentrum, LMU Klinikum, Germany*
[2]*Department of Urology, LMU Klinikum, Germany*
[3]*Department of Neurosurgery, LMU Klinikum, Germany*
e-mail: ronald.sroka@med.uni-muenchen.de

Neurosurgery suffered from discrimination of tumor to normal tissue during surgical tissue resection, but also for selective treatment of GBM. The application of photoactive drugs and their use for fluorescence guided resection, optical guided biopsy and photodynamic therapy in neurosurgery could support such requests. Besides the medical needs and boundary conditions, the physics and technical research and developments will be presented. Different clinical aspects of photodynamic therapy (PDT), like treatment planning, treatment and dosimetry protocols, spectral on-line-monitoring (SOM) as well as follow-up evaluation of clinical outcome, are of interest regarding further iPDT developments. Preliminary study results as well as the potential of optical dosimetry concepts based on light-tissue interaction and light-photosensitizer interaction are included summarizing the latest developments in this field.

Keywords: Intraluminal, Interstitial photodynamic therapy, iPDT, online monitoring, medical imaging, brain tumor.

REFERENCES

[1] Schwartz, C. et al. (2015) Interstitial Photodynamic Therapy for De-Novo Glioblastoma Multiforme WHO IV: A Feasibility Study, In: Proceedings of the 66th Annual Meeting of the German Society of Neurosurgery (DGNC) (Karlsruhe, Germany, 7-10 June 2015), DOI:10.3205/15dgnc304
[3] Lietke, S. et al. (2021) Interstitial Photodynamic Therapy Using 5-ALA for Malignant Glioma Recurrences, Cancers 13:1767, DOI:10.3390/cancers13081767
[4] Beck, T.J. et al. (2007) Interstitial photodynamic therapy of nonresectable malignant glioma recurrences using 5-aminolevulinic acid induced protoporphyrin IX, Lasers Surg Med 39:386-393, DOI:10.1002/lsm.20507
[5] Aumiller, M. et al. (2021) Investigation of Changes of Optical Tissue Properties up to 50°C, OSA Technical Digest (Optica Publishing Group, 2021), JW1A.6, DOI:10.1364/BODA.2021.JW1A.6
[6] Yassine, A.-A., et al. (2019) Optimizing interstitial photodynamic therapy with custom cylindrical diffuser, J Biophotonics 12(1):e201800153, DOI:10.1002/jbio.201800153
[7] Rühm, A., et al. (2014) 5-ALA based photodynamic management of glioblastoma, Proc SPIE 8928:89280E, DOI:10.1117/12.2040268
[8] Aumiller, M. et al. (2022) Interrelation between Spectral Online Monitoring and Postoperative T1-Weighted MRI in Interstitial Photodynamic Therapy of Malignant Gliomas, Cancers 14:120, DOI:10.3390/cancers14010120

Neutral atom quantum computing at QuEra Computing

O. Marković
QuEra Computing Inc.
Boston, USA
e-mail: omarkovic@quera.com

Quantum error correction is believed to be necessary for universal quantum computation due to its ability to correct inevitable errors arising in quantum computers. Recently, neutral atom quantum computers have demonstrated key aspects of scalable quantum error correction, such as the implementation of circuits with 48 logical qubits [1], magic state distillation [2] and architecture for universal fault-tolerant quantum processing [3].

In this talk, I will introduce QuEra Computing's approach to neutral atom quantum computing. I will discuss neutral atom qubits, the tools that are used to control them and the implementation of gate operations and qubit reconfigurability. With these basic building blocks, I will present a neutral atom quantum computing platform based on highly parallel operations and qubit shuttling. Next, I will present QuEra Computing's quantum computers, from the publicly accessible analog computer Aquila to our next-generation digital systems, along with the open-source software stack that exposes them to users. Finally, I will give an overview of recent demonstrations of scalable logical qubit processing in neutral atom platforms employing qubit shuttling, including implementation of logical magic state distillation [2].

REFERENCES

[1] Bluvstein, Dolev, Simon J. Evered, Alexandra A. Geim, Sophie H. Li, Hengyun Zhou, Tom Manovitz, Sepehr Ebadi, et al. "Logical Quantum Processor Based on Reconfigurable Atom Arrays." Nature 626, no. 7997 (February 2024): 58–65. https://doi.org/10.1038/s41586-023-06927-3.
[2] Rodriguez, Pedro Sales, John M. Robinson, Paul Niklas Jepsen, Zhiyang He, Casey Duckering, Chen Zhao, Kai-Hsin Wu, et al. "Experimental Demonstration of Logical Magic State Distillation." arXiv, December 19, 2024. https://doi.org/10.48550/arXiv.2412.15165.
[3] Bluvstein, Dolev, Alexandra A. Geim, Sophie H. Li, Simon J. Evered, J. Pablo Bonilla Ataides, Gefen Baranes, Andi Gu, et al. "Architectural Mechanisms of a Universal Fault-Tolerant Quantum Computer." arXiv, June 25, 2025. https://doi.org/10.48550/arXiv.2506.20661.

Tomography and Verification of Large-Scale Quantum Systems: Scalable Methods for Photonic Platforms

B. Dakić
University of Vienna, Faculty of Physics, Vienna Center for Quantum Science and Technology (VCQ), Boltzmanngasse 5, 1090 Vienna, Austria
Institute for Quantum Optics and Quantum Information (IQOQI), Austrian Academy of Sciences, Boltzmanngasse 3, 1090 Vienna, Austria
e-mail: borivoje.dakic@univie.ac.at

As quantum technologies scale up, the need for efficient and reliable verification of large entangled states becomes increasingly pressing. Full quantum state tomography, while comprehensive, faces exponential resource demands in both data acquisition and post-processing—making it impractical for systems beyond a modest number of qubits. This limitation is particularly acute in photonic platforms, where loss and probabilistic gates constrain the number of available state copies.

In this talk, we present a suite of scalable verification and tomography techniques designed for large-scale quantum systems under realistic experimental constraints. These methods combine tools from quantum information theory, probabilistic modeling, and post-processing optimization to make quantum verification and tomography feasible even in systems of arbitrary Hilbert space dimension. Our methods enable few-copy and even single-copy entanglement detection, sample-efficient and device-independent quantum state certification, and targeted tomography focused on physically-relevant observables. Particular emphasis is placed on their practical deployment in photonic quantum technologies, where challenges such as low detection efficiencies and limited data rates demand resource-efficient solutions to support the development of reliable quantum networks and processors and advancing photonic platforms toward real-world applications of quantum information processing.

ORCID: B.D. 0000-0001-9895-4889

Nonlinear disordered photonics for cryptography and optical isolation

F. Riboli[1,2], S. Nocentini[2,3], F. Maestri[4], A. Chabanov[5], L. Salvini[5], F. Tommasi[4], S. Cavalieri[4], D. S. Wiersma[3,4]
[1]*Istituto Nazionale di Ottica (INO), CNR, 50019 Sesto Fiorentino, Italy,*
[2]*European Laboratory for Non-linear Spectroscopy (LENS), Via Nello Carrara 1, 50019, Sesto Fiorentino (FI), Italy;*
[3]*Istituto Nazionale di Ricerca Metrologica (INRiM), Strada delle Cacce 91, Turin, 10135 Italy;*
[4]*University of Florence, Department of Physics and Astronomy, Via G. Sansone 1, 50019, Sesto Fiorentino (FI), Italy,*
[5]*Department of Physics and Astronomy, University of Texas at San Antonio, San Antonio, Texas 78249, USA*
e-mail: riboli@lens.unifi.it

The non-linear response of a disordered photonic system to a given stimulus allows to add functionalities to optical devices.

In this talk I will show how two different types of nonlinearities, namely the so called *structural nonlinearity* and the well know thermo optics and Kerr nonlinearities allows to realize highly secure nonlinear cryptographic primitives in the fist case, and optical limiters and isolators and the second case.

Structural nonlinearity is an optical phenomenon that occurs when the dielectric function of a scattering material is changed. The relationship between the dielectric configuration and the scattered field is not more linear even for a linear optical material. By using reconfigurable disordered photonic system made of Polymer Dispersed and Stabilized Liquid Crystals we have realized a nonlinear Physical Unclonable Functions. The entropy of the generated keys increase with respect to the linear case in which the dielectric function is static.

In a second example we exploit thermo optic and Kerr nonlinearity to realize an optical limiter based on the Parity-Time symmetry breaking of the reflectionless modes. By adding a slight structural disorder to the otherwise ordered photonic system, it is possible to turn the limiting behavior to optical isolation, thus obtaining asymmetric light transmission up to the case of unidirectional light propagation.

REFERENCES

[1] Nocentini, S., Rührmair, U., Barni, M. Wiersma, D.S., and Riboli, F., All-optical multilevel physical unclonable functions. Nature Materials 23, 369–376 (2024).
[2] Riboli, F. Kononchuk R, Tommasi F, Boschetti A, Suwunnarat S, Anisimov I, Vitebskiy I, Wiersma D S, Cavalieri S, Kottos T, Chabanov A. Optical LImiter based on PT-symmetry breaking of reflectionless modes, Optica 10, 1302–1309 (2023)

ORCID: F.R. 0000-0002-5553-9762, S.N. 0000-0003-2392-9077, A.C. 0000-0002-5886-4333, F.T. 0000-0002-3178-2514, D.S.W. 0000-0001-8150-7425

Progress Reports

Label-free characterization of red blood cells using advanced optical techniques

M. D. Radmilović[1], V. Lj. Ilić[2], A. Petakov[3], K. Lalić[3,4], M. D. Rabasović[1], A. J. Krmpot[1], I. T. Drvenica[2]
[1]*Institute of Physics Belgrade, University of Belgrade, Belgrade, Serbia*
Belgrade, Serbia
[2]*Institute of Medical Research, University of Belgrade, Belgrade, Serbia*
[3]*Clinic for Endocrinology, Diabetes and Metabolic Diseases, University Clinical Center of Serbia, Belgrade, Serbia*
[4]*Faculty of Medicine, University of Belgrade, Belgrade, Serbia*
e-mail: mihajlor@ipb.ac.rs

The interaction between femtosecond laser pulses and hemoglobin molecules, both in intact erythrocytes and in isolated form, was explored as a label-free strategy for erythrocytes imaging and characterization. It was observed that intrinsic fluorescent photoproducts are generated following the interaction of femtosecond laser pulses with hemoglobin [1]. Through systematic optimization of Two photon (TPEF) laser exposure parameters (excitation wavelength was set on 730nm, laser power was around 20mW), photostable and fluorescent molecular species were reproducibly formed and analyzed using TPEF and single-photon fluorescence microscopy, as well as UV-VIS absorption spectroscopy [2]. These photoproducts are formed during hemoglobin photodegradation, probably driven by porphyrin structure without necessity of Fe^{2+} ion presence [2]. Oxidative modifications, particularly through hydrogen peroxide or TBHP (tert-butyl hydroperoxide) treatment, significantly enhanced fluorescence emission intensity.

Spatially controlled formation of these photoproducts was achieved using TPEF microscopy on hemoglobin thin films, consequently enabling subcellular mapping of hemoglobin in intact erythrocytes [3]. The resulting fluorophore exhibited prolonged photostability and was successfully applied for selective *in situ* labeling of erythrocytes in whole blood as well [2], allowing visualization of hemoglobin distribution patterns without exogenous dyes.

Given the high stability of the fluorescent hemoglobin photoproduct formed by 730 nm femtosecond laser pulses, we were motivated to explore additional optics-based techniques to differentiate between healthy and altered erythrocyte subpopulations Flow cytometry revealed changes in fluorescence and light scattering (FSC/SSC) under induced oxidative stress, reflecting alterations in erythrocyte subpopulation morphology and internal composition [4]. It also confirmed corresponding impairments in erythrocytes deformability-an essential property for microcirculatory function, which was previously assessed by ektacytometry. These biophysical insights were further validated on erythrocytes from individuals with diabetes [5], confirming the diagnostic potential of the proposed label free approach.

This study demonstrates that integrating label-free nonlinear optical imaging with mechanical phenotyping enables precise, non-invasive assessment of hemoglobin dynamics and erythrocyte physiology, advancing diagnostics and research on hemoglobinopathies and erythrocyte-related diseases.

Acknowledgment: This research was supported by the Science Fund of the Republic of Serbia, Grant No. 4545, project "Advanced Biophysical Methods for Soil Targeted Fungi-Based Biocontrol Agents" BioPhysFUN.

REFERENCES

[1] E. A. Shirshin, B. P. Yakimov, S. A. Rodionov, N. P. Omelyanenko, A. V. Priezzhev, V. V. Fadeev, M. E. Darvin, Laser Phys. Lett. 15, 075604 (2018)
[2] M. D. Radmilović, I. T. Drvenica, M. D. Rabasović, V. Lj. Ilić, D. Pavlović, S. Oasa, V. Vukojević, M. Perić, S. N. Nikolić, A. J. Krmpot, Int. J. Biol. Macromol. 244, 125312 (2023)
[3] K. Bukara, S. Z. Jovanić, I. T. Drvenica, A. Stančić, V. Ilić, M. D. Rabasović, D. V. Pantelić, B. M. Jelenković, B. Bugarski, A. J. Krmpot, J. Biomed. Opt. 22, 026003 (2017)
[4] M. D. Radmilović, V. L. Ilić, D. D. Vučetić, D. I. Trivanović, M. D. Rabasović, A. J. Krmpot, I. T. Drvenica, Spectrochim. Acta A Mol. Biomol. Spectrosc. 327, 125420 (2025)
[5] M. D. Radmilović, V. Lj. Ilić, D. Trivanović, A. Petakov, K. Lalić, M. D. Rabasović, A. J. Krmpot, I. T. Drvenica, Opt. Quantum Electron. 56, 1225 (2024)

ORCID: M.D.R. 0000-0001-6578-2304, A.P. 0009-0000-8132-627X, V.I. 0000-0003-1119-1343, K.L. 0000-0002-8070-1899, M.R. 0000-0002-9235-4388, A.K. 0000-0003-2751-7395, I.D. 0000-0003-4985-1642

Multiphoton Live-Cell Metabolic Imaging and Femtosecond Laser Nanosurgery of Filamentous Fungi

T. Pajić[1], N. V. Todorović[2], K. Stevanović[1], M. D. Rabasović[3], M. Živić[1] and A. J. Krmpot[3]
[1]*Faculty of Biology, University of Belgrade, Serbia*
[2]*Institute for Biological Research "Siniša Stanković"- National Institute of the Republic of Serbia, University of Belgrade, Serbia*
[3]*Institute of Physics - National Institute of the Republic of Serbia, University of Belgrade, Serbia*
e-mail: tpajic@bio.bg.ac.rs

Filamentous fungi are of enormous ecological, medical and biotechnological importance. Studying their physiology and dynamics *in vivo* is crucial for understanding their interaction with the environment as well as for developing new therapeutic strategies for disease-causing pathogens. Nonlinear laser microscopy modalities, two-photon excitation fluorescence (TPEF) and third harmonic generation (THG) microscopy, were employed to image structural and functional changes in the cellular (lipid and energy) metabolism of model filamentous fungus *Phycomyces blakesleeanus*, at the single-cell level. Label-free THG method was used for the first time to image lipid droplets (LDs) in live filamentous fungi that predominantly have LDs smaller than 1 µm [1]. Under various environmental conditions, THG was able to detect changes in size, number and location of the LDs in tiny fungal cells. On the other hand, TPEF enabled the monitoring of morphological changes of mitochondria in real time under the same conditions as THG imaging.
To study fungal physiology, the first femtosecond IR laser nanosurgery was performed on the cell wall of filamentous fungi, enabling electrophysiological measurements on the protoplasts released from the hyphae [2]. The high precision of fs laser ablation allowed us to cut a small portion of the cell wall without damaging the cell membrane only a few micrometers away. A reproducible and highly precise (diffraction-limited, submicron resolution) method for obtaining viable protoplasts was developed. Protoplast release from the nanosurgery-generated incisions in the cell wall was achieved from different regions of the hyphae. The introduction of this method opened the way to investigate the physiology of ion channels directly on the cell membrane of filamentous fungi, which is otherwise inaccessible due to the presence of a rigid chitinous cell wall.

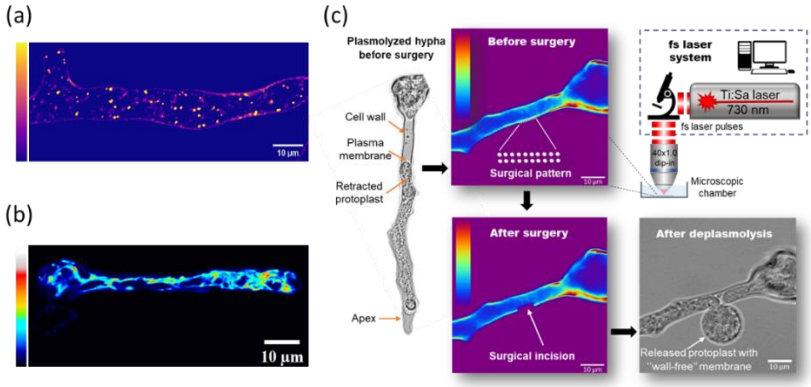

Figure 1. (a) Label-free THG image of lipid droplets in live *P. blakesleeanus* hypha (b) TPEF image of tubular mitochondria stained with 5 µM Rhodamine123 in live *P. blakesleeanus* hypha (c) *In vivo* femtosecond laser nanosurgery of chitinous cell wall of filamentous fungus *P. blakesleeanus*.

Acknowledgment: This research was supported by the Science Fund of the Republic of Serbia, Grant No. 4545, project "Advanced Biophysical Methods for Soil Targeted Fungi-Based Biocontrol Agents" BioPhysFUN.

REFERENCES

[1] T. Pajić, N.V. Todorović, M. Živić *et al*., Sci Rep 12, 18760 (2022).
[2] T. Pajić, K. Stevanović, N.V. Todorović *et al*., Microsyst Nanoeng 10, 47 (2024).

ORCID: T.P. 0000-0003-3794-7655, N.V.T. 0000-0003-2626-0794, K.S. 0000-0001-9733-2367, M.D.R. 0000-0002-9235-4388, M.Ž. 0000-0002-0314-5032, A.J.K. 0000-0003-2751-7395

Comparative Study of Ion Channels in Filamentous Fungi Following the Novel Development of Laser Nanosurgery for Cell Wall Removal

K. Stevanović[1], T. Pajić[1] A. Milovanović[1], N. V. Todorović[2], M. Živić[1], M. Milošević[1], A. J. Krmpot[3], M. D. Rabasović[3]
[1]*University of Belgrade, Faculty of Biology*
Belgrade, Serbia
[2]*Institute for biological research "Siniša Stanković", University of Belgrade, Serbia*
[3]*Institute of Physics, Belgrade, Serbia*
e-mail: katarina.stevanovic@bio.bg.ac.rs

The patch-clamp technique has been a standard method for the functional characterization of ion channels in living cells for several decades. However, despite the fungal kingdom's vast diversity and significance, the study of ion channels in filamentous fungi remains very limited due to the difficulty of electrically isolating membrane patches by creating a GΩ seal with a glass pipette. Cytoplasmic droplets (CDs) are a model system used in our research group that has so far yielded the most data on novel channels in the native membrane, but this approach is limited to the use of giant sporangiophores of *P. blakesleeanus*. CDs have been shown to be metabolically active, enclosed by a plasma membrane, and to contain many nuclei, making them suitable for studying membrane channels in their native physiological state [1].

The development of laser nanosurgery for precise cell wall removal enabled the first ion current recordings from *P. blakesleeanus* mycelium [2]. Results show differences in dominant activities compared to sporangiophore membrane, as well as the spatial distribution of distinct single ion channel activities along the hyphae. The osmotically sensitive, outwardly rectifying inactivating current (ORIC)—the dominant current of the CD membrane and the most thoroughly studied to date [3]—is absent in recordings from both the whole protoplast membrane and excised membrane regions, suggesting that its expression may be sporangiophore-specific. A dominant current in the protoplast membrane seen in all whole-protoplast recordings is an inward inactivating anionic current that resembles a rarely observed activity in CDs, that remains to be fully characterized. Various single channel activities were recorded under the same recording conditions on both CDs and mycelium protoplast in parallel. Besides ORIC, a 70 pS potassium current- one of the first single-channel currents described in the CD membrane [4]- has also not been observed in the mycelium membrane, while several activities suggest a novel type of ion channels specific for the mycelium.

The greatest advantage of using laser nanosurgery to obtain mycelial protoplasts is that the method can be further optimized for a wide range of filamentous fungi species. One ongoing project is focused on adjusting the protocol for phytopathogenic fungal species, to be followed by measurements of the currents induced by the insertion of peptides from biocontrol species of the genus Trichoderma. We have recently studied their effects on the growth inhibition of autochthonous phytopathogens [5], and it was further observed that peptaibol-containing extracts of *T. harzianum* exert an acute lethal effect on microscopic specimens of *R. solani* when applied extracellularly.

Overall, this strategy represents a significant step toward accelerating the discovery of novel ion channels and enabling the systematic exploration of their diversity and physiological roles in filamentous fungi.

Acknowledgment: This research was supported by the Science Fund of the Republic of Serbia, Grant No. 4545, project "Advanced Biophysical Methods for Soil Targeted Fungi-Based Biocontrol Agents" BioPhysFUN.

REFERENCES

[1] K.S. Stevanović, B Čepkenović, S. Križak, *et al* Živić Sci Rep. 13(1):11897 (2023)
[2] T. Pajić., K.S. Stevanović, N.V. Todorović *et al.* Microsyst Nanoeng 10, 47
[3] K. Stevanović, B. Čepkenović, S. Križak, *et al* J Fungi 9(6):637
[4] M. Zivić, M. Popović, B. Zivanović, Z.. Ann N Y Acad Sci. 1048:491-5.
[5] K. Atlagić, T. Cvetić Antić, Lukičić, *et al* J. Fungi, 11(7), 535.

ORCID: K.S 0000-0001-9733-2367, T.P 0000-0003-3794-7655, N.V.T. 0000-0003-2626-0794, M.Z. 0000-0002-0314-5032, M.M. 0000-0002-6138-6766, A.K. 0000-0003-2751-7395, M.R. 0000-0002-9235-4388

Analog Quantum Simulation and Digital Quantum Computation with Ultracold Atoms in Optical Lattices

P. Bojović[1], T. Hilker[1, 2], S. Wang[1], J. Obermeyer[1], M. Barendregt[1], D. Tell[1], T. Chalopin[1, 3], P.M. Preiss[1], I. Bloch[1, 4], T. Franz[1]
[1]*Max Planck Institute of Quantum Optics, Garching, Germany*
[2]*Department of Physics and SUPA, University of Strathclyde, Glasgow, United Kingdom*
[3]*Laboratoire Charles Fabry, Institut d'Optique Graduate School, CNRS, Université Paris-Saclay, 91127 Palaiseau, France*
[4]*Fakultät für Physik, Ludwig-Maximilians-Universität, Munich, Germany*
e-mail: petar.bojovic@mpq.mpg.de

In our quantum gas microscope experiment, we load fermionic ^{6}Li atoms into optical superlattices, and image the local density and spin by performing site-resolved projective measurements [1]. I will present how the exceptional control of optical superlattices and local measurements enables us to perform analog quantum simulation [2] and realize building blocks for digital quantum computation [3, 4].

We conduct systematic experimental quantum simulations of the Fermi-Hubbard model, a key model frequently used to study the physics of high-temperature superconductivity. Using multi-point spin and charge correlators, we perform thermometry, study magnetic polarons and their interactions, and directly observe traces of moving dopants, which are signatures of the strongly correlated states. Furthermore, we identify a universal scaling behavior in magnetic and spin-charge correlations, governed by a doping-dependent energy scale consistent with the pseudogap temperature T^*. Comparison with state-of-the-art numerical simulations confirms the quantitative accuracy of our analog quantum simulation [2].

In the digital approach, we implement high-fidelity collisional entangling gates with fermionic atoms in an optical superlattice, achieving Bell state lifetimes beyond 10 s and gate fidelities up to 99.75(6)%. We realize robust pair-exchange gates, enabling local characterization of spin-exchange and pair-tunneling dynamics [4]. These results demonstrate key building blocks for scalable, symmetry-preserving analog-digital hybrid quantum simulators [5, 6, 7].

REFERENCES

[1] M. Boll, T. Hilker, F. Salomon, et al. Science 353, 1257-1260 (2016)
[2] T. Chalopin, P. Bojović, S. Wang, et al. arXiv:2412.17801. (2024)
[3] T. Chalopin, P. Bojović, D. Bourgund, et al. Physical Review Letters 134, 053402 (2025).
[4] P. Bojović, T. Hilker, S. Wang, et al. arXiv:2506.14711. (2025)
[5] F. Gkritsis, D. Dux, J. Zhang, et al. Physical Review X Quantum 6, 010318 (2025)
[6] H. Schlömer, H. Lange, T. Franz, et al. Physical Review X Quantum 5, 040341 (2024)
[7] D.K. Mark., H.H. Hu, J. Kwan, et al. arXiv:2412.13186. (2024)

ORCID: P.B. 0009-0005-9647-4837

Propagation and Stability of Compact Localized Modes in 2D Photonic Flat-band Lattices

M. G. Stojanović
Vinča Institute of Nuclear Sciences, National Institute of the Republic of Serbia, University of Belgrade
Mike Petrovića Alasa 12-14, 11351, Belgrade, Serbia
e-mail: mirjana.stojanovic@vinca.rs

Photonic lattices with flat bands, characterized by the absence of dispersion and slow group velocity, support compact localized modes (CLMs) known as compactons. Light propagation can be controlled by tuning parameters such as waveguide spacing and wave profile. When the light intensity is sufficient, modulation instabilities can emerge, inducing a nonlinear response that alters propagation. Special attention is given to the Aharonov–Bohm effect and the influence of phase shifts and inhomogeneities on light dynamics and mode formation.

The propagation of light through photonic lattices can be modeled by a system of coupled difference-differential equations under the strong coupling approximation, with each waveguide interacting with its nearest neighbors. Assuming ideal conditions (no losses and infinite waveguides), and incorporating Kerr-type nonlinearity while neglecting diffraction and diffusion, this system reduces to a set of discrete nonlinear Schrödinger equations. Unit cells in photonic lattices are defined analogously to those in solid-state systems, enabling simplification of the governing equations.

We examined the existence and stability of both linear and nonlinear localized modes in 2D photonic lattices using three models: octagonal-diamond [1,2], dice [3], and plus-type [4,5]. The sixth-order Runge-Kutta method was applied to solve the governing equations. Analytical solutions were used to obtain eigenvalues of the Hamiltonian and the structure of CLMs. Linear stability analysis (LSA) provided equations for small perturbations, which were numerically solved to evaluate the stability of specific modes. By using analytical and numerical tools we confirmed the existence and behavior of both linear and nonlinear CLMs. While LSA offered useful insight into the stability spectrum of stationary solutions, it proved insufficient for capturing all features of compact modes, particularly in the presence of inhomogeneities. In such cases, direct numerical simulations were essential for verifying stability. These simulations revealed that the presence or absence of an external magnetic flux significantly affects the behavior and robustness of the observed modes.

REFERENCES

[1] M. G. Stojanović, M. Stojanović Krasić, A. Maluckov, M. Johansson, I. A. Salinas, R. A. Vicencio, M. Stepić, Phys. Rev. A 102, 023532 (2020).
[2] M. G. Stojanović, S. Gündoğdu, D. Leykam, D. G. Angelakis, M. S. Krasić, M. Stepić, A. Maluckov, Phys. Scri. 97 030006 (2022).
[3] M. G. Stojanović, A. Mančić, M. Stepić, A. Maluckov, Facta Universitatis, Series: Physics, Chemistry and Technology 20, 55-65 (2022).
[4] M. Stojanović Krasić, M. Stojanović, A. Maluckov, L. J. Maczewsky, A. Szameit, M. Stepić, Phys. Rev. E 102, 032207 (2020).
[5] A. Mančić, M. G. Stojanović, M. Stepić, Advanced Technologies (2022).

ORCID: 0000-0002-4376-7610

Real-time imaging using *Morpho didius* wing scales as biophotonic microcantilever pixels

P. Atanasijević[1], M. Mićić[1], D. Pavlović[2], B. Salatić[2], D. Pantelić[3] and P. Mihailović[1]
[1]*University of Belgrade, School of Electrical Engineering, Belgrade, Serbia*
[2]*University of Belgrade, Institute of Physics Belgrade, Belgrade, Serbia*
[3]*University of Belgrade, Senzor INFIZ, Belgrade, Serbia*
e-mail: petarat@etf.bg.ac.rs

For decades, wide spectral range imaging has continued to allure researchers to develop novel high-performing, yet affordable focal plane array (FPA) technologies. In a vast field of published approaches, microcantilever FPAs stand out as a strong commercial contender due to their high sensitivity and ease of manufacture. Furthermore, they offer a high-speed optical spatial filtering readout (OSFR) using a simple 4f system, overcoming the drawbacks of complex, heat-generating electronic readout integrated circuits [1]. Building upon the presented ideas, highly sensitive bioinspired alternatives utilizing wing scales of *Morpho* butterflies as biophotonic microcantilevers were proposed, although somewhat burdened by their less practical [2] or computationally heavy interrogation approaches [3].

In our research, we combine the speed and simplicity of the OSFR principle proposed in [1] with the highly sensitive *M. didius* wing scales as biophotonic microcantilevers [3]. We demonstrate a real-time acquisition system capable of capturing wide spectral range images, limited in bandwidth by the thermal transients of the microcantilevers. The system, shown in Fig. 1 (a), consists of a conventional 4f setup projecting the biophotonic sensor plane, illuminated by a 532 nm laser, to the plane of a lensless CMOS imager (Basler acA2440-75um camera). The adjustable slit in the spectrum plane of the 4f system is used to convert the light-induced scale displacements to an intensity change of the acquired sample image [1]. The slit is followed by a 532 nm, narrow bandpass filter (BPF), ensuring only the wavelengths originating from the interrogating light will pass from the sample to the camera. To test the operation of the proposed system, the sample was illuminated using a 4.4 mW, 638 nm laser, resulting in the imager's response presented in Fig. 1 (b).

Due to its high sensitivity of up to ~500 nm/K [3] and the 4f system's acquisition frame rate of over 50 Hz, we conclude that the proposed OSFR interrogated bioinspired imager presents a compelling choice, leading the next generation of uncooled wide spectral range FPAs.

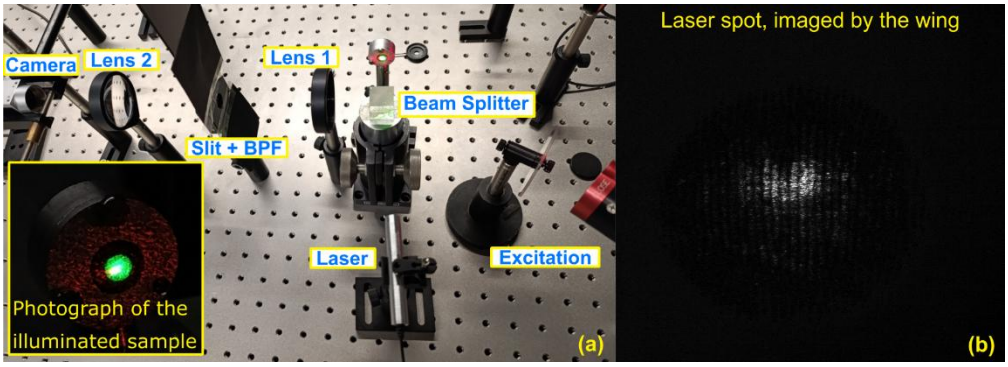

Figure 1. (a) The proposed 4f system, interrogating the *M. didius* wing. (b) The response of the imager to the 4.4 mW, 638 nm laser excitation.

Acknowledgment: The research was supported by the Serbian Ministry of Science, Technology, and Innovation (451-03-65/2024-03/200103). The research was partially conducted in the premises of the Palace of Science, Miodrag Kostić Endowment.

REFERENCES

[1] Y. Jin et al., Meas. Sci. Technol. 32 065202 (2021).
[2] A. Pris et al., Nature Photon 6, 195–200 (2012).
[3] P. Atanasijević et al., Opt. Laser Technol., 159, 108919 (2023).

ORCID: P.A. 0000-0001-7596-0266, M.M. 0009-0005-1769-4883, D.P. 0000-0003-4474-1209, B.S. 0009-0003-2165-9103, D.P. 0000-0002-2027-4696, P.M. 0000-0002-9720-1102

Illuminating the Brain: Pipedream or Impending Reality for Minimally Invasive Neurostimulation?

D. Galiakhmetova[1], A. Koviarov[1], V. Dremin[1], A. Gorodetsky[2], D. Stoliarov[1], D. Shcherbakova[3], M. Baloban[3], V. V. Verkhusha[3], S. Sokolovski[1], E. U. Rafailov[1]

[1]*Aston Institute of Photonic Technologies, Aston University, Birmingham, United Kingdom*
[2]*School of Physics and Astronomy, University of Birmingham, Birmingham, United Kingdom*
[3]*Department of Genetics and Gruss-Lipper Biophotonics Center, Albert Einstein College of Medicine, NY, USA*
e-mail: d.galiakhmetova@aston.ac.uk

Optogenetics has revolutionised the field of neuromodulation by enabling the monitoring and control of neural cell activity through the expression of light-sensitive proteins. However, the high absorption of visible light by the skin and skull presents a major obstacle for non-invasive modulation of neurons. We demonstrate a significant advancement in overcoming this challenge by employing near-infrared (NIR) light sources and exploiting the nonlinear photoconversion properties of phytochrome.

Firstly, the study delves into how visible and NIR light interacts with *ex vivo* mouse head tissues, highlighting the advantages of the NIR biological windows for deeper tissue penetration and reduced light absorption and scattering (Fig.1a). Our computer simulations and experimental results demonstrated that over 12% of initial light irradiation passes through skin and skull, reaching the brain cortex, potentially enabling minimally invasive neural activation [1]. Furthermore, our pioneering work in the two-photon (2P) photoconversion of novel genetically engineered monomeric variants of phytochrome demonstrates the 2P photoswitching efficiency of up to 71% in the NIR-II range (Fig.1b) and 2P NIR fluorescence using NIR-I laser radiation (Fig.1c,d). The excitation, fluorescence emission, and photoconversion NIR wavelengths indicate the potential use of new monomeric *Deinococcus radiodurans* bacterial phytochrome as a sensitive biological tool for high-resolution imaging, detection and treatment of neurological diseases [2].

Additionally, we introduce a versatile ultrashort pulsed fibre laser designed to operate within the NIR-I and NIR-II wavelength ranges. The laser is characterized by its remarkably low repetition rate of 600 kHz, resulting in high-peak-power pulses of 82 kW with an average power of 250 mW [3,4]. Since the laser has a compact size and high pulse stability, the source can be used for *in vivo* optogenetic research. These discoveries unveil possibilities for advanced biomedical applications in neurostimulation, promising enhanced tissue penetration and a non/minimal invasive approach.

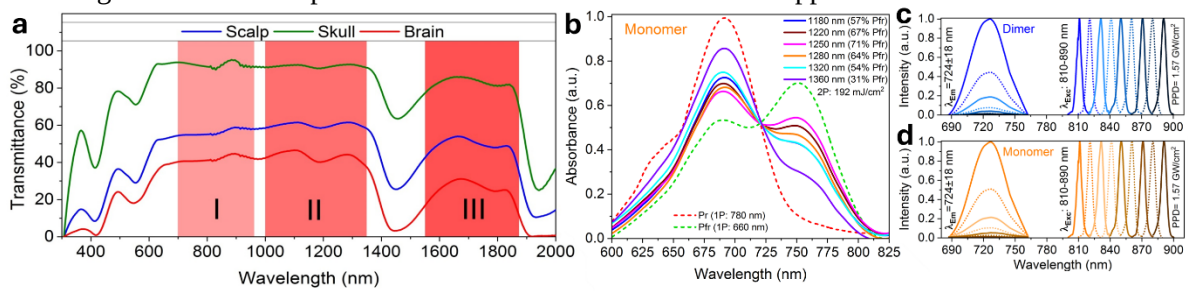

Figure 1. (a) Transmission spectra of mouse head samples; (b)1P and 2P Pr→Pfr conversion of monomeric bacterial phytochrome; 2P NIR fluorescence of (c) dimeric and (d) monomeric phytochromes.

Acknowledgements: The work was supported by COST CA22153 (EuroCurvoBioNet) and H2020 NEUROPA (863214).

REFERENCES

[1] D. Galiakhmetova et al., IEEE J. Sel. Top. Quantum Electron. 29.4: Biophotonics: 1-11 (2022).
[2] D. Galiakhmetova et al., Protein Science 34(5), e70118 (2025).
[3] D. Stoliarov et al., Scientific Reports 15.1, 1-8 (2025).
[4] D. Stoliarov et al., Optical Fiber Technology 72, 102994 (2022).

ORCID: D.G. 0000-0002-6222-2122, A.K. 0000-0002-2668-2367, V.D. 0000-0001-6974-3505, A.G. 0000-0001-5440-2185, D.S. 0000-0001-8635-2346, D.S. 0000-0003-3384-6363, M.B. 0000-0003-3919-1222, S.S. 0000-0001-7445-7204, E.R. 0000-0002-4152-0120

Electron-plasmon Scattering in Doped Graphene

J. Jakovac
Institut za fiziku, Zagreb, Croatia'
e-mail: jjakovac@ifs.

Decay mechanisms and plasmon satellites formed in the spectrum of a photo-excited hole in doped graphene is a phenomenon that has been investigated for a long time using Angle Resolved Photo-Emission Spectroscopy (ARPES) measurements [1–3]. The results I will present are produced by the ab-initio simulation of photo-emission spectra in electrostatically and chemically (KC_8) doped graphene, in the framework of our recently developed many-body RPA- G_0W_0 approximation. The decay width along the graphene π^+/π^- bands at the Fermi level features the exponential law $\Gamma \sim |E_{\sigma,\pi K} - E_{Fermi}|^{\alpha}$ (**Fig. 1a**), which perfectly fits the previous experimental results [1, 4], deviating from the standard Fermi liquid behavior $\alpha = 2$. At lower energies, the width of the π^+/π^- bands exhibits a peak due to the Dirac plasmon emission decay, also experimentally measured [1]. On the other hand, the plasmonic satellites appearing in the spectrum (**Fig. 1b**) feature much lower intensities than experimentally obtained [2, 3], except in the $E_{Dirac} < \omega < E_{Fermi}$ frequency range. Also, due to the Fermi liquid theory, we obtained a kink at the Fermi level in highly doped graphene (**Fig. 1b**).

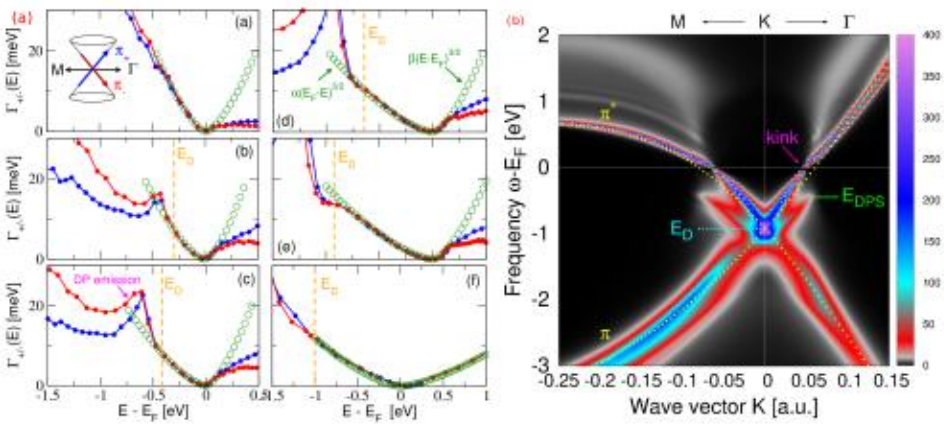

Figure 1. **a)** The imaginary part of self-energy along π^+/π^- bands in electrostatically doped [witt concentrations increasing (a)→(e)] and chemically (f) doped KC_8 graphene. **b)** The simulation of spectral intensity along the high symmetry path (M←K→ Γ) in electrostatically highly doped graphene (10^{14} cm^{-2}).

REFERENCES
[1] A. Bostwick, T. Ohta, T. Seyller, K. Horn and E. Rotenberg, Nature Phys. 3, 36 (2007).
[2] H. Zhang, S. Wang, E. Wang, et al, npj Quantum Mater. 6, 83 (2021).
[3] A. Bostwick, F. Speck, T. Seyller et al, Science 328, 999 (2010).
[4] J. Jakovac and V. Despoja, Phys. Rev. B 110, 195425 (2024).

ORCID: J.J. 0000-0003-0771-2150

AFM analysis of astrocyte membrane remodeling induced by immunoglobulin G from patients with amyotrophic lateral sclerosis

A. Jakovljević[1], D. Bijelić[1], F. Quiros-Corella[2], R. Pereira Reyes[3], J. R. Vega Baudrit[3], L. Radenović[1], P. Andjus[1], Y. R. Corrales Urena[3]

[1]*Center for laser microscopy, Institute for Physiology and Biochemistry "Jean Giaja", Faculty of Biology University of Belgrade, Belgrade, Serbia*

[2]*Advanced Computing Laboratory, National High Technology Center CeNAT CONARE, San Jose, Costa Rica*

[3]*National Laboratory of Nanotechnology, National High Technology Center CeNAT-CONARE, San Jose, Costa Rica*

e-mail: ana.jakovljevic@bio.bg.ac.rs

This study investigated whether immunoglobulin G (IgG) from Amyotrophic Lateral Sclerosis (ALS) patients induces subcellular and biophysical changes in cultured primary astrocytes. We applied Atomic Force Microscopy (AFM) and Scanning Electron Microscopy (SEM) to evaluate membrane morphology and stiffness in astrocytes treated with ALS or control IgGs, compared to untreated (Naïve) cells. AFM analysis revealed a significant increase in surface roughness and a decrease in Young's modulus following ALS IgG treatment, suggesting membrane remodeling and reduced cell stiffness. High-resolution AFM imaging also revealed structural features suggestive of membrane clustering, perforation, and potential phase separation, specifically in ALS IgG-treated cells. These changes may reflect protein aggregation or lipid domain reorganization, which are consistent with the decreased lacunarity observed in SEM-based fractal analysis. While both ALS and control IgGs increased microvilli area and surface complexity, only ALS IgGs led to significant disorganization of surface texture, as confirmed by texture and fractal analyses. Taken together, these findings demonstrate that ALS IgGs induce distinct and more pronounced alterations in astrocyte membrane biomechanics and organization compared to control IgGs, suggesting a role in early astrocytic dysfunction in ALS.

ORCID: A.J. 0000-0002-3035-1587, D.B. 0000-0002-7479-0186, L.R. 0000-0002-6632-0483, P.A. 0000-0002-8468-8513

Contributed papers

1. Quantum optics and ultracold systems
2. Nonlinear optics
3. Optical materials
4. Biophotonics
5. Devices and components
6. Optical communications
7. Laser spectroscopy and metrology
8. Ultrafast optical phenomena
9. Laser - material interaction
10. Optical metamaterials and plasmonics
11. Machine learning in photonics
12. Other topics in photonics

1. Quantum optics and ultracold systems

Exploring the Phase Diagram of Quantum Many-Body Scars with Programmable Rydberg Atom Arrays

A. Hudomal
Institute of Physics, Belgrade, Serbia
e-mail: ana.hudomal@ipb.ac.rs

Quantum many-body scarring is a form of weak ergodicity breaking, where specific initial states exhibit non-thermalizing dynamics despite the system's overall chaotic behavior [1]. We use programmable Rydberg atom arrays to explore the interplay between scarring and quantum criticality. Contrary to expectations [2], our previous numerical study revealed the persistence of quantum many-body scarring across the Ising critical point in the effective PXP model [3]. A detailed dynamical phase diagram of the one-dimensional PXP model with a varying chemical potential was mapped out using extensive numerical simulations. Notably, a continuous family of scarred states was identified, spanning both sides of the phase transition. We now experimentally verify this phase diagram using QuEra's Aquila device [4]. We also investigate the role of the Kibble-Zurek mechanism and defect formation during the preparation of the initial state, as well as the effects of defect density and type on the scarred dynamics. Finally, we discuss how our work can be extended to two spatial dimensions and various lattice geometries, where potentially richer phase diagrams and previously unseen families of scarred states may be discovered.

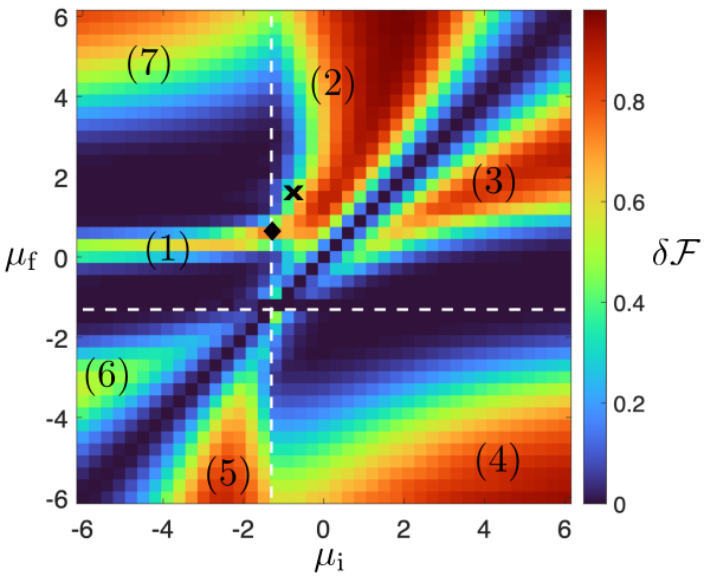

Figure 1. Dynamical phase diagram of the PXP model with chemical potential [3].

REFERENCES
[1] M. Serbyn, D. A. Abanin, and Z. Papić, Nat. Phys. 17, 675 (2021).
[2] Z. Yao, L. Pan, S. Liu, and H. Zhai, Phys. Rev. B 105, 125123 (2022).
[3] A. Daniel et al., Phys. Rev. B 107, 235108 (2023).
[4] J. Wurtz, et al., arXiv:2306.11727 (2023).

ORCID: A.H. 0000-0002-2782-2675

Acoustic Control of Quantum Emission: Toward Time-Bin Encoded Single-Photon Sources

S. Djurdjic Mijin[1, 2], S. Lazić[1, 3]
[1]*Departamento de Física de Materiales, Universidad Autónoma de Madrid, 28049 Madrid, Spain*
[2]*Institute of Physics Belgrade, University of Belgrade, Pregrevica 118, Belgrade, Serbia*
[3]*Instituto 'Nicolás Cabrera' and Instituto de Física de Materia Condensada (IFIMAC), Universidad Autónoma de Madrid, 28049 Madrid, Spain*
e-mail: sanja.djurdjic@uam.es

Photons are excellent carriers of quantum information, with multiple internal degrees of freedom available for qubit encoding. Although polarization encoding is widely used, it is highly sensitive to polarization mode dispersion in optical fibers, which limits its scalability over long distances. To address this, we present a pathway toward robust time-bin qubit implementation by acoustically modulating the emission properties of single-photon sources using surface acoustic waves (SAWs). SAWs are launched on piezoelectric $LiNbO_3$ substrates patterned with delay lines, onto which GaN/InGaN core-shell nanowires containing quantum-dot-like emitters have been mechanically placed. These emitters, formed by indium fluctuation-induced localization in the InGaN shell, demonstrate pronounced linear polarization and clear photon antibunching, confirming their quantum nature via polarization-resolved micro-photoluminescence and photon correlation measurements. Upon excitation with SAWs at ~330 MHz, the excitonic transitions undergo dynamic spectral modulation through acousto-mechanical coupling, with tuning amplitudes of approximately 2 meV. Stroboscopic time-resolved experiments reveal emission oscillations synchronized with the SAW phase, attributed to the simultaneous injection of photo-excited electrons and holes - unlike previously reported systems dominated by sequential carrier capture. By spectrally selecting SAW-shifted emission states, we achieve precise control over photon emission timing, effectively enabling time-bin qubit encoding. This approach circumvents polarization-related decoherence in optical fibers and supports secure quantum communication protocols such as quantum key distribution. Furthermore, the detection of biexcitonic emission opens the door to chip-integrated generation of entangled photon pairs at elevated operational temperatures. Our results demonstrate the potential of III-nitride-based, acoustically tunable quantum light sources as scalable components for future quantum information systems.

ORCID: S.Dj.M. 0000-0002-4597-8219

Characterization of the Tunable Mid Infrared Photon Pair Source realized in the nonlinear $AgGaS_2$ medium

F. Krajinić[1, 2], I. Firez[1], M. Lazic[1], S. Beric[3], M. M. Ćurčić[2], M. Lekić[2], B. Jelenković[2]
[1]*University of Belgrade, School of Electrical Engineering, Belgrade, Serbia*
[2]*University of Belgrade, Institute of Physics Belgrade, Belgrade, Serbia*
[3]*Universiry of Belgrade, Faculty of Physics, Belgrade, Serbia*
e-mail: filip@ipb.ac.rs

Quantum states of light provide a solid foundation for the realization of real-life systems based on quantum technologies. Quantum imaging exploits the properties of entangled photon pairs. The most efficient method to generate entangled two-photon states is spontaneous parametric down-conversion (SPDC). This process in the nonlinear crystal allows the conversion from a single pump photon into a correlated photon pair, referred to as the signal-idler photon pair. Newly generated photon pair holds spatial, spectral and polarization correlation and it can be highly non-degenerate in wavelength. Imaging technique, such as quantum imaging with undetected photons (QIUP), uses idler photons to probe the sample and read the gathered information by detecting only signal photons. By virtue of QIUP, one can image samples in a mid infrared spectrum without the need for detection in that region. Mid infrared spectrum holds absorption lines for many chemical molecules, which is why this spectral region is referred to as the fingerprint region.

A promising candidate to generate photons within the fingerprint region is SPDC in silver-gallium-sulfide (AGS) with its transparency from 500 nm to 12.5 μm [1]. Experimental realization of the AGS crystal as an infrared source from 1.8 μm to 6.3 μm was achieved by utilizing a tunable pump in the near infrared spectrum [2]. AGS crystal was also utilized in quantum spectroscopy in the mid infrared region from 7.4 μm to 8.4 μm [3], and quantum Fourier transform spectroscopy [4].

In our work, we built a setup for SPDC within the AGS crystal in the type-I configuration using a pump at the 660 nm wavelength. By angle tuning the phase matching condition of the bulk AGS crystal, we are able to generate idler photons in the fingerprint region from 5.6 μm up to 10.9 μm. Corresponding signal wavelength from 747 nm to 703 nm was measured with a scientific complementary metal-oxide-semiconductor camera and with a fiber-coupled spectrometer. Signal photon count as a function of pump optical power confirmed the low gain regime of the SPDC. The maximum brightness of the AGS photon pair source was calculated to be $3*10^4$ kHz/mW. In pursuit of building a future quantum imaging system in the mid infrared region, we also characterized the signal beam properties for different pump beam radii to achieve quantum microscopy resolution limited by the diffraction limit of the idler photons.

Acknowledgement: This work was supported by the Horizon WIDERA 2021-ACCESS-03-01 grant, #101079355 "BioQantSense".

REFERENCES

[1] G. Boyd, H. Kasper, and J. McFee, "Linear and nonlinear optical properties of AgGaS2, CuGaS2, and CuInS2, and theory of the wedge technique for the measurement of nonlinear coefficients," *IEEE J. Quantum Electron.*, vol. 7, no. 12, pp. 563–573, 1971, doi: 10.1109/JQE.1971.1076588.
[2] M. Kumar, P. Kumar, A. Vega, M. A. Weissflog, T. Pertsch, and F. Setzpfandt, "Mid-infrared photon pair generation in AgGaS2," *Appl. Phys. Lett.*, vol. 119, no. 24, p. 244001, 2021, doi: 10.1063/5.0074054.
[3] A. V Paterova, Z. S. D. Toa, H. Yang, and L. A. Krivitsky, "Broadband Quantum Spectroscopy at the Fingerprint Mid-Infrared Region," *ACS Photonics*, vol. 9, no. 6, pp. 2151–2159, Jun. 2022, doi: 10.1021/acsphotonics.2c00464.
[4] Y. Mukai, R. Okamoto, and S. Takeuchi, "Quantum Fourier-transform infrared spectroscopy in the fingerprint region," *Opt. Express*, vol. 30, no. 13, pp. 22624–22636, Jun. 2022, doi: 10.1364/OE.455718.

ORCID: F.K. 0009-0008-0284-9426, I.F. 0009-0003-4669-6349,
M.C. 0000-0001-6920-3461, M.L. 0000-0003-4814-2051, B.J. 0000-0001-8276-1169

Weighted Hartree-Fock-Bogoliubov method for interacting fermions

N. Kaschewski[1], A. Pelster[1] and C. Sa de Melo[2]
[1]*Physics Department and Research Center OPTIMAS, RPTU Kaiserslautern-Landau, Germany*
[2]*School of Physics, Georgia Institute of Technology, Atlanta, USA*
e-mail: axel.pelster@rptu.de

For several decades it has been known that divergences arise in the ground-state energy and chemical potential of unitary superfluids, where the scattering length diverges, due to particle-hole scattering. Leading textbooks [1] and research articles [2,3] recognize that there are serious issues but ignore them due to the lack of an approach that can regularize these divergences. We find a solution to this difficulty by proposing a general method, called the weighted Hartree-Fock-Bogoliubov theory, to handle multiple decomposition channels originating from the same interaction [4]. We distribute the interaction in weighted channels determined by minimization of the action, and we apply this idea to unpolarized Fermi superfluids. Using our method, we solve a long-standing difficulty in the partitioning of the interaction into Hartree, Fock, and Bogoliubov channels for Fermi superfluids, and we obtain a phase diagram at the saddle-point level, which contains multichannel nonperturbative corrections. We find a previously overlooked superfluid phase for weak interactions, which is dominated by particle-hole processes, in addition to the usual superfluid phase only containing particle-particle physics.

We emphasize that our method is so general, that it can be applied to any fermionic system that can support competing interaction channels. This includes systems from particle and nuclear physics, condensed matter physics, ultracold atoms, and even in astrophysical objects like the crusts of neutron stars.

REFERENCES

[1] L. Pitaevskii and S. Stringari, *Bose-Einstein Condensation and Superfluidity* (Oxford University Press, Oxford, 2016).
[2] M. Leskinen, J. Kajala, and J.J. Kinnunen, New J. Phys. **12**, 083041 (2010).
[3] A. Korolyuk, J.J. Kinnunen, and P. Törmä, Phys. Rev. A **89**, 013602 (2014).
[4] N. Kaschewski, A. Pelster, and C.A.R. Sá de Melo, Phys. Rev. Res. (in press).

ORCID: A.P. 0000-0002-5215-0348

Effect of dielectric environment on electronic and optical properties of spherical core/shell quantum dot: comparison of two models

Lj. Stevanović, V. Pavlović, M. Miladinović, M. Živković, S. Milenović, O. Stefanović and M. Perić
Department of Physics, Faculty of Sciences and Mathematics, University of Niš, Serbia
e-mail: vladan.pavlovic@pmf.edu.rs

Core/shell quantum dot (CSQD) is a quantum dot consisting of a core and a shell made of different semiconductor materials. The reason for studying CSQDs is their application in optoelectronics, bioimaging, quantum computing [1].

The subject of this study is the influence of dielectric environment on the energies and wave functions of electron in conduction band of CdSe/ZnS spherical CSQD and oscillator strength of 1s→1p intraband transition. We use two common approaches to take into account the effect of dielectric matrix, which consist in adding term Σ [2] or W [3] to the electron Hamiltonian. We perform calculations using effective mass approximation by imposing the corresponding boundary conditions on the values of wave function and its first derivative for the cases when CSQD is embedded in SiO_2 and HfO_2 dielectric matrix. The effect of CdSe/ZnS spherical CSQD radius on results is discussed.

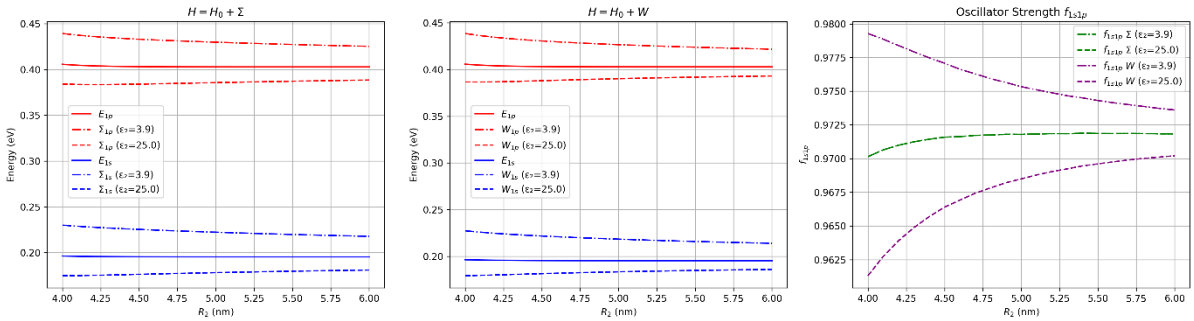

Figure. Energies of 1s and 1p states and oscillator strength of 1s→1p intraband transition in CdSe/ZnS spherical CSQD as functions of quantum dot radius.

We found that wave functions are the same in both models as for the plane CdSe/ZnS spherical CSQD. The model with term Σ in the Hamiltonian gives energy levels that are shifted up or down depending on dielectric constant of dielectric matrix and predicts the same value for the oscillator strength as for the plane quantum dot. On the other hand, inclusion of term W into Hamiltonian gives different energies and oscillator strength in comparison with the plane CdSe/ZnS spherical CSQD. Moreover, both models give very similar energy values.

REFERENCES

[1] A. Sahu, D. Kumar, J. Alloys Compd. 924, 166508 (2022).
[2] K. Hasanirokh, A. Naifar, Plasmonics 19, 2317 (2023).
[3] N. Yahayaoui, N. Zeiri, P. Baser, M. Said, S. Saadaoui, Plasmonics 18, 1489 (2023).

ORCID: Lj.S. 0000-0002-3662-3387, V.P. 0000-0002-2092-5620, M.P. 0009-0003-4137-7672

Collective dynamics of dipolar quantum droplets

D. Mujo[1], A. Balaž[1]
[1]*Center for the Study of Complex Systems, Institute of Physics Belgrade, University of Belgrade, Serbia*
e-mail: denis@ipb.ac.rs

Since the first experimental realization of droplets [1], it was proven that quantum droplets in a dipolar Bose system are stabilized due to quantum fluctuations, correcting the ground-state energy [2,3,4,5,6]. We examine the behavior of collective oscillation modes and dynamics of dipolar quantum droplets. Our focus will be on the cylindrical symmetry, which gives us two oscillatory modes: the breathing mode and the quadrupole mode. To induce the droplets dynamics we perturb and modify relevant parameters such as contact interaction strength and harmonic trap potential. We also variationaly derive equations of motion and the oscillatory modes from a given Lagrangian.

REFERENCES

[1] H. Kadau et al., Nature 530, 194 (2016).
[2] T.D. Lee, K. Huang, and C.N. Yang, Phys. Rev 106, 1135 (1957).
[3] A.R.P. Lima and A. Pelster, Phys. Rev. A 84, 041604(R) (2011).
[4] A.R.P. Lima and A. Pelster, Phys. Rev. A 86, 063609 (2012).
[5] F. Wächtler and L. Santos, Phys. Rev. A 93, 061603(R) (2016).
[6] F. Wächtler and L. Santos, Phys. Rev. A 94, 043618 (2016).

ORCID: D.M. 0009-0007-1837-2530, A.B. 0000-0002-5435-1688

2. Nonlinear optics

Solutions to variants of the resonant nonlinear Schrödinger equation using the Jacobi elliptic function expansion method

N. Petrović
Institute of Physics, University of Belgrade, Pregrevica 118, 11080 Belgrade, Serbia
e-mail: nzpetr@ipb.ac.rs

The resonant nonlinear Schrödinger equation (RNLSE) is an important modification to the nonlinear Schrödinger equation (NLSE) in which the so-called 'quantum potential' is added [1], named after its role in producing quantum effects in the closely-related Gross-Pitaevskii equation [1, 2]. In the context of nonlinear optics, the potential can be interpreted as a special form of diffraction, influencing the general form of the solutions [1]. Much work has been done in finding exact analytical solutions to the RNLSE and several techniques have been tried, including: the Hirota method [1], the self-similar method [2, 3], the Bernoulli sub-ODE method [4], the (G'/G)-expansion method [4] and others [5, 6]. In [7], a form of the Jacobi ellptic function (JEF) expansion method was used, but the method is applied to a slightly modified form of the RNLSE and one with constant coefficients next to the terms. In addition, the quadratic dependence on the phase, known as chirp [8], was not considered.

The JEF expansion method has been proven effective in finding both solitary and traveling wave solutions to the NLSE [9]. In [9] solutions were found to the NLSE with Kerr nonlinearity, while in [10] solutions were found for the NLSE with the single- and dual-power law nonlinearity, including the special case of the cubic-quintic nonlinearity, also known as the parabolic nonlinearity [5].

In this work, we generalize the Jacobi elliptic function (JEF) expansion method, developed in [9, 10], to find exact solutions to the RNLSE equations with distributed coefficients and with Kerr, cubic-quintic and general single- and dual-power law nonlinearities. The addition of the quantum potential turns out to be applicable in a straightforward way due to the form of the ansatz used in the JEF. The maximum degree of the JEF in the solutions is the same as maximum degrees of the corresponding solutions in the original papers. Solitary and traveling wave solutions to the RNLSE are obtained, both with and without chirp, and the effects on the solutions of adding the quantum potential is analyzed.

REFERENCES

[1] O. K. Pashaev, J. H. Lee, Mod. Phys. Lett. 17, 1601 (2005)
[2] S. Meradji et. al., Chaos Solitons Fractals 141, 110441 (2020)
[3] A. Das et. al., Nonlinear Dyn. 111, 15347 (2023)
[4] K. S. Nisar et. al., Results Phys. 33, 105153 (2022)
[5] H. Triki et. al., Opt. Laser Technol. 44, 2223 (2012)
[6] H. M. Srivastava et. al., Math. Methods Appl. Sci. 42, 7210 (2019)
[7] E. M. E. Zayed, R. M. A. Shohib, Optik 158, 970 (2018)
[8] S. Chen, L. Yi, Phys. Rev. E 71, 016606 (2005)
[9] M. Belić, N. Z. Petrović, et. al., Phys. Rev. Lett. 101, 123904 (2008)
[10] N. Z. Petrović, Nonlinear Dyn. 93, 2389 (2018)

ORCID: N. P. 0000-0002-1297-3163

Various rogue wave clusters of the higher-order nonlinear Schrödinger equation

S. N. Nikolić[1], and M. R. Belić[2]
[1]*Institute of Physics Belgrade, University of Belgrade, Pregrevica 118, 11080 Belgrade, Serbia*
[2]*College of Science and Engineering, Hamad Bin Khalifa University, Doha, Qatar*
e-mail: stankon@ipb.ac.rs

We analyze a few types of rogue wave (RW) clusters for the quintic nonlinear Schrödinger equation (QNLSE) on a flat background. The exact QNLSE solutions are generated using the Darboux transformation (DT) scheme and they are composed of the higher-order Akhmediev breathers (ABs) and Kuznetsov-Ma solitons (KMSs) [1]. We analyze the dependence of their shapes and intensity profiles on the eigenvalues and evolution shifts in the DT scheme and on three real quintic parameters. The first type of RW clusters, characterized by the periodic array of peaks along the evolution or transverse axis, is obtained when the condition of commensurate frequencies of DT components is applied. The elliptical RW clusters are computed from the previous solution class when the first *m* evolution shifts in the DT scheme of order *n* are equal and nonzero. For both AB and KMS solutions a periodic structure is obtained with the central RW and *m* ellipses, containing the first-order maxima that encircle the central peak. We show that RW clusters built on KMSs are significantly more vulnerable to the application of high values of QNLSE parameters, in contrast to the AB case. We next present non-periodic long-tail KMS clusters. They are characterized by the rogue wave at the origin and *n* tails above and below the central point containing the first-order KMSs. We also show that the breather-to-soliton conversion can transform the shape of RW clusters by careful adjustment of the real parts of DT eigenvalues, while remaining parameters are left unchanged.

REFERENCES

[1] S.N. Nikolić, N.B. Aleksić, M.R. Belić, Optical and Quantum Electronics 56, 1182 (2024).

ORCID: S.N.N. 0000-0002-2082-9954, M.R.B. 0000-0002-2622-6425

Edge modes in nonlinear zig-zag modulated waveguide arrays with zero average modulation

P. P. Beličev[1], G. Gligorić[1], M. Stepić[1], M. Johansson[2], R. A. Vicencio[3, 4] and A. Maluckov[1]
[1]*COHERENCE Centre, Department of Atomic Physics, Vinča Institute of Nuclear Sciences, National Institute of the Republic of Serbia, University of Belgrade, Belgrade, Serbia*
[2]*Department of Physics, Chemistry and Biology (IFM), Linköping University, SE-581 83 Linköping, Sweden*
[3]*Departamento de Física, Facultad de Ciencias Físicas y Matemáticas, Universidad de Chile, Chile*
[4]*Millenium Institute for Research in Optics - MIRO, Chile*
e-mail: petrab@vin.bg.ac.rs

Topological edge states in periodically driven (Floquet) systems have attracted significant interest in recent years, particularly in photonic platforms, where their experimental realization and manipulation are highly controllable [1]. Among the key features of such systems are the so-called π-modes — robust edge-localized states with quasienergies locked at half the driving frequency — which are unique to time-periodically modulated lattices and have no static analog [1-5]. While extensive studies have addressed linear Floquet topological phases, the impact of nonlinearity remains an active area of research with many open questions [1].

In this work, we examine edge π-modes in nonlinear Su-Schrieffer-Heeger (SSH) lattices driven by zero-average time-periodic modulation as shown in Figure 1. Building on prior studies that identified nonlinear Floquet edge solitons bifurcating from linear π-modes in the high-frequency regime [6, 7], we extend the analysis to examine their nonlinear continuation under Kerr-type interactions and explore their behavior across both fast and slow driving regimes. We aim to map the stability properties of the resulting nonlinear π-mode family through detailed Floquet linear stability analysis.

In addition, we consider the emergence of topological mode bifurcations induced by nonlinearity, focusing on transitions between distinct families of edge-localized states and the onset of dynamical instabilities. These findings contribute to the broader understanding of nonlinear Floquet topological phases and open pathways for engineering robust edge-localized excitations in photonic systems governed by time-periodic driving.

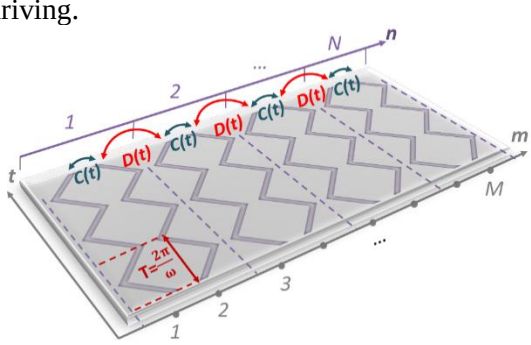

Figure 1. Schematic representation of longitudinally modulated zig-zag photonic lattice with periodically alternating coupling constants. Indices m and n stand for number of waveguides and 'dimers', respectively.

REFERENCES

[1] Y.V. Kartashov et al., Phys. Usp. 67, 1095-1110 (2024).
[2] V. Dal Lago, M. Atala, L.E.F. Foa Torres, Phys. Rev. A 92, 023624 (2015).
[3] Q. Cheng et al., Phys. Rev. Lett. 122, 173901 (2019).
[4] S. Wu et al., Opt. Express 30, 44983-44991 (2022).
[5] Z. Chen et al., Phys. Rev. B 109, L020302 (2024).
[6] H. Zhong et al., Phys. Rev. A 107, L021502 (2023).
[7] M. Arkhipova et al., Science Bulletin 68, 2017–2024 (2023).

ORCID: P.P.B. 0000-0002-2267-7202, G.G. 0000-0003-1890-7324, M.S. 0000-0002-0623-5113, M.J. 0000-0001-6708-1560, R.A.V 0000-0002-5825-9117, A.M. 0000-0002-6474-360X

Deterministic aperiodic lattices generation with Weber beams

I. J. Vlaović Mitić[1], A. Ž. Tomović[2], V. P. Jovanović[2], D. V. Timotijević[2], and D. M. Jović Savić[1]
[1]*Institute of Physics, University of Belgrade, P.O. Box 68, 11001 Belgrade, Serbia*
[2]*Institute for Multidisciplinary Research, University of Belgrade, Kneza Višeslava 1, 11030, Belgrade, Serbia*
e-mail: isidora@ipb.ac.rs

Light propagation in periodic photonic structures is controlled by spatial and temporal photonic band gaps; however, the manipulation of light in deterministic aperiodic and complex photonic structures remains poorly understood and unexplored for practical applications [1]. Nondiffracting beams, characterized by their propagation-invariant intensity profiles, are well-suited for creating photonic lattices in photosensitive media [2,3]. A method for generating deterministic aperiodic photonic lattices through the interference of two coherent Weber beams is presented [4]. These patterns are used to induce refractive index modulations in a photorefractive SBN crystal via single-pass optical induction. Various two-dimensional truncated aperiodic lattices were realized by adjusting the beams' parabolicities, relative phases, orientations, and spatial displacements. The resulting structures exhibit asymmetric domains, localized and extended defects, and enclosed macro-defect regions, offering diverse configurations suitable for studying wave localization, photonic surface states, and light manipulation in aperiodic systems. The formation and properties of the induced lattices were predicted through numerical simulations based on an anisotropic model. Their existence and guiding behavior were experimentally confirmed by probing with an extraordinarily polarized Gaussian beam. This approach provides a robust and versatile platform for the fabrication of deterministic aperiodic photonic media using structured light, with potential applications in integrated photonic devices, nonlinear optics, and topological light control.

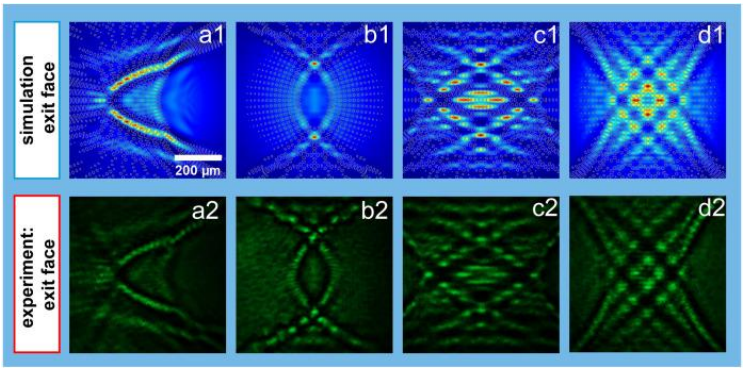

Figure 1. Verification of deterministic aperiodic photonic lattices inscribed in a photorefractive SBN crystal through probe beam propagation. Intensity distributions of the probe beam at the exit face of the crystal obtained numerically (the top row) and experimentally (the bottom row). Contours in numerical results indicate waveguide position.

REFERENCES

[1] Z. V. Vardeny, A. Nahata, A. Agrawal, Nat. Photonics 7, 177 (2013).
[2] M.A. Bandres, J.C. Gutiérrez-Vega, S. Chávez-Cerda, Opt. Lett. 29, 44–46 (2004).
[3] J. M. Vasiljević, A. Zannotti, D. V. Timotijević, C. Denz, D. M. Jović. Savić, Phys. Rev. A 96, 023840 (2017).
[4] A. Ž. Tomović, I. J. Vlaović Mitić, V. P. Jovanović, D. V. Timotijević, D. M. Jović Savić, Optical Materials 157, 116334 (2024).

ORCID: I.V. M. 0009-0003-1794-4278, A.T. 0000-0001-5972-6760, V.J. 0000-0001-6640-4575, D.T. 0000-0003-4538-3140, D.J.S, 0000-0002-1081-0141

Excitation of self-induced surface states in parabolic geometry

D. V. Mitić[1], J. M. Vasiljević[1], D. V. Timotijević[2], and D. M. Jović Savić[1]
[1]*Institute of Physics, University of Belgrade, P.O. Box 68, 11001 Belgrade, Serbia*
[2]*Institute for Multidisciplinary Research, University of Belgrade, Kneza Višeslava 1, 11030, Belgrade, Serbia*
e-mail: damir@ipb.ac.rs

Non-diffracting beams are a class of optical waves that maintain their transverse intensity profile over long propagation distances, exhibiting self-healing properties [1-5]. These beams have found applications in the field of optical trapping, high-resolution imaging, and laser material processing, where precise beam control and long-depth focusing are essential [6]. They are a significant promise for a new class of optical lattice-writing light within their stability range [7], but their potential in nonlinear photonics remains unexplored [8]. Truncating photonic lattices leads to the formation of localized surface states demonstrated in 1D waveguide arrays and 2D photonic lattices [9]. The geometrical characteristics of Weber beams offer a specific level of control over the topology of lattice surface.

We achieve the progress of these fields extending the concept of surface state generation by investigating the nonlinear propagation of non-diffracting Weber beams in photorefractive media. We present an approach for generating self-induced parabolic surface states in a photorefractive SBN crystal, utilizing a single-pass experimental setup with the optical induction technique. We systematically examined how these surface states characteristics depend on the beam parameters, orientation, and the strength of the nonlinearity. The formation of these surface states was observed without a pre-inscribed photonic lattice. This approach enhances the predictability and control of parabolic surface states, enabling new ways to manage diffraction, localization, and exploring novel nonlinear optical effects. Also, we investigate the linear propagation of a narrow Gaussian probe beam in a Weber aperiodic lattice inscribed in an SBN crystal to study surface effects. Such photonic lattices are naturally truncated, therefore build-up processes such as multiplexing or some kind of occlusion is avoided for their generation. Under specific parameter regimes, we observe oscillatory surface states near the lattice boundary, characterized by cyclic energy exchange between adjacent lattice sites. In both cases, such specific parabolic states are observed in the form of surface states extending across multiple adjacent parabolas, or edge parabolic states localized along the border parabola.

REFERENCES

[1] J. Durnin, J. Opt. Soc. Am. A 4, 651 (1987).
[2] J. Durnin, J. J. Miceli, and J. H. Eberly, Phys. Rev. Lett. 58, 1499 (1987).
[3] E. G. Kalnins and J. W. Miller, J. Math. Phys. 17, 331 (1976).
[4] J. C. Gutiérrez-Vega, M. D. Iturbe-Castillo, and S. Chávez-Cerda, Opt. Lett. 25, 1493 (2000).
[5] M. A. Bandres, J. C. Gutiérrez-Vega, and S. Chávez-Cerda, Opt. Lett. 29, 44 (2004).
[6] M. Woerdemann, C. Alpmann, M. Esseling, and C. Denz, Laser Photon. Rev. 7, 839 (2013).
[7] P. Rose, M. Boguslawski, and C. Denz, New Journal of Physics14, 033018 (2012).
[8] B. Freedman, G. Bartal, M. Segev, R. Lifshitz, D. N. Christodoulides, and J. Fleisher, Nature 440, 1166 (2006).
[9] S. Suntsov, at. al, Journal of Nonlinear Optical Physics & Materials 16, 401 (2007).
[10] D.V. Mitić, J. M. Vasiljević, D. V. Timotijević, and D. M. Jović Savić, *Self-induced parabolic surface states* Submitted in Optical Materials.

ORCID: D.M. 0009-0003-0085-9448, J.V. 0000-0001-9092-5223, D.T. 0000-0003-4538-3140, D.J.S, 0000-0002-1081-0141

Counterpropagating Peregrine-like soliton

A. Strinić[1], M. Petrović[1], I. Ilić[2] and M. R. Belić[3]
[1]*Institute of Physics, University of Belgrade, P.O. Box 68, 11080 Belgrade, Serbia*
[2]*Mathematical Grammar School (MGS), Kraljice Natalije 37, 11000 Belgrade, Serbia*
[3]*College of Sciences and Engineering, Hamad Bin Khalifa University, 23874 Doha, Qatar*
e-mail: strinic@ipb.ac.rs

We investigated numerically mutual interaction of two Peregrine-like solitons travelling in the opposite directions. Both beams are adjusted such that their inputs and outputs overlap on both ends of the nonlinear medium. Peregrine solitons are one of the solutions of the cubic nonlinear Schrödinger equation (NLSE), and can be used to model rogue waves [1, 2]. We found that for small propagation distances and input intensities, both beams propagate in a straight line. Larger propagation distances and initial intensities lead to a transverse shift of the two counter-propagating discrete solitons through the beam bending [3].

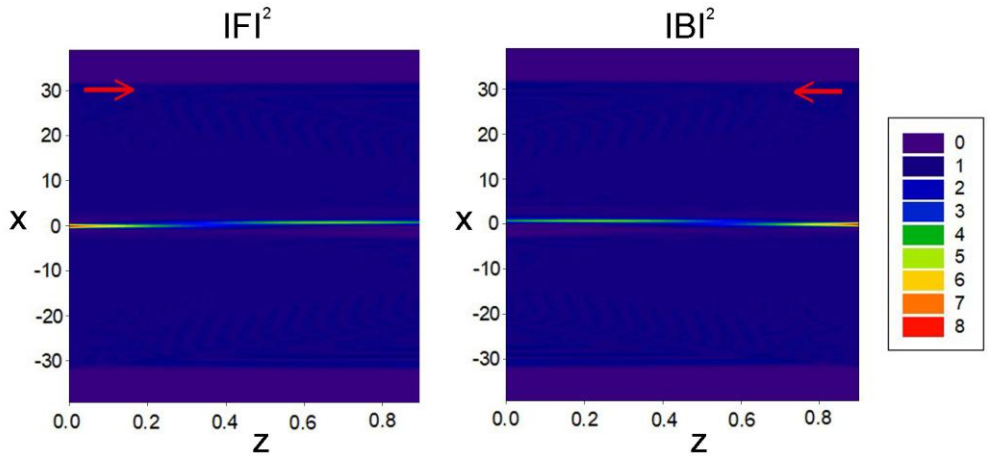

Figure 1. Counterpropagating rogue waves: input is Peregrine-like soliton for both forward (F) and backward (B) propagating beams.

REFERENCES
[1] Y. Zhang *et al.*, Phys. Rev. E **89**, 032902 (2014).
[2] Y. Zhang *et al.*, Phys. Rev. E **91**, 032916 (2015).
[3] M. Petrović *et al.*, Las. Phot. Rev. **5**, 214-233 (2011).

ORCID: A.S.0000-0001-9002-3764, M.P.0000-0002-6874-4407, M.B.0000-0002-2622-6425

The nonlinear Talbot effect of counterpropagating rogue waves

M. Petrović[1], A. Strinić[1], N. Petrović[2] and M. R. Belić[3]
[1]*Institute of Physics, University of Belgrade, P.O. Box 68, 11080 Belgrade, Serbia*
[2]*Mathematical Grammar School (MGS), Kraljice Natalije 37, 11000 Belgrade, Serbia*
[3]*College of Sciences and Engineering, Hamad Bin Khalifa University, 23874 Doha, Qatar*
e-mail: petrovic@ipb.ac.rs

The Talbot effect (TE) is an image recurrence phenomenon manifested by a periodic repetition of planar field distributions in some types of wave fields [1]. The nonlinear TE of rogue waves was demonstrated in [2, 3]. Here, we investigated numerically mutual interaction of two Ahkmediev-like breathers travelling in the opposite directions. Ahkmediev breathers (ABs) can be used to model rogue waves because they are one of the solutions of the cubic nonlinear Schrödinger equation (NLSE). We observed the formation of perfect nonlinear Talbot carpets for small input intensities.

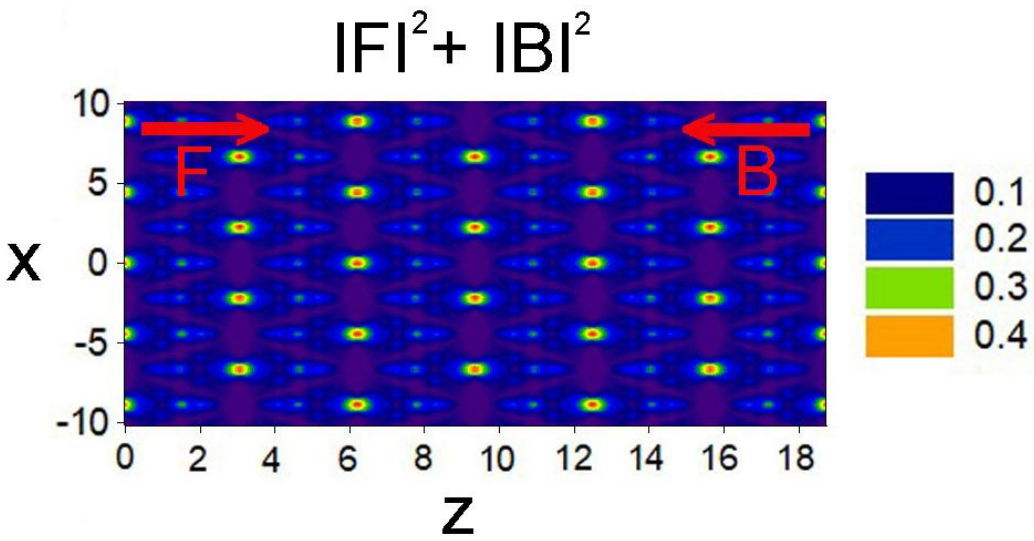

Figure 1. The nonlinear Talbot effect of counterpropagating rogue waves: input is Ahkmediev breather for both forward (F) and backward (B) propagating beams.

REFERENCES

[1] J. Wen *et al*., Adv. in Opt. and Phot. 5, 83-130 (2013).
[2] Y. Zhang *et al.*, Phys. Rev. E 89, 032902 (2014).
[3] Y. Zhang *et al.*, Phys. Rev. E 91, 032916 (2015).

ORCID: M.P.0000-0002-6874-4407, A.S.0000-0001-9002-3764, M.B.0000-0002-2622-6425

Nonlinear Optical Properties of Poly-Lactic Acid (PLA) for Photonic Applications

R. Stefanov[1], K. Shumanov[1], V. Atanasova[1], E. Yordanova[1], S. Karatodorov[1], R. Mincheva[2], G. Yankov[1]
[1]*Institute of Solid State Physics, Bulgarian Academy of Sciences (ISSP–BAS), 1784 Sofia, Bulgaria*
[2]*Laboratory of Polymeric and Composite Materials (LPCM), Center of Innovation and Research in Materials and Polymers (CIRMAP), University of Mons, 7000 Mons, Belgium*
e-mail: gyankov@issp.bas.bg

We investigate the nonlinear optical properties of poly-lactic acid (PLA), a biodegradable polymer with high transparency in the UV and near-infrared (NIR) spectral regions, using the Z-scan technique under femtosecond laser irradiation (35 fs, 408 nJ, 1 kHz). PLA samples were prepared via compression molding method. Our results show that PLA exhibits a nonlinear refractive index and multiphoton absorption coefficient that exceed those of fused silica by approximately one order of magnitude and are comparable to those of borosilicate glass.

Additionally, filamentation in PLA occurs at significantly lower pulse energies compared to borosilicate and quartz, providing strong evidence for its enhanced nonlinear response. These characteristics, combined with excellent processability and optical clarity, position PLA as a strong candidate for use in photonic structures requiring high nonlinearity, low energy thresholds, and environmentally friendly materials.

Funding: This work was supported by the Extreme Light Infrastructure – European Research Infrastructure Consortium (ELI ERIC), under contract DO1-102/26.06.2025.

Nonlinear Optical Properties of Borosilicate Glasses with Silver Nanoparticles for Photonic Applications

K. Shumanov[1], R. Stefanov[1], E. Yordanova[1], V. Atanasova[1], S. Karatodorov[1], N. Nedyalkov[2], L. Aleksandrov[3], G. Yankov[1]
[1]*Institute of Solid State Physics, Bulgarian Academy of Sciences (ISSP–BAS), 1784 Sofia, Bulgaria*
[2]*Institute of Electronics, Bulgarian Academy of Sciences (IE–BAS), 1784 Sofia, Bulgaria*
[3]*Institute of General and Inorganic Chemistry, Bulgarian Academy of Sciences (IGIC-BAS), 1113 Sofia,* Bulgaria e-mail: gyankov@issp.bas.bg

Borosilicate glass and fused silica are well-established materials in photonic technologies due to their broad optical transparency in the ultraviolet (UV) and near-infrared (NIR) spectral ranges, combined with stable nonlinear optical characteristics. In this study, we investigate the nonlinear optical properties of borosilicate glasses doped with silver nanoparticles using the Z-scan technique and femtosecond laser pulses of 35 fs duration, 408 nJ energy, and 1 kHz repetition rate.

The measured nonlinear refractive index (n_2) and multiphoton absorption coefficient (β) of the doped glasses were found to be an order of magnitude higher than those of reference fused silica. Furthermore, filamentation in silver-doped borosilicate glass was observed at significantly lower pulse energies, further confirming the higher optical nonlinearity of the medium. These findings highlight the potential of such glasses for nonlinear photonic applications, including optical memory and integrated photonic circuits.

Acknowledgment: This work was supported by the Extreme Light Infrastructure – European Research Infrastructure Consortium (ELI ERIC), under contract DO1-102/26.06.2025.

3. Optical materials

Semiconductor-driven tunable nanostructured metamaterial with epsilon-near-zero transition layer

T. Gric[1], E. U. Rafailov[2]
[1] *Department of Electronic Systems, Vilnius Gediminas Technical University, Vilnius, Lithuania*
[2]*Aston University, Birmingham, United Kingdom*
e-mail: tatjana.gric@vilniustech.lt

The metamaterials offer much-needed atypical material features to help with the subwavelength concentration of electromagnetic fields, which is the focus of nanophotonics research. By investigating propagation of surface plasmon polaritons (SPPs) at the boundary of semiconductor based nanostructured metamaterial with epsilon-near-zero transition layer, we demonstrate that the surface plasmon's dispersion along with the absorption is altered by a continuous dielectric function that is temperature dependent opening the wide avenues for sensing applications. A continuous function $\varepsilon(z)$ of the normal to the interface coordinate z describes the properties of the nanostructured metamaterial structure due to the existence of the transition layer. It should be topologically equal to a kink, however the major results for the spectrum of SPP are not sensitive to the particular form of $\varepsilon(z)$. Here, we'll look at a semiconductor-based metamaterial heterostructure made up of stacked anisotropic semiconductor sheets separated by dielectric layers, as schematically shown in Figure 1.

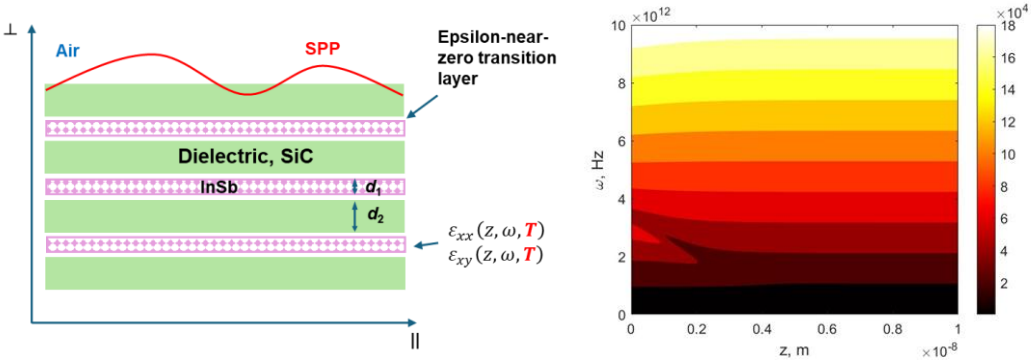

(a) (b)

Figure 1. Diagram showing the contact between air and an infinitely layered nanostructured metamaterial made of alternating dielectric and semiconductor layers (a). Real part of the propagation constant β (b). Herein, d_1=6 nm, d_2=10 nm, T=350K.

To describe the optical response of such a system, we employ the effective-medium technique, which is suitable when the wavelength of the light in question is substantially larger than the thickness of any layer. It should be mentioned that the frequency range of surface wave existence may be significantly controlled by adjusting the permittivities and thicknesses of the layers [1] utilized in the metamaterial. One must evaluate the tangential components of the electric and magnetic fields at the interface and generate a single surface mode with the propagation constant in order to determine the unique dispersion relation for the surface modes restricted at the interface between metamaterial and air.

$$\beta(z,\omega) = k\sqrt{\frac{\left(1-\varepsilon_{||}(z,\omega)\right)\varepsilon_{\perp}(z,\omega)}{1-\varepsilon_{\perp}(z,\omega)\varepsilon_{||}(z,\omega)}}, \quad (1)$$

where k is the wavevector's absolute value in vacuum and β is the wavevector component parallel to the interface.

REFERENCES

[1] T. Gric, Prog. Electromagnetics Res. 46, 165–172 (2016).

ORCID: T.G. 0000-0002-7850-2778

Morphological transformation of (In,Ga)N nanoshells grown around pencil-like GaN nanowires

J. Obradović[1], M. Tinoco[2], L. Monge Bartolomé[3], V. J. Gómez[3], A. Torres-Pardo[2], S. Fernández-Garrido[1], Á. Guzmán[1], Ž. Gačević[1]
[1]*Institute for Optoelectronic Systems and Microtechnology (ISOM), Universidad Politécnica de Madrid, Madrid, Spain*
[2]*Inorganic Chemistry Department, Chemical Sciences Faculty, Universidad Complutense de Madrid, Madrid, Spain*
[3]*Nanophotonics Technology center, Universitat Politècnica de València, Valéncia, Spain*
e-mail: j.obradovic@upm.es

GaN/(In,Ga)N/GaN pencil-like nanowires (NWs) are promising nanostructures for the development of single photon sources with highly tunable emission wavelengths and lifetimes [1]. A major challenge in advancing these structures lies in the limited understanding and control of in incorporation. One reason for complicated in incorporation into the NW shells could be the NW geometrical transition from r- (10-12) to s- (10-11) semi-polar crystal plane, observed from GaN to (In,Ga)N growth. In this work, we study and propose a growth model of (In,Ga)N nanoshells grown around (0001) oriented pencil-like GaN nanowires.

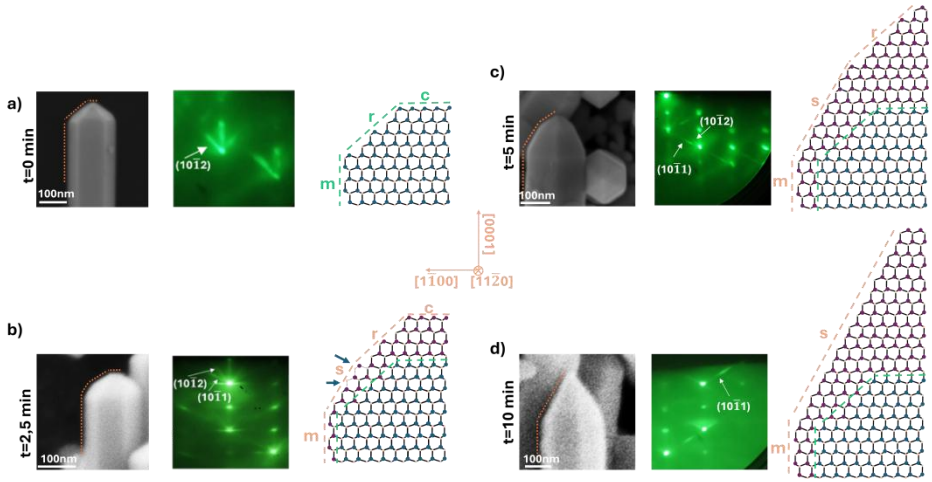

Figure 1 a)- d): Stages of the (In,Ga)N nanoshell growth, illustrated by a cross-view SEM images of single representative NW - RHEED diffraction patterns obtained along [11-20] azimuth, and an atomic sketches of the NW tip.

All samples were grown by plasma-assisted molecular beam epitaxy on commercial GaN-on-sapphire substrates, with a deposited Ti mask with nanoholes prior to the growth, so that growth selectivity can be achieved. The growth was performed in 2 steps: (i) GaN NWs growth, with fixed parameters, and (ii) (In,Ga)N nanoshell growth, with increasing growth time from sample H1 to sample H4 (0 min - 10 min, Figures 1 a)- d)). With addition of (In,Ga)N nanoshell, the initial GaN nanowires [Figure 1a)], progressively undergo through morphological changes, as shown in Figures 1b) and 1c). In this transition, semi-polar s- crystal planes appear and grow at the expense of r- and c- crystal planes, resulting in a structure dominated by m- and s- planes (Figure 1 d)). We propose a model of this geometrical transformation based on minimization of surface energy [2]. Furthermore, considering the instability of certain crystal planes we investigate In incorporation on the NW tops and sidewalls through two additional growth series, varying In impinging flux or growth temperature of the (In,Ga)N shell. These studies provide additional insights into both In incorporation and the (In,Ga)N luminescence in such nanostructures.

REFERENCES

[1] Ž. Gačević et al., ACS Photonics 4, 657 (2017).
[2] H. Liet al., Phys. Rev. Lett. 115, 085503 (2015).

ORCID: M.T. 0000-0003-2490-8059, L.M.B. 0000-0002-0125-6142, V.J.G. 0000-0003-2364-8814, A.T.P. 0000-0002-1667-4072, S.F.G 0000-0002-1246-6073, A.G. 0000-0001-5386-0360, Ž.G. 0000-0003-0552-2169

Impact of Growth Pressure on the Physical Properties of Two-Step Grown Sb_2Se_3 Absorbers for Thin Film Solar Cell Applications

A. Cantas
Department of Electric and Energy, Pamukkale University, Denizli, Türkiye
e-mail: abagdas@pau.edu.tr

As a result of growing population density and industrialization, the energy demand has been rising continuously. To meet the growing demand of energy consumption in the world, clean energy-based technology, such as photovoltaic technology, has been widely developed. The primary component of a solar cell system is the absorber layer. Thin-film solar cells rely on inorganic absorbers. However, the low stability and the high toxicity of some absorber layers could prevent the commercialization of these solar cells. Finding a novel, earth-based, and environmentally acceptable material for thin-film solar cells is crucial in this situation. Recently, Sb_2Se_3 thin film has drawn a lot of attention from researchers as a potentially useful photovoltaic absorber material. Earth-abundant and non-toxic, antimony selenide (Sb_2Se_3) has a direct bandgap of 1.1–1.3 eV and a high absorption coefficient (more than 10^5 cm^{-1}) [1]. These good properties make antimony selenide an extremely suitable absorber layer for thin-film solar cells. Although the theoretical studies have predicted that the conversion efficiency of Sb_2Se_3 can reach 30%, these values have not yet been reached experimentally [2]. Many methods have been used to prepare Sb_2Se_3 thin films. Still, most of them employ toxic chemicals and solvents or easily introduce impurities into the film as a result of the processes. Therefore, the two-step method has been preferred to deposit Sb_2Se_3 thin films. Firstly, the magnetron sputtering technique (Fig.1) has been used to grow Sb_2Se_3 thin films under different pressures, and then the selenization process has been applied. The different growth pressures have been applied to obtain the Sb_2Se_3 thin films (Fig.2) with desired properties. Scanning electron microscopy (SEM), energy dispersive X-ray (EDX), X-ray diffraction (XRD), Raman spectroscopy, X-ray photoelectron spectroscopy (XPS), UV/VIS/NIR spectroscopy, and the Hall system have all been used in this study to describe the complete characterization.

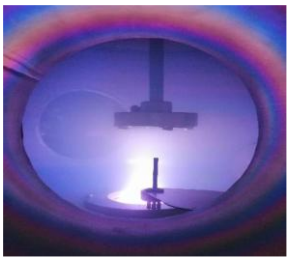

Figure 1. Growth of Sb_2Se_3 thin film.

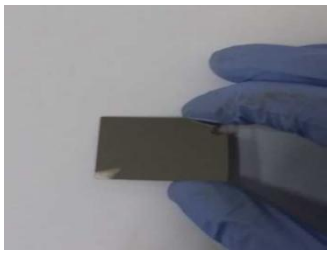

Figure 2. Sb_2Se_3 thin film.

The grown absorber films have different atomic compositions and have band gap energy values in the range of 1.2-1.4 eV. They exhibited an orthorhombic crystal structure with different preferred orientations. Electrical measurements of Sb_2Se_3 thin films demonstrated a p-type characteristic with varied resistivity. Substrate or superstrate thin film solar cells will be fabricated with absorber layers having the properties required for photovoltaic applications, and their efficiency values will be discussed.

'This work was supported by The Scientific and Technological Research Council of Turkey (TÜBİTAK) under the 2224-A Grant Program for Participation in Scientific Meetings Abroad.

REFERENCES

[1] X. Huang, Y. Zhang, L. Fang, X. Zhou, Q. Yu, K. Meng Results in Optics 16, 100734 (2024).
[2] A. Cantas, Phys. Scr. 99, 105993 (2024).

ORCID: Cantas.A. 0000-0002-6536-5516

Fiber optic sensors enhanced by diamond structures for biomedical and environmental sensing

M. Kosowska
Faculty of Telecommunications, Computer Science and Electrical Engineering, Bydgoszcz University of Science and Technology, Bydgoszcz, Poland
e-mail: monika.kosowska@pbs.edu.pl

Sensors have become an integral part of today's world due to their ability to deliver precise data on variety of parameters, either on-demand or in real-time. Current research trends focus on the development of advanced materials, AI-driven analysis, multimodality, and miniaturization [1,2]. As a result, there is a growing interest in fiber optic sensors, which offer high sensitivity, compact size, resistance to electromagnetic interferences, non-invasive and contactless operation mode. Additionally, the ability to functionalize the fiber surface enables a selective detection of specific biomarkers [3]. Therefore, enhancing and tailoring fiber optic sensors can lead to their broad application in biomedical measurements or environmental monitoring.

In this study, fiber optic sensors integrated with diamond structures (boron-doped diamond film, nitrogen-doped diamond film, nanocrystalline diamond sheet) are presented. Diamond structures offer mechanical robustness, chemical stability, biocompatibility, and possibility of tuning their properties towards specific applications [4]. They are also known for their exceptional hardness, which improves durability of the sensors components.

The design and development of interferometric optical fiber sensors are presented. Several configurations and example applications of the optical sensors are discussed, eg. sensor of hemoglobin level [5], setup for monitoring of electrochemical processes [6], sensor for bisphenol A investigation [7]. The system is based on a superluminescence diode, an optical spectrum analyzer, 2x1 fiber coupler, micromechanical setup, and a PC.

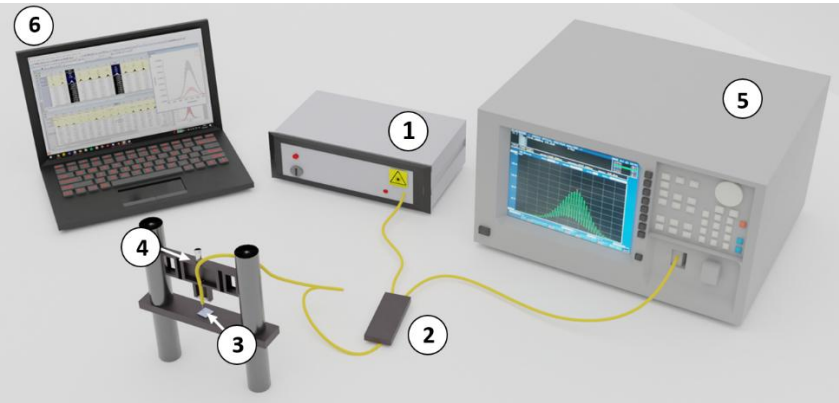

Figure 1. Laboratory measurement setup for the experiments: 1 – light source, 2 – coupler, 3 – measurement head, 4 – micromechanical setup, 5 – optical spectrum analyzer, 6 - PC

REFERENCES

[1] A. Venketeswaran, N. Lalam, J. Wuenschell, et al., Adv. Intell. Syst. **4**(1), 2100067 (2022).
[2] M. Szczerska, K. Cierpiak, M. Kosowska, et al., Sens. Actuators Rep. **10**, 100346 (2025).
[3] P. Wityk, M. Kosowska, J. Kwon, et al. Opt. Quant. Electron. **56**(8), 1303 (2024).
[4] M. Kosowska, S. Pawłowska, K. J. Sankaran, et al. Diam. Relat. Mater. **111**, 108221 (2021).
[5] D. Majchrowicz, M. Kosowska, K. J. Sankaran, et al. Materials **11**(1), 109 (2018).
[6] M. Kosowska, P. Jakóbczyk, M. Rycewicz, et al. Sci. Rep. **11**(1), 12600 (2021).
[7] M. Szczerska, M. Kosowska, P. Listewnik, et al. Measurement **189**, 110495 (2022).

ORCID: M.K. 0000-0002-3163-778X

Plasma, UV Radiation and Ozone for Microplastics Degradation: Optical Characterization of Polystyrene, Polyethylene and Polypropylene Degradation using FTIR and Raman Spectroscopy

M. Ćurčić[1], P. Kolarž[1], B. Hadžić[1], I. Stajčić[2], Z. Lazarević[1], D. Maletić[1], M. A. Urošević[1], A. Ž. Ilić[1]
[1]*Institute of Physics, University of Belgrade, Pregrevica 118, 11080 Belgrade, Serbia*
[2]*Institute Vinca, University of Belgrade, P.O. Box 522, 11001 Belgrade, Serbia*
e-mail: milicap@ipb.ac.rs

This study comprehensively examined the alterations in the optical and structural properties of three commonly encountered microplastic polymers—polypropylene (PP), polyethylene (PE), and polystyrene (PS)—when subjected to different degradation treatments. The microplastic samples were exposed to three distinct experimental conditions: ozone (O_3) treatment, ultraviolet (UV) radiation, and cold plasma, each representing an advanced oxidation or energetic degradation environment relevant to both environmental and industrial contexts. Controlled laboratory experiments were designed to simulate realistic degradation pathways and to systematically assess how each treatment influences the integrity and chemical structure of the selected polymers. The progression of degradation was monitored through Fourier-transform infrared spectroscopy (FTIR) and Raman spectroscopy, which provided detailed spectral fingerprints of the evolving chemical bonds and functional groups [1]. The spectroscopic data revealed treatment-specific molecular transformations, such as oxidation, chain scission, and the formation of new surface functionalities. These changes were manifested through the appearance or shifting of characteristic peaks, indicating alterations in crystallinity, the emergence of carbonyl and hydroxyl groups, and the breakdown of polymer backbones. This multi-technique approach enabled a nuanced understanding of the degradation mechanisms and the relative persistence of each microplastic type under different environmental stressors [2].

Overall, the study contributes valuable insights into the photochemical and oxidative degradation behavior of microplastics, with implications for environmental monitoring, remediation strategies, and the design of more degradable polymeric materials.

REFERENCES

[1] Alimi, O.S., Farner Budarz, J., Hernandez, L.M., Tufenkji, N., 2018. Microplastics and nanoplastics in aquatic environments: aggregation, deposition, and enhanced contaminant transport. Environ. Sci. Technol. https://doi.org/10.1021/acs.est.7b05559.
[2] Bandaru, S., Ravipati, M., Busi1, K.B., Phukan, P., Bag, S., Chandu, B., Dalapati, G.K., Biring, S., Chakrabortty, S., 2024. A review on the fate of microplastics: their degradation and advanced analytical characterization. J. Polym. Environ. 32, 2532–2550.
https://doi.org/10.1007/s10924-023-03102-7.

ORCID: M.C. 0000-0001-9239-0912, P.K. 0000-0002-9886-8494, B.H. 0000-0001-5459-7461, I.S.0000-0001-8278-4491, Z.L. 0000-0002-8397-1659, D.M. 0000-0002-0368-6568, M.A.U.0000-0001-6917-5368, A. I. 0000-0003-0859-6358

First-Principles Investigation of the Optical Properties of Layered Phyllosilicates

L. Filipović, A. Khasiyeva, A. Šolajić, J. Pešić
Laboratory for 2D Materials, Center for Solid State Physics and New Materials, Institute of Physics Belgrade, University of Belgrade, Pregrevica 118, 11080 Belgrade, Serbia
e-mail: lenka@ipb.ac.rs

In recent years, the focus of the 2D materials community has increasingly shifted toward phyllosilicates—a diverse group of naturally occurring van der Waals layered minerals. These materials display a broad spectrum of electronic, magnetic, and optical properties, many of which remain under active investigation. Their intrinsic robustness and stability under ambient conditions further enhance their appeal for various applications.

Talc, the most well-known member of the phyllosilicate family, is a wide-band-gap insulator characterized by a highly anisotropic crystal structure. It comprises stacked TOT layers—two tetrahedral (T) sheets strongly bonded to a central trioctahedral (O) sheet—held together by weak van der Waals forces [1]. The octahedral sheet consists of magnesium-centered octahedra, while the tetrahedral sheets contain silicon–oxygen units, arranged to reinforce the layered integrity of the structure. Remarkably, talc retains its structural and electronic stability even when exfoliated down to the monolayer limit.

This work investigates the optical properties of phyllosilicates, with a particular focus on talc. First-principles calculations were carried out using the Quantum ESPRESSO package [2], based on density functional theory (DFT) with plane-wave basis sets and projector augmented-wave (PAW) pseudopotentials. Exchange-correlation interactions were treated using the PBE-GGA functional, and Grimme-D2 van der Waals corrections were included to account for interlayer interactions. Optical response was evaluated at the random phase approximation (RPA) level. Current efforts aim to expand this study to other phyllosilicate species, supporting their potential use in optoelectronics, nanocomposites, and 2D heterostructure engineering.

REFERENCES

[1] “Ion implantation in phyllosilicates”, Muhammad Zubair Khan *et al*, *In preparation*
[2] Giannozzi P et al. J Phys Condens Matter. 30;21(39):395502 (2009)

ORCID: L.F.0009-0003-4401-7656, A.Š. 0000-0002-0553-0858, J.P. 0000-0002-8600-7187

Strain-Induced Corrugation and Its Impact on Electronic and Optical Properties of hBN-GaS, -GaSe, and -InS heterostructures

A. Šolajić and J. Pešić
Laboratory for 2D Materials, Center for Solid State Physics and New Materials, Institute of Physics Belgrade, University of Belgrade, Pregrevica 118, 11080 Belgrade, Serbia
e-mail: solajic@ipb.ac.rs

Two dimensional group IIIa monochalcogenides are promising two-dimensional semiconductors, known for their high carrier mobility and strong optical absorption in the visible and UV range. When integrated with hexagonal boron nitride (hBN) in van der Waals heterostructures, these materials benefit from the atomically flat and inert nature of hBN, which helps preserve their intrinsic electronic quality and enhances overall device performance. In our previous studies, hBN-based heterostructures with these monolayers exhibited favorable band alignment and optoelectronic characteristics [1,2,3].

In this work, we investigate the role of strain in shaping the structural and electronic behavior of hBN/GaS, hBN/GaSe, and hBN/InS heterostructures using first-principles DFT calculations. Contrary to heterostructures previously reported in the literature, these three systems develop a pronounced corrugated geometry as a result of compressive strain and lattice mismatch, coupled with the buckled nature of the monochalcogenide layers. We analyze how this strain-induced out-of-plane distortion modifies interlayer coupling, charge redistribution, band structure, and optical absorption spectra.

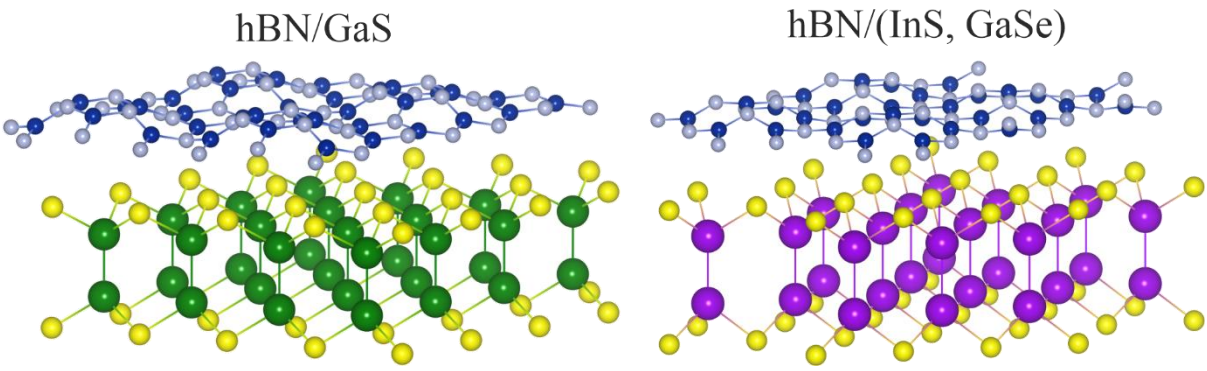

Figure 1. Crystal structure of corrugated heterostructures (hBN/InS, hBN/GaS, hBN/GaSe)

REFERENCES
[1]Šolajić, A., Pešić, J., *Journal of Physics: Condensed Matter*. **34(34)**:345301, 2022.
[2]Šolajić, A., Pešić, J., *Scientific Reports*, **14(1)**:1081, 2024.
[1]Šolajić, A., Pešić, J., *Optical and Quantum Electronics*, **56(7)**:1186, 2024.

ORCID: A.Š. 0000-0002-0553-0858, J.P. 0000-0002-8600-7187

An exploration of the electromagnetic boundary conditions for two-dimensional materials with out-of-plane polarization

A. Hansen and Z. Mišković
Department of Applied Mathematics, University of Waterloo, Waterloo, Ontario, Canada
e-mail: zmiskovic@uwaterloo.ca

We have re-derived the set of electromagnetic boundary conditions applicable to the macroscopic Maxwell's equations in the presence of a conductive 2D material, modelled as an infinitesimal sheet, placed in an interface between two distinct isotropic, lossless, dielectric media, where both the in-plane conductivity and the out-of-plane polarizability of that material are included [1,2]. Two important issues were addressed: identifying the effective electric fields that drive the response of the 2D material and exploring the possible screening effects of the out-of-plane response by the nearby dielectrics. This is done by first placing the 2D material inside a finite vacuum gap between the dielectrics and solving the Fresnel's problem, followed by "closing" the gap. The resulting theoretical model was tested against ellipsometric measurements and revealed significant influence from the out-of-plane response even at optical frequencies and in a graphene on substrate configuration, as shown in Figure 1. The comparison data included fixed frequency ($\hbar\omega$=1.95 eV) angular sweeps across the pseudo-Brewster angle [3], and fixed angle frequency sweeps across the range 1 eV < $\hbar\omega$ < 5 eV [4]. *Ab initio* computed in-plane and out-of-plane sheet conductivities were used to model the undoped graphene [5]. Finally, we tested the model for doped graphene at the THz to the midinfrared frequencies and observed significant alteration to the in-plane plasmon mode as a result of interaction with the out-of-plane polarizability when the nearby media have different permittivities [6].

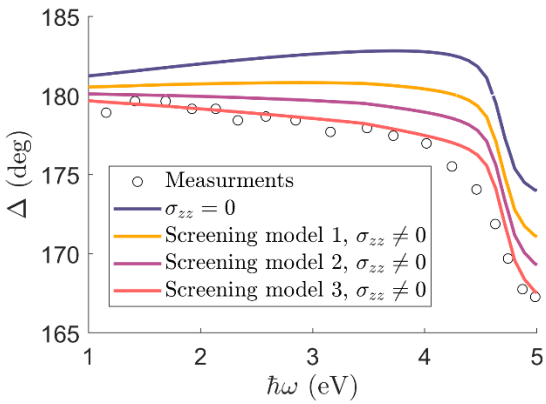

Figure 1. Comparison between three model predictions based on *ab initio* conductivity data for graphene and ellipsometric phase measurements [4] at a fixed incident angle of $\theta_i = 50°$.

REFERENCES

[1] M Idemen, et al. Boundary conditions of the electromagnetic field. Electronics Letters, 13(23):704–705, 1987.
[2] T Senior, et al. Sheet simulation of a thin dielectric layer. Radio Science, 22(07):1261–1272, 1987.
[3] Z Xu, M Merano, et al. Optical detection of the susceptibility tensor in two-dimensional crystals. Communications Physics, 4(1):215, 2021.
[4] F Nelson. Study of the Dielectric Function of Graphene from Spectroscopic Ellipsometry and Electron Energy Loss Spectroscopy. [PhD thesis, College of Nanoscale Science and Engineering], State University of New York at Albany, 2012.
[5] L Matthes, et al. Influence of out-of-plane response on optical properties of two-dimensional materials: First principles approach. Physical Review B, 94(20):205408, 2016.
[6] Y Bludov, et al. A primer on surface plasmon-polaritons in graphene. International Journal of Modern Physics B, 27(10):1341001, 2013.

ORCID: Z.M. 0000-0003-3882-8930

Rapid vs. Conventional Annealing: Impact on Optical Losses in TiN Thin Films

M. Novakovic[1], D. Jugovic[2], D. Tosic[1] and M. Popovic[1]
[1]*Vinca Institute of Nuclear Sciences - National Institute of the Republic of Serbia, University of Belgrade, Belgrade, Serbia*
[2]*Institute of Technical Sciences of SASA, Belgrade, Serbia*
e-mail: mnovakov@vinca.rs

Titanium nitride (TiN) is emerging as a promising alternative to noble metals for plasmonic and photonic applications, offering stability and CMOS compatibility [1,2]. This study investigates the effects of 150 keV Au ion implantation followed by rapid thermal annealing (RTA) and conventional annealing on the optical and metallic properties of sputtered TiN thin films. Ion implantation modifies the dielectric function by introducing damage and smaller crystallites, which reduces the metallic character and optical losses (Figure 1). Post-implantation RTA significantly enhances the metallic response, decreasing plasma frequency and Drude broadening, thus minimizing optical losses. Comparable results are achieved by conventional annealing; however, it requires longer processing time. At 500 °C, conventional annealing leads to the formation of Au nanoparticles, introducing additional absorption due to scattering. Overall, RTA proves to be a more efficient route for tuning the plasmonic performance of TiN films, making it highly suitable for applications in the visible–NIR range where low optical losses and defined metallic behavior are essential.

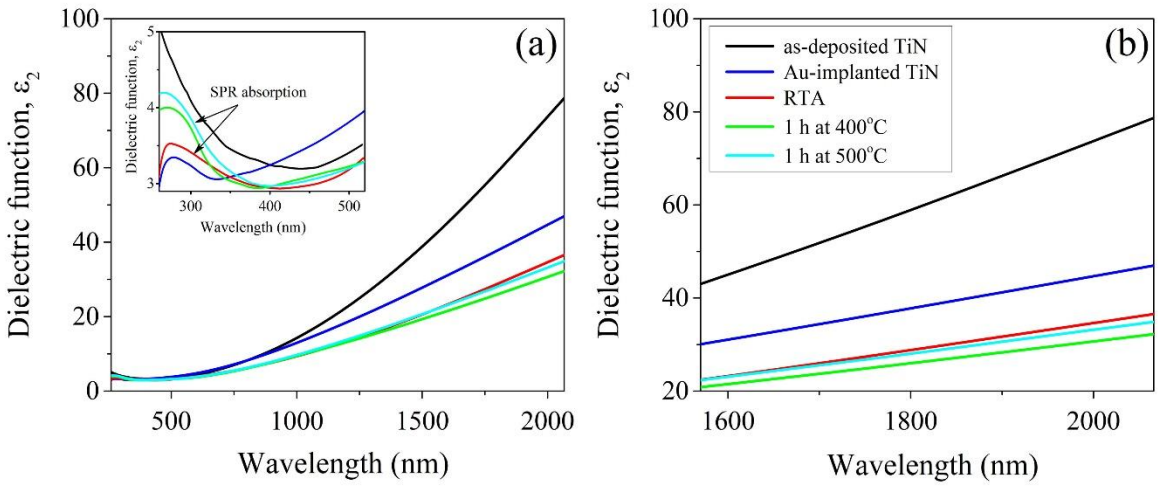

Figure 1. Imaginary part of the dielectric function for TiN films: as-deposited, Au-implanted (150 keV, 5×10^{16} ions/cm^2), and post-annealed (RTA/conventional, 400–500 °C, 1 h); (a) 260–2066 nm with SPR peaks (inset); (b) high-wavelength region detail.

REFERENCES
[1] M. Dasog, Chem. Mater. 34, 4249 (2022).
[2] U. Mahajan, M. Dhonde, K. Sahu, P. Ghosh, P.M. Shirage, Mater. Adv. 5, 846 (2024).

ORCID: M.N. 0000-0001-7103-0117, D.J. 0000-0001-6363-0825, D.T. 0000-0001-7289-6959, M.P. 0000-0002-0659-1732

Temperature tunable biopolymer photonic structure

S. Savic-Sevic[1], B. Muric[1] and J. Potocnik[2]
[1]*Institute of Physics, Belgrade, Serbia*
[2]*Vinca Institute of Nuclear Sciences, Belgrade, Serbia*
e-mail: savic@ipb.ac.rs

Tunable biopolymer photonic structures responsive to temperature changes are investigated. Two types of biopolymers are employed: pullulan, characterized by a linear polysaccharide structure, and dextran, which has a branched configuration. The photonic structures are fabricated by holographic recording in dichromate-doped pullulan and dextran. Properties of pululan [1,2] and dextran [3] films as holographic material - surface gratings, its diffraction efficiency, copying and environmental stability, were previously investigated.

Photonic structures, fabricated using a simple counter-propagating beam holographic setup, consist of multilayered biopolymer configurations, separated and supported by nanopillars. This complex morphology is formed through the combined action of holographic recording and nonsolvent-induced phase separation.

The optical properties of the resulting biopolymer photonic structures were analyzed during heating and cooling cycles. A Peltier element was used to control the sample temperature, while reflection spectra from white halogen light were recorded using a fiber-optic spectrometer. During heating, the reflectance peaks shifted toward shorter wavelengths (blue-shifted), showing a negative spectral shift of 60 nm for pullulan and 27 nm for dextran with a temperature increase of +50 K. Upon cooling, the spectral peaks nearly returned to its original position.

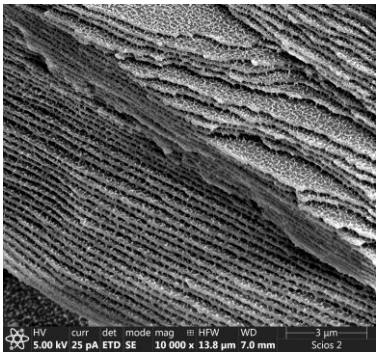

Figure 1. A cross-section of dextran structure.

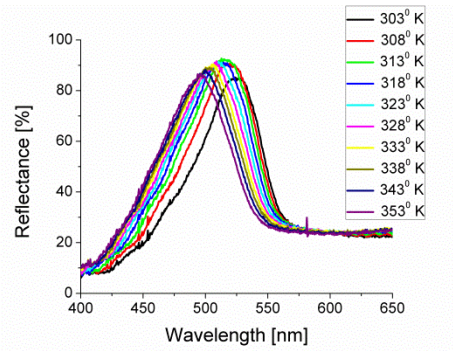

Figure 2. Reflectance spectra of dichromate-sensitized dextran photonic structure as a function of temperature

REFERENCES

[1] S. Savic-Sevic, D. Pantelic, Appl. Opt. 46, 287 (2007).
[2] S. Savic-Sevic, D. Pantelic, Optics Exp. 13, 2747 (2005).
[3] S. Savic-Sevic, D. Pantelic, Optical Mater. 30, 1205 (2008).

ORCID: S.S-S. 0000-0002-6406-0745, B.M. 0000-0003-3003-1708, J.P. 0000-0001-7206-5952

4. Biophotonics

Thermal Damage Modeling of CO2 Fractional Laser Induced Skin Micro-Tunnels

A. Shirkavand[1], A. Shorakaie[2], E. Nahvifard[3], L. A. Fashtami[4], E. Mohajerani[5]
[1]*Ph. D, Assistant Prof of Biophotonics/Medical Physics, Department of Photodynamic, Medical Laser Research Center, Yara Institute, ACECR, Tehran, Iran*
[2]*MSc of Physics, Physics Department, Science Faculty, Imam Khomeini International University, Qazvin, Iran*
[3]*Ph. D, Assistant Prof of Physics, Physics Department, Science Faculty, Imam Khomeini International University, Qazvin, Iran*
[4]*MD, Assistant Prof of Dermatology, Skin cell therapy Department, Regenerative medicine, Royan Institute, ACECR, Tehran, Iran,*
[5]*PhD, Professor of Photonics, Photonics Department, Laser and Plasma Research institute, Shahid Beheshti University, Tehran, Iran*
e-mail: shirkavand@acecr.ac.ir

Introduction: thermal damage pattern following the light absorption in tissue, can be useful for treatment optimization. More than rejuvenating, microtunnels that are induced due to CO2 fractional, are also considered in drug delivery. To lessen the risks of thermal damage, we modeled thermal damage patterns of these Micro-Tunnels in skin induced by the CO2 fractional laser in various laser parameters. **Methods:** In this modeling, COMSOL software was applied. The skin was modeled as three homogenous layers of epidermis, dermis, and hypodermis. Opto-thermal coefficients of the modeled tissue and its components in addition to the laser parameters (CO2, 10600 nm) were input data. The Bioheat Module and diffusion equations were applied. **Results**: The outcomes of this modeling show that power of 10w with different time pulses creates a better microtunnel in the tissue while preventing unwanted injuries. At a power higher than 15 watts and 5 pulses, the tissue will be damaged inconsiderably. Fractional laser creates heat only at the desired point of the treatment, and this heat is absorbed through the tissue, and microtunnels in it form the tissue. Also, 10w power with a low time width does not have a good effect on the tissue, but with an increase in the pulse width, it causes less damage to the surroundings. With a power higher than 15w, fractional laser irradiation creates wider microtunnels which might damage the tissue due to the adjacent microtunnels. **Conclusions:** COMSOL seems as a promising software for optimizing laser treatment plans before the clinical treatments for the specialists.

Keywords: Modeling, COMSOL, Thermal Damage, CO2 Fractional Laser

REFERENCES

[1] L Ataie-Fashtami, A Shirkavand, S Sarkar, M Alinaghizadeh, M Hejazi et al. Photomed Laser Surg. 29(7):509-15 (2011).
[2] A Shirkavand, L Ataie-Fashtami, S Sarkar, MR Alinaghizadeh, et al. Photomed Laser Surg.30(7):374-80 (2012).

ORCID: A.S. 0000-0002-6454-8847, E.N. 0000-0002-85453847, L.A.F. 0000-0002-8998-4063, E.M. 0000-0002-9243-9410

Novel Phosphorene-based Photodetector for biomarker analysis at UV range

M. Suplewski, M. Szczerska , P. Jakóbczyk
Department of Metrology and Optoelectronics, Faculty of Electronics, Telecommunications and Informatics, Gdańsk University of Technology, Poland
e-mail: suplewskimichal@gmail.com

We present a novel ultraviolet (UV) photodetector based on few-layer black phosphorus (FLBP) encapsulated in nitrocellulose, enabling highly stable and sensitive detection of UV light within the solar-blind spectral region, specifically around 260-280 nm. The device exhibits a pronounced and reversible change in electrical resistance upon exposure to 260-280 nm UV radiation, demonstrating its applicability for bio-photonic sensing without the need for external optical filters. Encapsulation in nitrocellulose significantly enhances environmental stability, overcoming the rapid degradation issues typical of black phosphorus materials [1-5].

The capability of this detector to sensitively measure UV absorption near 270 nm opens new possibilities for biomolecular analysis, particularly in the quantification and purity assessment of nucleic acids such as DNA and RNA. DNA and RNA nucleotides exhibit strong absorption maxima near 270 nm due to their aromatic bases; precise measurement in this spectral range enables rapid and non-destructive quantification of nucleic acid concentration and purity, essential in molecular biology and biomedical diagnostics [6].

The use of UV absorbance ratios (e.g., A260/A280) is a widely established method to assess sample contamination by proteins or other impurities [6-7]. Our FLBP-based UV detector provides a compact, flexible, and highly sensitive platform for such measurements, potentially integrating into portable biomedical devices for real-time nucleic acid quality monitoring.

Acknowlegment: This project is supported by DS programs of the Faculty of Electronics, Telecommunications and Informatics of Gdańsk Tech, 3/1/2024/IDUB/III.1a/Ra grant under the Radium Learning Through Research program at Gdańsk Tech, 7/1/2024/IDUB/III.4c/Tc grant under the Technetium Talent Management Grant, DEC-6/1/2025/IDUB/III.4a/Pu, 2025 under the Plutonium Supporting Student Research Teams program at Gdańsk Tech, Ministry of Science and Higher Education of the Republic of Poland under agreement no. MNiSW/2024/DPI/433. Additional support was provided by the COST Action CA21159.

REFERENCES

[1] M. Szczerska et al., “Investigation of the Few-Layer Black Phosphorus Degradation by the Photonic Measurements” Adv. Mater. Interfaces 10, 2202289 (2023)
[2] P. Jakóbczyk et al., “Low-power microwave-induced fabrication of functionalised few-layer black phosphorus electrodes: A novel route towards Haemophilus Influenzae pathogen biosensing devices” Applied Surface Science, 539, 148286 (2021)
[3] D. Roy et al., "Advancement in phosphorene: Synthesis, properties, and applications," Applied Materials Today, 35, 101944 (2023).
[4] W. Li et al., "Phosphorene Degradation: Visualization and Quantification of Nanoscale Phase Evolution by Scanning Transmission X-ray Microscopy," Chem. Mater., 32, 1272–1280 (2020).
[5] L. Peng et al., "Black Phosphorus: Degradation Mechanism, Passivation Method, and Application for In Situ Tissue Regeneration," Adv. Materials Interfaces, 7, 2001538 (2020).
[6] Thermo Fisher Scientific, "Extinction Coefficients and Purity of Nucleic Acids," Application Note TR0006, https://assets.thermofisher.com/TFS-Assets/LSG/Application-Notes/TR0006-Extinction-coefficients.pdf.
[7] Technology Networks, "A guide to DNA and RNA quantification and quality," https://www.technologynetworks.com/genomics/articles/a-guide-to-dna-and-rna-quantification-and-quality-392900.

ORCID: 0009-0002-2559-8400, 0000-0003-4628-6158, 0000-0002-6528-3713

Fiber Optic Based Sensors For Viral Biomarkers Detection

P. Sokołowski[1], M. Babińska[1], W. Brzezińska[2], J. Raczak-Gutknecht[2], P. Wityk[1,2], M. Szczerska [1]
[1]*Gdańsk University of Technology, Gdańsk, Poland*
[2]*Medical University of Gdańsk, Gdańsk, Poland*
[3]*Institute of Physics, Belgrade, Serbia*
e-mail: patsokol@pg.edu.pl

The development of optical biosensing platforms for the rapid detection of immunological and inflammatory biomarkers is essential to support clinical diagnostic. We present optical methods integrating fiber sensors techniques for sensitive biomarkers detection in complex biological matrices like urine and wastewater. Fiber optic sensors provide near real-time measurement capabilities, making them particularly useful for epidemic monitoring and early pathogen detection. The ability to establish sensor networks enables large-scale monitoring, which is essential for widespread diagnostic applications.

In this study, we introduce a fiber optic sensor functionalized with a sensing probe for biomarker detection based on antibodies and viral RNA. The sensor employs a microsphere design at fiber tip, enhanced with biofunctionalized layers to achieve high sensitivity and specificity toward selected viruses. The multilayer structure at tiber tip creates an optically responsive surface, allowing for the real-time detection of changes in optical properties registered in recorded spectra. The sensor operates based on optical interference, reflection on the surface of the microsphere is highly dependent on geometry and refractive index and properties of the functionalized layer, which covers the fiber tip. Presented sensor can be adapted for various viruses or pathogens with probe modification. The use of a single-mode telecommunication optical fiber, making integration into existing fiber optic networks possible, enhancing its applicability in near real-time medical diagnostics and biomarkers monitoring.

Acknowlegment: This research was supported by Ministry of Education and Science under project NdS-II/SP/0438/2024/01 of Gdansk Medical University, by DS programs of Faculty of Electronics, Telecommunications and Informatics of Gdańsk University of Technology, by 6/1/2025/IDUB/III.4a/Pu grant under the Plutonium Grants and by COST Action [CA21159]

REFERENCES

[1] P. Sokołowski, P. Wityk, J. Raczak-Gutnecht, W. Brzezińska, M. Sobaszek, P. Kalinowski, S. Garcia-Galan, M. Szczerska, Optical Method for the Detection of Viral RNA Using an Optical Fiber Sensor, Journal of Biophotonics, 2025, **https://doi.org/10.1002/jbio.202500063**
[2] M. Szczerska, K. Cierpiak, M. Kosowska, P. Wityk, S. Garcia-Galan, P. Sokołowski, S. Fudala-Książek, M. T. Tomczak, B. Ye, A. Łuczkiewicz, Remote real-time wastewaters surveillance by the optical sensor supported by machine learning, Sensors and Actuators Reports, 2025, https://doi.org/10.1016/j.snr.2025.100346
[3] K. Cierpiak, P. Wityk, M. Kosowska, P. Sokołowski, T. Talaśka, J. Gierowski, M. J. Markuszewski, M. Szczerska, C-reactive protein (CRP) evaluation in human urine using optical sensor supported by machine learning, Scientific Reports, 2024, https://doi.org/10.1038/s41598-024-67821-0

ORCID: P.S. 0000-0002-3524-4836, P.W. 0000-0001-8612-727X, M.Sz. 0000-0003-4628-6158

Tissue optics for low invasive diagnostics

S. Nemcova, U. Finaeva, J. Cap, P. Denk and J. Dvorak
Czech Technical University in Prague,
Prague, Czech Republic
e-mail: uliana.finaeva@fs.cvut.cz

Lung cancer is the leading cause of cancer death worldwide [1]. In the Czech Republic it comprised 10.7 % (approx. 6 600 cases per year) of new cancers and 18.2 % of cancer deaths in 2021, yet only 10.5 % are detected at stage I [2]. Early detection dramatically improves outcomes: one-year survival is 81–85 % at stage I versus 15–19 % at stage IV [3,4].

One of the early manifestations of lung cancer are solitaire pulmonary nodules (SPNs). A small, round opacity in the lung, surrounded by healthy tissue that can be both malignant and benign [5]. Options of diagnostics are immediate open chest surgery for critical cases [6], lung biopsy under CT or ultrasound navigation and pulmonary endoscopic biopsy. The nodules that are under 20 mm in size and the ones located distally are the most problematic from the diagnostics point of view: bronchoscopy methods often cannot reach the distal parts of the lung because of small airways size or have troubles navigating through the lung parenchyma. Transthoracic approach may be helpful, however, there is a higher risk of pneumothorax.

Our team was contacted with the proposition of work with bronchologist on design of diagnostic devices for SPNs using NIR transmittance spectroscopy. NIR spectroscopy was employed in study [7] to access the CT/PET found SPNs using two fiber system, collecting the spectral signal of back scattered light and in similar manner in study [8] for caries detection. However, transmittance NIR camera imaging has not been reported for lung lesions diagnostics. The market research of pulmonary diagnostic instruments shows no available ready-to-buy tools for transmittance NIR spectroscopic camera imaging. Based on our measurements we have defined the optimal lung transmittance wavelength and there are no bronchoscopes with this wavelength light delivery. This means that for Transluminance NIR spectroscopy it is necessary to develop a new diagnostic tool set. The approach is a bronchoscope with NIR source and pleuroscope with NIR camera. This will enable minimally invasive diagnostics and low post operative risks, allowing for real time SPN registration and assessment.

We performed a review of popular ways and methods to describe tissue optics so it can direct the optical design of the diagnostic toolset. However, the price and sophistication of equipment and the great disadvantage of used sample thickness varying from hundredths of millimeters to couple of millimeters led us to development of own measurement tool as the application in question requires description of lung-light interaction within at least 20 mm. The new method allows the measurement of diffused transmittance and calculation of attenuation coefficient. The validation of the results was performed by comparing the attenuation coefficients with literature data. Our device is simple, cost effective and mobile. It allows extraction of the tissue optics data, directing values for the low invasive medical toolset development for solitary pulmonary nodules diagnostics.

REFERENCES

[1] https://acsjournals.onlinelibrary.wiley.com/doi/10.3322/caac.21262
[2] https://www.uzis.cz/res/f/008447/novotvary2019-2021.pdf
[3] S. B. Knight et al., Open Biology, 7(9), 170070, (2017).
[4] ONS, Newport, UK, Statistical Bulletin, (2016).
[5] https://www.ncbi.nlm.nih.gov/books/NBK556143/
[6] H. MacMahon, et al., Radiology, 284(1):228-243, (2007).
[7] A. Fantin, et al., Life (Basel), 13(2):254, (2023).
[8] E. Stratigaki,et al., J Dent, 103S:100025, (2020).

ORCID: U.F. 0009-0003-2684-5423, S.N. 0000-0002-4260-0907, J.C. 0000-0002-5252-7395, P.D. 0000-0001-7863-8985

Near-infrared Light-Driven Nanomotors: Toward Ballistic Transport of Medicaments Across the Cell Membrane

D. K. Božanić[1], D. Danilović[1], J. Pajović[2], B. Ristić[3], A. Abu el Rub[1], V. Djoković[1], T. Mišeljić[4]
[1]*Vinča Institute of Nuclear Sciences – National Institute of the Republic of Serbia, University of Belgrade, Belgrade, Serbia*
[2]*Faculty of Physics, University of Belgrade, Belgrade, Serbia*
[3]*Institute of Medical Research, University of Belgrade, Belgrade, Serbia*
[4]*The Danish National Research Foundation and Villum Foundation's Center for Intelligent Drug Delivery and Sensing Using Microcontainers and Nanomechanics, Department of Health Technology, Technical University of Denmark, Lyngby, Denmark*
e-mail: bozanic@vinca.rs

Nanotechnology-based drug or gene delivery relies on effective internalization of molecular cargo in cells. However, external material is typically taken up via clathrin- or caveolae-mediated endocytosis, leading to localization of nanoparticles within lysosomes upon internalization. This endo-lysosomal pathway typically results in degradation of molecular cargo, rendering delivery inefficient and possibly inducing cell death. In this study, we outline a strategic framework to address this challenge by introducing an innovative method that utilizes near-infrared (NIR) light-driven nanomotors [1] for the ballistic transport of molecular cargo across cellular membranes (Figure 1.).

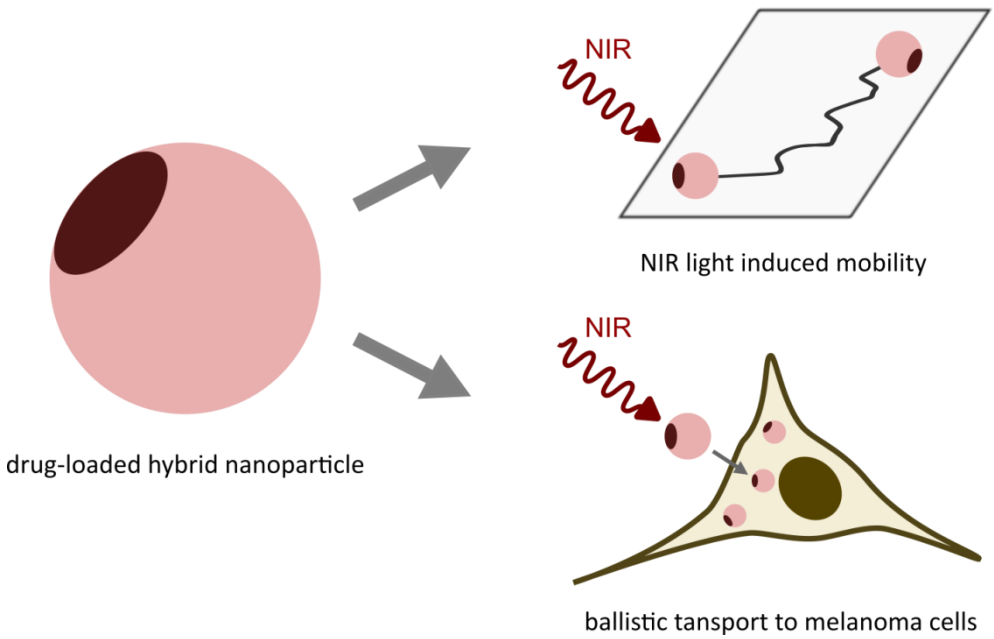

Figure 1. Roadmap to development of hybrid nanosystems capable of near-infrared light-induced ballistic transport of molecular cargo across the cell membrane.

REFERENCES

[1] D.Danilović, T. Maric, D.K. Božanić. J. Pajovic, G. Garcia, L. Nahon, Z. Zhang, A. Boisen, V.Djokovic, Nano research 18, 94907505 (2025)

ORCID: D.B. 0000-0001-8246-9635, D.D. 0000-0001-8402-1850, J.P. 0000-0002-3644-0118, B.R. 0000-0002-7255-6556, A.A. 0000-0001-9164-3965, V.Dj. 0000-0001-8237-1101, T.M. 0000-0002-6847-251X

X-ray assisted photodynamic therapy for pancreatic cancer

M. Stepić[1], M. Živanović[2], M. D. Nešić[1], J. Žakula[3], I. A. Popović[1], V. Ž. Ralić[1], L. Korićanac[3], P. Lobachevsky[4], A. N. Bugay[4], O. O. Vinogradova[4], V. S. Vinogradova[4] and M. Ž. Petković[1]
[1]*COHERENCE Centre, Department of Atomic Physics, VINČA Institute of Nuclear Sciences, National Institute of the Republic of Serbia, University of Belgrade, 11000 Belgrade, Serbia*
[2]*Department of Radiation and Environment Protection, VINČA Institute of Nuclear Sciences, National Institute of the Republic of Serbia, University of Belgrade, 11000 Belgrade, Serbia*
[3]*Department of Molecular Biology and Endocrinology, VINČA Institute of Nuclear Sciences, National Institute of the Republic of Serbia, University of Belgrade, 11000 Belgrade, Serbia*
[4]*Laboratory of radiation biology, Joint Institute of Nuclear Research, 141980 Dubna, Moscow Region, Russia*
e-mail: mstepic@vin.bg.ac.rs

Conventional treatments for cancer, such as chemotherapy, radiotherapy, and surgical resection, have shown limited healing efficacy and may cause severe side effects, poor targeting, and drug resilience for monotherapies, which strongly restrict their clinical application. Thus, various combinatorial strategies, such as photodynamic therapy (PDT), are investigated in detail to combat cancer. PDT [1] is a controllable, non-invasive, and non-cumulative two-step treatment that combines a nontoxic and biocompatible photosensitiser (PS), oxygen, and light to annihilate tumour cells and tissues. Upon light activation, the PS generates reactive oxygen species (ROS), which selectively destroy the targeted malignant tissue.

Deep-seated tumours, such as those in the lungs, pancreas, ovaries, colorectum, and kidneys, are challenging to treat with PDT because visible or near-infrared light has a tissue penetration depth of less than 3 cm, thus limiting PDT treatment to superficial tissues. This obstacle may be eliminated by X-PDT, a PDT based on X-ray irradiation, which penetrates deeper than visible or infrared light [2]. X-PDT utilises a scintillator (e.g., lanthanides) to convert external X-ray photons into visible light photons, which in turn activate the PS to trigger PDT-mediated processes within the tumour tissue.

Pancreatic cancer is among the most deadly forms of cancer globally, with one of the lowest survival rates. In this work, we experimentally examined the viability of MIA PaCa-2 pancreatic cancer cells as a function of the concentration of the photosensitive molecule protoporphyrin IX doped with a rare-earth element, Gd (pPIXGd). For the concentration range from 1.56 µg/mL to 50 µg/mL, the minimal cell viability was 43%. In parallel, we explore the *in-vitro* viability of MIA PaCa-2 cells under irradiation with X-rays of different doses (from 0.5 to 6 Gy). Finally, we combine a concentration of pPIXGd that exhibits low cytotoxicity (the mortality rate ≈ 26%) with the lowest X-ray dose, which weakly kills cancer cells (the mortality rate ≈ 11%), and observe a notable synergistic effect, resulting in total cell viability reduced to ≈ 51%.

REFERENCES

[1] M. Matijević et al., Photochem. Photobio. Sci. 2036, 1087 (2021).
[2] O. Sahin et al., Sci. Adv.11, eadr 4008 (2025).

ORCID: M.S. 0000-0002-0623-5113, M.Ž. 0000-0003-2965-1897, M.D.N. 0000-0002-9167-6553, J.Ž. 0000-0001-7280-3273, I.A.P. 0000-0003-1120-8985, V.Ž.R. 0000-0002-3206-1831, L.K. 0000-0001-5497-284X, P.L. 0000-0001-6539-7625, A.N.B 0000-0001-5334-346X, O.O.V.0000-0001-5914-930X, V.S.V. 0009-0003-6544-4411, M.Ž.P. 0000-0002-8354-995X

Towards NIR and MIR quantum microscopy of biosamples with undetected photons

M. M. Ćurčić[1], T. Pajić[2], M. Lekić[1], F. Krajinić[1] and B. Jelenković[1]
[1]*Institute of Physics, University of Belgrade, Serbia*
[2]*Faculty of Biology, University of Belgrade, Serbia*
e-mail: marijac@ipb.ac.rs

Method of quantum imaging with undetected light (QIUL) [1] has been decisive in extending the accessible spectral range for probing and imaging of biological samples. The classical and conventional NIR and MIR imaging techniques use infrared sources and detectors which are costly, noisy and with a poor performance in respect to the visible and NIR counterparts. On the other hand, microscopic imaging with QIUL scheme is a cost effective and powerful method for hyperspectral imaging which could help to reliably distinguish between different cells and tissues morphologies. Additionally, imaging at the single photon level prevents photo- and thermal damage of the bio-samples.

We report progress on the development of quantum interferometric set-up, exploiting induce coherence phenomena [2], while employing nonlinear crystal as a medium for generation of entangled, highly nondegenerate photon pair (signal and idler) via SPDC (spontaneous parametric down-conversion) process. The interferometer, in Michelson configuration, is formed in a double pass of the pump through 2 mm long ppKTP crystal, while the QIUL operation is based on momentum correlations. The bio-sample to be imaged is put on the path of the idler photons (λ_i=1345 nm), whereas the information on the absorption and the phase of the idler upon the interaction with the object is obtained solely from the detected signal photons (λ_s=880 nm).

Our results establish a foundation for efficient QIUL-based microscopy and outline the system's potential for high-fidelity imaging of biological samples, at our Center for Quantum Biophotonics. These findings pave the way for the future enhancements in design, sensitivity, and spectral versatility of QIUL systems meant for microscopy.

Acknowledgement: This work was supported by the Horizon WIDERA 2021-ACCESS-03-01 grant, #101079355 "BioQantSense" and bilateral project "Classical and quantum biophotonics" (HU-SRB).

REFERENCES

[1] G. B. Lemos, V. Borish, G. D. Cole, S. Ramelow, R. Lapkiewicz, and A. Zeilinger, Nature **512**, 409 (2014).
[2] X. Y. Zou, L. J. Wang, and L. Mandel, Phys. Rev. Lett. **67**, 318 (1991).

ORCID: M.Ć. 0000-0001-6920-3461, T.P. 0000-0003-3794-7655, M.L. 0000-0003-4814-2051, F.K. 0009-0008-0284-9426, B.J. 0000-0001-8276-1169

Nonlinear Laser Scanning Microscopy for noninvasive imaging of cells labeled by up-converting $NaY_{0.65}Gd_{0.15}F_4:Yb_{0.18}Er_{0.2}$ nanoparticles

M. Piljević[1], I. Dinić[2], L. Mancic[2], M. Vuković[2], M. Tomić[2], M. E. Rabanal[3], M. Lazarević[4], M. D. Rabasović[1]

[1]*Photonic Center, Institute of Physics Belgrade, University of Belgrade, Pregrevica 118, Zemun, 11080, Belgrade, Serbia*

[2]*Institute of Technical Sciences of SASA, Kneza Mihaila St. 35, 11000, Belgrade, Serbia*

[3]*Department of Materials Science and Engineering and Chemical Engineering, Universidad Carlos III de Madrid and IAAB, 28903, Madrid, Spain*

[4]*School of Dental Medicine, University of Belgrade, dr Subotica 8, 11000, Belgrade, Serbia*

e-mail: miljana@ipb.ac.rs

Nonlinear Laser Scanning Microscopy (NLSM) is a modern technique that utilizes ultrafast-pulsed lasers in the near-infrared wavelength range, which makes it suitable for noninvasive imaging of living cells. In this study, $\alpha NaY_{0.65}Gd_{0.15}F_4:Yb_{0.18}Er_{0.2}$ nanoparticles were synthetized and their potential for non-specific cell labeling was investigated using NLSM. These up-converting nanoparticles (UCNPs) have a significant potential in biomedical sciences as fluorescent probes for early cancer detection. Upon excitation by near-infrared light UCNPs are able to emit visible or ultraviolet photons, enabling deep noninvasive tissue imaging. The solvothermal synthesis applied chitosan, a polymer that ensures biocompatibility of synthetized UCNPs. Their morphological and structural characterization included following analyses: X-ray powder diffraction, scanning electron microscopy coupled with energy-dispersive X-ray spectroscopy, transmission electron microscopy, Fourier transform infrared spectroscopy and photoluminescence spectroscopy. Cell lines tested for labeling and visualization were HS-5 fibroblast healthy cells and SCC–25 oral cancer cells. Following nanoparticles incubation in these, NLSM was performed using Ti:Sapphire laser (Coherent, Mira 900-F) as a laser light source, operating in both, femto-second pulse mode and continuous wave mode. In order to visualize cells through their autofluorescence, excitation wavelength of 730 nm in femtosecond mode was used, while for their visualization through excitation of incubated nanoparticles continuous wavelength of 976 nm was used. Obtained images implied that the UCNPs were located adjacent to the plasma membrane in the cytoplasmic region of both healthy and cancer cells, without disturbing the morphology of cells. Besides this, UCNPs exhibited relative temperature sensitivity of ~1.3% K^{-1} indicating their potential for measuring the temperature in tissues.

ORCID: M.P. 0000-0002-6367-8316, I.D. 0000-0002-0909-8230, L.M. 0000-0002-6620-9582, M.V. 0000-0001-5824-3484, M.T. 0000-0003-1436-2208, M.E.R. 0000-0002-5090-6498, M.L. 0000-0003-1330-5332, M.D.R. 0000-0002-9235-4388

The Subtle Interplay of Microfluidics and Optics in Nature

D. Pavlović[1], B. Salatić[1] and D. Pantelić[2]
[1]*Institute of Physics, Belgrade, Serbia*
[2]*Senzor INFIZ, Pregrevica 118, Belgrade, Serbia*
e-mail: danicap@ipb.ac.rs

Environmental stimuli such as water and light play a critical role in shaping the structural adaptations of living organisms. Among insects, certain species have evolved sophisticated photonic nanostructures that facilitate dynamic color modulation, serving diverse biological functions including camouflage, communication, thermoregulation, and water regulation. In this study, we examine a beetle species known for its vivid, water-responsive coloration, characterized by a reversible shift from green to reddish-brown upon hydration. Through detailed structural and optical analyses, we identify a complex micro/nano-optofluidic architecture within the beetle's elytra and scales as the basis of this phenomenon. Water infiltration into the cuticle triggers capillary-driven transport through internal lacunae and petal-like nanostructures within the scales, displacing air and altering the refractive index contrast—thereby inducing a rapid and reversible color change. Remarkably, this system operates under capillary pressures estimated at ~15 bar, ensuring efficient fluid uptake and distribution. Optical modeling highlights the influence of the superhydrophilic cuticle on light scattering and reflectance, underpinning the observed chromatic shift. These reversible photonic changes are hypothesized to offer ecological advantages such as adaptive camouflage or thermal control. Beyond their biological relevance, the reproducible and structurally encoded fluidic pathways present in this natural system inspire novel approaches for the design of biomimetic materials. Potential applications include responsive sensors, microfluidic platforms, targeted drug delivery systems, and security technologies based on physically unclonable functions (PUFs).

ORCID: D.P. 0000-0003-4474-1209 B.S. 0009-0003-2165-9103

Parallel Factor Analysis of Essential Oils via Fluorescence Spectroscopy

A. Zhelyazkova[1] and Ts. Genova[1]
[1]*Institute of Electronics, Bulgarian Academy of Sciences, Sofia, Bulgaria*
e-mail: alexandra_jivkova@abv.bg

The integration of Parallel Factor Analysis (PARAFAC) with fluorescence excitation-emission matrix (EEM) spectroscopy has emerged as a robust tool for characterizing essential oils (EOs), offering rapid and cost-effective solutions for quality control and authentication in food, cosmetics, and pharmaceuticals [1, 2]. This methodology provides particular advantages for analyzing complex mixtures and commercial formulas, where traditional chromatographic methods may be time-consuming and expensive, while PARAFAC decomposition of fluorescence data can identify individual fluorophore components within multi-component essential oil systems. PARAFAC serves as a powerful chemometric tool for decomposing these complex fluorescence matrices into individual component profiles. The technique enables the identification and quantification of specific fluorophore signatures within essential oil samples, even when multiple components are present simultaneously [2]. That capability is particularly valuable for essential oil analysis because these natural products typically contain dozens to hundreds of chemical compounds, many of which contribute to the overall fluorescence profile.

However, the limited availability of recent research specifically focused on PARAFAC analysis of essential oils suggests that this field remains underexplored despite its apparent potential. Future research efforts should focus on developing comprehensive databases of fluorescence fingerprints for commercially important essential oils, establishing standardized analytical protocols, and validating the methodology against traditional analytical approaches [3]. The integration of PARAFAC-EEM analysis with existing quality control frameworks could provide enhanced analytical capabilities while supporting regulatory compliance requirements across multiple industries.

The methodology presented in the current experimental research shows particular promise for applications involving complex commercial formulations where traditional analytical approaches may be limited by time or cost constraints. As the essential oil market continues to grow and regulatory requirements become more stringent, rapid analytical methods like PARAFAC-EEM spectroscopy will likely play increasingly important roles in ensuring product quality and consumer protection.

Acknowledgements: The investigations were supported by the Ministry of Education and Science NRRI 2020-2027 funding agreement #D01–352/13.12.2023 "National Centre of Biomedical Photonics".

REFERENCES

[1] Kazi Monowar Abedin, Methaq Awadh Al-Yaqoobi, Laser-induced fluorescence spectroscopy of certain essential oils by blue and violet diode laser excitation, Results in Optics, Volume 16, 100693 (2024)
[2] Wu XJ, Pan Z, Zhao YP, Liu HL, Zheng LJ., Application of fluorescence spectra and parallel factor analysis in the classification of edible vegetable oils, 34(8):2137-42 (2014)
[3] Claudia X. Ramírez at all, Analyst, 145, 3414-3423 (2020)

ORCID: A.Zh. 0000-0001-9523-0308, Ts.G. 0000-0002-7792-8259

Optimizing Optical Coherence Tomography for Tooth Lesions Diagnosis Through Optical Clearing Agents

Ts. Genova[1] and A. Zhelyazkova[1]
[1]*Institute of Electronics, Bulgarian Academy of Sciences, Sofia, Bulgaria*
e-mail: ts.genova@gmail.com

Optical Coherence Tomography (OCT) has emerged as an imaging modality in dentistry, offering high-resolution cross-sectional and three-dimensional visualization of dental tissues without the use of ionizing radiation. This non-invasive technology is particularly effective for the early detection and characterization of carious lesions, enamel demineralization, and structural defects in teeth. Recent advances in swept-source OCT systems enable rapid acquisition of volumetric datasets with axial and lateral resolutions on the order of 7.4 µm, allowing detailed assessment of enamel, dentin, and the dentin-enamel junction [1].

In dental OCT imaging, sound enamel appears nearly transparent at near-infrared wavelengths (~1300 nm), while demineralized or carious regions manifest as bright zones due to increased light scattering. The ability to generate 3D images through raster scanning and multiplanar visualization overcomes limitations of 2D imaging, such as suboptimal projection angles and imaging artifacts, thereby improving lesion localization and diagnostic confidence. Quantitative analysis of OCT intensity profiles and attenuation coefficients further aids differentiation between sound and diseased dental structures.

To enhance OCT imaging depth and contrast, a number of optical clearing agents (OCAs) have been investigated. Recently natural oils were purposed as a biocompatible and cost-effective OCAs [2]. Appropriate natural oil will reduce the refractive index mismatch at the enamel surface, thereby decrease the light scattering and increase optical penetration.

The application of robust OCAs in dental OCT results in increased image contrast and penetration depth, enabling clearer visualization of subsurface carious lesions and microstructural features. It offers clinicians a safe, efficient, and highly sensitive tool for detecting and monitoring caries and other dental pathologies, potentially reducing reliance on traditional radiography. This improvement facilitates earlier and more accurate diagnosis, which is critical for timely and minimally invasive dental treatment.

Acknowledgements: The investigations were supported by the Ministry of Education and Science NRRI 2020-2027 funding agreement #D01–352/13.12.2023 "National Centre of Biomedical Photonics".

REFERENCES

[1] Janjua OS, Jeelani W, Khan MI, Qureshi SM, Shaikh MS, Zafar MS, Khurshid Z, Use of Optical Coherence Tomography in Dentistry, International Journal of Dentistry, 4179210 (2023)
[2] Banerjee A, Indoliya A, Poddar R, Edible oil based optical clearing for optical coherence tomography angiography imaging, Microvasc Res.,154:104671 (2024)

ORCID: Ts.G. 0000-0002-7792-8259, A.Zh. 0000-0001-9523-0308

Photonic Biosensors for Discriminating Sepsis, UTI, and Bladder Cancer via Biofunctionalized Optical Probes

P. Wityk[1,2], W. Brzezińska[1], P. Sokołowski[2], J. Raczak-Gutknecht[1], M. Szczerska[2]
[1]*Medical University of Gdańsk, Gdańsk, Poland*
[2]*Gdańsk University of Technology, Gdańsk, Poland*
e-mail: pawel.wityk@pg.edu.pl

We report on the development and validation of a fiber-coupled photonic biosensor platform for the differential analysis of urine samples from patients with sepsis, urinary tract infections (UTI), and bladder cancer. The system employs custom-engineered optical probes operating in the 200–1000 nm spectral range, allowing simultaneous acquisition of absorbance, fluorescence, and scattering signatures.

The sensing surface is biofunctionalized with disease-specific monoclonal antibodies, enabling molecular recognition of inflammatory cytokines, oxidative stress markers and tumor-derived metabolites (Fig. 1). The optical interface operates in a reflective mode, ensuring maximal contact with analyte-containing fluid and enhancing photon collection efficiency.

High-sensitivity detection is achieved via integrated low-noise spectrofotometer, narrow-band optical filtering, and real-time spectral deconvolution. Preliminary clinical validation on a pilot cohort demonstrated distinct biomolecular optical signatures for each disease group, with sensitivity and specificity exceeding 85% and total acquisition times below 5 minutes per sample [1, 2, 3]

This portable, label-free, and non-invasive photonic technology holds strong potential for rapid bedside stratification of patients in emergency care, with prospective applications in point-of-care diagnostics, infection control, and oncological screening.

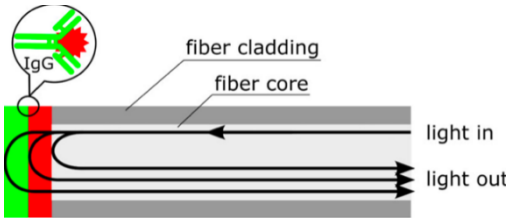

Figure 1. Schematic representation of biofunctionalized probe.

REFERENCES
[1] Wityk, Paweł, et al. "Optical method supported by machine learning for urinary tract infection detection and urosepsis risk assessment." Journal of Biophotonics 16.9 (2023): e202300095.
[2] Krawczyk, Beata, et al. "Uropathogenic Escherichia coli Associated with Risk of Urosepsis—Genetic, Proteomic, and Metabolomic Studies." International Journal of Molecular Sciences 26.12 (2025): 5681.
[3] Sokołowski, Patryk, et al. "Optical method supported by machine learning for dynamics of C-reactive protein concentrations changes detection in biological matrix samples." Journal of Biophotonics (2024): e202300523.

ORCID: P.W. 0000-0001-8612-727X P.S. 0000-0002-3524-4836 J.RG. 0000-0002-1856-0001 M.Sz. 0000-0003-4628-6158

Multimodal optical imaging and label-free sensing on-chip for monitoring intracellular and extracellular cellular processes

F. Torrini[1,2], M. Rojas Rodríguez[2], C. Dallari[1,2], L. Ponticelli[1,2], A. Jakovljević[3], M. Catarzi[2], T. Pajić[3], S. Donato[1,4], C. Capitini[2], M. Calamai[2], P. Andjus[3], B. Jelenković[5], S. Scarano[6], S. Nocentini[1,4], C. Credi[1,2]
[1]*National Institute of Optics, National Research Council (INO-CNR), Via Nello Carrara 1, 50019 Sesto Fiorentino, Italy*
[2]*European Laboratory for Non-linear Spectroscopy (LENS), Via Nello Carrara 1, 50019 Sesto Fiorentino, Italy*
[3]*Institute of Physiology and Biochemistry "Ivan Djaja", Faculty of Biology, University of Belgrade, Studentski trg 3, 11001, Belgrade, Serbia*
[4]*National Institute of Metrology (INRiM), Strada delle Cacce 91, 10135, Turin, Italy*
[5]*Institute of Physics Belgrade, University of Belgrade, National Institute of the Republic of Serbia, Pregrevica 118, 11080 Belgrade, Serbia*
[6]*Department of Chemistry "Ugo Schiff", University of Florence, 50019, Sesto Fiorentino, FI, Italy*
e-mail: francesca.torrini@lens.unifi.it

Integrated microfluidic lab-on-chip devices, combined with 3D printing and photonic technologies, hold significant potential for advancing the study of biophysical and biomedical processes. In this framework, we developed a modular LoC device that integrates two functional units: one for live-cell imaging and one for downstream, label-free optical sensing, enabling in-line analysis of both intracellular processes and extracellular secretome signatures.

The chip prototype is fabricated using stereolithography and a molding replication process based on perfluoropolyether, a UV-curable polymer with excellent anti-fouling properties, which minimize non-specific biomolecule adsorption [1,2]. By combining these two functionalities on a single chip, we designed a novel device to investigate the brain-periphery pathway using a simplified model. As a case study, we investigated the amyloidogenic cleavage of the amyloid precursor protein (APP) by the β-secretase Bace1, a well-characterized molecular event involved in the early stages of Alzheimer's disease (AD), which leads to the release of soluble APP β (sAPPβ). APP processing dynamics and particularly the secretion of sAPPβ, recently re-evaluated as potential AD early biomarker in biofluids [3], were investigated in neuronal cell models (SH-S5Y). Specifically, cells were transfected with APP fused to monomeric fluorescent proteins at both termini (mChAPPmGFP), allowing the visualization of proteolytic cleavage events through changes in the blue/green fluorescent ratio [4]. To mimic a neuroinflammation state and investigate biochemical and bioanalytical changes relative to a healthy baseline, cells were co-transfected with Bace1 to enhance APP cleavage.

Three compartmentalized cell culture chambers are used for cell confinement and phenotyping under physiological conditions. The integration of a valve enables fluidic connection with the downstream detection module for biomolecule tracking via a trapping surface functionalized with bioreceptors for specific analyte detection. The opening of the valve is designed to simulate the passage of biomolecules across a damaged or breakdown blood-brain barrier, as occurs during neuroinflammatory conditions. Fluorescence imaging was first performed off-chip to validate the construct, followed by on-chip integration. sAPPβ levels in the culture medium were initially quantified using a flow cytometer bead-based immunoassay. In parallel, an affinity-based detection strategy was developed using surface plasmon resonance system and a portable interferometric sensor to characterize binding kinetic/affinity parameters and analytical figures of merit (selectivity, repeatability, limit of detection and quantification). The portable sensing module was then connected in-line with the microfluidic chip, enabling real-time correlation between intracellular dynamics and secretome analysis. This integrated platform holds significant potential for monitoring the effects of disease-modifying therapies and for studying the diagnostic potential of biomarkers reflecting the brain status in peripheral fluids [4], with important implications for non-invasive diagnosis of neuropathologies, especially in the era in which in vitro models are increasingly approaching clinical relevance.

REFERENCES

[1] C. Credi, M. Levi et al., Appl. Surf. Sci. 404, 268-275 (2017).
[2] C. Credi, C. Dallari et al., Bioengineering 10 (6), 676 (2023).
[3] C. Capitini, A. Bigi et al., iScience 26, 106611 (2023).
[4] F. Torrini, M. Gil-Garcia et al., Trends Pharmacol. Sci. 46, 468-479 (2025).

Prospects for heart failure diagnostics using photoplethysmography

M. Tiosavljevic[1], P. Tadic[1], A. Lazovic[2], V. Atanasoski[2], M. Ivanovic[2], M. Stojanovic[2], P. P. Beličev[2], A. Maluckov[2], LJ. Hadzievski[2], A. Ristic[3], V. Vukcevic[3], J. Petrović[2]
[1]*School of Electrical Engineering, University of Belgrade, Serbia*
[2]*Vinca Institute of Nuclear Sciences, Belgrade, Serbia*
[3]*Faculty of Medicine, University of Belgrade, Serbia*
e-mail: masa.tiosavljevic@etf.bg.ac.rs

Heart failure (HF) is a serious condition that affects 64 million people worldwide, has high mortality and treatment costs. As it is primarily caused by mechanical malfunction of heart, the tests used in primary care, such as ECG, do not accurately detect it. Hence, a combination of tests and clinical evaluations, including a blood test, chest X-ray, magnetic resonance, and echocardiogram as a gold standard for the assessment of ejection fraction (EF), is used, however, often too late when the condition has already progressed towards the fatal outcome.

This study presents deep learning approaches for HF detection and classifying its subtypes based on simultaneous mechanical cardiac signals, with a primary focus on photoplethysmogram (PPG) due to their optical, non-invasive measurement modality.

Two neural network architectures were developed: the first processes PPG, phonocardiogram (PCG), and seismocardiogram (SCG) signals independently, extracting features via convolutional and LSTM layers. The second model aligns these signals temporally by adapting their sampling frequencies through adjusted convolutional and pooling layers, enabling joint feature extraction that considers inter-signal relationships.

We used an interim database from the ongoing SensSmart clinical study comprising 407 recordings from 82 subjects (46 HF patients, 36 healthy). HF patients were further categorized into three subtypes: preserved, mid-range, and reduced EF. PPG recordings, acquired at the brachial artery, alongside PCG and SCG recordings, were preprocessed and passed to the neural network models.

In binary classification tasks, accuracies exceeded 73%, with sensitivities reaching up to 93%, indicating a high true positive rate in identifying pathological cases. Multiclass classification, which aimed to distinguish HF subtypes, showed accuracy around 64%.

These results demonstrate the added value of using the PPG, in addition to other mechanical cardiac signals, in HF diagnostics. Importantly, all signals can be acquired via non-invasive, wearable solutions—highlighting the promise of integrating deep learning with accessible health technologies for early cardiovascular risk screening.

ORCID: M.T. 0009-0003-1916-9551, P.T. 0000-0002-8845-997X, A.L. 0000-0002-4581-0459, V.A. 0000-0003-1695-6341, M.I. 0000-0002-7218-6575, M.S. 0000-0002-4376-7610, P.B. 0000-0002-2267-7202, A.M. 0000-0002-6474-360X, LJ.H. 0000-0002-3955-628X, A.R. 0000-0002-0713-1180, V.V, J.P. 0000-0002-1002-241X, V.V. 0000-0002-8590-1152

A reflective holographic setup for simultaneous micro- and macro-scale imaging of biological samples

A. Minić[1], P. Atanasijević[1] D. Pavlović[2], B. Salatić[2], D. Pantelić[3] and P. Mihailović[1]
[1]*University of Belgrade, School of Electrical Engineering, Belgrade, Serbia*
[2]*University of Belgrade, Institute of Physics Belgrade, Belgrade, Serbia*
[3]*University of Belgrade, Senzor INFIZ, Belgrade, Serbia*
e-mail: minicana50@gmail.com

Simultaneous imaging at multiple spatial scales can be essential for analyzing biological structures due to their complex nature, often exhibiting an intrinsic coupling of a wide range of multiphysics phenomena. A glowing example is the entangled opto-thermo-mechanical response of the *Morpho didius* butterfly's wing to the incoming infrared photons. It is shown that the opto-thermally induced displacements result in both the macro bending of the wing membrane and the micro bending of the wing scales, as well as the changes in the reflection spectrum of the whole sample [1,2].

Digital holography presents itself as a suitable approach for imaging of optical and mechanical changes on the sample's surface, at both the macro- and the microscopic level. However, standard reflective digital holographic setups typically operate at a distinct magnification scale, as the need for the microscope objective to be very close to the sample's surface prevents simultaneous macro-scale imaging. In this study, we demonstrate a compact reflection-configured off-axis digital holographic setup, enabling simultaneous micro- and macro-scale imaging of biological membrane samples with complex photonic structures on both sides. We overcome the difficulties in dual-scale holographic recording by separating the macro- and micro-scale imaging to the opposite membrane sides using two distinct optical paths. The photograph of the setup is shown in Fig. 1 (a). It consists of a single laser source at 532 nm, illuminating both sides of the sample, and two synchronized cameras, one capturing the wide-field image and the other capturing the real, magnified image after the microscope objective. To demonstrate the operation of the proposed holographic macro-microscope, we image the wing of a *M. didius* butterfly suspended in air. The reconstructed macroscopic and microscopic intensity images are shown in Fig. 1 (b) and (c), respectively. Both images show distinct structural features – scale patterns on the membrane and the overlapping scales. Based on the results presented, the proposed reflective macro-microscope shows promise in imaging a wide range of complex biophotonic specimens, enabling comprehensive analysis of their inseparable structural multiphysics at a dual scale.

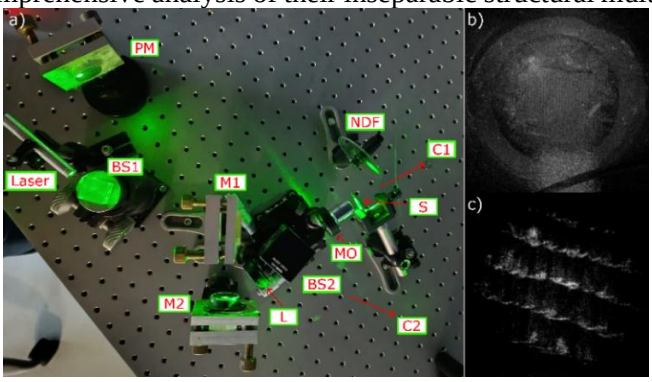

Figure 1. a) Photograph of the proposed macro-microscope. M. didius macro-scale (b) and micro-scale (c) intensity images. BS – beam splitter, M – mirror, PM – parabolic mirror, L – lens, C – camera, S – sample, NDF – neutral density filter.

Acknowledgment: The research was supported by the Serbian Ministry of Science, Technology, and Innovation (451-03-65/2024-03/200103). The research was partially conducted in the premises of the Palace of Science, Miodrag Kostić Endowment.

REFERENCES

[1] A. Pris et al., Nature Photon **6**, 195–200 (2012).
[2] P. Atanasijević et al., Opt. Laser Technol., 159, 108919 (2023).

ORCID: A.M. 0009-0009-4589-2667, P.A. 0000-0001-7596-0266, D.P. 0000-0003-4474-1209, B.S. 0009-0003-2165-9103, D.P. 0000-0002-2027-4696, P.M. 0000-0002-9720-1102

Performance Evaluation of Galvanometric Mirrors for Fast Scanning in Multimodal Laser Microscopy

M. Bukumira[1], S. N. Nikolić[1], M. D. Rabasović[1], T. Pajić[2], N. V. Todorović[3], K. Stevanović[1], M. Živić[1], A. J. Krmpot[1]
[1]*Institute of Physics Belgrade, University of Belgrade, Belgrade, Serbia*
[2]*Faculty of Biology, University of Belgrade, Serbia*
[3]*Institute for Biological Research "Siniša Stanković"- National Institute of the Republic of Serbia, University of Belgrade, Serbia*
e-mail: marta@ipb.ac.rs

In the development of a versatile nonlinear microscope optimized for multimodal imaging of biological samples, we implemented a custom-built setup combining two-photon excitation fluorescence, second harmonic generation and up-conversion imaging modalities. While the core system has been previously validated and applied to diverse samples ranging from starch granules to fungal hyphae, further improvements in imaging precision motivated a more detailed investigation into the role of galvanometric scanner performance.

In this work, we present a comparative characterization of two different pairs of galvanometric mirrors used in beam steering within our system. To evaluate how scanner dynamics – including step response behavior, dynamic artefacts such as overshoot, settling time and possible jitter – affect both beam position accuracy and image quality, we implemented several image acquisition modes operating at different scanning speeds. A custom-developed software platform allows full control of galvo driving signals and scanning trajectories, enabling precise and programmable scan patterns optimized for various imaging tasks. This flexibility enables a direct comparison of scanner performance under matched conditions and allows testing under regimes such as point-by-point acquisition. Preliminary measurements were conducted using photodetector and oscilloscope-based monitoring of scanner response to control signals as well as test imaging on simple samples. Results indicate notable differences in response profiles, which could be relevant for applications requiring rapid and precise scanning.

Acknowledgment: This research was supported by the Science Fund of the Republic of Serbia, Grant No. 4545, project "Advanced Biophysical Methods for Soil Targeted Fungi-Based Biocontrol Agents" BioPhysFUN.

ORCID: M.B. 0000-0003-2313-7344, S.N.N. 0000-0002-2082-9954, M.D.R. 0000-0002-9235-4388, T.P. 0000-0003-3794-7655, N.V.T. 0000-0003-2626-0794, K.S. 0000-0001-9733-2367, M.Ž. 0000-0002-0314-5032, A.J.K. 0000-0003-2751-7395

5. Devices and components

Fluorescent proteins as perspective elements of optoelectronic devices

A.S. Kudriavtseva[1,2], N.P. Nekrasov[3], I. Bobrinetskiy[2,4]
[1]*Prokhorov General Physics Institute of the Russian Academy of Sciences, Moscow, Russia*
[2]*Moscow Institute of Physics and Technology, Moscow Region, Russia*
[3]*National Research University of Electronic Technology, Moscow, Russia*
[4*]*BioSense Institute - Research and Development Institute for Information Technologies in Biosystems, University of Novi Sad, Novi Sad, Serbia*
e-mail: bobrinet@gmail.com

Fluorescent proteins (FPs) are widely used in biomolecular research due to their high quantum yield and stability. A broad range of engineered FPs have been developed, enabling tuning their spectral sensitivity, wavelength conversion, and chemical modifications. Recently, FPs were proposed as a light converter for photovoltaics and bioelectronics applications.

In this work, we demonstrate the functionalization of field-effect transistors based on individual single-walled carbon nanotubes (SWCNT-FETs) with FPs to introduce novel optoelectronic properties (Figure 1a). We employed a developed protein immobilization approach on carbon nanomaterials, that have been used also for biosensor development [1].

First, the sensitivity of green FPs (GFPs) photochemically immobilized on carbon lattices was investigated and specific photoresponse at 470 nm (Figure 1b) was shown [2]. Two types of engineered proteins have been studied with different positions of introduced non-natural amino acids containing phenyl-azide chemistry: the barrel wall of GFP and the bottom side. We demonstrated that the photoresponse is site-specific, and influenced by the number of charge traps associated with the hydrophobicity of the protein surface (Figure 1c).

Additionally, for SWCNT-FETs functionalized with red FPs, we used a PBASE linker adsorbed onto the nanotube surface [3]. These devices exhibit an unexpected gating effect on channel conductivity under FP-specific light irradiation. In this configuration, electrons can only transfer from the FPs when the gate voltage is below the threshold voltage, resulting in a negative photoresponse. Thus, engineering of FPs pave a way for novel optoelectronic devices with tunable properties.

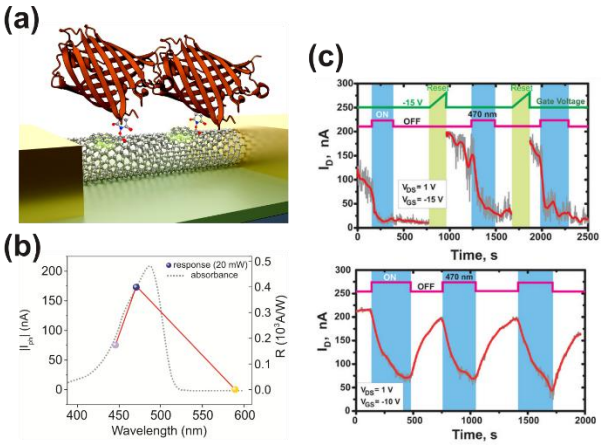

Figure 1. The performance of FP/SWCNT FET. (a) Scheme of SWCNT-FET with immobilized fluorescent proteins. (b) Spectral selectivity of bio-FET response. (c) The role of FPs immobilization site with memory response (top) and photodetector mechanism (bottom).

REFERENCES

[1] N. Nekrasov, S. Jaric, D. Kireev, et al. Biosens. Bioel. 200, 113890 (2022).
[2] A.S. Kudriavtseva, N.P. Nekrasov, D.V. Krasnikov, et al., Adv. Electron. Mater. 11, 2400329 (2025).
[3] R.E. Gwyther, N.P. Nekrasov, A.V. Emelianov, et al., Adv. Funct. Mater. 32, 2112374 (2022).

ORCID: I.B. 0000-0003-2380-2594, A.K. 0000-0002-2239-4691
*The work was made in part by I.B. during stay in this affiliation

TERA-MIR Photonic Functionalities and Applications

M.F. Pereira[1,2], H. Zafar[1], A. Al-Ateqi[1], A. Apostolakis[2] and V. Vaks[3]
[1]*Department of Physics, Khalifa University, Abu Dhabi, UAE*
[2]*Institute of Physics of the Czech Academy of Sciences, Prague, Czech Republic*
[3]*Institute for Physics of Microstructures, Nizhny Novgorod, Russia*
e-mail: mauro.pereira@ku.ac.ae

This talk covers photonics theory, simulations device fabrication, testing and applications in the TERA-MIR (Terahertz and Mid-Infrared) range starts with a discussion of superlattice nonlinearities and their applications THz metabolomics [1-4]. Evolving from detection in the THZ to the MIR, we present an update on detection in the by discussing the evolution of a sensor system incorporating a state-of-the art quantum cascade laser emitting at 9 μm in resonance with the absorption line of NH3 located at 1103.46 cm–1. Our initial instrument demonstrated sensitivity at a low ppm level for the ammonia, enabling precise detection of ammonia traces in water [5].

Next, we review light polarization control devices, focusing on silicon-on-insulator (SOI) platforms. We analyze polarizers, polarization splitters, and polarization splitters/rotators using silicon nanowires, ridge waveguides, hybrid plasmonic waveguides, and subwavelength grating waveguides. We start with some of our Near-Infrared (NIR) designs and show how they outperform existing devices in the literature [6-10].

Finally, we show how our designs are being modified for the MIR, with a discussion of existing [11-12] and forthcoming solutions.

REFERENCES

[1] Pereira, M.F., Nanomaterials 2022, 12, 1504.
[2] Al-Ateqi, A., Pereira, M.F., Opt Quant Electron 55, 1287 (2023).
[3] Vaks, V., Anfertev, V., Chernyaeva, M. et al., Sci Rep 12, 18117 (2022).
[4] Pereira, M.F., *et al.*, *Sci Rep* **10**, 15950 (2020).
[5] Apostolakis et al, ACS Omega 2024, 9, 17, 19127–19135.
[6] Zafar, H. et al, Opt. Express 31, 21389-21398 (2023)
[7] Zafar, H. et al, Opt. Express 2022, 30, 10087-10095.
[8] Zafar, H. et al, IEEE Journal of Selected Topics in Quantum Electronics, vol. 29, no. 6: Photonic Signal Processing, pp. 1-9, Nov.-Dec. 2023, Art no. 4400109
[9] Zafar, H. et al, AIP Advances 2020, 10, 125214.
[10] H. Zafar, M. F. Pereira, Laser Photonics Rev 2024, 2301025.
[11] H. Zafar and M. F. Pereira, in IEEE Access, vol. 12, pp. 48294-48300, 2024.
[12] Zafar, H., Pereira, M.F. , *Sci Rep* **15**, 5160 (2025).

ORCID: M.F.P: 0000-0002-2276-2095

Cross waveguide design for color-centers in diamond

A. Miranda[1,2], R. Ishihara[1,2] and S. Nur[1]
[1]*Department of Quantum Computer Engineering, Faculty of Electrical Engineering Mathematics and Computer Science, Delft University of Technology, Delft, The Netherlands*
[2] *QuTech, Delft University of Technology, Delft, The Netherlands*
e-mail: a.m.d.miranda@tudelft.nl

Color centers in diamond for quantum networking and computing are experiencing a growing interest because of their peculiar optical and spin properties [1]. Nevertheless technological and cost issues hinder the use of diamond for a complete quantum circuit. To cope with these limitations it is convenient to fabricate a diamond chiplet containing the color center(s) which is then heterogeneously integrated to a receptor fabricated on other platforms (e.g. by pick and place technology, P&P) [1,2,3]. The chiplet consists of a diamond multimode interferometric cross waveguide embedding the color center as well as port waveguides (WGs) for collecting excitation and emission (with eventual tapers and gratings for loss and crosstalk suppression), and tethers to connect it to a frame; the receptor, consists of adiabatic couplers, WGs, and other photonic components. In addition to P&P, this design can find application in any integration scheme such as transfer printing or DOI monolithic.

In order for the system to function properly each component must be designed in order to maximize the excitation to emission conversion and transmission efficiency, working bandwidth, fabrication feasibility and tolerance. Here we propose a methodology to perform this optimization for each component of the chiplet, of the receptor and of their combination: after a comparison of various alternatives presented in the literature, we show a complete study for the chosen solution. Apart from the proposed application, this methodology is of interest for a wider audience because it offers a strategy of optimization for components commonly used in other areas of photonics.

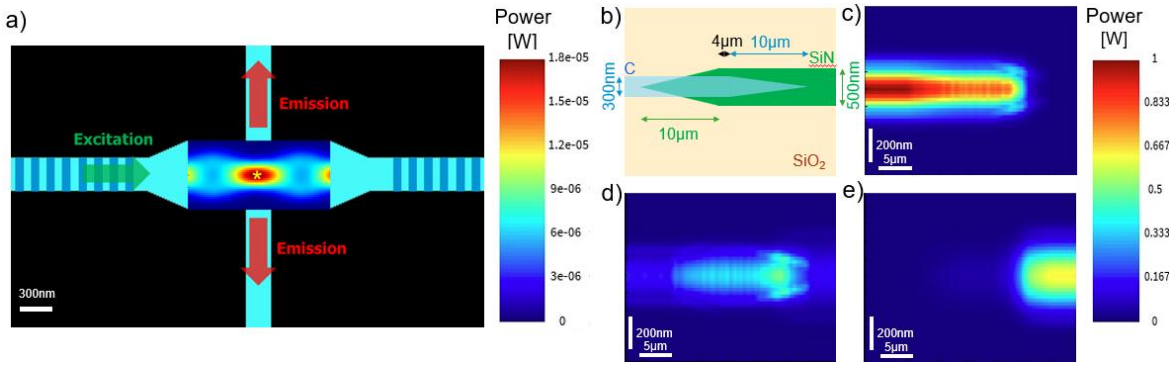

Figure 1. a) structure and power distribution of an adiabatically tapered MMI (1.6µm x 600nm) with Bragg reflectors at the horizontal diamond WGs (300nm x 250nm). b) structure of overlapping diamond and SiN adiabatic couplers (10µm long with 100nm ending and overlap of 4 µm) and corresponding power distribution in c) diamond coupler, d) interface between the couplers, e) the SiN coupler to SiN WG (500nmx250nm).

We gratefully acknowledge support from the joint research program "Modular quantum computers" by Fujitsu Limited and Delft University of Technology, co-funded by the Netherlands Enterprise Agency under project number PPS2007.

REFERENCES

[1] M. Ruf, N. H. Wan, H. Choi, D. Englund, R. Hanson, J. Appl. Phys. 130, 070901 (2021).
[2] N. H. Wan, Ts.-J. Lu, K. C. Chen, M. P. Walsh, M. E. Trusheim, L. De Santis, E. A. Bersin, I. B. Harris, S. L. Mouradian, I. R. Christen, E. S. Bielejec, D. Englund, Nature 583, 226 (2020).
[3] R. Ishihara, J. Hermias, S. Neji, K. Y. Yu, M. van der Maas, S. Nur, T. Iwai, T. Miyatake, S. Miyahara, K. Kawaguchi, 2023 IEEE International Interconnect Technology Conference (IITC) and IEEE Materials for Advanced Metallization Conference (MAM), 1 (2023).

ORCID: A.M. 0000-0003-4794-882X, R.I. 0000-0002-2114-4236, S.N. 0000-0002-2700-7769

Optimized AR Facet Coatings for 4.6 µm QCLs in Directed Infrared Countermeasures

M. Ozdemir[1], K. Aras[2], S. Eroğlu[2], M. Ekmekcioglu[1,2] and L. Ozyuzer[1]
[1]*Teknoma Technological Material Inc. IZTECH Campus, Urla, 35430, İzmir, Türkiye*
[2]*Department of Physics, Izmir Institute of Technology, Urla, 35430, İzmir, Türkiye*
e-mail: mehtapozdemir@teknoma.net

Mid-wave infrared (MWIR) Quantum Cascade Lasers (QCLs) are useful for applications such as remote spectral sensing, chemical spectroscopy, breath analysis, free space communications, and infrared countermeasure [1]. Directed Infrared Countermeasure (DIRCM) is especially important in military application. It is possible to confuse heat-seeking missiles guidance systems by mid-infrared source in order to protect aircrafts. Most of these application needs high output power and high-efficiency lasers. There are several ways to increase the output power. One of them is increase the number of active region stages. While this method results in higher peak power in pulsed mode, it leads to increase of temperature in the active region. Unlike other approaches, increasing the cavity length does not cause additional heating in the active region or degrade the beam quality [2]. Therefore, controlling the facet reflectivity emerges as a crucial design consideration for optimization. Two main methods are used to reduce laser facet reflectivity: angled-facet waveguides, which are effective but add optical complexity, and dielectric anti-reflection (AR) coatings, which are simpler and widely adopted. Applying these optical coatings to the front facets of QCLs reduces internal reflections and enhances the emitted optical power [3]. In this study, AR coatings were designed for the front facet of the laser as shown in Figure 1.a to enhance the optical efficiency and output power of QCLs, particularly for DIRCM applications at 4.6 µm, where aircraft strongly emit CO_2 radiation and heat-seeking missiles have high sensitivity. The AR coating was optimized to reduce reflectance to below 10% at this wavelength. Multilayer thin-film structures of AlN and Al_2O_3 on a GaAs substrate were modeled and simulated using OpenFilters programme. The optimal simulation was achieved with an AlN (200 nm) / Al_2O_3 (190 nm) / GaAs (2.0 mm) configuration, resulting in ~7% reflectance at 4.6 µm, as shown in Figure 1.b. After the modeling study, the Al_2O_3 and AlN layers were deposited on GaAs respectively using magnetron sputtering without breaking vacuum, yielding a total thickness of 410 nm. Reflectance measurements with a Bruker Vertex V80 FTIR spectrometer showed ~15% reflectance at 4.6 µm. The details of the fabrication of AR coatings and comparison of results with simulations will be discussed.

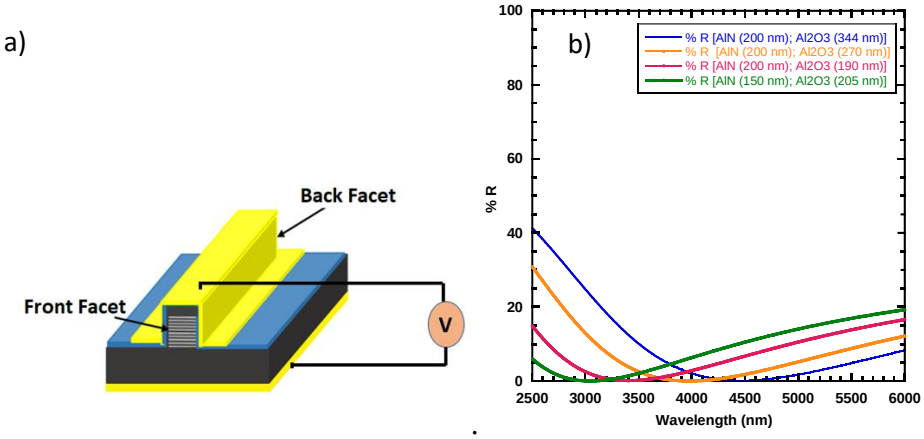

Figure 1. a) Front facet of the QCL b) Simulation results of the AR coatings

This work was partially supported by TUBITAK project number 22AG072. The authors would like to acknowledge the facilities of Research and Application Center for Quantum Technologies (RACQUT) of IZTECH.

REFERENCES

[1] D. Niewczas, D. Pierscinska, G. Sobczak, P. Kozlowski, A. Krząstek, T. Stefaniuk, K. Pierscinski, Appl. Phys. B 130, 192 (2024).
[2] R. Maulini, A. Lyakh, A. Tsekoun, R. Go, C. Pfluegl, L. Diehl, F. Capasso and C. Patel, Appl. Phys. Lett. 95, 151112 (2009).
[3] Y. Matsuoka, M.P. Semtsiv, S. Peters, W.T. Masselink, Opt. Lett. 43, 4723 (2018).

ORCID: M.O. 0000-0002-0453-6852, L.O. 0000-0001-7630-3938, K.A. 0000-0003-4066-8884, M.E. 0000-0002-8303-2264, S.E. 0009-0006-7250-6723

Etching-Based Mesa Formation for Quantum Cascade Laser Waveguides

K. Aras[1], S. Eroğlu[2], S. N. Basal[2], Y. Demirhan[2], M. Ozdemir[3] and L. Ozyuzer[2,3]
[1]*Department of Photonics, Izmir Institute of Technology, Izmir, Türkiye*
[2]*Department of Physics, Izmir Institute of Technology, Izmir, Türkiye*
[3]*Teknoma Technological Materials Industrial and Trading Inc. IZTECH, Izmir, Türkiye*
e-mail: kubraaras@iyte.edu.tr

Quantum cascade lasers (QCLs) play a vital role as laser emitters in the mid-infrared (MIR) and terahertz regions [1]. They are compact, fast, coherent semiconductor-based sources with broad applications in spectroscopy, monitoring, communications, diagnostics, and security [2]. QCLs require high power, causing self-heating. Reducing the pumped area helps lower the driving current [3], which in turn reduces self-heating. Additionally, high-quality deep mesa structures with smooth waveguide sidewalls help minimize lateral current spreading and optical losses [4]. Besides waveguide design, metal choice and interface purity are critical for QCLs. A high-vacuum system was developed for oxidation-free Cu–Cu bonding on GaAs waveguides, which can improve QCL efficiency and performance. [5]. In this study, the wet etching process was optimized using GaAs samples to fabricate mesa structures for the development of QCLs. The fabrication process began with spin-coating the sample surface with photoresist (PR) at 3000 RPM, followed by a soft bake step. The waveguide was designed using Layout Editor software, and pattern transfer was performed with a maskless lithography system (Heidelberg Instruments µMLA). Exposed PR regions were developed using developer, while the unexposed areas underwent a hard bake to enhance resist durability. For the etching step, various solutions were prepared and optimized, and the sample was immersed in the solution. After etching, the sample was rinsed with deionized water and dried with nitrogen gas. Residual PR was removed using acetone. The depth of the etched regions was optimized depending on etching time and measured using a surface profilometer. Figure 1 shows an SEM image of one of the samples, the wet etching process yielded well-defined mesa sidewalls, confirming a controlled and uniform fabrication.

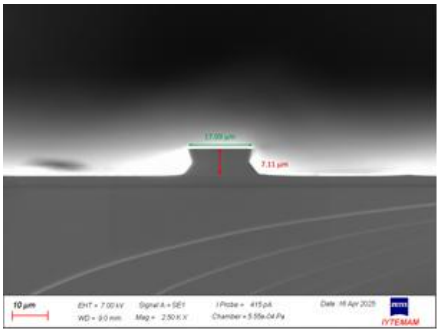

Figure 1. SEM Image of the fabricated Mesa

This work was partially supported by TUBITAK project number 22AG014. The authors would like to acknowledge the facilities of Research and Application Center for Quantum Technologies (RACQUT) of IZTECH.

REFERENCES

[1] M. Razeghi, Q. Y. Lu, N. Bandyopadhyay, W. Zhou, D. Heydari, Y. Bai, S. Slivken, Opt. Express 23, 8462 (2015).
[2] A. Kuźmicz, E. Pruszyńska-Karbownik, K. Pierściński, P. Gutowski, D. Pierścińska, K. Janus, K. Michalak, G. Sobczak, M. Sakowicz, Infrared Phys. Technol. 118, 103902 (2021).
[3] A. Szerling, K. Kosiel, M. Kozubal, et al., Semicond. Sci. Technol. 31, 075010 (2016).
[4] A. Szerling, P. Karbownik, K. Kosiel, J. Kubacka-Traczyk, E. Pruszyńska-Karbownik, M. Płuska, M. Bugajski, Acta Phys. Pol. A, 116 (2009).
[5] S. Rouhi, M. Ozdemir, M. Ekmekcioglu, S. Yigen, Y. Demirhan, A. Szerling, K. Kosiel, M. Kozubal, R. Kruszka, P. Prokaryn, M. Ertugrul, J. L. Reno, G. Aygun, L. Ozyuzer, J. Mater. Sci.: Mater. Electron. 32, 18684 (2021).

ORCID: K.A. 0000-0003-4066-8884, S.E. 0009-0006-7250-6723, S.N.B. 0009-0001-0641-3848, Y.D. 0000-0002-7782-4468, M.O. 0000-0002-0453-6852, L.O. 0000-0001-7630-3938

Single-Frequency DFB Laser based on High-Yb-doped photosensitive fiber

A. Shigapov, E. Seregin, M. Likhachev and Yu. Gromova
GREITLEX PHOTONICS DOO, Belgrade, Serbia
e-mail: mike@greitlex-photonics.com

Single-frequency fiber lasers are one of the important tools in number of applications (first of all - lidars). Laser based on distributed feedback (DFB) resonators are most suitable for mass production due to reduction of fabrication steps (only single π-shifted fiber bragg grating should be fabricated) and guarantee of operation in single-frequency regime. To date lack of such lasers was coursed by absence of highly Yb-doped photosensitive fibers. Recent progress in development of highly Yb-doped silica-based fibers [1, 2] open new possibilities in development of DFB Yb-doped fiber lasers. Home-made highly-Yb-doped photosensitive fiber with ability to maintain polarization was used in the current work. A record-short (10 mm in length) DFB laser operated near 1064 nm was fabricated by direct whitening of fiber Bragg grating in the active fiber. Scheme of the laser is shown in Fig.1 (upper insert). Single-mode pump diode (Pump), was coupled to DFB resonator based on active fiber using polarization maintaining single-mode pump and signal combiner (WDM). Output signal was passed through WDM. Full power generated by DFB laser (see Fig.1) and polarization extinction ratio of more than 23 dB were measure just after WDM. To measure output spectra (see bottom insert to Fig.1) we added polarization-maintaining Isolator. Linewidth was found to be smaller than resolution of optical spectrum analyzer (0.02 nm), which confirm the operation of the laser in single-frequency regime (according our estimations distance between own modes of the resonator, i.e. between polarization modes was of about 0.2 nm).

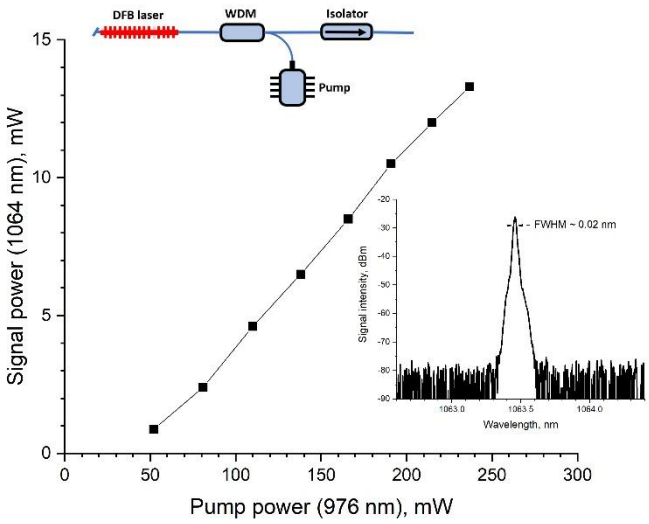

Figure 1. Dependence of output single-frequency signal power on pump power. Upper insert: scheme of DFB fiber laser; bottom insert: output spectrum of the DFM fiber laser.

REFERENCES

[1] K.K.Bobkov, E.K. Mikhailov, T.S. Zaushitsyna, A.A. Rybaltovsky, S.S. Aleshkina, M.A. Melkumov, M.M. Bubnov, D.S. Lipatov, M.V. Yashkov, A.N. Abramov, A.A. Umnikov, A.N. Guryanov, M.E. Likhachev, "Properties of silica based optical fibers doped with an ultra-high ytterbium concentration", J. of Lightwave Technology, 40(18), 6230-6239 (2022).
[2] Y.Li, X.Deng, S.Fu, Q.Sheng, C.Shi, J.Zhang, L.Zhang, W.Shi, and J. Yao, "High-power, high-efficiency single-frequency DBR fiber laser at 1064 nm based on Yb3+-doped silica fiber," Opt. Lett. 48, 598-601 (2023).

ORCID: M.L. 0000-0001-6767-3486

Design and Fabrication of Thin Film for All Solid-State Lithium-Ion Batteries

N. Karadeniz[1,2], N. Esen[1], S. Karpuz[1], U. Unal[3], A. Cantas[4], L. Ozyuzerr[1,2], M. Ozdemir[2], K. Kosiel[5], A. Szerling[5], R. Socha[6], G. Aygun[1]
[1]*Department of Physics, Izmir Institute of Technology, Izmir, Türkiye*
[2]*Teknoma Technological Material Inc., Iztech Campus, Izmir, Türkiye*
[3]*Department of Chemistry, Koc University, Istanbul, Türkiye*
[4]*Department of Electric and Energy, Pamukkale University, Denizli, Türkiye*
[5]*Łukasiewicz Research Network-Institute of Microelectronics and Photonics, Warsaw, Poland*
[6]*CBRTP S.A., 36 Czarnowiejska St. 30-054 Cracov, Poland*
e-mail: nurcinkaradeniz@iyte.edu.tr

Organic liquid electrolytes, commonly used in commercial Lithium-ion batteries, are susceptible to fire due to their low flash point, particularly at high voltages. This flammability raises safety concerns in practical applications [1]. Thus, current concerns over lithium-ion battery safety are leading to exciting developments in all solid-state lithium-ion batteries (ASSLIBs), fueled by the promise of unparalleled safety and boosted energy density. ASSLIBs eliminate the risks like leakage and combustibility associated with liquid electrolytes. Performance parameters of ASSLIBs such as cycle life, stability and capacity can be improved by both increasing the ionic conductivity of the electrolyte layer and improving the electrode/electrolyte interface [2]. A previous study in our group investigated the influence of substrate temperature on the surface, structural, and chemical properties of RF magnetron sputtered $LiCoO_2$ (LCO) thin films for ASSLIB cathodes [3]. Another study focused on the preparation of crystalline $Li_{0.5}La_{0.5}Ti_{1-x}Al_xO_3$ (LLTAlO) targets using conventional solid-state reactions. The effect of Al substitution on the lithium-ion conductivity of LLTO was investigated [4].

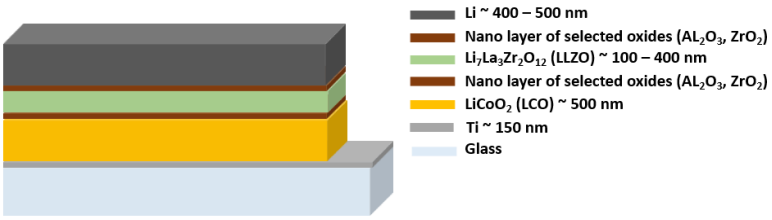

Figure 1. The schematic diagram of all solid-state thin film battery designed on a glass substrate.

This work focuses on the fabrication of thin film components for ASSLIBs that were prepared using RF magnetron sputtering for LCO and $Li_7La_3Zr_2O_{12}$ (LLZO), along with thermal evaporation for lithium metal. In our structure Titanium is used as a current collector, LCO is the cathode, LLZO is the electrolyte, and Li is the anode layer. Due to undesirable phases that may occur on both the cathode and anode of the electrolyte layer, the nanolayer of selected oxides will act as buffer layers (Fig.1). The cathode–electrolyte interface was carefully investigated using 2.85 nm Al_2O_3, ZrO_2, and Al_2O_3–ZrO_2 buffer layers deposited by atomic layer deposition (ALD) to improve contact and stability. The characterization of samples with SEM, XRD, Raman, XPS and electrochemical tests will be discussed and the design of efficient all solid-state batteries will be presented.

This research was supported by TUBITAK with project number 122N516 under MERANET program. The authors would like to acknowledge the facilities of Research and Application Center for Quantum Technologies (RACQUT) of IZTECH.

REFERENCES

[1] S. Liu, L. Zhou, J. Han, et al. Adv. Energy Mater. **12**, 2200660 (2022).
[2] C. Wang, J. Liang, J. T. Kim, X. Sun, Sci. Adv. **8**, eadc9516 (2022).
[3] P. Ozcan, N. Esen, A. Cantas, L. Ozyuzer, M. Ozdemir, K. Kosiel, A. Szerling, G. Aygun, Vacuum, **239**, 114439 (2025).
[4] S. Ulusoy, S. Gulen, G. Aygun, L. Ozyuzer, M. Ozdemir, Solid State Ion. **324**, 226-232 (2018).

ORCID: N. K. 0000-0001-5452-5513, N. E. 0009-0005-5580-2523, S. K. 0009-0001-2998-5582, E. A. 0000-0002-4763-9923, U. U. 0000-0003-4718-1243, A.C. 0000-0002-6536-5516 L. O. 0000-0001-7630-3938, M. O. 0000-0002-0453-6852, K. K. 0000-0001-5076-4621 A. S. 0000-0002-3664-467, R. S. 0000-0003-4072-2393, G. A. 0000-0003-0860-2914.

Electromagnetic Shielding Performance of Transparent ZTO/Ag/ZTO Multilayer Electrodes Deposited on Polymer Substrates

M. Ekmekcioglu[1,2], S. Akar[1,2], N. Karadeniz[1,2], S. Demirbas[1], F. Erbas[1], S. Surucu[3], N. Erdogan[3], G. Aygun[1], L. Ozyuzer[1,2] and M. Ozdemir[2]
[1]*Department of Physics, Izmir Institute of Technology, Urla, Izmir, Turkiye*
[2]*Teknoma Technological Materials Inc., IZTECH Campus, Urla, Izmir, Turkiye*
[3]*Turkish Aerospace Industries Inc., Advanced Material, Process and Energy Technology Center, Ankara, Turkiye*
e-mail: merveekmekcioglu@iyte.edu.tr

Advanced thin film coatings are extensively utilized in numerous critical sectors, including transportation vehicles, defense and aerospace platforms, space technologies, and electronic systems [1]. These coatings play a crucial role in minimizing the electromagnetic visibility of structures and enhancing their electromagnetic shielding performance. Among these, transparent conductive oxides (TCO) have gained prominence due to their combination of high optical transmittance, low sheet resistance, and compatibility with flexible or polymer-based substrates. Although Indium Tin Oxide (ITO) is the most widely adopted TCO due to its superior optical and electrical characteristics, its brittleness and high production cost have driven the search for viable alternatives [2]. Zinc Tin Oxide (Zn_2SnO_4, ZTO), characterized by its wide bandgap, high refractive index, excellent optical transparency, and ability to form uniform thin films even at relatively low deposition temperatures, which is advantageous for flexible polymer substrates, has emerged as a promising candidate [3]. To further enhance its functional performance, dielectric/metal/dielectric configurations, particularly ZTO/Ag/ZTO (ZAZ) structures, have been investigated for their ability to simultaneously provide high conductivity and high optical transparency [4,5]. In this work, ZAZ electrodes were deposited onto acrylic (Poly (methyl methacrylate)–PMMA) substrates via DC magnetron sputtering. Structural, morphological, optical, and electrical properties of electrodes were comprehensively characterized using XRD, SEM, AFM, Raman spectroscopy, and EDS. The resulting films exhibited an amorphous microstructure, smooth and uniform surface morphology, 89.2% optical transmittance at 550 nm, and sheet resistance in the range of 8–9 Ω/sq. These results demonstrate the suitability of ZAZ multilayer electrodes for electromagnetic shielding applications. In addition to experimental characterization, electromagnetic simulations were conducted using CST Studio Suite to assess the radar absorption performance of transparent ZAZ multilayer electrode structures. A three-layer polycarbonate model incorporating ITO and ZAZ thin films demonstrated an absorption bandwidth of 11.6 GHz between 3.0 and 14.6 GHz, achieving a maximum reflection loss of –16.1 dB. These findings confirm that transparent ZAZ multilayer electrodes not only represent an effective alternative to conventional ITO films but also serve as high-performance, broadband, and optically transparent electromagnetic shielding and radar absorbing material solutions for next-generation defense and aerospace systems.

This work was partially supported by TUBITAK TEYDEB project number 3230445. The authors would like to acknowledge the facilities of Research and Application Center for Quantum Technologies (RACQUT) of IZTECH.

REFERENCES

[1] A. F. Khan, Z. Ul Abadeen, M. B. Hanif, M. S. Saleem, K. Naveed, K. Bashir, I. Ahmad, Mater. Chem. Phys. **272**, 125009 (2021).
[2] O. Tuna, Y. Selamet, G. Aygun, L. Ozyuzer. J. Phys. D: Appl., **43**, 055402 (2010).
[3] M. Ekmekcioglu, N. Erdoğan, A. T. Astarlıoğlu, S. Yigen, G. Aygun, L. Ozyuzer, M. Ozdemir, Vacuum, **187**, 110100 (2021).
[4] F. Turkoglu, H. Koseoglu, M. Ekmekcioglu, A. Cantas, M. Ozdemir, G. Aygun, L. Ozyuzer, J. Mater. Sci.: Mater. Electron. **33**, 10955-10964 (2022).
[5] A. T. Astarlioglu, Y. Oz, E. Unal, N. B. Kilic, C. Celikli, M. Ozdemir, L. Ozyuzer, H. V. Demir, N. Erdogan, J. Phys. D: Appl. **57**, 325301 (2024).

ORCID: M. E. 0000-0002-8303-2264, S. A. 0009-0006-1449-5640, N. K. 0000-0001-5452-5513, S. D. 0009-0005-3990-2233, F. E. 0009-0000-4424-964X, N. E. 0000-0001-6891-7964, A. T. 0000-0002-5048-6286, L. O. 0000-0001-7630-3938, M. O. 0000-0002-0453-6852,

Effect of pulse energy on the formation of Laser-Induced Periodic Surface Structure on Nb/Ti multilayer thin films

S. Petrović[1], N. Božinović[1], V. Rajić[1], D. Canteli[2], C. Munoz Garcia[2], C. Molpecres[2]
[1]*Vinča Institute of Nuclear Sciences, University of Belgrade, P.O.Box 522, 11001 Belgrade, Serbia*
[2]*Centro Laser, Universidad Politecnica de Madrid, Alan Turing 1, 28038 Madrid, Spain*
e-mail: spetro@vin.bg.ac.rs

The possibilities of creating Laser-Induced Periodic Surface Structure (LIPSS) on Nb/Ti multilayer structures were investigated through surface modification with picosecond laser radiation. Using DC ion sputtering, fifteen (Nb/Ti) bilayers were deposited to create multilayer thin films with a total thickness of 440 nm on (100) Si wafers. Dynamic laser modifications, such as laser-etched lines, were performed using picosecond (15 ps) laser pulses of a Nd: YVO4 laser operating at 532 nm, with pulse energies ranging from 1.5 to 2.8 µJ. The development of LIPSS was accompanied by different morphological features depending on the applied pulse energy; the different absorbed energy stimulated diverse processes in a multilayer 15x(Nb/Ti)/Si system. By gradually increasing the pulse energy at a constant scanning speed (5 mm s^{-1} and 1 mm s^{-1}), the development of LIPSS included the following morphological changes: (i) initial surface melting with the formation of clusters, (ii) elongation of melted regions and formation of HSFL (high spatial frequency LIPSS); (iii) separation of droplets and their arrangement in LSFL (low spatial frequency LIPSS); (iv) cracks appearance corresponding to positions of LSFL; (v) material recrystallization; and (vi) material ablation at the highest pulse energies. The analysis of changes in composition after laser modification revealed the presence of oxygen in a higher concentration than in the untreated area, realizing the possibility of forming an ultra-thin oxide layer composed of Nb- and Ti-oxides. The obtained results for the development of periodic structures in the form of LIPSS, depending on the pulse energy (fluence) at the selected scan speeds, provide a relatively satisfactory prediction of the LIPSS formation with the desired morphological characteristics.

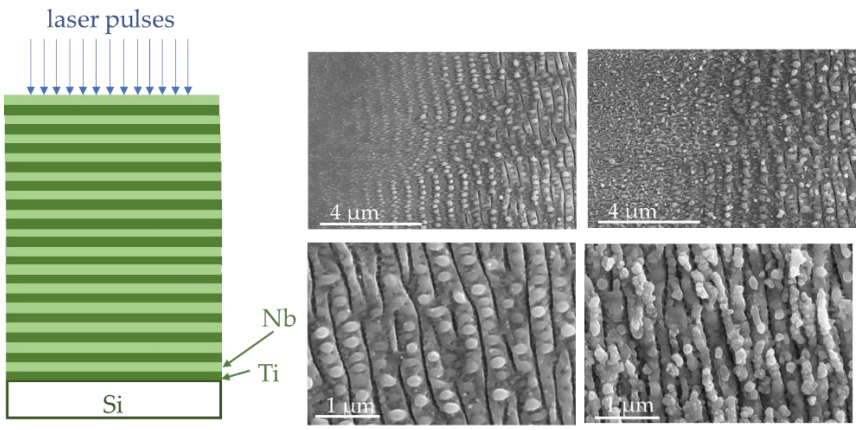

Figure 1. Schematic view of the multilayer 15x(Nb/Ti)/Si system with SEM images of the centre of the laser-inscribed lines on the surface of the 15x(Nb/Ti)/Si multilayer system at a constant scanning speed of 5 mm s^{-1} for: 1.5 µJ, 1.8 µJ, 2.0 µJ, and 2.4 µJ.

REFERENCES

[1] S. Petrovic, et al. J. Appl. Phys. 122, 115302 (2017)
[2] S. Petrovic, et al. Materials Chemistry and Physics 143, 530-535 (2014)

ORCID: S.P. 0000-0003-0930-6455, N.B. 0000-0002-4762-4115, V.R. 0000-0001-7053-572X

Magnetron Sputtered Grown $LiCoO_2$ and Li7La3Zr2O12 Thin Film Layers for All-Solid-State Lithium-ion Batteries

N. Esen[1], S. Karpuz[1], N. Karadeniz[1,2], L. Ozyuzer[1,2], M. Ozdemir[2], U. Unal[3], A. Cantas[4], K. Kosiel[5], A. Szerling[5], R. Socha[6], G. Aygun[1]

[1]*Department of Physics, Izmir Institute of Technology, Izmir, Türkiye*
[2]*Teknoma Technological Material Inc., IZTECH Campus, Izmir, Türkiye*
[3]*Department of Chemistry, Koc University, Istanbul, Türkiye*
[4]*Department of Electric and Energy, Pamukkale University, Denizli, Türkiye*
[5]*Łukasiewicz Research Network-Institute of Microelectronics and Photonics, Warsaw, Poland*
[6]*CBRTP S.A., 36 Czarnowiejska St. 30-054 Cracov, Poland*
e-mail: gulnuraygun@iyte.edu.tr

All solid-state batteries have attracted considerable research interest in recent years due to their potential to provide higher energy density, improved thermal stability, and enhanced safety compared to conventional liquid-electrolyte lithium-ion batteries [1,2]. Among the key solid electrolyte materials, $Li_7La_3Zr_2O_{12}$ (LLZO) stands out for its high ionic conductivity and good chemical stability [3]. Moreover, $LiCoO_2$ (LCO), a widely used cathode material, continues to be investigated in solid-state systems, particularly with respect to its interfacial compatibility with solid electrolytes [4]. To mitigate issues such as interfacial chemical instability and lithium dendrite formation between LLZO and LCO, an Al_2O_3 buffer layer grown by atomic layer deposition (ALD) has been introduced as an interfacial modification strategy. In this context, the crystal structure of LLZO, its lithium-ion conduction mechanisms, and its interaction with LCO through the Al_2O_3 interlayer are considered key physical parameters in evaluating and optimizing the performance and cycle life of all solid-state lithium-ion battery (ASSLIB) technologies.

This study focuses on the deposition and characterization of thin film layers for ASSLIBs. LCO and LLZO layers were successfully deposited by radio-frequency magnetron sputtering (Fig.1 (a)), while the integration of lithium metal as the anode layer is planned for future stages of the project by thermal evaporation. LLZO target was fabricated to obtain sputtering material for thin film deposition. Titanium was selected as the current collector due to its high electrical conductivity and interfacial stability. To enhance structural integrity and electrochemical performance, thin oxide buffer layers were incorporated at both the cathode–electrolyte and anode–electrolyte interfaces. Al_2O_3 buffer layer between cathode and electrolyte layer was grown by ALD technique (Fig.1 (b)) to improve interfacial contact and chemical stability of ASSLIBs. The resulting multilayer thin film structures were comprehensively characterized using SEM, XRD, Raman spectroscopy, XPS, and electrochemical measurements. Details of the fabrication and characterization processes will be discussed.

Figure 1. Images of **(a)** glove box and **(b)** ALD systems

This research was supported by TUBITAK with project number 122N410 under MERANET program. The authors would like to acknowledge the facilities of Research and Application Center for Quantum Technologies (RACQUT) of IZTECH.

REFERENCES

[1] P. U. Nzereogu, et al., Hybrid Advances, **8**, 100339 (2025).
[2] S. Ulusoy, et al., Solid State Ionics, **324**, 226-232 (2018).
[3] R. Murugan, V. Thangadurai, W. Weppner, Angew. Chem. Int. Ed., **46**, 7778–7781 (2007).
[4] P. Ozcan, et al., Vacuum, **239**, 114439 (2025).

ORCID: N. E. 0009-0005-5580-2523, S. K. 0009-0001-2998-5582, N. K. 0000-0001-5452-5513, L. O. 0000-0001-7630-3938, M. O. 0000-0002-0453-6852, U. U. 0000-0003-4718-1243, A.C. 0000-0002-6536-5516, K. K. 0000-0001-5076-4621 A. S. 0000-0002-3664-467, R. S. 0000-0003-4072-2393, G. A. 0000-0003-0860-2914.

Laser-Induced Graphene and MXene on Biocompatible Polymer Substrates as Physical Sensors

M. Spasenović, T. Vićentić, A. Gavran, V. Vojnović, I. Pešić, K. Tošić, M. Rašljić-Rafajilović, S. Ilić, M. V. Pergal
Center for Microelectronic Technologies, Institute of Chemistry, Technology and Metallurgy – National Institute of the Republic of Serbia, Belgrade, Serbia
e-mail: marko.spasenovic@ihtm.bg.ac.rs

Laser-induced graphene (LIG) offers a highly adaptable platform for applications such as physiological sensing, electrode fabrication, gas detection, and biosensing [1, 2]. Traditionally, research has centered on commercial polyimide (PI) tape as the substrate for LIG production. While PI enables the formation of LIG with favorable electronic properties, its limited adhesion and lack of stretchability pose challenges for wearable device integration. To overcome these constraints, we introduce a novel strategy: laser induction of graphene on biocompatible, synthesized cross-linked polymers. These include sodium alginate, PDMS/PEG composites, cross-linked polyurethanes (PUs) derived from ethoxypropyl-terminated PDMS macrodiol, and custom-synthesized polyimides. These materials exhibit desirable mechanical strength, non-cytotoxicity, and biocompatibility, making them promising candidates for wearable sensor platforms. Our study systematically identifies optimal chemical formulations and laser processing conditions for generating LIG on these substrates. Additionally, we explore MXene ($Ti_3C_2T_x$) layers as alternative active sensing components. The resulting devices are thoroughly characterized using optical, mechanical, biological, and chemical techniques. Finally, we demonstrate the real-world utility of LIG and MXene-based wearable patches for monitoring vital signs such as heartbeat, respiration, and limb movement. These findings lay the groundwork for next-generation, biocompatible, unobtrusive, and cost-effective thin-film sensors designed for continuous physiological monitoring.

This research was supported by the Science Fund of the Republic of Serbia, #4950, Polymer/graphene heterostructures for physiological sensors – Polygraph.

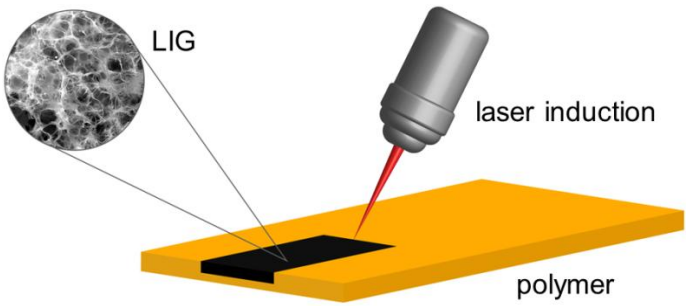

Figure 1. Representation of Laser Induction of Graphene on Polymer Substrate.

REFERENCES
[2] Wang, M., Yang, Y., and Gao, W., *Trends Chem*. **3,** 969-981 (2021).
[3] Vićentić, T., et al, *Sensors* **22**, 6326 (2022).

ORCID: M.S. 0000-0002-2173-0972, T.V. 0000-0002-3460-6137, A.G. 0009-0004-7465-3087, V.V. 0009-0005-2304-0958, I.P. 0009-0005-2304-0958, K.T. 0000-0003-1141-4340, M.R.R. 0000-0001-8170-746X, M.V.P. 0000-0001-6078-2006

All optical fiber whispering gallery mode resonator

D. N. Wang[1], Y. L. Mei[2], Qiaoben Wang[2] and Chao Wang[3]
[1]*College of Urban Transportation and Logistics, Shenzhen Technology University, Shenzhen, China*
[2]*College of Optical and Electronic Technology, China Jiliang University, Hangzhou 310018, China*
[3]*School of Future Technology, Shenzhen Technology University, Shenzhen, China*
e-mail: wangdongning@sztu.edu.cn

Whispering gallery mode (WGM) resonator can strongly confine light within the structure by continuous total internal reflection [1], and is widely used in optical filters, modulators, micro-lasers, frequency comb generators, nonlinear optics and high-sensitivity sensor devices. However, most of WGM resonators are usually discrete optical devices, which have integration difficulties with optical fiber system.

Here we present a new type of optical fiber WGM resonator based on cylindrical cavity, which is located in the multimode fiber (MMF) core as shown in Fig. 1. When the light transmission path in the fiber core is tangent to the cylindrical cavity wall, it is coupled into the cylindrical cavity through the evanescent field, circulates along the cylindrical cavity wall and excites WGM resonance in the glass wall before leaving the cylindrical cavity in the same tangential path and traveling along the fiber core again.

The WGM resonator is fabricated by femtosecond laser micromachining together with fast hydrofluoric acid etching techniques. Firstly, a ring structure is carved on the surface of the MMF. Then the focused laser beam moves downward to start inscribing the same ring structure again. Such a process continues until a cylindrical structure is formed, as shown in Fig. 2(a). Next, a small amount of hydrofluoric acid solution is dropped at the cylindrical structure position to from a cylindrical cavity as shown in Fig. 2(b).

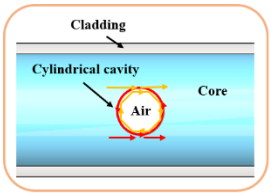

Figure 1. Schematic of the WGM resonator

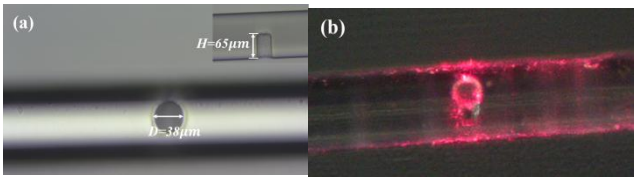

Figure 2. Microscope image of the WGM resonator. (a) Top view. Inset: the cross-section view. (b) Top view under the red light illumination.

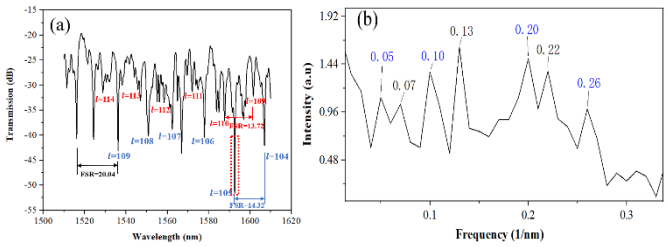

Figure 3. (a) The transmission spectrum of the optical fiber WGM cylindrical cavity resonator with diameter of 38 μm. (b) The corresponding spatial frequency spectrum.

Fig. 3(a) shows the transmission spectrum of the WGM resonator. The corresponding spatial frequency spectrum is shown in Fig. 3(b). It can be observed that the first two peaks are located at 0.05 nm^{-1} and 0.07 nm^{-1}, respectively, and the rest peaks are multiples of these two peak frequencies. It can be determined that these two peaks correspond to WGM resonator operation.

REFERENCES

[1] A. Matsko and V. Ilchenko, IEEE J. Sel. Topics Quantum Electron., 12, 3 (2006).

ORCID: D. N. Wang 0000-0002-7748-4272

Multifractal analysis of heart dynamics after running with PPG sensor

D. B. Stojanović, A. Maluckov, M. Miletić, and J. Petrović
Vinca Institute of Nuclear Sciences- National Institute of the Republic of Serbia, University of Belgrade, Belgrade, Serbia
e-mail: sandram@vin.bg.ac.rs

Heart dynamics changes markedly at increased effort, which is used routinely to assess the heart condition, for example via electrocardiographic (ECG) stress test. However, the intricate nonlinear changes in heart dynamics are not easy to measure during short routine tests, but the ECG holter recordings are used instead [1]. Thereby, heart-rate variability is used as a base biomarker. The problem is that it requires annotation of heartbeats, which can be a cumbersome process in a noisy out-of-hospital measurement, such as holter around-the-clock measurement or in fitness rooms. Moreover, while the market is saturated by new wearables measuring mechanical function of the cardiovascular system, little attention has been paid to exploit them in assessment of complex heart dynamic.

To overcome these limitations, we perform a multifractal analysis on 30-second recordings of photoplethysmogram (PPG), ECG, accelerometer (ACC), and phonocardiogram (PCG) signals. The data stem from the SensSmartTech study [2,3], involving synchronized multimodal physiological recordings collected at rest, immediately after treadmill exercise, and during recovery. We focus here on the PPG signal due to its suitability for wearable cardiovascular monitoring**.**

As a benchmark of fitness level, we adopt the Heart Rate Recovery (HRR) index, a clinically validated marker of autonomic reactivation following exertion [4]. The multifractal spectrum was used to extract key features related to cardiovascular complexity—namely, the position of the spectral peak, spectrum width, and asymmetry. These features were used to classify fitness states via supervised logistic regression.

Classification results are presented for the PPG sensor, with and without K-fold cross-validation and class balancing. Cross-validation improves stability and generalizability of the model, yielding better separation between physiological states. Our results demonstrate that short-term, optically acquired PPG signals—when analyzed via multifractal dynamics—can serve as a compact, non-invasive tool for characterizing post-exercise heart adaptation and individual fitness levels.

REFERENCES

[1] P. Ivanov et al, Nature 399, 461-465, 1999.
[2] J. Petrović et al., 11th International Conference on Electrical, Electronic and Computing Engineering (IcETRAN), Nis, Serbia, IEEE, 1-5, 2024.
[3] A. Lazović et al.. PhysioNet. https://doi.org/10.13026/fy9p-n277, 2024.
[4] D. Mongin, et al. Research in Sports Medicine 31, 157-170,2023.

ORCID: A.M. 0000-0002-6474-360X, M.M. 0000-0002-8476-4141, J.P. 0000-0002-1002-241X

Modelling of Terahertz Quantum Cascade Laser Self-Mixing Dynamics

N. Stanojević[1, 2], N. Vuković[1], M. Ignjatović[1] and J. Radovanović[1]
[1]*School of Electrical Engineering, University of Belgrade, Serbia*
[2]*Vlatacom Institute of High Technologies, Belgrade, Serbia*
e-mail: novak.stanojevic@vlatacom.com

Quantum cascade lasers operating at terahertz frequencies (THz QCLs) [1, 2] emit in the traditionally hard-to-reach far-infrared part of the spectrum, which has enabled their growing use in fields such as medical diagnostics, chemical detection, and imaging. In this work, we use a theoretical model developed in [3] based on the effective semiconductor Maxwell–Bloch equations (ESMBEs) [4] to study the dynamics of a THz QCL in a Fabry–Perot (FP) configuration. The model incorporates the key features of the semiconductor active medium, such as asymmetric, frequency-dependent gain and refractive index, as well as phase–amplitude coupling described by the linewidth enhancement factor. This approach accounts for standing wave formation in the resonator, resulting in spatial hole burning. We study the self-mixing dynamics of an experimentaly grown GaAs/AlGaAs bound to continuum THz QCL designed for emission at 2.0 THz [5] using transport parameters calculated via the density matrix model. The simulation results show that adding external feedback for a QCL operating at the threshold current density leads to the spectrum of the emitted light changing from a single-mode to a multimode regime as well as a significant increase in both the average output power and steady-state time. The model predicts high sensitivity of the QCL output power to changes in the external resonator length. For numerical calculation of the ESMBEs we use the finite difference method to discretize the variables both in time and space and solve in a travelling wave manner.

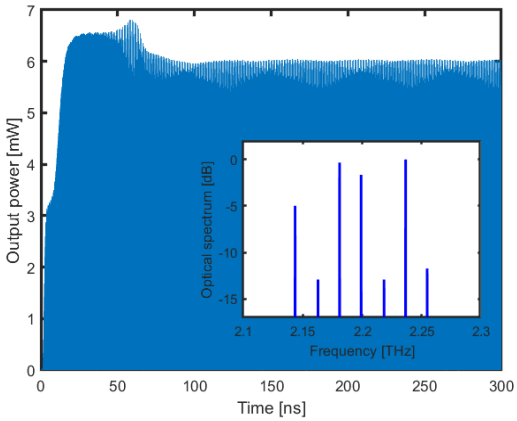

Figure 1. Output power waveform at threshold current for a QCL with external feedback. The inset shows the optical spectrum of the emitted light where the QCL is emitting in a multimode regime.

Acknowledgment: This work was financially supported by the Vlatacom Institute of High Technologies under project 178, the Ministry of Science, Technological Development and Innovation of the Republic of Serbia under contract number: 451-03-65/2024-03/200103, Science Fund of the Republic of Serbia, Grant No. 10504, "Ultra-short pulsations from TERAhertz quantum cascade laser using passive mode-LOCKing with graphene saturable absorber"-TERALOCK, European Cooperation in Science and Technology (COST) Action CA21159 PhoBioS.

REFERENCES

[1] J. Faist, et al., Science 264, 553-556 (1994).
[2] R. Köhler, et al., Nature, 417(6885), 156-159, (2002).
[3] C. Silvestri, L. L. Columbo, M. Brambilla, and M. Gioannini, Opt. Express 28(16), 23846–23861, (2020).
[4] C. Z. Ning, R . A. Indik, and J. V. Moloney, IEEE J. Quantum Electron. 33(9), 1543–1550, (1997).
[5] A. Demić, et al. IEEE Transactions on Terahertz Science and Technology 7, 368–377, (2017).

ORCID: N.S. 0009-0007-5122-2219, N.V. 0000-0002-4941-2546, M.I. 0000-0001-6066-8764, J.R. 0000-0003-3031-7802

Wavelength demultiplexers based on coupled waveguide arrays with nonuniform lengths

K. Bugarski[1], M.G. Stojanović [1], A. Maluckov [1] and J. Petrović[1]
[1]*Vinca Institute of Nuclear Sciences, Belgrade, Serbia*
e-mail: kolja.bugarski@vinca.rs

We propose a demultiplexer based on linearly coupled waveguide array, implemented through a simple photonic lattice layout. Straight waveguides minimize propagation losses then bent waveguides, while choosing appropriate distances between waveguides enables us to tune the output wavelength and bandwidth.

For two input wavelengths, spatial divide is achieved when a shorter wavelength perfectly transfers it's power from first to last, then back to the first waveguide, while longer wavelength's power perfectly transfers from the first to last waveguide for the same length of waveguide array. Any waveguide array which supports periodic propagation and perfect transfer of light supports such multiplexing [1]. However, by selecting Clebsch–Gordan coupling coefficients, bandwidth can be controlled simply by changing the number of waveguides in an array, with the full-width at half-maximum narrowing with the square root of the waveguide number. An experimental proof of this concept was provided by fabricating the demultiplexers in borosilicate glass using femtosecond laser writing [2, 3].

Building upon these designs, we propose a more elaborate structure that introduces non-uniform waveguide lengths to enhance spectral separation for multiple wavelengths. In this configuration, only the input waveguide and its nearest neighbour retain equal lengths, while each subsequent waveguide is progressively shorter. We show results for a 3-wavelength demultiplexer with the maximum insertion loss of $1.22dB$ and the minimum cross talk of $-22.02dB$. For a 4-wavelength demultiplexer the maximum insertion loss is $2.76dB$ and the minimum cross talk is $-17.43dB$.

REFERENCES

[1] J. Petrović, J. Kršić, A. Maluckov, J.J.P Veerman "High-density optical interconnects based on self-imaging in coupled waveguide arrays", J. Opt. Las. Technol. 163, 109381 (2023)
[2] M. G. Stojanović, P. Vildoso, K. Bugarski, P. M. Parra, A. Maluckov, R. A. Vicencio, and J. Petrović, "Wavelength demultiplexers based on finite photonic lattices" J. Opt. 27, 055801 (2025).
[3] D. Guzmán-Silva, G. Cáceres-Aravena, and R. A. Vicencio, "Experimental Observation of Interorbital Coupling" Phys. Rev. Lett. 127, 066601 (2021).

ORCID: K.B. 0000-0002-4924-1564, M.G.S. 0000-0002-4376-7610, A.M. 0000-0002-6474-360X, J.P. 0000-0002-1002-241X

Method of registration of the different times of optical signals in multichannel laser systems

Z. I. Valerievich[1], K. P. Vyacheslavovich[1], T. A. Alekseevich[1], K. V. Gennadievich[1], A. Y. Dmitrievich[1]
[1]*The Federal State Unitary Enterprise Dukhov Automatics Research Institute (VNIIA), Moscow, Russia*
e-mail: igor.denikin7@yandex.ru

Direct conversion interferometers began to be used in experiments on measuring the mass velocity of matter with the advent of lasers, since laser radiation has sufficient spatial and temporal coherence for measurements. Initially, they were different variations of a two-beam interferometer [2, 3]. With the development of technologies, the improvement of photo recording systems and, in particular, telecommunications equipment, the PDV (Photonic Doppler Velocimeter) system has become widespread today [1, 4].

Synchronization of multichannel PDV complexes is an urgent task, since in order to study fast gas-dynamic processes it is necessary to record the change in the velocity of an object at different points on its surface, but due to the fact that the acceleration of the object under study is uneven, a problem arises associated with determining the initial time of surface motion. Initially, this problem was solved by synchronously supplying an electric pulse to start the recording complexes and to start the gas-dynamic process. But this solution does not take into account the difference in optical paths in different channels of the used complexes, which may occur during the laying of the fiber route from the experimental assembly to the equipment. At present, a method is used to determine the time difference of optical lines of multichannel complexes of the PDV type, the error of which can reach up to 100 ns. In this regard, a method for recording the time difference is proposed, allowing synchronization of multichannel complexes of the PDV type, due to probing fiber bays with a laser broadband pulse, which will increase the accuracy of the experimental results to 3 ns.

The aim of the work is to develop a method for binding different types of fiber-optic measuring laser-heterodyne complexes to a single point in time. The proposed synchronization method consists of mixing laser pulses into the channel of the complex so that reference time marks are registered on the experimental oscillogram, which show the time of passage of the optical signal along the fiber line.

REFERENCES:
[1] B.J. Jensen, D.B. Holtkamp, P.A. Rigg, D.H. Dolan / Accuracy limits and window corrections for photon Doppler velocimetry // *Journal of Applied Physics*, № 101, p. 013523, doi: 10.1063/1.2407290, 2007.
[2] Yu.V. Kolomiytsev / Interferometers. // Leningrad: "Mashinostroenie". 296 p., 1976.
[3] V.P. Klochkov, L.F. Kozlov, I.V. Potykevich, M.S. Soskin / Laser anemometry, remote spectroscopy and interferometry // Kyiv: Naukova Dumka, 759 p., 1985.
[4] O.T. Strand, D.R. Goosman, C. Martinez, T.L. Whitworth / Compact system for highspeed velocimetry using heterodyne techniques // Rev. Sci. Instr., Vol. 77, № 8, 083108, doi: 10.1063/1.2336749, 2006.

Transition from normal to inverted band structure type in HgTe/CdTe nanowires

D. Z. Jakovljević[1], V. V. Arsoski[1] and M. Ž. Tadić[1]
[1]*School of Electrical Engineering, University of Belgrade,*
P.O. Box 35 – 54, 11120 Belgrade, Serbia
e-mail: jakovljevic@etf.bg.ac.rs

In recent years, HgTe-based structures have raised significant attention due to their feature to exhibit the quantum spin Hall (QSH) effect [1], a topologically nontrivial phase characterized by the presence of helical edge or surface states protected by time-reversal symmetry. Although initial studies of the QSH effect have been focused on graphene [2], it was later discovered that this phase is more likely to manifest in materials composed of heavy elements. Here, the strong spin-orbit coupling arising from relativistic effects plays a critical role. Shortly after theoretical prediction, the QSH effect was experimentally confirmed in thin HgTe/CdTe quantum wells [3]. Beyond two-dimensional systems, theoretical investigations have shown that topological phases can also emerge in low-dimensional structures such as quantum wires [4], where quantum confinement leads to significant modifications of the electronic band structure.

In this work, we investigate the electronic properties of HgTe/$Cd_xHg_{1-x}Te$ nanowires considering both cylindrical and square cross-sectional geometries. The band structure is calculated using the Kane $\mathbf{k} \cdot \mathbf{p}$ theory within the framework of the eight-band model, which subtly captures the coupling between the Γ_6, Γ_7, and Γ_8 bands [5]. Material parameters, such as band edges and effective masses, are assumed to change abruptly at interfaces, while the band offsets are interpolated linearly with the mole fraction.

Our results indicate that band inversion can occur in the structures studied, revealing the presence of a topologically nontrivial phase. The transition point for band inversion strongly depends on the nanowire's cross-sectional geometry, dimensions, and the compositional profile of the surrounding barriers. Considering the possibility of switching topological phases by an external electrical field, these findings highlight the potential of nanowire heterostructures as a versatile platform for next-generation electronic and spintronic devices.

REFERENCES

[1] B. A. Bernevig, T. L. Hughes, S. C. Zhang, Science **314**, 1757 (2006).
[2] C. L. Kane and E. J. Mele, Phys. Rev. Lett. **95**, 226801 (2005).
[3] M. König, S. Wiedmann, C. Brüne, A. Roth, H. Buhmann, L. W. Molenkamp, X. Qi, S. Zhang, Science **318**, 766 (2007).
[4] R. Li, Phys. Scr. **100,** 055918 (2025).
[5] E. G. Novik, A. Pfeuffer – Jeschke, T. Jungwirth, V. Latussek, C. R. Becker, G. Landwehr, H. Buhmann, and L. W. Molenkamp, Phys. Rev. B **72**, 035321 (2005).

ORCID: D. J. 0000-0002-8635-6117, V. A. 0000-0002-9326-7809

Next-Generation Load Sensing: FBG Sensors vs. Classic Strain Gauge Approach

J. S. Bajić[1], A. Joža[1], M. Dramićanin[1], M. Kovačević[2]
[1]*Faculty of Technical Sciences, University of Novi Sad, Novi Sad, Serbia*
[2]*Faculty of Sciences, University of Kragujevac, Kragujevac, Serbia*
e-mail: bajic@uns.ac.rs

Load cells represent one of the most important types of sensors in force measurement applications across various industries, with conventional strain gauge-based load cells being the standard one [1]. However, Fiber Bragg Grating (FBG) sensors are emerging as a promising alternative due to their unique measurement features [2], [3], [4]. In this work an industrial-grade (FBG) load cell designed for demanding applications is presented as a next-generation alternative to conventional strain gauge load cells. Accordingly, a comprehensive study and comparison between FBG-based and traditional strain gauge load cells is conducted, focusing on performance metrics such as accuracy, sensitivity, durability, and environmental resilience. Experimental evaluation conducted in laboratory conditions under different stress and temperature inputs, confirms that FBG load cells can achieve precision comparable to commercial strain gauge systems while offering unique features like additional outputs such as temperature and torque, as well as remote sensing and spectral multiplexing. Despite higher initial costs, the scalability, robust design, and potential of operability in extreme conditions provide FBG load cells a significant competitive edge important in demanding industries like aerospace, automotive, and smart manufacturing.

Fig. 1 illustrates sensors evaluated and compared in this work. In Fig. 1a conventional strain gauge load cell is depicted, while FBG-based cell is given in Fig. 1b. Equivalent response of the evaluated load cells are presented in Fig. 1c under tension and compression loading.

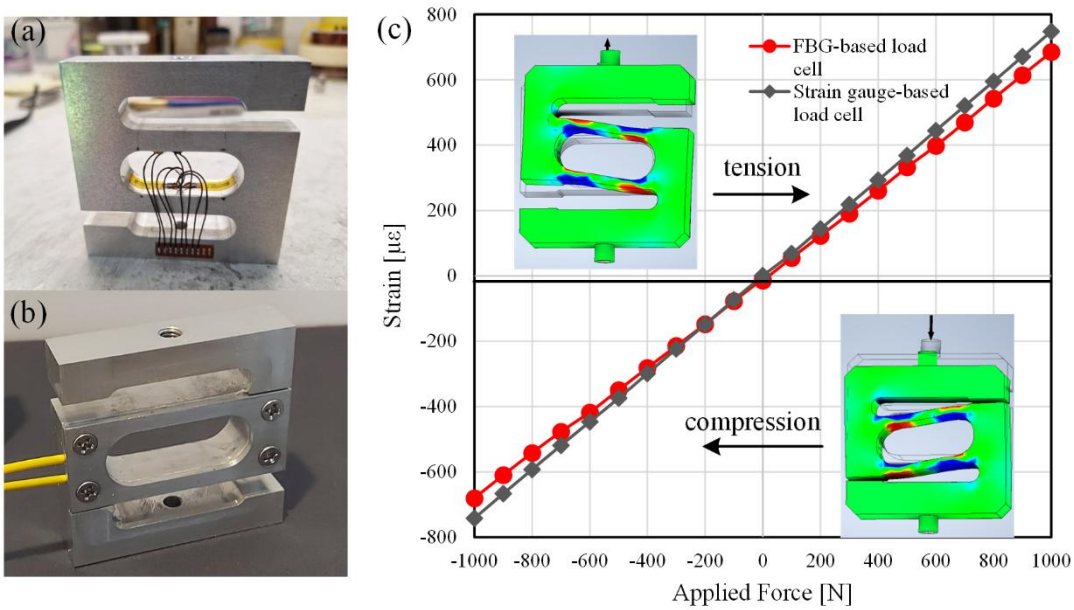

Figure 1. a) Strain gauge load cell, b) FBG load cell and c) Equivalent response of the evaluated load cells under tension and compression loading.

REFERENCES

[1] O. S. Al-Dahiree, M. O. Tokhi N. H. Hadi, N. R. Hmoad, R. A. R. Ghazilla, H. J. Yap, A. Albaadani, Sensors, 22 (2022).
[2] G. Ma, C. Li, J. Jiang, Y. Luo, Y. Cheng, Cold Regions Science and Technology, 71 (2012).
[3] A. Gautam, A. Kumar, K. Kinjalk, J. Thangaraj, V. Priye, IEEE Sensors Journal, 20 (2020).
[4] M. Bocciolone, G. Bucca , A. Collina, L. Comolli, Journal of Rail and Rapid Transit (2018).

ORCID: J.S.B. 0000-0002-8823-5423, A.J. 0000-0002-0768-6864,
M.D. 0000-0002-9079-0864, M. K. 0000-0001-7643-9886

High-power gold vapor laser operating in ultraviolet and deep ultraviolet spectral ranges

I. Kostadinov, K. Temelkov, S. Slaveeva and G. Yankov
Georgi Nadjakov Institute of Solid State Physics, Bulgarian Academy of Sciences, 72 Tzarigradsko Chaussee, 1784 Sofia, BULGARIA
e-mail: temelkov@issp.bas.bg

Metal vapor lasers operating on the atomic self-terminating transitions of different chemical elements, such as copper (Cu), gold (Au), strontium, lead, iron, etc., are still very promising, because of the possibility to deliver significant average laser power at relatively high efficiency in any spectral range, namely from ultraviolet (UV) to middle infrared ones. Even the average output power of the copper vapor laser (CVL) is still the highest one in the visible spectral diapason so far. Nevertheless, the well-developed UV laser sources, such as excimer lasers and frequency-converted solid state lasers, prevail in the UV spectral range. Unfortunately, the gold vapor laser (GVL) is the only one laser source that operates on the atomic Au self-terminating transition in the UV spectral diapason. The GVLs are less researched and developed in comparison with the CVLs and their various versions, due to the severe difficulties related to the extremely high operating temperature for both atomic Au 627.8- and 312.2-nm lines and the impossibly contradictory gas-discharge conditions for the UV laser line. The highest average output power of 20 W at the 627.8-nm line has been delivered by a laser tube with an active volume of 2376 cm^3 (55 mm inside diameter and 100 cm length) at a pulse repetition frequency of 5.5 kHz and average electrical power of 15.7 kW [1]. A laser tube with an active volume of 232 cm^3 (22 mm inside diameter and 61 cm length) has produced at the 627.8-nm line an average laser power of 11.6 W at a pulse repetition frequency of 27.5 kHz and average electrical power of 3.9 kW [2]. These results correspond to a wall-plug efficiency of 0.30 % and a specific average output power (SAOP) of 0.050 $W.cm^{-3}$ [2], which are the highest efficiency and SAOP reported for the GVL. For comparison, the efficiency and SAOP presented in [1] are 0.13 % and 0.008 $W.cm^{-3}$, respectively. The record-high average output power of 1.20 W has been declared in 1978 [3] at the atomic Au 312-nm line by a laser tube with an active volume of 140.7 cm^3 (16-mm inside diameter and 70-cm length). Since then the only observed UV laser oscillation at the atomic Au 312.2-nm line reported only in [2] has been so weak that it has been unmeasurable.

An active volume scaling of the GVL is carried out. The highest average laser power of 1.04 W at the atomic Au 312-nm line is delivered by a laser tube LT1 with an active volume of 49.5 cm^3 (10-mm inside diameter and 63-cm length), i. e. SAOP is 17.8 $mW.cm^{-3}$. The highest SAOP of 46.5 $mW.cm^{-3}$, i. e. more than 5 times higher than the SAOP reported in [3], is produced through a discharge tube LT2 delivering average laser power of 251 mW with an active volume of 5.4 cm^3 (a 4-mm bore and an active length of 43 cm). Polarized diffraction-limited ($M^2 = 1$) laser beam is produced for the first time placing the LT2 in a negative-branch unstable cavity with magnification $M = 20$, which incorporates a Glan prism for linear polarization of the laser beam. Laser beam is focused with a 25-cm concave mirror into a 5-mm-long nonlinear crystal made of β-Barium Borate (BBO) and recollimated by a 15-mm lens made of CaF_2. DUV laser oscillation is obtained for the first time at a new spectral line with a wavelength of 208.5 nm via Sum Frequency Generation (SFG) of the two atomic Au 312.2- and 627.8-nm lines.

Acknowledgements: This work was supported by Bulgarian National Science Fund under Grant KP-06-H77/8 of 04.12.2023.

REFERENCES

[1] S. Gabay, I. Hen, M. Lando, Proceedings of SPIE 1225, 260 (1990).
[2] G. D. Marshall, D. W. Coutts, IEEE Journal of Quantum Electronics 49(8), 711 (2013).
[3] S. V. Markova, G. G. Petrash, V. M. Cherezov, Quantum Electronics 5(7), 904 (1978).

ORCID: I.K. 0009-0000-1877-1530, K.T. 0000-0002-5540-9992, S.S. 0000-0003-0800-4885, G.Y. 0009-0008-4831-7871

High-power ultraviolet laser system based on frequency-converted copper vapor laser

I. Kostadinov, K. Temelkov, S. Slaveeva, G. P. Yankov and L. Stoychev
Georgi Nadjakov Institute of Solid State Physics, Bulgarian Academy of Sciences, 72 Tzarigradsko Chaussee, 1784 Sofia, BULGARIA
e-mail: stefka@issp.bas.bg

Precise micromachining with laser ablation requires ultraviolet and deep ultraviolet (UV and DUV) laser radiations, since the processed area size after focusing linearly depends on the laser radiation wavelength. In addition to the high resolution, the UV and DUV laser radiations have sufficiently high enough photon energy to induce some phenomena in different materials, such as material and its surface modification, fluorescence, image recording, etc. Nonlinear frequency conversion is a well-known method for oscillating in the UV and DUV spectral ranges. Several UV and DUV laser sources have been well developed and investigated, such as frequency-quadrupled and frequency-tripled Nd:YAG and Nd:YLF lasers, frequency-doubled argon ion lasers, and frequency-doubled dye lasers.

DUV laser sources based on nonlinear frequency conversion of the copper vapor laser (CVL) radiation at the atomic copper (Cu) 510.6- and 578.2-nm lines is quite competitive alternative. DUV radiation at 255.3 nm, 289.1 nm and 271.2 nm has been obtained by frequency doubling the CVL output and Sum Frequency Generation (SFG) of the two atomic Cu lines [1-3]. Unfortunately, the CVL pulse energy and hence the CVL peak pulse power at laser pulse duration of about 15–40 ns are considerably lower in comparison with the frequency-converted solid state lasers, which requires the laser beam focusing and hence increases the hazard of optical breakdown of the nonlinear crystal. Applying spherical optics for the laser beam focusing in a β-barium borate (BBO) nonlinear crystal, the maximal DUV laser power at the 255.3-nm laser line has been 450 mW through frequency doubling the 510.6-nm output [1]. Utilizing cylindrical optics instead of spherical ones to reduce the hazard of nonlinear crystal damage at high average pump laser power [2, 3], the DUV laser power has been consecutively increased from 1.3 W [2] to 3 W via nonlinear BBO crystals [3] and up to 15 W with a nonlinear crystal made of cesium lithium borate (CLBO) [3].

Various types of Master Oscillator – Power Amplifier (MO–PA) Cu and copper bromide (CuBr) vapor laser systems are studied as pump laser sources for a 15-mm-long BBO nonlinear crystal. Focusing is made by spherical mirrors and lenses with focusing distances of 20 cm, 40 cm, 75 cm, and 100 cm. The highest average laser power at 255.3-nm line is 1.6 W at an average pump power of 7.2 W, i. e. the frequency-conversion efficiency is 22.2 %. Using a new innovative technique to diminish the optical breakdown hazard, which consists in the laser beam aperturing in horizontal direction, a maximal frequency-conversion efficiency of 36.0 % is obtained at an average DUV laser power of 144 mW and an average pump power of 0.4 W. Though the new technique achieves the effect of the laser beam focusing through cylindrical lens, it significantly simplifies the optical scheme eliminating the necessity of reduction in the laser beam diameter to the transverse dimensions of the nonlinear crystal via a telescope made of two spherical lenses.

Acknowledgements: This work was supported by Bulgarian National Science Fund under Grant KP-06-H77/8 of 04.12.2023.

REFERENCES

[1] T. S. Petrov, N. V. Sabotinov, S. T. Trendafilov, F. Lin, G. Zhang, Journal of Physics **D**: Applied Physics 25, 1169 (1992).
[2] M. J. Withford, D. J. W. Brown, IEEE Journal of Selected Topics in Quantum Electronics 1(3), 779 (1995).
[3] D. J. W. Brown, M. J. Withford, Optics Letters 26(23), 1885 (2001).

ORCID: I.K. 0009-0000-1877-1530, K.T. 0000-0002-5540-9992, S.S. 0000-0003-0800-4885, G.Y. 0009-0008-4831-7871, L.S. 0000-0001-6336-5494

6. Optical communications

Data transmission rate estimates for OAM-carrying waves generated by various discrete EM radiating sources

A. Ž. Ilić[1], J.Z. Trajković[1,2], S.V. Savić[3], and M.M. Ilić[3]
[1]*Institute of Physics Belgrade, University of Belgrade, Serbia*
[2]*Faculty of Physics, University of Belgrade, Serbia*
[3]*School of Electrical Engineering, University of Belgrade, Serbia*
e-mail: andjelijailic@ieee.org

In progressing towards the ubiquitous connectivity of short-range beyond-5G and 6G systems, the millimeter-wave and optical waves carrying the orbital angular momentum (OAM) are expected to be amongst the key technological enablers [1], [2]. In the millimeter-wave wireless communication systems (WCS), the generation of OAM waves by the employment of electrically large antenna arrays has been proven as a cost-effective solution, also allowing relatively easy OAM mode reconfiguration and multiplexing of different OAM modes through a single aperture. The use of OAM modes generated by the discrete OAM EM wave source arrangements could also be of interest for other frequency ranges, e.g. free-space optical communications, as different parts of radiating metasurfaces or optical light modulators could be used to stream separate information channels. However, the source discretization affects generated OAM EM fields, producing unwanted sidelobes and radiation spikes in many directions, and also, reducing the OAM mode purity of the useful transmitted waves. Therefore, system optimization has to be carried out to adjust the power/phases of a limited number of discrete radiating sources for the best performance.

Data transmission rates in line-of-sight (LoS) scenarios can be estimated from the radiation characteristics of an antenna array [3]. Considering the unlicensed millimeter-wave frequency band around 60 GHz, and both the commonly used uniform circular antenna arrays (UCA) and sets of non-uniform linear or rectangular antenna arrays (LAA/RAA), we analyze the effects of source discretization on the EM field quality as well as the possibility to achieve the desired total data transmission rates by the use of multiple OAM modes simultaneously.

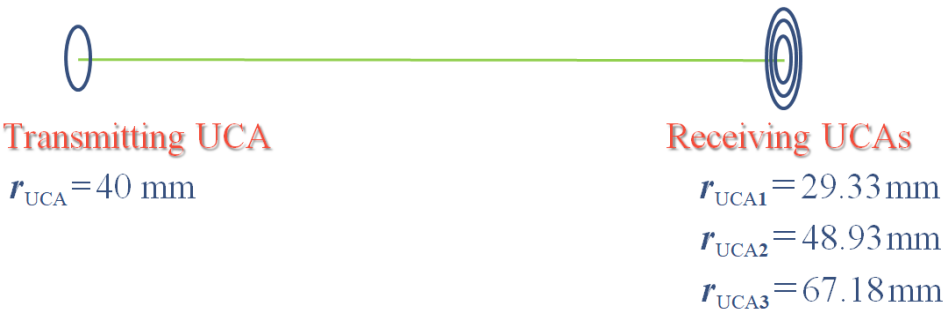

Figure 1. An example of the optimal sizing of the receiving UCAs for 60 GHz mm-wave transmission at the link range of 0.8 m. The OAM UCA source discretization, concerning the radial and azimuthal coordinates, affects the quality of an OAM wave representation. In the case of OAM waves produced by the sets of linear antenna arrays, additional effects due to the non-uniformity of spatial arrangements are observed.

Acknowledgments: The authors acknowledge funding provided by the Institute of Physics Belgrade and School of Electrical Engineering, University of Belgrade, through the grants by the Ministry of Science, Technological Development, and Innovations of the Republic of Serbia.

REFERENCES

[1] S. Chen, Y. Liang, S. Sun, S. Kang, W. Cheng, M. Peng, IEEE Wirel. Commun. 27, 218–228 (2020).
[2] P. Yang, Y. Xiao, M. Xiao, S. Li, IEEE Netw. 33, 70–75 (2019).
[3] A.Ž. Ilić, N.M. Vojnović, S.V. Savić, N. Maletić, E. Grass, M.M. Ilić, Performance assessment for OAM antenna arrays, 2019 IEEE-APS Topical Conf. Antennas and Propagation in Wireless Comm. (APWC), Granada, Spain, 171–173, (2019). https://doi.org/10.1109/APWC.2019.8870549

ORCID: A.Ž.I. 0000-0003-0859-6358, J.Z.T. 0000-0002-2246-0097, S.V.S. 0000-0002-0759-6041, M.M.I. 0000-0003-4196-3594

Reconfigurable NAND/NOR/S-R latch all-optical circuit based on a dual injection-locked Fabry-Pérot laser

M. Krstić, P. Atanasijević, M. Banović, M. Mićić, J. Aleksić, P. Smiljanić, S. Petričević, P. Mihailović, J. Crnjanski, D. Gvozdić
University of Belgrade-School of Electrical Engineering, Serbia
e-mail: marko.krstic@etf.bg.ac.rs

Rapidly increasing global demand for high-performance computing is constantly inspiring further developments in electronic computers, which are, however, starting to face bottlenecks in terms of response speed and bandwidth, followed by exaggerated heat dissipation and power consumption. On the other hand, optical logic gates, i.e., the optical implementation of the fundamental building blocks of a digital computer, enabling the optical computing paradigm, have been attracting growing research attention in recent years [1, 2, 3]. This new technology is seen to provide a framework for increasing the operational speed, the amount of processed information and consequently bandwidth, while reducing the losses and power consumption. A variety of optical logic gates implementations have been analyzed and reported, including schemes residing on spatial encoding of the light, highly nonlinear fibers, photonic crystals, micro- and nano-scale waveguides and resonators, and nonlinear effects in semiconductor amplifiers [4]. Even though the cascading of universal photonic logic gates is largely adopted to achieve programmable digital photonics, a high degree of reconfigurability in a single element photonic digital device remains challenging, especially in the all-optical arena.

In this research, we exploit a dispersive nonlinearity of an injection-locked semiconductor laser for the realization of three different all-optical logic circuits. Our approach resides on a simple, low-power scheme, capable of on-chip photonic integration, including two master lasers optically injecting a Fabry-Pérot slave laser, enabling its parameter dependent multistability [5, 6]. Within this framework, we successfully engineer a three-in-one all-optical digital circuit comprising NAND, NOR, and S-R latch operations, readily reconfigurable by tuning one or two injection parameters, e.g., bias current, or frequency of injected light. By using discrete, off-the-shelf components, we experimentally demonstrate device operation and report operating speeds up to 1 GHz with extinction ratios between logic 0 and 1 up to ≈16 dB, depending on the logic in operation. The proposed all-optical device encloses both the universal gate and memory functionalities in a single element, promising a significant advance toward low-complexity programmable photonics.

Acknowledgment: The research was supported by Science Fund of the Republic of Serbia (#7750121, ORCA-LAB), and by Serbian Ministry of Science, Technology and Innovation (451-03-65/2024-03/200103). The research was partially conducted in the premises of the Palace of Science, Miodrag Kostić Endowment.

REFERENCES

[1] Xu, J., Zhang, C., Wang, Y. *et al.* All-in-one, all-optical logic gates using liquid metal plasmon nonlinearity. *Nature Communication*, vol. 15, 1726 (2024)
[2] Paolo Minzioni *et al.* Roadmap on all-optical processing, *Journal of Optics*, vol. 21, 063001 (2019)
[3] F. Ashtiani, Programmable photonic latch memory, *Optics Express* vol. 33, 3501-3510 (2025)
[4] Jiao S.M., Liu J.W., Zhang L.W., Yu F.H., Zuo G.M. *et al*. All-optical logic gate computing for high-speed parallel information processing. *Opto-Electronic Science*, vol 1, 220010 (2022)
[5] M. Ž. Banović, P. A. Atanasijević, M. M. Krstić, P. M. Mihailović, J. V. Crnjanski, S. J. Petričević, and D. M. Gvozdić, Reconfigurable all-optical bistability/tristability in dual injection-locked Fabry–Perot laser diodes, *Optics Letters*, vol. 48, 4165-4168 (2023)
[6] S.Z. Zarić, J.V. Crnjanski, and M.M. Krstić, Optical switching in dual injection-locked Fabry-Pérot laser diodes, *Optical and Quantum Electronics*, vol. 48, 5 (2016)

ORCID: M.K. 0000-0001-5284-4959, P.A. 0000-0001-7596-0266, M.B. 0009-0001-1843-6326, J.C. 0000-0003-0685-4093, D.G. 0000-0003-0917-5280, M.M. 0009-0005-1769-4883, P.M. 0000-0002-9720-1102

Design and first tests of the optical setup for experiments with the free-space OAM waves

J.Z. Trajković[1,2], S.V. Savić[3], B. Kasalica[1], I. Belča[1] and A.Ž. Ilić[2]
[1]*Faculty of Physics, University of Belgrade, 11000 Belgrade, Serbia*
[2]*Institute of Physics Belgrade, University of Belgrade, 11080 Belgrade, Serbia*
[3]*School of Electrical Engineering, University of Belgrade, 11000 Belgrade, Serbia*
e-mail: jelena.trajkovic.ff@gmail.com, andjelijailic@ieee.org

Within the last decade, waves carrying orbital angular momentum (OAM) have been recognized as one of the key technological enablers of high-data-rate wireless communications and free-space optical communications [1], [2]. Moreover, data encryption schemes using the composite OAM waves consisting of different combinations of multiple OAM modes have been proposed for the combined capacity and security enhancements [3], [4]. Towards the development of novel data encryption algorithms and their experimental verification, as well as carrying out different other experiments, we have designed and assembled an experimental setup using the transmissive light modulator (TLM) plate for the precise control of phase modulation of the transmitted Gaussian beam (Figure 1). The Gaussian beam has been produced by the HeNe laser source (~632.8 nm wavelength), whereas the received waves are being monitored by the CCD camera and post-processed by the custom-designed algorithms.

Here we report on the system design and the observed system performances. We present a summary of the results from the first trials of our experimental equipment, with special emphasis on the production of composite OAM waves and their decryption on the receiving side.

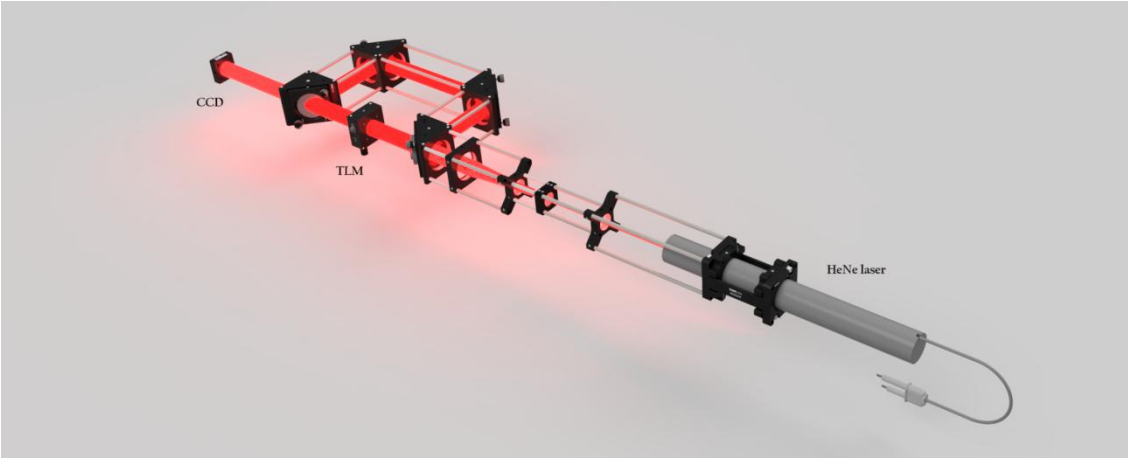

Figure 1. Proposed layout of the experimental setup.

Acknowledgments: This work was financially supported by the SEED Research Grant of the Institute of Physics Belgrade (for young researchers), through the SAIGE Project (Serbia Accelerating Innovation and Growth Entrepreneurship), as well as by the grants to the Institute of Physics Belgrade, Faculty of Physics and School of Electrical Engineering, provided by the Ministry of Science, Technological Development, and Innovations of the Republic of Serbia.

REFERENCES

[1] S. Tripathi, N.V. Sabu, A.K. Gupta, H.S. Dhillon, Millimeter-wave and terahertz spectrum for 6G wireless; In: Y. Wu, et al., 6G Mobile Wireless Networks, Computer Communications and Networks, Springer, Cham (2021). https://doi.org/10.1007/978-3-030-72777-2_6
[2] J. Wang, J. Liu, S. Li, Y. Zhao, J. Du, L. Zhu, Nanophotonics 11(4), 645–680 (2022).
[3] I.B. Djordjevic, IEEE Access 5, 16416–16428 (2017).
[4] X. Yu, J. Fan, X. Li, H. Zhu, S. Nie, J. Ma, C. Yuan, J. Light. Technol. 43(6), 2535–2543 (2025).

ORCID: J.Z.T. 0000-0002-2246-0097, S.V.S. 0000-0002-0759-6041, B.K. 0000-0002-8300-6234, I.B. 0000-0001-6124-5333, A.Ž.I. 0000-0003-0859-6358.

Simulation and adaptation of DPS and DQPS QKD protocols for practical implementation and coexistence within PON architecture

N. Miljković, P. Matavulj
School of Electrical Engineering, University of Belgrade, Serbia
e-mail: mnemanja92.etf@gmail.com

Technology of quantum computing and quantum computers is no longer topic of the future but the topic which represents one of the main focuses of nowadays research with fast traction and concrete practical results in last years. Taking this into account it became clear that all modern encryption algorithms will face serious challenges in incoming years especially if secure key exchange can't be guaranteed. One of considered approach to overcome this problem is technology of Quantum Key Distribution (QKD) that guarantees key exchange security by the laws of fundamental physics. Previous decades of research led to various practical implementations of QKD with constant pressure for further improvement of performances while lowering down costs of the placement of this new technology within existing optical network infrastructure. Result of this urge are new protocols and new methodologies with one goal to simplify and expand possibilities of integration within modern optical networks including Passive Optical Network (PON).

Due to the fact that implementing QKD within PON has some specific requirements, like simple and low-cost integration and multi-user scalability, there was a need for pairing it with newly developed protocols like Differential Phase Shift QKD (DPS QKD) and Differential Quadrature Phase Shift QKD (DQPS QKD) [1]. Results of recent studies, covering practical network implementation [2], also showed that these protocols are probably the best fit for first generation of Quantum Access Network (QAN).

In our previous work we were focused on most mature and most widely implemented QKD protocols BB84 and B92 where we proposed generalized QKD authentication architecture to enhance security of authentication mechanism [3]. We performed simulation and system characterization for this architecture with main focus on comparing performances of three proposed schemes.

In this paper our focus is on simulation, characterization and adaptation of DPS-QKD and DQPS-QKD aimed for integration and coexistence within PON architecture, with special focus on state-of-the-art versions of GPON and NG-PON2 [4]. Following principles from our previous research we are investigating which adaptations of mentioned protocols and their combination can result in most secure and yet most easy to implement solution for QKD integration within PON. General authentication architecture is proposed for this set of protocols and different variations of the setup are simulated and compared.

Acknowledgement: This work was financially supported by the Ministry of Science, Technological Development and Innovation of the Republic of Serbia under contract number: 451-03-137/2025-03/200103.

REFERENCES:

[1] H. Takesue et al., 2008 First ITU-T Kaleid. Academ. Conf. 229-236 (2008).
[2] N. Vokić et al., IEEE J. Sel. Top. Quant. Electron. 26, 3, 1-9 (2020).
[3] N. Miljkovic et al., Opt. Quant. Electron. 50, 319 (2018).
[4] https://www.itu.int/rec/T-REC-G.989.2

ORCID: N.M. 0000-0002-1146-8739, P.M. 0000-0001-6635-5152

7. Laser spectroscopy and metrology

A calibration method for laser interferometric instrument complexes based on stimulated Mandelstam-Brillouin scattering effect

T. A. Aleksandrovich[1], K. P. Vyacheslavovich[1], T. A. Alekseevich[1], K. V. Gennadievich[1], A. Y. Dmitrievich[1]
[1]*The Federal State Unitary Enterprise Dukhov Automatics Research Institute (VNIIA), Moscow, Russia*
e-mail: alaltav@mail.ru

The work is dedicated to the study of nonlinear effects in optical fibers as a source of calibration signals for PDV and VISAR systems, as well as to the development of a method for generation calibration lines for laser interferometric instrument complexes intended for use in gas-dynamic experiments. In such experiments, the registration of the displacement (as well as the velocity and/or acceleration) of a moving surface of complex shape and multiple points. This problem is solved by measuring the Doppler shift of the frequency of scattered laser radiation from a moving surface. Interference of scattered laser radiation with a reference radiation (PDV) [1] or with itself, delayed in time by a fiber optic line (VISAR) [2] is used to determine the magnitude of the Doppler shift. Calibration of measurement systems using certified objects is necessary, so the development of a calibration method for these complexes that allows comparing measurement results obtained by different methods is a pressing task.

The presented work is aimed at solving the problem of creating a universal method for calibrating laser-optical measuring systems and expanding the operating range of measuring speeds. The report presents the results of assessments and experimental studies of the influence of nonlinear optical effects based on stimulated light scattering in optical fibers on the characteristics of Doppler laser diagnostic systems.

The proposed method is based on the occurrence of the nonlinear effect of stimulated Mandelstam-Brillouin scattering under the influence of laser radiation in optical fibers. Experimental verification of this method has been conducted on laser interferometric instrument complexes such as PDV and VISAR, which are used in gas-dynamic experiments in conjunction with other control and measurement equipment and technical means.

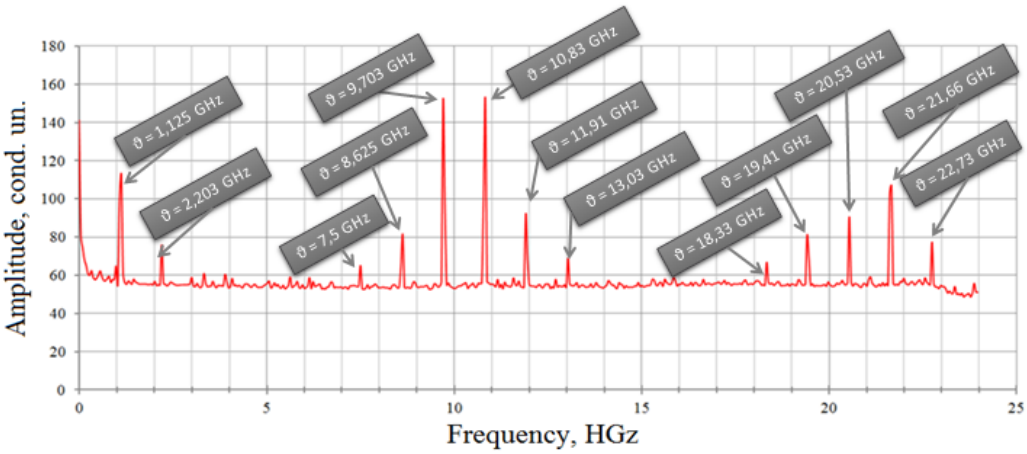

Figure 1. General calibration spectrum.

REFERENCES
[1] D.H. Dolan / Extreme measurements with Photonic Doppler Velocimetry (PDV) // *Rev. Sci. Instrum.* № 91, doi: 10.1063/5.0004363, 2020.
[2] Lynn M. Barker / The development of the VISAR, and its use in shock compression science // *AIP Conf. Proc.* 505, c.11-18, doi: 10.1063/1.1303413, 2000.

Wood Phantoms as Reference Material for Machine Learning Optical Spectroscopy of Construction Wood

K. Słowiński[1], J. Nyga[1], M. Szczerska[1], M. Babińska[1], J. Bąbińska[2], A. Dąbrowska[2], and A. Władziński[1]

[1]*Department of Metrology and Optoelectronics, Faculty of Electronics, Telecommunications and Informatics, Gdańsk University of Technology, Gdańsk, Poland*

[2]*Department of Building Engineering, Faculty of Civil and Environmental Engineering, Gdańsk University of Technology, Gdańsk, Poland*

e-mail: s188973@student.pg.edu.pl

Construction wood is one of the most common materials used in construction [1, 2], so it's important to make sure that the natural wood used is of high quality. Traditional methods for checking wood quality often depend on human judgment, which can be inconsistent [2]. Optical techniques offer a more accurate and repeatable way to analyze wood that can determine its content [3, 4]. This study looks at using wood phantoms – artificial samples made from cellulose and resin – as reference materials in optical spectroscopy. The end goal is to develop a reliable method for identifying and classifying construction wood based on how it interacts with light.

This research focuses on Raman spectroscopy as the main technique to study the wood samples. It compares different phantom samples with varying amounts of cellulose to see how the mixture affects the results. Wood phantoms are useful because their ingredient – cellulose and resin – can be carefully measured and mixed, allowing for consistent and repeatable samples, unlike natural wood where each sample is different.

In this study, data were collected using an 830 nm laser (in the near-infrared range) to minimize fluorescence background [5]. Next, the data were preprocessed using simple baseline correction before being input for machine learning models, that will be used for classification of wood and phantoms (Figure 1). Initial results have shown that Raman spectroscopy not only makes it possible to detect the presence of lignin and cellulose but also allows for the determination of their relative concentrations across samples. This capability makes it possible to distinguish between samples based on variations in cellulose content.

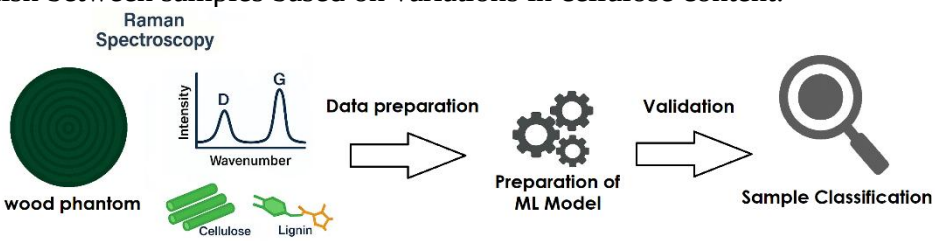

Figure 1. - Proposed workflow.

REFERENCES

[1] M. H. Ramage et al., "The wood from the trees: The use of timber in construction," Renewable and Sustainable Energy Reviews, doi: 10.1016/j.rser.2016.09.107.

[2] R. Ross, Wood handbook: Wood as an engineering material Wood handbook: Wood as an engineering material, https://research.fs.usda.gov/treesearch/62200

[3] V. Ondrejka, et al., "Innovative methods of non-destructive evaluation of log quality," Central European Forestry Journal, vol, doi: 10.2478/forj-2020-0021.

[4] X. Wang, R. J. Ross, In-Forest Wood Quality Assessments—Where Are We with NDT Technologies?, https://www.fpl.fs.usda.gov/documnts/pdf2022/fpl_2022_wang005.pdf

[5] A. Władziński, et al., "Biomarker Detection in the Wastewater Phantom," Journal of Biophotonics, doi: 10.1002/jbio.202500003.

This research was supported by the "Excellence Initiative – Research University" (IDUB) program: Technetium Talent Management Grants (7/1/2024/IDUB/III.4c/Tc), by the "European Cooperation in Science and Technology" (COST Action CA21159), and by the Gdańsk University of Technology, Faculty of Civil and Environmental Engineering Project Fund (NR038216).

Raman spectroscopy as a predictive tool for Laser-Induced Graphene from wooden biomass

J. Nyga[1], K. Słowiński[1], A. Władziński [1], M. Szczerska [1], J. Bąbińska[2], A. Dąbrowska[2], M. Babińska [1]
[1]*Department of Metrology and Optoelectronics, Faculty of Electronics, Telecommunications and Informatics, Gdańsk University of Technology, Gdańsk, Poland*
[2]*Department of Building Engineering, Faculty of Civil and Environmental Engineering, Gdańsk University of Technology, Gdańsk, Poland*
e-mail: s188631@student.pg.edu.pl

The synthesis of laser-induced graphene (LIG) is a relatively new and rapidly developing field of materials engineering, offering new opportunities for fabricating functional carbon structures for optoelectronic and sensing applications [1, 2]. However, the wooden materials, despite their promising properties, remain poorly understood in the context of LIG formation [3].

In this work, the use of Raman spectroscopy as a predictive, pre-LIG diagnostic tool to assess wood as a precursor. Presented data obtained from wood samples - spruce, in raw form as offcuts. Raman spectra were collected using an 830 nm laser (near infrared - to reduce background fluorescence) [4], revealing key fingerprints related to cellulose/lignin ratio and sample unity. These factors appear to influence the result of LIG structure - morphological uniformity, low defect density, and potential electronic conductivity relevant for sensing applications.

Preliminary results of spectroscopy show high potential of material carbonization [3]. A relatively simple workflow is proposed, using baseline correction, and highlight peaks, to pre-select wood and extract well-structured graphene-like carbon parts, as illustrated in Figure 1. Raman spectroscopy appears to be a promising predictive tool to suggest which wooden materials can form into effective bio-microelectrodes with potential utility in optical and electrochemical sensing fields.

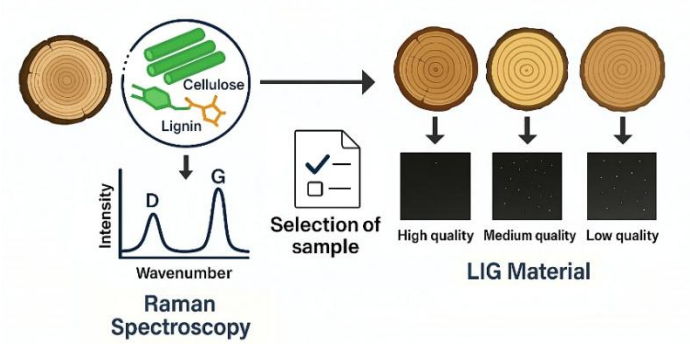

Figure 1. Raman spectroscopy for wooden material classification.

This research was supported by the "Excellence Initiative – Research University" (IDUB) program: Technetium Talent Management Grants (7/1/2024/IDUB/III.4c/Tc), by the "European Cooperation in Science and Technology" (COST Action CA21159), and by the Gdańsk University of Technology, Faculty of Civil and Environmental Engineering Project Fund (NR038216).

REFERENCES

[1] S. K. Lengger *et al.*, "Laser-induced graphene formation on different wood species: Dependence of electronic performance on intrinsic features of certain types of wood", doi: 10.1016/j.susmat.2024.e00936.
[2] K. Avinash and F. Patolsky, "Laser-induced graphene structures: From synthesis and applications to future prospects", doi: 10.1016/j.mattod.2023.10.009.
[3] R. Ye *et al.*, "Laser-induced graphene formation on wood", doi: 10.1002/adma.201702211.
[4] A. Władziński *et al.*, "Biomarker detection in the wastewater phantom", doi: 10.1002/jbio.202500003.

Synthesis of Bimetallic Germanium-Copper Oxide Nanoparticles by Pulsed Laser Ablation in Liquids: Potential Application for LIBS Signal Enhancement

S. Zivkovic[1], M. Momcilovic[1], N. Krstulovic[2], G. Galbacs[3]
[1]*Department of Physical Chemistry, Vinca Institute of Nuclear Sciences, University of Belgrade, Belgrade, Serbia*
[2] *Centre for Advanced Laser Techniques, Institute of Physics, Zagreb, Croatia*
[3]*Department of Molecular and Analytical Chemistry, University of Szeged, Szeged, Hungary*
e-mail: sanjaz@vin.bg.ac.rs

A novel laser-based strategy was developed for the synthesis of functional germanium–copper oxide nanoparticles, with the aim of enhancing the analytical performance of LIBS. A thin germanium film was deposited onto a copper substrate by pulsed laser deposition (PLD) in vacuum, using an Nd:YAG laser ($\lambda = 1064$ nm, ≈300 mJ per pulse, 5 Hz repetition rate, 4 ns duration), with the target and substrate placed ~1 cm apart and rotated continuously for uniform coating, over 3000 pulses. The resulting material was then used to fabricate nanoparticles using the laser ablation technique in liquids. This target was immersed into 3 ml of Milli-Q water, and the surface area of approximately 25 mm² was continually scanned by a pulsed laser beam in order to achieve homogeneous ablation of the sample using an Nd:YAG laser (7 mJ, 10 Hz, 150 ps pulse duration, wavelength of 1064 nm). Characterization of the formed bimetallic nanocolloids was performed by measuring the SPR band using UV-VIS spectrophotometry and TEM microscopy.

Additionally, nanoparticles were used for Nanoparticle-Enhanced Laser-Induced Breakdown Spectroscopy (NELIBS) of an aluminum sample. LIBS measurements were performed using a TEA CO_2 laser-based setup with an Avantes spectrometer and optical triggering. Bimetallic nanocolloid solution was applied by the drop-and-dry technique [1]. Preliminary results have shown an improvement in analytical sensitivity for the detection of Mg in aluminum.

a) *b)*

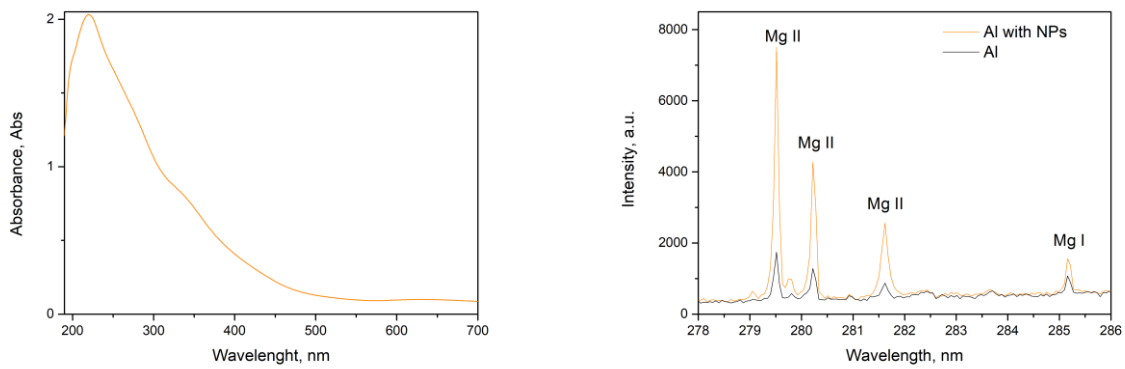

Figure 1. a) UV Vis spectrum of LASIS nanoparticles, b) obtained LIBS spectra of aluminum sample with and without nanoparticles

REFERENCES:
[1] M. Momcilovic, J. Petrovic, M. Nemoda, J. Ciganovic, N. Krstulovic, M. Ognjanovic, S. Zivkovic, Appl. Phys. B 129, 62 (2023).

ORCID: S.Z. 0000-0003-1499-1645, M.M. 0000-0001-9117-5903, N.K. 0000-0001-6443-2417, G.G. 0000-0002-1799-5329

8. Ultrafast optical phenomena

Controllable Splitting and Coherently Recombining Intense Femtosecond Pulses Using Structured Light

L. I. Stoyanov[1, 2], Y. Zhang[3,4], A. Dreischuh[1,2,5] and G. G. Paulus[3,4]
[1]*Department of Quantum Electronics, Faculty of Physics,*
Sofia University "St. Kliment Ohridski", Sofia, Bulgaria
[2]*National Centre of Excellence Mechatronics and Clean Technologies, Bulgaria*
[3]*Institute of Optics and Quantum Electronics, Friedrich Schiller University, Jena, Germany*
[4]*Helmholtz Institute Jena, Jena, Germany*
[5]*Bulgarian Academy of Sciences, Sofia, Bulgaria*
e-mail: l.stoyanov@phys.uni-sofia.bg

It is generally known that at high energies/powers intense femtosecond beams/pulses are prone to instabilities (see e.g., [1]). These effects, to some extent, could be mitigated through the controlled splitting of the beam into sub-beams. However, this approach is only viable if there exists a reliable method to coherently recombine the sub-beams following their spectral broadening. To achieve this, we use known objects from the field of singular optics, namely optical vortex lattices [2-4]. Such beams enable controllable and reversible break-up into an ordered array of well-defined intensity peaks in the focal plane of a lens (i.e., in the artificial far field, where the intensity is high). A typical example of a square-shaped optical vortex lattice is shown in Fig. 1.

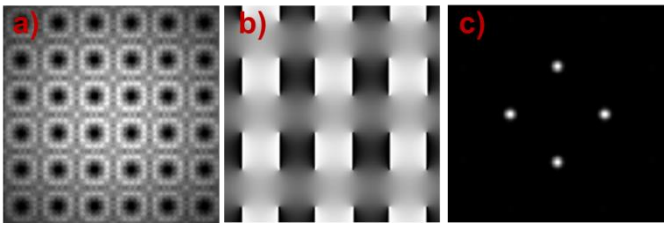

Figure 1. Numerical intensity and phase distributions (a) and (b) of a square-shaped optical vortex lattice composed by singly-charged optical vortices with alternative signs. (c) – intensity profile of the square-shaped optical vortex lattices in the focal plane of a lens.

In this talk, we will present our recent advances [5] in addressing spectral broadening and temporal compression of high-energy femtosecond pulses by the controllable splitting and coherent beam recombining of femtosecond beams/pulses using structured light, more precisely square-shaped optical vortex lattice. Moreover, the compression in time (down to the Fourier transform limit) of the spectrally broadened pulses will be demonstrated and discussed as well. In our view, the obtained results serve as a strong motivation for further optimization and investigation serving as potential alternative to the established methods for coherent beam recombining.

We acknowledge funding of the Bulgarian National Science Fund (project КП-06-Н78/6). The work was also supported by the Bulgarian Ministry of Education and Science as a part of National Roadmap for Research Infrastructure, project ELI ERIC BG and by the European Regional Development Fund under "Research Innovation and Digitization for Smart Transformation" program 2021-2027 under the Project BG16RFPR002-1.014-0006 "National Centre of Excellence Mechatronics and Clean Technologies".

REFERENCES

[1] A. Braun, G. Korn, X. Liu, D. Du, J. Squier, and G. Mourou, Opt. Lett. 20, 73-75 (1995).
[2] L. Stoyanov, G. Maleshkov, M. Zhekova, I. Stefanov, D. N. Neshev, G. G. Paulus and A. Dreischuh, J. Opt. Soc. Am. B, vol. 35, pp. 402-409 (2018).
[3] L. Stoyanov, G. Maleshkov, M. Zhekova et al., Journal of Optics, vol. 20, Art. No. 095601 (2018).
[4] L. Stoyanov, G. Maleshkov, M. Zhekova et al., Scientific Reports, vol. 9, Art. No. 9:2128 (2019).
[5] L. Stoyanov, G. Maleshkov, M. Zhekova et al., Opt. Express **32**, 48758-48771 (2024).

ORCID: L.S. 0000-0002-2723-8639, Y.Z. 0000-0002-0962-6371, A.D. 0000-0003-4812-3520

Laser Polarization Control of High Harmonics in Centrosymmetric and Non-Centrosymmetric Semiconductors

T. Apostolova[1, 2], B. Obreshkov[1]
[1]*Institute for Nuclear Research and Nuclear Energy, Bulgarian Academy of Sciences, Sofia, Bulgaria*
[2] *Institute for Advanced Physical Studies, New Bulgarian University, Sofia, Bulgaria*
e-mail: tzveta.apostolova@nbu.bg

We investigate high harmonic generation (HHG) in semiconductors driven by mid-infrared femtosecond laser pulses, focusing on the dependence of harmonic emission on the laser polarization angle relative to fixed crystal axes. Experiments on silicon (centrosymmetric) and c-cut zinc oxide (ZnO, non-centrosymmetric) reveal distinct symmetry-dependent responses influenced by both crystal structure and laser field strength.

In ZnO, harmonic spectra exhibit clear symmetry signatures: as the linear polarization is rotated within the (0001) plane, odd-order harmonics display six-fold rotational symmetry, while even-order harmonics exhibit two-fold symmetry, consistent with the hexagonal wurtzite lattice and lack of inversion symmetry. In silicon, HHG yields vary with polarization direction, with enhancements along high-symmetry axes such as [100] and [110]. Notably, at higher laser intensities, even-order harmonics also emerge, indicating field-induced dynamical symmetry breaking in this otherwise centrosymmetric material.

To interpret these results, we perform multi-band time-dependent Schrödinger equation (TDSE) simulations under experimental laser conditions [1]. The simulations reproduce the angular dependence and harmonic yields in both materials. These findings highlight how crystal symmetry, laser polarization, and field strength together govern the HHG response in solids, and establish polarization-resolved HHG as a tool for probing symmetry and ultrafast dynamics in semiconductors.

Acknowledgements: Authors acknowledge project ELIUPM4-92_MIR_HHGSOLID_TA and MIR Laser group at ELI-ALPS and support from COST Action CA20129, COST Action CA21128 (T.A.) and Peta SC Discoverer supercomputer resources under project EPICURE.

REFERENCES

[1] B. Obreshkov, T. Apostolova, arXiv: 2405.01571, (2024), accepted Applied Physics B, (2025) .

ORCID: T.A. 0009-0002-5548-2900

9. Laser - material interaction

Terahertz wave generation from laser-irradiated near-critical-density plasmas

V. Yu. Bychenkov[1, 2], A.V. Brantov[1, 2], M.G Lobok[1, 2] and A.S. Kuratov[1, 2]
[1]*Dukhov Research Institute of Automatics, Moscow, Russia*
[2]*P.N. Lebedev Physical Institute of the Russian Academy of Sciences, Moscow, Russia*
e-mail: mglobok@me.com

Femtosecond laser pulse propagation in a relativistic self-trapping (RST) regime within near-critical-density plasma enhances electron acceleration, maximizing both total charge and laser-to-electron energy conversion [1]. This process efficiently generates intense, coherent terahertz (THz) transition radiation. Three-dimensional particle-in-cell (PIC) simulations reveal that THz emission occurs as accelerated electrons exit into vacuum—either directly from the low-density plasma or after traversing a thin foil at the target rear [2].

The RST regime proves superior to conventional foil targets with preplasma, enabling significantly stronger THz generation. Optimized laser-plasma matching allows a 2-J femtosecond laser to produce quasi-unipolar THz pulses with energies exceeding 100 mJ.

REFERENCES

[1] M.G. Lobok, A.V. Brantov, D.A. Gozhev, V.Yu. Bychenkov, Plasma Phys. Control. Fusion *60*(8) (2018).
[2] V. Yu. Bychenkov, A.V. Brantov, M.G. Lobok, A. S. Kuratov, Phys. Rev. E, 110(6), (2024).

ORCID: V.Yu. B. 0000-0001-9624-3813, A.V. B. 0000-0002-6743-1513
M.G.L. 0000-0003-4661-5943, A.S.K. 0000-0002-7434-8224

Enhancement of LIBS Signal via NELIBS and LIPSS for Biomedical Applications

M. Vinić[1,2], I. C. Tommasi[2], A. De Giacomo[3], C. Gaudiuso[4],
F. P. Mezzapesa[4], A. Santagata[5], M. L. Pace[5], L. Catanzaro[6], L. D'Urso[6], G. R. Compagnini[6], R. Gaudiuso[2]
[1]*Institute of Physics, University of Belgrade, Serbia*
[2]*Department of Chemistry, University of Bari "A. Moro", Italy*
[3]*Department of Translational Biomedicine and Neurosciences, University of Bari "A. Moro", Italy*
[4]*Institute of Photonics and Nanotechnology – CNR, Bari, Italy*
[5]*Institute of Structure of Matter – CNR, Potenza, Italy*
[6]*Department of Chemical Sciences, University of Catania, Italy*
e-mail: rosalba.gaudiuso@uniba.it

Laser-Induced Breakdown Spectroscopy (LIBS) has emerged as a promising technique for elemental analysis in complex matrices, including biological fluids. However, its sensitivity - especially for trace elements - remains a critical limitation when targeting subtle biochemical differences such as those potentially associated with neurodevelopmental disorders like Autism Spectrum Disorder (ASD) [1]. In this context, signal enhancement strategies are essential to increase LIBS performance and unlock its potential in clinical diagnostics.

In this work, we present our preliminary results on two distinct signal enhancement approaches: Nanoparticle-Enhanced LIBS (NELIBS) and the application of Laser-Induced Periodic Surface Structures (LIPSS). Both methods aim to improve signal intensity and reproducibility in LIBS measurements by altering the physical properties of the substrate or sample–substrate interface.

Our experimental setup involves the analysis of aqueous $PbCl_2$ solutions and blood serum microdroplets deposited and dried on solid substrates. For NELIBS, substrates were functionalized with noble metal nanoparticles, known to facilitate localized plasma confinement and improved ablation efficiency. In parallel, LIPSS were fabricated on the same substrates using controlled laser irradiation, creating periodic nanostructures that enhance light–matter interaction during plasma generation.

The enhanced LIBS spectra were compared with conventional LIBS for both $PbCl_2$ and serum samples, focusing on signal-to-noise ratio, emission intensity, and spectral reproducibility. Our findings confirm that both NELIBS and LIPSS contribute to notable signal enhancement. The observed enhancements suggest increased sensitivity for trace element detection in complex biological fluids.

These results represent a first step toward applying advanced LIBS-based techniques for biomedical diagnostics. The long-term objective of our research is to develop a robust metallomic profiling method capable of detecting elemental biomarkers potentially associated with ASD. Future work will focus on applying these optimized LIBS protocols to real blood serum samples from pediatric subjects with ASD and neurotypical controls.

This study highlights the promise of physical and chemical substrate modifications for pushing the analytical limits of LIBS and opens new perspectives for its application in non-invasive and rapid diagnostic workflows.

Acknowledgements: This work has been partially supported by the European Union, PRIN-PNRR 2022. "Finanziato dall'Unione europea- Next Generation EU, Missione 4 Componente 1 CUP H53D23007820001".

Reference:

[1] J.K. Kern et al, Journal of Trace Elements in Medicine and Biology 38 (2016) 8.

ORCID: M.V. 0000-0001-7438-7058

Ultrafast laser–tissue interaction modeled via two-electron-temperature and free-carrier dynamics

H. Delibašić Marković[1], V. Petrović[1] and V. Srećković[2]
[1]*University of Kragujevac, Faculty of Science, Radoja Domanovića 12, 34000 Kragujevac, Serbia*
[2]*University of Belgrade, Institute of Physics Belgrade, Pregrevica 118, 11080 Belgrade, Serbia*
e-mail: hristina.delibasic@pmf.kg.ac.rs

We present a numerical study of femtosecond laser interaction with skin-like biological tissue using a two-electron-temperature and free-electron-density framework. The model resolves nonequilibrium energy transfer between nonthermal and thermalized electrons, coupled with the generation and spatiotemporal evolution of free carriers. Originally applied to metals [1] and later extended to wide-bandgap materials [2], this approach is adapted here to describe a soft, heterogeneous, water-rich medium with embedded absorbers. The governing system includes balance equations for high- and low-energy electron populations, as well as a rate equation for the free electron density. The latter accounts for multiphoton ionization, cascade processes, and chromophore-mediated photoionization, which is particularly relevant in pigmented or vascular tissue. Electron–phonon coupling is modeled as effective energy transfer to the surrounding matrix [3, 4], enabling thermalization on sub-picosecond timescales. Several physical effects, essential for realistic modeling, are incorporated: nonlinear absorption, local field enhancement near chromophores, and transient changes in the refractive index due to free carriers. Additionally, saturation of absorption, carrier diffusion, and heat dissipation through water content are considered. These elements are critical for understanding early energy localization and avoiding over-simplified energy deposition models [5]. Simulations are carried out in one dimension using an explicit finite-difference scheme under Gaussian pulse excitation. The model captures the dynamic interplay between ultrafast ionization, localized heating, and optical property modulation. Results suggest that the inclusion of distinct electron populations and chromophore-specific effects significantly alters the predicted damage thresholds and spatial confinement. This work builds upon recent extensions of the two-temperature model in nonequilibrium systems [6], offering a flexible basis for investigating ultrafast photothermal interactions in biological contexts.

Acknowledgements: Authors would like to acknowledge the support received from the Science Fund of the Republic of Serbia, #GRANT 6821, Atoms and (bio)molecules-dynamics and collisional processes on short time scale - ATMOLCOL. Our appreciation also goes to the Serbian Ministry of Education, Science and Technological Development (Agreement No. 451-03-137/2025-03/ 200122).

REFERENCES

[1] S.I. Anisimov, B.L. Kapeliovich, T.L. Perelman, Sov. Phys. JETP 39, 375 (1974).
[2] B. Rethfeld, D.S. Ivanov, M.E. Garcia, S.I. Anisimov, J. Phys. D: Appl. Phys. 50, 193001 (2017).
[3] V.E. Alexopoulou, A.P. Markopoulos, Arch. Comput. Methods Eng. 31, 93 (2024).
[4] U. Ritzmann, P.M. Oppeneer, P. Maldonado, Phys. Rev. B 102, 214305 (2020).
[5] B. Rethfeld, A. Kaiser, M. Vicanek, G. Simon, Phys. Rev. B 65, 214303 (2002).
[6] M. Uehlein, S.T. Weber, B. Rethfeld, Nanomaterials 12, 1655 (2022).

ORCID: H.D.M. 0000-0002-8391-4179, V.P. 0000-0002-7865-523X, V.S. 0000-0001-7938-5748

Surface Modification for bioactivity improvement of Polyetheretherketone (PEEK) via Femtosecond Laser Microprocessing

L. Angelova[1], A. Daskalova[1], E. Filipov[1], F. Lemaire[2] and H. Kerdjoudj[2]
[1]*Institute of Electronics, Bulgarian Academy of Sciences, Sofia, Bulgaria*
[2]*University of Reims Champagne Ardenne, Reims, France*
e-mail: liliyaangelova9@gmail.com, lily1986@abv.bg

The increasing prevalence of orthopedic disorders and technological advances have significantly improved the design and functionality of orthopedic implants and have carved the way for the growth of the orthopedic implants market. Materials used in the design and production of bone implants include metals, ceramics, polymers, and their composites. Among polymers, polyetheretherketone (PEEK) and its composites have been employed as biomaterials for trauma, cranio and maxillofacial, orthopedic, and spinal implants. Due to its strong biocompatibility and mechanical properties, PEEK has become a main competitor to metallic implants, still used as a gold standard in bone tissue engineering. However, the chemical inertness is the main reason explaining the poor osseointegration and fixation of PEEK implants to the recipient bone tissue. Recent development in surface micro- and nanostructuring by ultra-short femtosecond laser-induced surface processing suggests the high potential of the method to tailor surface roughness, and as a consequence - precisely-controlled wettability. The interplay between wettability and surface roughness is the basis of achieving enhanced osteointegration of the implants as the femtosecond laser processing approach provides a unique tool to produce micro/nano-rough surfaces, with improved interface adhesion characteristics. High precision and tunability of the laser radiation parameters provide a possibility for creating diverse micro and nano surface designs, resembling an effective and green alternative to the developed chemical methods by offering permanent surface structuring without residual toxicity. Due to ultra-short irradiation periods and ultra-high intensities applied, the created structures have such advantages as precise control over surface roughness and wettability, processing accuracy, and reproducibility. The main research goal of this work is to apply and study laser-induced micro/nano surface modification of PEEK for enhanced osseointegration. To achieve this, developing of various texturing designs of PEEK surface interfaces via femtosecond laser modification is performed. Detailed morphological and chemical evaluation of the obtained results is carried out (by means of SEM, EDX, XRD, 3D profilometer and WCA analyses) and preliminary biological evaluation of the structured PEEK substrates is done. The results obtained show that the created ultra-short laser surface designs of the bone PEEK implants can essentially enhance their bioactivity properties, which could improve osteointegration capacity of the as created micro/nano structured PEEK scaffolds in engineering of personalized bone tissue.

Acknowledgments: This research was funded by BULGARIAN NATIONAL SCIENCE FUND (NSF) under grant number No. ***KP-06-Rila/6 (2024–2026)*** *"Improving the efficiency of PEEK implants for bone tissue regeneration by femtosecond laser functionalization ". The research was carried out with the help of infrastructure purchased under the National Roadmap for Scientific Infrastructure* ***(ELI-ERIC-BG)****, project* ***D01-351****.*

ORCID: L.A. 0000-0002-1702-862X, A.D. 0000-0003-1131-6900, E.F. 0000-0002-8373-6034, F.L. 0009-0001-6772-5191, H.K. 0000-0002-8072-9728

Comparison of laser-induced graphene on different types of synthesized crosslinked polyimides

K. Tošić[1], M. Pergal[1], M. Bošković[1], I. Pašti[2], D. Bajuk-Bogdanović[2], M. Spasenović[1]
[1]*Center for Microelectronic Technologies, Institute of Chemistry, Technology and Metallurgy, National Institute of the Republic of Serbia, University of Belgrade, Belgrade, Serbia*
[2]*Faculty of Physical Chemistry, University of Belgrade, Belgrade, Serbia*
e-mail: katarina.tosic@ihtm.bg.ac.rs

Laser-induced graphene (LIG) has emerged as a promising material in recent years, mainly due to the unique advantages offered by the laser induction process itself. This technique enables the direct and efficient conversion of carbon-rich precursors into graphene, offering a rapid, straightforward and cost-effective alternative to conventional graphene production methods for certain applications. Potential applications of LIG range from flexible, wearable electronics to electrodes for electrochemistry, to gas and biosensors. Among the various precursors, polyimides have proven to be particularly suitable for LIG formation due to their thermal stability and carbon content [1]. While most current research is based on commercially available polyimides, research on LIG from synthetically produced polyimides is still limited. However, laser induction on such tailored substrates opens up new possibilities for tuning the biocompatibility, electrical performance, structural integrity and physicochemical properties of the resulting LIG, which is crucial for optimizing material performance for a target application [2].

In this work graphene was induced on a series of newly synthesized polyimide substrates. The polyimides were obtained by polymerization in solution at elevated temperatures using *N*-[3-(2,5-dioxo-2,5-dihydro-1H-pyrrol-1-yl)phenyl]acetamide in combination with selected diamine compounds with terminal amino groups: urea, 4-[(4-aminophenyl)sulfonyl]aniline and 1,2-diaminoethane. The structures of the precursors and polyimides were characterized by ^{1}H NMR, ^{13}C NMR and FTIR spectroscopy. After graphene induction, the resulting materials were analyzed to determine their nanomechanical and electrical properties, with a focus on potential applications in electrochemical systems. Characterization techniques included Raman and FTIR spectroscopy, SEM-EDS, XRD analysis and sheet resistance measurements. The results provide valuable insights into the correlation between the molecular structure of polyimide and the efficiency and quality of laser-induced graphene, underlining the promise of these materials in electrode applications.

Acknowledgements: This research was supported by the Science Fund of the Republic of Serbia, #4950, Polymer/graphene heterostructures for physiological sensors – Polygraph.

REFERENCES

[1] I. Lawan, P. Luengrojanakul, K. Charoensuk, H. Argunam, C. Ahn, S. Rimdusi, Nanoscale Adv., 6, 1556 (2024)
[2] A. Iqbal, B. Amna, I. ul Islam, Z. Yuchi, H. M. Siddiqi, J. Zai, X. Qian, Polymer, 319, 128016 (2025)

ORCID: K.T. 0000-0003-1141-4340, M.P. 0000-0001-6078-2006, M. B. 0000-0003-1428-9346, I.P. 0000-0002-1000-9784, D.B.B. 0000-0003-2443-376X, M.S. 0000-0002-2173-0972

Grated target reflectivity evolution during laser prepulse irradiation

A. Zubarev[1], M. Cuzminschi[1,2]
[1]*National Institute for Laser, Plasma and Radiation Physics, 077125 Magurele, Ilfov, Romania*
[2]*Department of Theoretical Physics, ''Horia Hulubei'' National Institute for Physics and Nuclear Engineering, 07125 Magurele, Ilfov, Romania*
e-mail: alxubarev@gmail.com

The laser-driven experiments are a promising way to produce accelerated particles and x-rays or to reproduce astrophysical phenomena in laboratory conditions. Laser target interaction can be significantly improved by choosing an appropriate target and the temporal profile of laser intensity. For the high performance of the laser-driven experiment, maximal radiation absorption is required.
In this work, we study the preplasma generation during prepulse target interaction and its influence on the target reflectivity. The prepulse influence on target reflectivity was studied numerically using the FLASH simulation program [1] and analytically using the effective refractive index model and Bloch wave approximation. The laser radiation heats the target and the material is ablated [2]. The preplasma distribution in front of the target for flat and grated targets is shown in Fig. 1 (a) and (b). The numerical simulations show that laser absorption is lower for a grated target than for a grated one (Fig. 1 (c)). The angle of incidence is about 15 degrees, which ensures the best radiation absorption for the grated target.

The analytical model predictions are in agreement with numerical simulation results. The reflectivity of the grated target decreases after the preplasma generation. During the preplasma generation its density increases and the reflectivity changes. After the preplasma density reaches critical value the reflectivity increases fast.

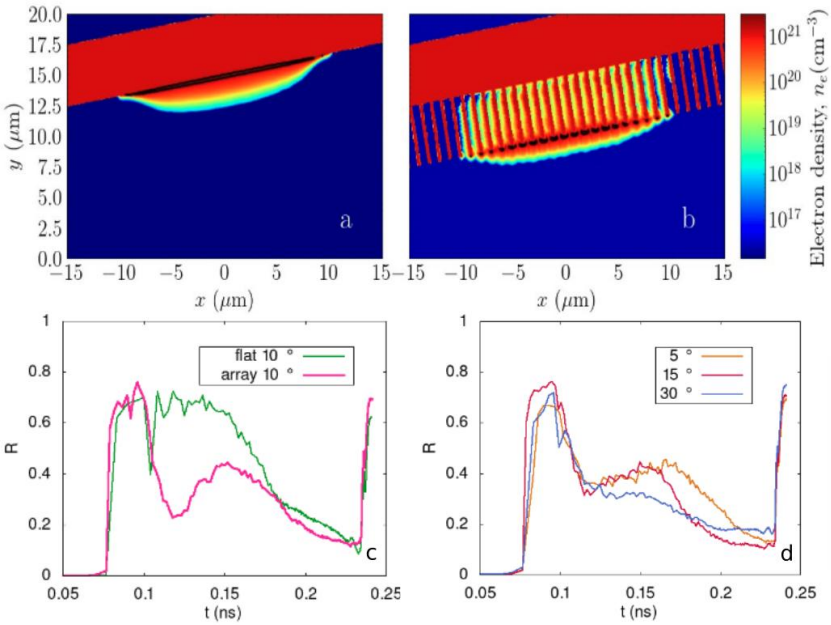

Figure 1. Preplasma evolution during prepulse iradiation in front of flat (a) and grated (b) targets. Reflectivity evolution during the irradiation for flat and grated tagets (c) and for grat targets for different angles of incidence (d). Figure reproduced from [3].

Funding: UEFISCDI PN-IV-P7-7.1-PED-2024-079, PN-IV-P2-2.1-TE-2023-1102 and IOSIN

REFERENCES

[1] Fryxell, Bruce, et al. Astrophys. J Suppl. Ser. 131.1 (2000): 273.
[2] Ong, J. F., et al. Sci. Reports 13.1 (2023) 20699.
[3] Zubarev, A., et al. An. West Univ. Timis. Phys. Ser. 0001, Vol. LXVII, 2025

ORCID: A.Z. 0000-0002-3906-965X, M.C. 0000-0002-4084-8642

Solid targets heating during laser prepulse

A. Zubarev[1], M. Cuzminschi[1,2]
[1]*National Institute for Laser, Plasma and Radiation Physics, 077125 Magurele, Ilfov, Romania*
[2]*Department of Theoretical Physics, ''Horia Hulubei'' National Institute for Physics and Nuclear Engineering, 07125 Magurele, Ilfov, Romania*
e-mail: alxubarev@gmail.com

The main stages of high-intensity laser pulse with a target interaction are prepulse and main pulse. Prepulse stage is crucial for plasma expansion and energy absorption. During the prepulse stage, preplasma generation occurs because of ablation and ionization of target atoms. Prepulse parameters have a significant influence on results of high-intensity laser-driven experiments. Particularly, laser prepulse strongly impacts the intensity and energetic spectra of accelerated particles. For optimization of and optimization of experimental condition of laser-driven particle acceleration interaction of laser prepulse with a target needs to be thoroughly studied.

This study is centered around prepulse-target interaction before the formation of preplasma. Employing first-principles simulations, such as time-dependent density functional theory (TDDFT), enables a more detailed characterization of the coupled electronic and structural dynamics underlying preplasma formation.

In our study, we use Salmon [1] (Scalable Ab-initio Light-Matter simulator for Optics and Nanoscience) software for TDDFT to determine laser-matter interaction at atomic scale. It is capable of performing TDDFT simulations by solving the time-dependent Kohn-Sham equations in real time and real space, utilizing norm-conserving pseudopotentials. SALMON begins by performing ground-state calculations based on density functional theory to establish the system's initial state. It then simulates the electron dynamics triggered by an applied electric field.

This research explores laser-matter interactions by simulating the propagation of pulsed light through thin films of various materials, including Si, Cu, Al, and SiO_2. We analyze the incident, reflected, and transmitted pulses, as well as the electric field and excitation energy at material surfaces. Additionally, we examine the spatial distributions of the electric field and current density. The onset of preplasma formation is identified by a sudden rise in excited or ionized electron populations, a rapid drop in bound electron density, and a significant increase in energy absorption. We anticipate that preplasma will form earlier in metals than in silica or bulk silicon.

Funding: UEFISCDI PN-IV-P7-7.1-PED-2024-079, PN-IV-P2-2.1-TE-2023-1102 and IOSIN

REFERENCES

[1] M. Noda, et. al., Comp. Phys. Comm., 235 356-365 (2019).

ORCID: A.Z. 0000-0002-3906-965X, M.C. 0000-0002-4084-8642

Laser-Induced Nanostructuring and Surface Phonon Behavior in ZnO/MnO Nanocomposites

B. Hadžić[1], M. Ćurčić[1], I. Kuryliszyn-Kudelska[2], M. Romcevic[1], W.D. Dobrowolski[2] and N. Romcevic[1]

[1]*Institute of Physics Belgrade, Pregrevica 118, 11080 Belgrade, Serbia*
[2]*Institute of Physics, Polish Academy of Sciences, Al. Lotników 32/46, 02-668Warsaw, Poland*
e-mail: branka@ipb.ac.rs

In this study, we investigate the influence of laser power on nanocrystalline ZnO(Mn) samples synthesized via a wet chemical co-precipitation method followed by calcination at 300 °C. The initial mixtures were prepared with varying concentrations of MnO dopant, ranging from 5% to 95%. X-ray diffraction (XRD) analysis confirmed the presence of ZnO and $ZnMn_2O_4$ phases. At the same time, Raman spectroscopy and scanning electron microscopy (SEM) provided additional insights into the structural and morphological evolution of the samples.

Non-resonant Raman scattering spectra were recorded across the 100–1600 cm^{-1} range for samples irradiated at multiple laser power densities. The results reveal that laser-induced heating leads to characteristic broadening and red-shifting peaks associated with ZnO and Mn-based phases. These spectral modifications are attributed to nanostructuring effects and partial decomposition processes triggered by localized thermal energy.

As the dopant concentration and laser power increase, significant changes in the behavior of surface optical phonons (SOP) are observed, including a gradual suppression of SOP modes associated with the ZnO matrix. The data suggest the formation of secondary phases such as $Zn_{1-x}Mn_xO$ and $Zn_yMn_{3-y}O_4$, resulting from the interplay between laser-induced nanostructuring and dopant-induced modifications of the host lattice.

This comprehensive investigation highlights the complex relationship between laser power, dopant concentration, phase evolution, and optical phonon dynamics in ZnO/MnO nanocomposites. It underscores the utility of laser processing as a tool for fine-tuning the structural and vibrational properties of multifunctional oxide materials.

ORCID: B.H.0000-0001-5459-7461, M.C. 0000-0001-9239-0912, I.K-K. 0000-0003-1433-264X, M. R. 0000-0003-3753-7680, W.D.D. 0000-0001-6630-761X, N. R. 0000-0002-5064-175X

Surface Modification of Wide Bandgap Semiconductor GaN Using Femtosecond Laser Induced Periodic Surface Structuring (LIPSS)

M. Shehadi[1], D. Tsankov[2], L. Stoychev[1], T. Petrov[3]
[1]*Institute of Solid State Physics, Bulgarian Academy of Sciences, Sofia, Bulgaria*
[2]*Department of Electrical Motion Automation Systems, Faculty of Automatics, Technical University of Sofia, Bulgaria*
[3]*Department of Applied Physics, Faculty of Applied Mathematics and Informatics, Technical University of Sofia, Bulgaria*
e-mail: mshehadi@issp.bas.bg

Femtosecond laser induced periodic surface structures (LIPSS) is a no contact, low-cost technique used for structural surface modifications of wide bandgap (WBG) transparent materials, at dimensions equal or smaller than the laser wavelength. Experiments showed LIPSS to be much more cost-effective and accurate technique to use for machining of WBG at micro- and nano-resolutions, compared to other conventional chemical or mechanical techniques, mainly thanks to its simple experimental setup, high reproducibility, and applicability to vast range of materials (semiconductors, metals and isolators) [1].

In our study, we observe femtosecond laser radiation (λ=1030 nm, τ=180 fs) interaction with the surface of transparent crystal GaN under different experimental conditions (number of pulses, energy of pulse, scanning direction, polarization of laser radiation and irradiation mode), to obtain a database of optimal experimental parameters that allow us to control the characteristics of formed LIPSS, in order to achieve highly reproducible structures on larger surface areas. The results are discussed regarding the potential applications of LIPSS, such as: surface characteristic control (wettability), fabrication of quantum dots and quantum-wires (LEDs, solar cells), and enhancement of optical properties (photoluminescence, absorption) [2].

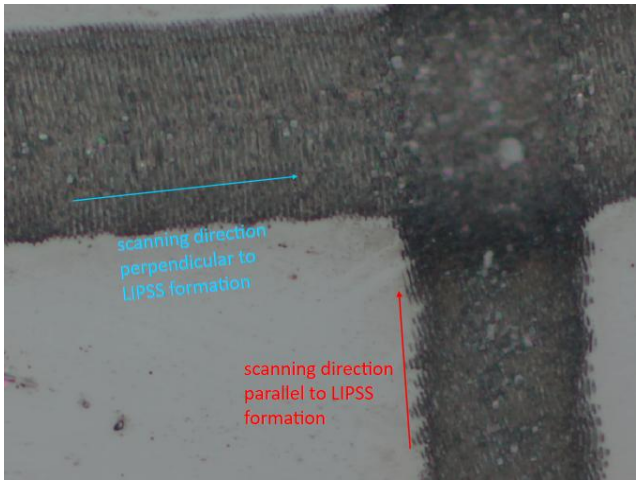

Figure 1. Comparison of characteristics of formed LIPSS at different scanning directions.

REFERENCES

[1] J. Bonse, S. Höhm, S. V. Kirner, A. Rosenfeld, and J. Krüger, Laser-induced periodic surface structures—A scientific evergreen. IEEE Journal of selected topics in quantum electronics, 23(3), (2016).
[2] Q. Hua, B. Ma and W. Hu., Aluminum, Gallium, and Indium Nitrides. Encyclopedia of Materials: Technical Ceramics and Glasses 3, 74-83, (2021).

ORCID: M.S. 0009-0006-0079-4295, D. T. 0000-0001-9426-8160

Effects of high heat flux obtained by pulsed laser irradiation on PM 316L alloy

J. Ruzic[1], D. Bozic[1], M. Simic[1], A. Zekic[2], B. Vucetic[2] and J. Stasic[1]
[1]*Department of Materials, "Vinča" Institute of Nuclear Sciences - National Institute of the Republic of Serbia, University of Belgrade, Serbia*
[2]*Faculty of Physics, University of Belgrade, Serbia*
e-mail: jruzic@vin.bg.ac.rs

316L alloy, known for its excellent mechanical properties up to 600 °C and massive application in various industries, is considered as one of the important candidates for fusion reactor construction materials, as well as matrix for other potential materials with this purpose. It belongs to the class of austenitic steels, which are only lately considered as a basis for the so-called oxide dispersion strengthened (ODS) steels, where ceramic nanoparticles ensure endurance of the material at temperatures over 700 °C, under high pressure and neutron irradiation. Austenitic ODS steels, including 316L-based, are still being developed and, although ferritic steels are studied as well, they are expected to perform better in regards to certain high temperature properties [1]. 316L steel can be synthesized through different routes – aside from conventional casting, it can be obtained from powders by novel method of selective laser method (SLM), as well as contemporary techniques of powder metallurgy (PM) used in this work. Samples were then subjected to laser irradiation in vacuum which, in one approximation, could simulate high heat fluxes present in the reactor. Since materials are also exposed to the effects of light species, preliminary results of conventionally obtained 316L irradiated by ultrashort laser pulses in He atmosphere are also given. Synthesis of 316L alloy comprised hot pressing of powders, using following process parameters: temperature 1150 °C, holding time 2 h, pressure 40 MPa, argon atmosphere. Density of the obtained samples, determined by Archimedes method, was about 90% of the theoretical value. Laser irradiation was done using picosecond Nd:YAG laser with energies up to 30 mJ at different number of delivered pulses (up to 500). XRD analysis has identified austenite as dominant phase with FCC crystal structure. Microstructural characterization was performed using SEM-EDS. Based on the obtained SEM images of the surface damages in vacuum, damage threshold for 500 pulses was estimated to be about ~0.9 J/cm^2.

Acknowledgement: This research was supported by the Science Fund of the Republic of Serbia, Grant No. 7365, Development of dispersion-strengthened metal-based materials for applications in fusion reactor - DisSFusionMat; and by the Ministry of Education, Science and Technological Development of the Republic of Serbia, Contract No. 451-03-136/2025-03/200017.

REFERENCES

[1] B. Bandriyana, B. Sugeng, R. Salam, D. Hairani, A. Sujatno, N. Shabrina, M. Silalahi, Synthesis and microstructure evaluation of ODS steel 316L with zirconia dispersion, Journal of Physics: Conference Series, 1912 (2021) 012002.

ORCID: J.R. 0000-0002-8076-0012, D.B. 0000-0002-0556-4708, M.S. 0000-0003-4474-0257, A.Z. 0000-0001-7720-5846, B.V. 0000-0001-9621-0376, J.S. 0000-0002-3900-3298

10. Optical metamaterials and plasmonics

Graphene Based Plasmon-Induced Terahertz Metamaterial for High-Performance Multispectral Detecting

Y. Demirhan[1,2], N. A. Tertemiz[4], S. Balcı[4], H. Altan[5], G. Aygün[1], L. Özyüzer[1,3]
[1]*Department of Physics, İzmir Institute of Technology, İzmir, Turkey*
[2]*Center for Materıals Research, Integrated Research Centers, İzmir Institute of Technology, İzmir, Turkey*
[3]*Teknoma Technologıcal Materials Industrial and Tradıng ınc, İzmir, Turkey.*
[4]*Department of Photonıcs, İzmir Instıtute of Technology, İzmir, Turkey*
[5]*Department of Physics, Mıddle East Technical Unıversıty, Ankara, Turkey*
e-mail: yasemindemirhan@iyte.edu.tr

The invention of metamaterials has attracted significant academic and technological interest due to their extraordinary electromagnetic (EM) properties, which are not readily achievable with conventional photonic and optical materials [1-3]. Among the various types of metamaterials, plasmonic metamaterials stand out by harnessing surface plasmons (SPs), which exhibit some of the most compelling EM characteristics [4]. Graphene and other two-dimensional (2D) materials have opened new possibilities for next-generation optoelectronic devices, including ultrafast photodetectors. Graphene supports tightly confined surface waves with low losses and tunable properties, making it a strong candidate for terahertz (THz) detection. Plasmonic metamaterials with multiband and broadband responses provide a promising approach for detector design. Using graphene-coated mesa structures can enhance light–matter interaction through plasmonic effects in the THz range. Additionally, three-dimensional graphene-based structures enable the excitation of higher-order plasmonic modes and multiple resonance frequencies. In this study, a high-performance terahertz metamaterial structure based on graphene and induced by surface plasmon resonance is proposed, featuring tunable resonance frequencies. Graphene-coated mesa metamaterial structures were designed and fabricated as integrated photodetector arrays on a single chip. These structures inherently enable plasmonic enhancement without the need for separate metamaterial integration. THz lenses were incorporated into the multispectral photodetector chips to improve performance. Metamaterial unit cells with varying mesa dimensions (70 x 70 um^2 – 90 x 90 um^2), (85 x 85 um^2 – 100 x 100 um^2), (115 x 115 um^2 – 135 x 135 um^2), were optimized through CST Microwave Studio simulations for operation at 1.1, 0.9, and 0.6 THz. Fabrication was carried out on high-resistivity silicon substrates using UV lithography and reactive ion beam etching, followed by graphene deposition via Plasma-Enhanced Chemical Vapor Deposition (PECVD). The electromagnetic response of the devices was characterized using both THz Time-Domain Spectroscopy and continuous-wave THz imaging systems. The effects of graphene thickness and Fermi level on the reflection spectrum have been determined. Furthermore, the characteristics of the plasmonic resonance modes were qualitatively analyzed and compared with experimental results.

Acknowledgement: This research is partially supported by TUBITAK (Scientific and Technical Research Council of Turkey) project number 221M087. We would like to thank the Research and Application Center for Quantum Technologies (RACQUT) of IZTECH for the experimental facilities.

REFERENCES:

[4] M.Tonouchi, Cutting edge THz technology, Nat. Photonics 97, 1 (2007).
[5] L. Ozyuzer et al., Emission of THz waves from superconductors, Science 318, 1291 (2007).
[6] Y. Demirhan et al., Fourcross shaped metamaterial filters fabricated from high temperature superconducting YBCO and Au thin films for terahertz waves" Supercond. Sci. Technol. 30 074006 (9pp) (2017).
[4] B. Akyurek, A. Noori, Y. Demirhan, L. Ozyuzer, K. Guven, H. Altan, & G. Aygun, VO2-Based Dynamic Coding Metamaterials for Terahertz Wavefront Engineering. Journal of Infrared, Millimeter, and Terahertz Waves, 46(1), 1-19, (2025).

Studying electronic properties and plasmonic reactivity of (functionalized) nanoparticles by x-ray aerosol photoelectron spectroscopy (XAPS)

A. R. Milosavljević[1], D. Danilović[2], R. Schürmann[3], R. Dojčilović[2], D. K. Božanić[2] and I. Bald[4]
[1]*Synchrotron SOLEIL, L'Orme des Merisiers, 91190 Saint-Aubin, France*
[2]*Vinca Institute of Nuclear Sciences, Belgrade, Serbia*
[3]*Physikalisch-Technische Bundesanstalt (PTB), Abbestr. 2-12, 10587 Berlin, Germany*
[4]*Institute of Chemistry – Hybrid Nanostructures, University of Potsdam, Karl-Liebknecht-Straße 24-25, 14476 Potsdam, Germany*
e-mail: aleksandar.milosavljevic@synchrotron-soleil.fr

We present the experimental technique for x-ray aerosol photoelectron spectroscopy (XAPS) at the PLEIADES beamline of the SOLEIL synchrotron (France) [1,2]. It allows us to measure the electronic properties of (functionalized) nanoparticles (NPs) isolated in the gas-phase, free of any solvent or substrate, therefore, to study the intrinsic physicochemical properties of such complex targets. This could help to develop new materials and improve our understanding of the light interaction with such materials. Furthermore, the corresponding theoretical results could be compared to the experiment, therefore further improving our understanding of newly developed materials.

In the present contribution, we will show results for two types of NPs. The first class corresponds to the lead halide perovskite nanocrystals [3], as well as silver-bismuth iodide nanoplatelets [2,4]. The former NPs belong to the hybrid perovskite materials that have attracted extensive research interest in recent years as they exhibit optical and semiconducting properties favorable for the fabrication of optoelectronic devices such as solar cells, light-emitting diodes, and photodetectors. The later Ag-Bi-I NPs have been considered as a possible more stable and lead-free replacement for methylammonium lead halides. The second class of materials that we will present corresponds to the functionalized noble metal NPs. Such system can undergo localized surface plasmon resonances that can induce and drive reactions of adsorbed ligand molecules [5]. They have been intensively investigated in recent years as they provide opportunities in chemical synthesis, optoelectronics etc. (see [5] and references therein).

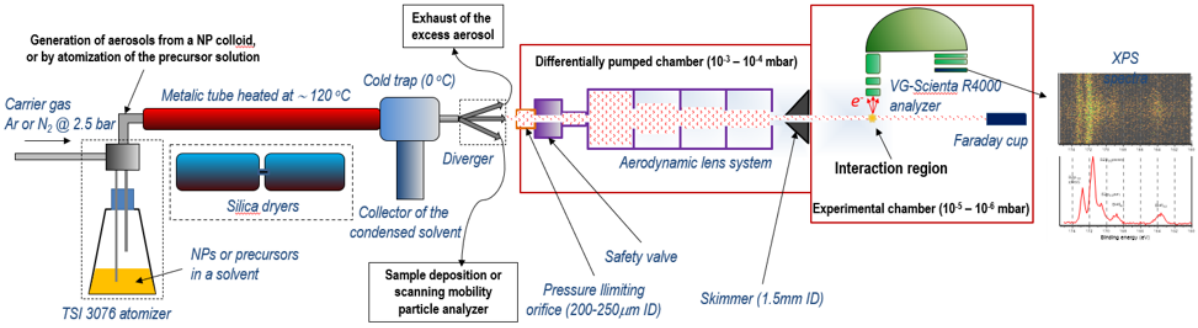

Figure 1. XAPS setup at PLEIADES, SOLEIL [2].

REFERENCES
[1] A. Lindblad et al., Rev. Sci. Instrum. 84, 113105 (2013)
[2] D. Danilović et al., J. Phys. Chem. C 124, 23930 (2021)
[3] A. Milosavljevic et al, J. Phys. Chem. Lett. 9, 3604 (2018)
[4] D. Danilović et al., J. Phys. Chem. C 1126, 13739 (2022)
[5] R. Schürmann et al., J. Chem. Phys. 157, 084708 (2022)

ORCID: A. M. 0000-0003-3541-8872

Electron energy loss function in a graphene-hBN-graphene heterostructure

I. Radović[1], A. Kalinić[1], L. Karbunar[2] and Z.L. Mišković[3]
[1]*Department of Atomic Physics, Vinča Institute of Nuclear Sciences - National Institute of the Republic of Serbia, University of Belgrade, Belgrade, Serbia*
[2]*School of Computing, Union University, Belgrade, Serbia*
[3]*Department of Applied Mathematics, University of Waterloo, Waterloo, Ontario, Canada*
e-mail: iradovic@vin.bg.ac.rs

In our previous publications [1-4], we studied the effects of plasmon-phonon hybridization in a sandwich-like structure consisting of two doped graphene sheets separated by a layer of aluminum oxide (Al_2O_3) [1-4], silicon dioxide (SiO_2) [4], and hafnium dioxide (HfO_2) [4]. In all those publications, we considered only isotropic insulators between two graphene sheets.

In this work, we investigate for the first time two graphene layers separated by an insulating slab that exhibits anisotropy of a uniaxial crystal. We choose an anisotropic layer of hexagonal boron nitride (hBN) because van der Waals heterostructures based on graphene and hBN layers with different stacking modes have been attracting a great deal of interest in the last few years owing to their potential applications [5-8]. The objective is to explore the effects of anisotropy of hBN in the graphene-hBN-graphene heterostructure. In particular, we examine the plasmon-phonon hybridization in the range of frequencies corresponding to the Reststrahlen bands of hBN, where the phonon modes of this material exhibit hyperbolic dispersion.

The expression for the effective surface electron energy loss (EEL) function (the imaginary part of the negative value of the surface response function [9]) of the graphene-hBN-graphene composite system is derived following and generalizing the continued fraction method of Ref. [10]. The response function of each graphene is obtained using the dynamic polarization function of doped graphene within the random phase approximation for its π electrons described as Dirac's fermions. The response of the anisotropic hBN layer is described by a diagonal dielectric tensor consisting of the in-plane and axial components.

We compare the effective surface EEL functions of the graphene-hBN-graphene systems in the cases of the anisotropic and fictitious isotropic (with the dielectric functions equal to the in-plane or axial components) hBN layers.

REFERENCES

[1] V. Despoja, T. Djordjević, L. Karbunar, I. Radović, Z.L. Mišković, Phys. Rev. B 96, 075433 (2017).
[2] V. Despoja, I. Radović, L. Karbunar, A. Kalinić, Z.L. Mišković, Phys. Rev. B 100, 035443 (2019).
[3] A. Kalinić, V. Despoja, I. Radović, L. Karbunar, Z.L. Mišković, Phys. Rev. B 106, 115430 (2022).
[4] A. Kalinić, I. Radović, L. Karbunar, V. Despoja, Z.L. Mišković, Nanomaterials 14, 1951 (2024).
[5] D.A. Mylnikov, M.A. Kashchenko, K.N. Kapralov, D.A. Ghazaryan, E.E. Vdovin, S.V. Morozov, K.S. Novoselov, D.A. Bandurin, A.I. Chernov, D.A. Svintsov, npj 2D Mater. Appl. 8, 34 (2024).
[6] N. Golenić, S. de Gironcoli, V. Despoja, npj 2D Mater. Appl. 8, 37 (2024).
[7] H. Abdelsalam, M.A.S. Sakr, N.H. Teleb, O.H. Abd-Elkader, W. Zhilong, Y. Liu, Q. Zhang, Chin. J. Phys. 90, 237 (2024).
[8] Yu.N. Khanin, E.E. Vdovin, S.V. Morozov, K.S. Novoselov, JETP Lett. 118, 433 (2023).
[9] B. Gumhalter, Prog. Surf. Sci. 15, 1 (1984).
[10] Ph. Lambin, J.P. Vigneron, A.A. Lucas, Phys. Rev. B 32, 8203 (1985).

ORCID: I.R. 0000-0002-8402-9585, A.K. 0000-0002-3541-0531, L.K. 0000-0002-3319-5823, Z.L.M. 0000-0003-3882-8930

Monitoring Adsorption and Reduction Kinetics in a Plasmonic Microreactor Using Methylene Blue as a Model System

O. Jakšić[1], K. Radulović[1], M. Bošković[1], M. Obradov[1] and D. Vasiljević-Radović[1]
[1]*Department of Microelectronic Technologies, Institute of Chemistry, Technology and Metallurgy—National Institute of the Republic of Serbia, University of Belgrade, Njegoševa 12, 11000 Belgrade, Serbia*
e-mail: olga@nanosys.ihtm.bg.ac.rs

We explore a plasmonic microreactor concept designed for real-time monitoring of surface adsorption and catalytic transformations. As a model system, we study the adsorption and subsequent reduction of methylene blue (MB) on a gold surface, forming leuco-methylene blue (LMB). The proposed reaction is represented by a stoichiometric equation and schematically shown in Fig 1 (left).

To interpret the temporal sensor response, we develop a kinetic model that describes the evolution of MB in solution, its adsorption onto gold, and its conversion to LMB. The model incorporates rate constants for adsorption, desorption, and surface-bound reduction, along with a conservation law for total surface binding sites and MB molecules. For a realistic parameter set [1], Fig 1 (right) shows exponential relaxation toward a steady state, a numerical solution to the model, illustrating the dynamic changes in molecular populations.

$$\mathrm{MB\ (sol)} + S \underset{k_d}{\overset{k_a}{\rightleftharpoons}} \mathrm{MB}_S \xrightarrow{k_r} \mathrm{LMB\ (sol)} + S$$

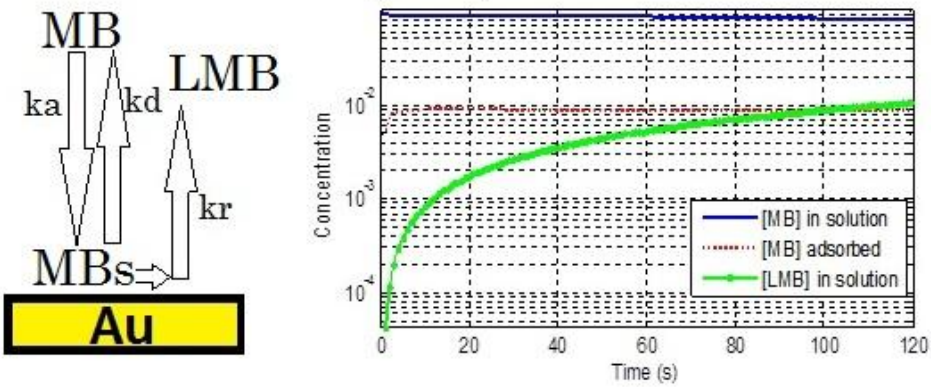

Figure 1. Top: Stoichiometric equation showing how free surface site S gets occupied byu an MB molecule and released again after MB catalytically reduces to LMB (which does not stay on the surface and does not re-adsorb). Left: schematic block diagram. Right: Temporal response of reactants assuming concentration of the reducing agent is constant and in large excess.

The refractive index change is proportional to the change in surface-bound MB population, so plasmonic read-out in these microreactors supports the integration of photonic devices allowing for simultaneous plasmonic sensing and reaction monitoring.

Further model refinement involves multicomponent adsorption, surface heterogeneity (e.g., gold microstripes), spatially varying reactivity and system alterations and optimizations with respect to practical problems [2]. This approach enables dual-function microreactors where optical read-out assists both in-situ detection and quantitative modeling of surface reactions.

REFERENCES

[1] Sharma, K., Sharma, S., Sharma, V., Mishra, P. K., Ekielski, A., Sharma, V., & Kumar, V. (2021). Methylene blue dye adsorption from wastewater using hydroxyapatite/gold nanocomposite: Kinetic and thermodynamics studies. *Nanomaterials*, *11*(6), 1403.

[2] Aravind, A., Dhinasekaran, D., & Rajendran, A. R. (2025). Titanium Mxene: A Promising Material for Next-Generation Optical Biosensors and Machine Learning Integration. Analysis & Sensing, 5(2), e202400095.

ORCID: O.J. 0000-0002-0937-3677, K.R. 0000-0001-5898-6130,
M.B. 0000-0003-1428-9346, M.O. 0000-0001-8559-9048, D. V-R. 0000-0002-7609-8599

Influence of the GaN phonon excitations on the EELS spectra of a hole-doped graphene-GaN-graphene system

T. Đorđević[1], A. Kalinić[1], J. P. Georgijević[1] and J. Jakovac[2]
[1]*Vinca Institute of Nuclear Sciences, PO Box 522, 11 351, Belgrade, Serbia*
[2]*Institute of Physics, Bijenička 46,10000 Zagreb, Croatia*
e-mail: tijanam@vin.bg.ac.rs

Two-dimensional (2D) nanomaterials occupy the scientific community interest with the increasing need for minimization of devices. The discovery of graphene in 2004 significantly expands the field of research into 2D structures, among which, in addition to graphene itself, are MoS2, borophene, and phosphorene. Wide band-gap semiconductors such as GaN and SiC stand out as potential substrates for their application in nanodevices. In this poster, we analyze the graphene-GaN-graphene system. The Dirac plasmon (DP) dominates the electron energy loss (EELS) spectra of doped graphene [1], while GaN is characterized by phonon branches [2] in the same lower ω(Q) regime, that hybridizes with the DP. Understanding plasmon-phonon coupling in this system is critical for further development of optoelectronic devices. In addition to the fact that GaN has interesting dielectric properties, it is also widely used [3] in photonics, optoelectronics and sensor technology etc. The dielectric function of GaN and the polarization function of graphene are obtained by the ab initio method. As a result, the EELS spectra of the observed system is presented.

REFERENCES

[1] V. Despoja, J. Jakovac, N. Golenić, L. Marušić, Npj 2D Mater. Appl. 4, 51 (2020).
[2] Z. Zhang, T. Wang, H. Jiang, X. Xu, J. Wang, Z. Wang, F. Liu, Y. Yu, Y. Zhang, P. Wang, P. Gao, B. Shen, X. Wang, Nat. Commun. 15(1) (2024).
[3] G. Li, M. Zhu, Z. Guo, Y. Yang, H. Li, J. Shang, Y. Feng, Y. Lu, F. Gao, S. Li, J. Mater. Chem. C 12, 12150 (2024).

ORCID: T.Đ. 0000-0003-0022-9334, J.P.G. 0000-0001-5858-4772, J.J. 0000-0003-0771-2150

11. Machine learning in photonics

Computational capacity of LA-VCSEL devices with complex resonator shapes

L. Cardenas-Razo[1], A. Skalli[1], M. Marciniak[2], M. Gebski[2], S. Reitzenstein[3], J. A. Lott[3], T. Czyszanowski[2] and D. Brunner[1]
[1]*Institut FEMTO-ST, Université Marie et Louis Pasteur, CNRS UMR, 6174, Besancon, France*
[2]*Institute of Physics, Lodz University of technology, Wólczańska 217/22190-005 Łódź, Poland*
[3]*Institut für Festkörperphysik, Technische Universität Berlin, Hardenbergstraße 36, 10623 Berlin, Germany*
e-mail: lucero.cr@femto-st.fr

In our current era of data and information, the amount of energy required to sustain modern AI is reaching formidable levels. Motivated by this, novel hardware architectures such as optical neural networks (ONN) have emerged as a high-performance, energy-efficient and scalable alternatives.

We have recently demonstrated a ONN using a semiconductor multimode vertical-cavity surface-emitting laser (LA-VCSEL) [1] as the nonlinear neuron substrate, realizing spatial multiplexed photonic neurons with trainable input and output weights, see Fig. 1(a). This network is inherently autonomous, parallel and fully realized in hardware, using off-the-shelf components. Training was achieved using model-free training algorithms, obtaining 93% test accuracy, outperforming the digital linear classifier, hence highlighting the nonlinear transformation produced by the laser.

However, the link between a LA-VCSEL's area, shape and operating conditions and an ONN's computational dimensionality is non-trivial. Here, we perform a detailed, data-driven study to link different physical parameters of the ONNs to general computational metrics, such as the number of neurons. Furthermore, we explore circular as well as chaotic resonator shapes and their impact on these principle performance predictors.
In these experiments, we recorded with a camera the response of LA-VCSELs with different chaotic cavity geometries and aperture sizes to each image in the MNIST training dataset. Additionally, we scanned different injection laser positions inside the laser aperture. We applied Principal Component Analysis (PCA) to carry out a dimensionality study on the acquired images. The number of linearly independent principal components (PCs) determines the LA-VCSEL's computational dimensionality, i.e., the neurons in our system. To account for the noise in the ONN, we used a criterion presented in [2] to separate the dimensions resulting from real data variations from those where noise was predominant, thus arriving at a more physically meaningful dimensionality. To link the dimension of the device to a performance metric, we performed classification of MNIST digits under the same injection conditions. Our results identify a potential link between dimensionality and ONN computing performance, see Fig. 1 (b).
In conclusion, this study established a bridge between the computational performance of LA-VCSELs through a simple and fast measurement to determine the system's dimensionality, and through that provides physical insights to guide the design of novel LA-VCSELs for optical computing.

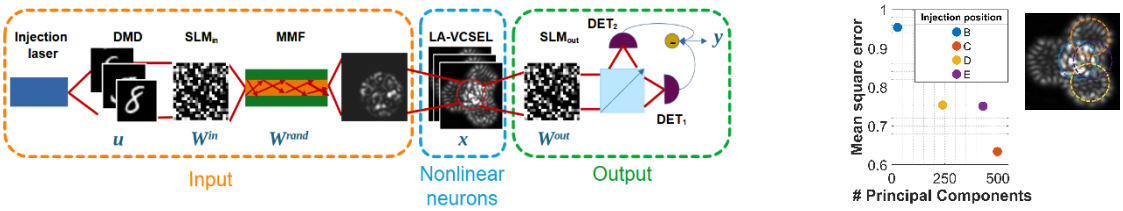

Figure 1. (a) Experimental setup of the ONN. (b) Computing power vs dimensionality represented by plotting MSE (mean square error) vs number of PCAs/ neurons in the LA-VCSEL.

REFERENCES

[1] Skalli, A., et al. (2025). Model-free front-to-end training of a large high performance laser neural network.https://arxiv.org/abs/2503.16943
[2] Skalli, A., et al. (2022). Computational metrics and parameters of an injection-locked large area semiconductor laser for neural network computing. https://doi.org/10.1364/OME.451524

ORCID: L.C.R. 0009-0004-8080-0733, A.S. 0000-0002-7039-926X, D.B. 0000-0002-4003-3056

Optical reservoir computing with controlled complexity

N. Marinin[1] and M. Rafayelyan
[1]*PhotonicsAI lab, Yerevan State University, Armenia*
e-mail: nikita.marinin@ysu.am

Reservoir Computing (RC) is a computational approach based on a Recurrent Neural Network. There are many implementations of Optical Reservoir Computing [1]. In other works, different reservoir schemes with different connectivities and interconnections were explored [2]. We propose an advanced optical scheme using a Liquid Crystal Cell (LCC) with a voltage-controlled scattering as a reservoir.

The amount of scattering in the LCC and, as a result, the complexity of reservoir in corresponding RC scheme changes under different applied voltages. Our experimental results show gradual transition from dense, Gaussian-distributed to the identity diagonal matrix in a simple retrieval task.

In a high scattering case, results were comparable with the results of experiments with a fixed high-scattering media. Steady transformation of a retrieved transmission matrix from a Random Gaussian type (high scattering cases) to an identity diagonal type (low scattering cases) is shown.

Besides that, we compared the time predictions of spatiotemporal chaotic datasets obtained from the Kuramoto-Sivashinky equation, obtained with optical setup in different scattering cases, to the results of simulations with corresponding parameters of the reservoir. The results show the change in prediction quality for different reservoir complexities. Adjusting the reservoir according to the task may allow us to achieve better performance.

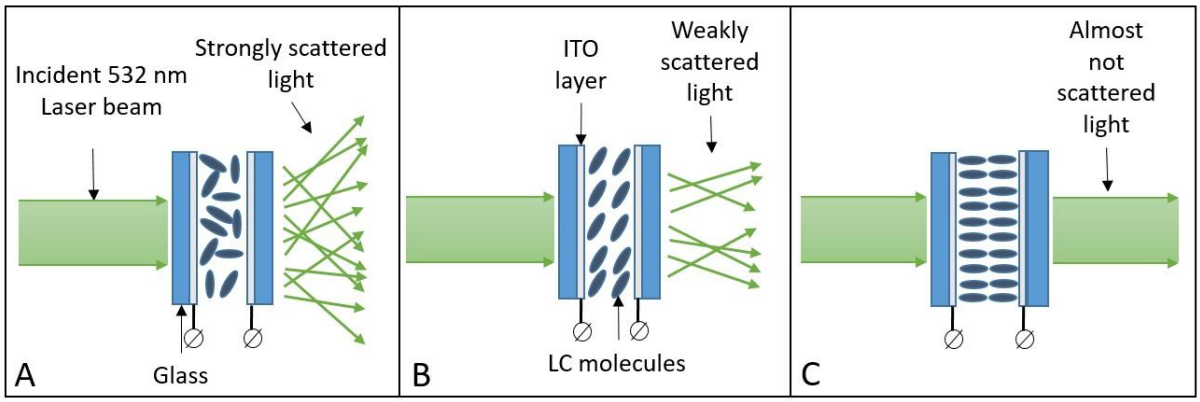

Figure 1. Different scattering cases for LCC. (A) No voltage. The LC molecules inside the cell are disordered. Light undergoes many scattering events inside the LCC. (B) Medium voltage. The LC molecules begin to orient themselves in the direction of the applied electric field. Light undergoes less scattering events inside the LCC. (C) High voltage. The LC molecules are oriented in the direction of the electric field. Light undergoes insignificant amount of scattering events inside the LCC.

REFERENCES

[1] M. Rafayelyan, J. Dong, Y. Tan, F. Krzakala, S. Gigan, “Large-scale optical reservoir computing for spatiotemporal chaotic systems prediction,” Physical Review X, 10(4), 041037 (2020).
[2] Pathak, Jaideep, et al. "Model-free prediction of large spatiotemporally chaotic systems from data: A reservoir computing approach." *Physical review letters* 120.2 (2018): 024102.

ORCID: N.M. 0009-0005-6092-201X, M.R. 0000-0001-7615-6579

The interference effects in injection-locking-based reservoir computing: a case study of a Fabry-Perot laser diode under optical injection

M. Banović, N. Bratić, P. Atanasijević, J. Crnjanski, M. Krstić, and D. Gvozdić
School of Electrical Engineering, University of Belgrade, Serbia
e-mail: mladen@etf.rs

Photonic neural networks (PNNs) offer a fast and energy-efficient platform for machine learning, with two dominant architectures: multilayer perceptrons (MLPs) and recurrent neural networks (RNNs). MLPs rely on feedforward summation and nonlinear activation, while RNNs incorporate feedback to process temporal data. An efficient photonic RNN variant is time-delayed reservoir computing (RC), which uses a single nonlinear element with delayed feedback, often implemented using semiconductor lasers and optical fibers [1-4].

Regardless of the specific architecture, a common requirement in all PNNs is the ability to combine multiple optical input contributions and apply a nonlinear transformation. In coherent photonic systems, this summation process is affected by optical interference, making the experimental realizations of PNNs highly susceptible to environmental optical path length variations, coherence degradation, and wavelength instabilitiess.

In all-optical implementations of time-delayed RC, based on laser diodes driven by optical injection, a particularly problematic case arises, as the phase sensitivity between overlapping pulses in the delay loop alters internal state evolution, reducing memory capacity and task performance [3]. In the experimental realizations, the newly incoming pulse interferes with the previous pulse from the feedback loop, often 10-1000 m long. Even though both pulses originate from the same coherent source, they are substantially delayed by the loop length, giving rise to the pronounced beating signal with a frequency equal to the notorious frequency drift of the laser source. Moreover, the difficulty in environmental stabilization of an interferometer with unbalanced branches surges as the branch path lengths increase. Finally, an optically injected laser diode, serving as a nonlinear activator, suffers from the inherently present frequency chirping due to rapid carrier induced phase oscillations [5], furthering the problem of beating in all-optical summation.

In our research, we delve deep into the experimental time-delayed RC realizations for Gb/s speeds based on Fabry-Pérot laser diodes under optical injection, ensuring reliable computations using different mitigation strategies, creating a novel paradigm of interference-aware RC design.

Acknowledgment: The research was supported by Science Fund of the Republic of Serbia (#7750121, ORCA-LAB), and by Serbian Ministry of Science, Technology and Innovation (451-03-65/2024-03/200103). The research was partially conducted in the premises of the Palace of Science, Miodrag Kostić Endowment.

REFERENCES

[1] A. Tsakyridis *et al*, APL Photonics 9, 011102 (2024).
[2] D. Brunner, M. Soriano, C. Mirasso, *et al*. Nat. Commun. 4, 1364 (2013).
[3] R. Nguimdo, G. Verschaffelt, J. Danckaert, G. der Sande, Opt. Express 24, 1238-1252 (2016).
[4] J.-Y. Tang, B.-D. Lin, Y.-W. Shen, *et al.* Opt. Express 31, 2456–2466 (2023).
[5] J. Liu and D. Botez, *J. Appl. Phys.*, 113, 063104, (2013).

ORCID: M.B. 0009-0001-1843-6326, N.B. 0009-0003-7621-8831, P.A. 0000-0001-7596-0266, J.C. 0000-0003-0685-4093, M.K. 0000-0001-5284-4959, D.G. 0000-0003-0917-5280

Inverse Design for Femtosecond-Laser Photonic Surfaces with Direct Gradient Optimization

A. Haboub[1], A. Khelif [2], and B. Aissa[1]
[1]*Qatar Environment and Energy Research Institute, Materials Center, Hamad Bin Khalifa University, Doha, Qatar.*
[2]*College of Science and Engineering, Hamad Bin Khalifa University, Doha, Qatar.*
e-mail: amhaboub@hbku.edu.qa

The inverse design of photonic surfaces produced by high-throughput femtosecond laser processing is limited by a strongly non-linear, many-to-one mapping from laser parameters (power, speed, hatch spacing) to the resulting optical spectrum. Tandem Neural Networks (TNNs) mitigate this ill-posedness by pairing a forward surrogate with a separately trained inverse network, but they still rely on artificial noise injection to uncover diverse solutions and still explore the design space only sparsely. We propose Direct Gradient Optimization (DGO), a single-network alternative that treats the pre-trained forward surrogate as a differentiable proxy for the laser–material interaction and back-propagates errors all the way to the process parameters. This strategy (i) eliminates inverse-model training, (ii) allows the embedding of practical constraints such as laser-power penalties to be encoded directly in the loss function, and (iii) yields transparent sensitivity information through native gradients and SHapley Additive exPlanations (SHAP).

Two optimization modes are assessed: a single-start DGO and a parallel multi-start "Tournament" DGO that launches multiple random seeds, runs a brief qualification phase, and refines only the five most promising candidates. Across 10000+ inverse-design tasks, Tournament-DGO cuts the average spectral root-mean-squared error (RMSE) from 1.29 % (best TNN) to 0.70 %, and boosts design novelty (quantified by the Normalized Euclidean Parameter Distance, NEPD) from 0.26 to 0.38. A SHAP-based meta-analysis shows that convergence is dominated by the initial hatch spacing, explaining why broad sampling followed by pruning addresses this sensitivity. DGO delivers state-of-the-art accuracy, enhanced robustness, and diverse inverse solution without noise heuristics or extra model training. Its ability to embed manufacturability constraints directly in the optimization loop establishes a powerful, energy-aware platform for scalable photonic devices, thermal emitters, and meta surfaces.

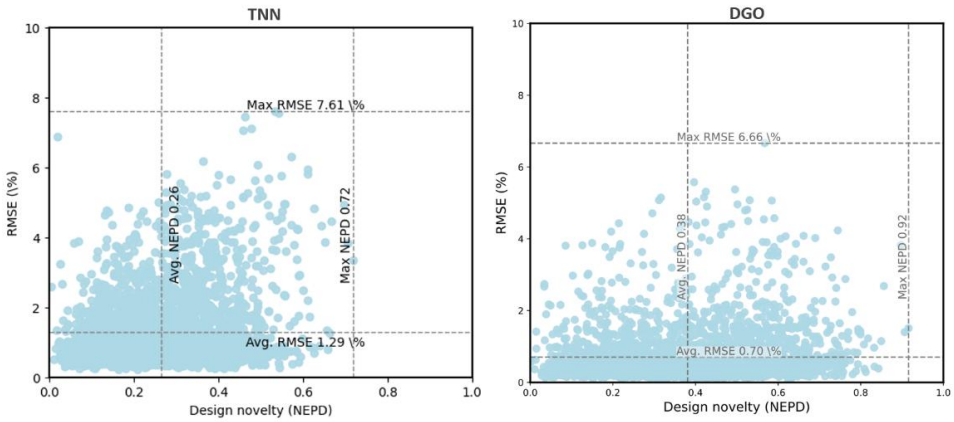

Figure 1. Comparison of TNN (left) and DGO (right) across 10,000+ inverse-design tasks. Points show spectral RMSE vs design novelty (NEPD). DGO achieves lower mean error (0.70\% vs 1.29\%) and higher novelty (0.38 vs 0.26).

REFERENCES

[1] M. Park, L. Grbčić, et al., Adv. Sci. 11(26), 2401951 (2024).
[2] L. Grbčić, M. Park, et al., npj Comput. Mater. 11(1), 35 (2025).

ORCID: A.H. 0000-0002-0766-2272, A.K. 0000-0001-8712-824X, B.A. 0000-0002-4768-9891

Principal Component Analysis for Photoacoustic Experiment Optimization: Evaluating Correlation vs. Covariance Approaches

S.M. Kovacevic[1], M.N. Popovic[1], M. Jordovic Pavlovic[2], D.D. Markushev[1], D.K. Markushev[1]
[1]*Institute of Physics, Belgrade, Serbia*
[2]*Faculty of Mechanical Engineering and Civil Engineering in Kraljevo, University of Kragujevac, Kragujevac, Serbia*
e-mail: slavica.kovacevic@ipb.ac.rs

Background – Photoacoustic material characterization is a non-destructive technique for assessing samples' optical, thermal, and mechanical properties. In this paper we utilize two approaches to PCA, covariance-based and correlation-based, to identify key modulation frequencies for neural network (NN) input, enabling accurate predictions. Using simulated data from a composite piston model [1], we analyzed thermoelastic photoacoustic signals from aluminum samples at varying thicknesses (l) and cut-off frequencies (f_0), across 300 modulation frequencies (10 Hz–10 MHz) in an open-cell setup (Fig 1a).

Results – The data pre-processing of input variables involved transforming amplitudes into decibels. For the covariance approach, the input data to PCA was scaled using maximum absolute (MA) scaling while for the correlation-based approach we used Z-scaled data as input, since $Cor(MA-scaled) = Cov(Z-scaled)$[].When using covariance-based PCA, five phases were selected with modulation frequencies ranging from 1 kHz to 38 kHz. In contrast, the correlation-based approach captured one amplitude and four phases, with frequencies between 22 kHz and 363 kHz.

The NN used had an input layer of 5 nodes, 5 and 10 nodes in the hidden layers and an output layer with 2 nodes, corresponding to l and f_0. For better performance, logarithmic values of output features were used, and both input and output features of the NN were scaled using MA scaling. NN trained on the correlation-based set has smaller mean relative errors (0.03% for l and 0.05% for f_0) compared to the NN trained on the covariance-based set (0.1% for l and 0.18% for f_0) on the independent test data (data outside of the original set used for training).

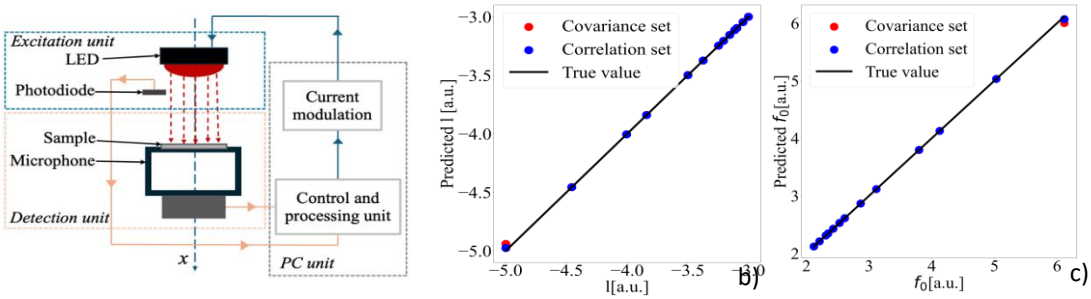

a) Figure 1. Open-cell experimental setup (a) where the sample placed directly on the microphone is periodically heated by a current modulated LED. Independent test results for l (b) and f_0 (c).

Conclusion – Current analysis shows that an NN with 5 thermoelastic signal points, selected using either of the two approaches, as input features predicts values of l and f_0 with adequate precision and accuracy (<5% relative error). While the correlation-based selected variables cover a wider range of modulation frequencies, covariance selected variables capture only phases at significantly lower frequencies, closer to the working range of photoacoustic, from 20 Hz to 20kHz, and thus is a better fit.

REFERENCES

[1] McDonald, F. A. & Wetsel, G. C. Generalized theory of the photoacoustic effect. J. Appl. Phys. 49, 2313–2322 (1978).
[2] Djordjević, K. Lj. et al. Influence of data scaling and normalization on overall neural network performances in photoacoustics. Opt. Quantum Electron. 54, 501 (2022).
[3] Choi, J. & Yang, X. Asymptotic properties of correlation-based principal component analysis, J. Econometrics, 229 (2022)

ORCID: S.M.K. 0009-0008-7502-250X, M.N.P. 0000-0001-8550-4862, M.I.J.P. 0000-0003-4038-6537, D.D.M. 0000-0002-0330-3600, D.K.M. 0000-0003-1270-4606

Fiber optic interferometer sensor for condition surfaces monitoring

K. Rychert[1], M. Szczerska[2], K. Cierpiak[1], and M. Szczerska[1]
[1]*Department of Metrology and Optoelectronics, Faculty of Electronics, Telecommunications and Informatics, Gdańsk University of Technology, Poland*
[2]*GUT Optica Student Chapter, Gdańsk University of Technology, Poland*
e-mail: s190601@student.pg.edu.pl

The increasing dependence on real-time data acquisition and analysis in industrial processes, electronic communications, and manufacturing requires precise and scalable monitoring methods. This research explores the potential of a fiber optic interferometry based system for metal surface condition monitoring, addressing challenges in predictive maintenance and process optimization [1, 2]. Through integration of optical sensing with large-scale data processing, the system enables high-precision diagnostics of surface degradation and monitors key parameters like distance and clearance to maintain geometry and machine performance under continuous motion [3]. Measurements on various materials ranged from 10 to 500 µm in 5 µm increments. Signal changes from the interferometer allowed abrasion levels to be determined. The collected data is processed using machine learning algorithms to improve accuracy and support real-time diagnostics, machine learning algorithms were employed for classification of material wear based on spectral data collected from the fiber-optic interferometer. A set of 52 features was extracted from each spectrum, including peak morphology, intensity distribution, and spectral entropy. Using feature selection and ensemble classifiers such as Random Forest and Extra Trees, the models achieved up to 83% accuracy in distinguishing four wear levels with micrometer precision [4]. These models effectively captured non-linear relationships between optical features and degradation patterns, demonstrating the potential of data-driven approaches in predictive maintenance applications.

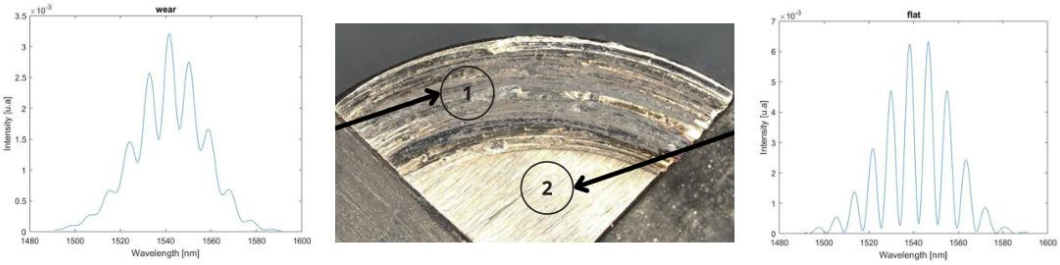

Figure 1. Obtained signal of flat and wear surfaces of measured stainless steel sample.

Acknowledgment: The project is co-financed by DS programs of Faculty of Electronics, Telecommunications and Informatics of Gdańsk Tech, and by the 7/1/2024/IDUB/III.4c/Tc grant under the TECHNETIUM Talent Management Grants program and by 6/1/2025/IDUB/III.4a/Pu grant under the Plutonium Supporting Student Research Teams, which is herein gratefully acknowledged.

REFERENCES

[1] M Jedrzejewska-Szczerska, *at all* Low-coherence fiber-optic interferometric sensors, (2011), Acta Physica Polonica A 120 (4), 621-624
[2] D. Milewska, *at all*, Application of thin diamond films in
low-coherence fiber-optic Fabry Pérot displacement sensor, Diamond and Related Materials, Volume 64, 2016, https://doi.org/10.1016/j.diamond.2016.02.015.
[3] P. Sokołowski, *at all* "Fiber optic interferometer as a sensor for surface conditions measurement",(2024), Proc. SPIE 13187, Advances in 3OM: Opto-Mechatronics, Opto-Mechanics, and Optical Metrology 3OM 2023, 1318707; https://doi.org/10.1117/12.3021424
[4] Cierpiak, K., *at all* (2023). Application of fiber optic sensors using Machine Learning algorithms for temperature measurement of lithium-ion batteries. Photonics Letters of Poland, 15(3), 36–38. https://doi.org/10.4302/plp.v15i3.1207

Hardware matrix multiplication through silicon photonics

R. Minnullin, A. Sapegin, M. Makarov, A. Marakhin, A. Italyantsev
JSC Molecular Electronics Research Institute, Zelenograd, Moscow, Russia
e-mail: rminnullin@niime.ru

Matrix multiplication is of the utmost need and use in data processing. It has been used in a variety of applications including image processing and various types of data analysis, however substantial expansion of artificial intelligence and neural network technologies in recent years have made them primary contributors to the development of hardware matrix multiplication approaches. Vast research in this field have resulted in occurrence of specialized electronic integrated circuits for matrix multiplication, namely, application specific integrated circuits (ASICs), tensor processing units (TPUs) and neural processing units (NPUs), besides GPUs and field-programmable gate arrays (FPGAs) that have already been used for this purpose since the appearance of hardware acceleration concept [1]. Meanwhile, rapid progress in integrated photonics has also evoked outstanding opportunities for performing matrix multiplication on a hardware level with the use of light.

Variety of different approaches to realization of matrix multiplication in photonics can be classified into 4 principal groups:

1) mathematical matrix is represented as physical matrix of modulators: ring resonators or elements including phase change materials [2, 3] (Figure 1a);
2) mathematical matrix is factorized through singular value decomposition into a product of two unitary matrices and a rectangular diagonal matrix, which are further physically represented by the appropriate set of Mach–Zehnder interferometers and attenuators [4] (Figure 1b);
3) matrix coefficients are physically encoded into the specific geometry of a multimode interferometer (MMI) [5] (Figure 1c);
4) mathematical matrix is represented as physical matrix of attenuators but light propagates in free space out of the plane of a photonic chip in contrary to in-plane propagation in previous approaches – so called 3D approach [6] (Figure 1d).

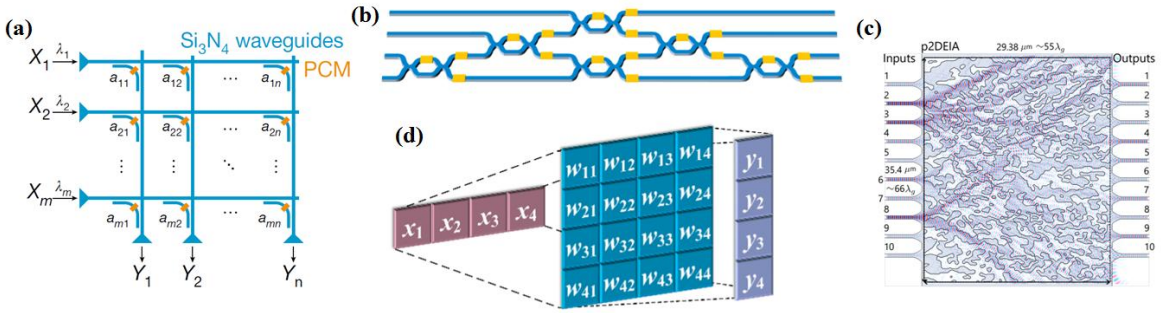

Figure 1. Approaches to photonic matrix multiplication

In this paper we review the latest research on realization of matrix multiplication in silicon photonics classifying them by approach into the aforementioned 4 groups, we briefly discuss the basic principles of these approaches noting their benefits and drawbacks, and report on our elaboration on the topic.

REFERENCES

[1] Reuther A., Michaleas P., Jones M. et al. 2020 IEEE HPEC Conf. 2020, pp. 1–12
[2] Feldmann, J., Youngblood, N., Wright, C.D. et al. *Nature* **569**, 208–214 (2019)
[3] Feldmann J., Youngblood N., Karpov M. et al. *Nature* **589**, 52–58 (2021)
[4] Zhang H., Gu M., Jiang X.D. et al. *Nat. Commun.* **12**, 457 (2021)
[5] Nikkhah V., Pirmoradi A., Ashtiani F. et al. *Nat. Photon.* **18**, 501–508 (2024)
[6] Lin X., Rivenson Y., Yardimci N.T. et al. *Science*, **361**, 1004–1008 (2018)

Reconfigurable all-optical sigmoid-like activator based on a Fabry-Pérot laser diode with multi-wavelength output capacity

J. Crnjanski, A. Dakić, P. Atanasijević, M. Banović, M. Krstić and D. Gvozdić
School of Electrical Engineering, University of Belgrade, Serbia
e-mail: jasna.crnjanski@etf.bg.ac.rs

Reconfigurable photonic activation functions (AFs) play a key role in advancing neuromorphic computing by enabling ultra-fast and energy-efficient information processing in optical neural networks [1, 2].

In this study, we build upon the foundations of all-optical AFs in Fabry-Pérot laser diodes (FP-LDs) under optical injection shown in [3], achieving AF wavelength conversion and multiple simultaneous sigmoid-like AFs at different wavelengths. To achieve the multi-output operation of our nonlinear element (NLE), we use the dual optical injection (DOI) paradigm, where two input signals are simultaneously coupled into different longitudinal side modes of the FP-LD. Unlike the DOI shown in [3], both optical inputs are pulsed. The DOI pulse trains are Gaussian-shaped, at a repetition rate of 0.5 Gb/s with a FWHM of ~400 ps. The first input operates at a wavelength λ_c, frequency detuned by −15 GHz (red shifted) with respect to the m = +5 longitudinal side mode of the FP-LD (blue shifted with respect to the central FP-LD mode), delivering a continuous train of fixed-peak-power pulses. The second input at λ_p, used to insert the data, is injected near the m = +3 FP-LD side mode, with a variable detuning in the −15 to −21 GHz range (Fig. 1(a)). The data patterns comprise both linearly increasing and randomized sequences of peaks modulated in power, allowing for a realistic investigation of the system's nonlinear behavior. The AFs can be extracted either at λ_c or λ_p, by adjusting the tunable bandpass filter (BPF) providing the NLE with two concurrent, apparently distinct, outputs, as shown in Fig. 1(b). While the AF at λ_p follows a previously demonstrated trend [2,3], the wavelength converted AF at λ_c exhibits a more pronounced saturation, with a lower ON-OFF power level ratio.

We further extend the known detuning reconfigurability of λ_p AFs [3], exploiting the observed interplay between the signals at λ_c and λ_p within the FP-LD, and demonstrate the 0.55 to 0.75 mW λ_c AF threshold shift by varying the λ_p detuning in the −15 to −21 GHz range. This adaptivity, shown in Fig. 1(c), enables dynamic shaping and real-time reconfiguration of the wavelength-shifted nonlinear response, creating a programmable NLE suitable for all-optical activation in multiwavelength photonic neural networks, enhancing the parallelism and scalability for future demonstrations.

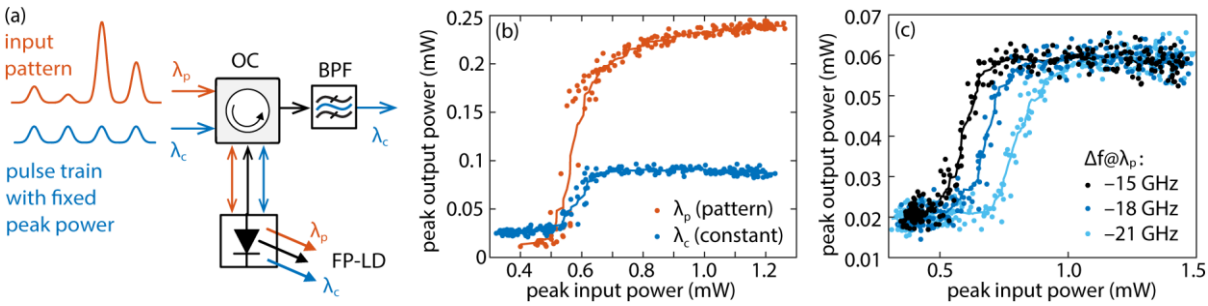

Figure 1. (a) The schematic of the experimental setup. (b) Comparison of nonlinear responses at both outputs. (c) Detuning-dependent nonlinear response at λ_c.

*Acknowledgment: The research was supported by Science Fund of the Republic of Serbia (#7750121, ORCA-LAB), and by Serbian Ministry of Science, Technology and Innovation (451-03-65/2024-03/200103). The research was partially conducted in the premises of the Palace of Science, Miodrag Kostić Endowment.*REFERENCES

[1] A. Tsakyridis *et al*, APL Photonics 9, 011102 (2024).
[2] J. Crnjanski *et al.*, Optics Letters 49, 1153 (2024).
[3] M. Banović *et al.*, arXiv:2503.21603, (2025).

ORCID: J.C. 0000-0003-0685-4093, A.D. 0009-0005-5140-6101, P.A. 0000-0001-7596-0266, M.B. 0009-0001-1843-6326, M.K. 0000-0001-5284-4959, D.G. 0000-0003-0917-5280

Coupled phase-intensity bistability in Fabry-Pérot lasers under optical injection

P. Atanasijević, K. Jović, M. Banović, J. Crnjanski, M. Krstić and D. Gvozdić
University of Belgrade, School of Electrical Engineering, Serbia
e-mail: gvozdic@etf.bg.ac.rs

The concept of real-valued photonic neural networks has recently been extended to complex-valued and Kramers–Kronig neural networks, which process data using inputs, weights, and activation functions that account for both magnitude and phase [1,2]. In this work, we experimentally demonstrate that dispersive bistability in Fabry–Pérot laser diodes (FP-LDs) under optical injection can produce stationary optical phase hysteresis accompanied by optical intensity hysteresis, linked through the Kramers–Kronig relations.

To enable the coherent detection of the FP-LD's output, the experimental setup used in the investigation of quasi-static injection locking (IL) of FP-LDs [3] is complemented with an additional local oscillator (LO) branch and a balanced photodiode (BPD), creating an interferometer illustrated in Fig. 1(a). The master laser's (ML) optical output with a wavelength λ_m is injected into the $m = -3$ side mode of the FP-LD, for several different values of frequency detuning ranging from −15 to −21 GHz (negative values corresponding to a red shift with respect to the central mode). The FP-LD's output signal at λ_m is spectrally selected using an optical bandpass filter (BPF) and interrogated using the interferometer. ML's power is gradually varied, shifting the FP-LD between the IL and the free-running states, experimentally verifying the coupling between the intensity and phase hysteresis loops [4] shown in Figs. 1(b) and (c). The arrows highlight the different directionality of the coupled loops, leading to the conclusion that the transition to the IL state is accompanied by a rise in power and a decline in the phase difference between the ML and the FP-LD. Increasing the magnitude of the frequency detuning in the investigated range is shown to yield wider regions of the coupled intensity-phase bistabilities, achievable for higher input powers. Thus, the complex-valued response is shown to be reconfigurable, with experimentally demonstrated extinction ratios of up to ~8 dB and phase jumps of up to 0.9 rad.

These findings indicate that, in a dynamical regime under optical pulse injection, an FP-LD can serve as an activation unit, providing simultaneous nonlinear responses in both signal intensity and phase, demonstrating the existence of their Kramers–Kronig relation.

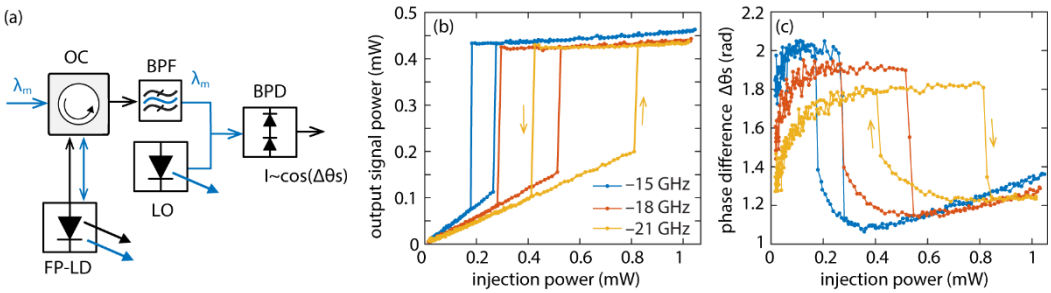

Figure 1. (a) The schematic of the experimental setup used for injection locking of the FP-LD and coherent detection. Static (b) intensity and (c) phase hysteresis loops for different frequency detunings.

Acknowledgment: The research was supported by Science Fund of the Republic of Serbia (#7750121, ORCA-LAB), and by Serbian Ministry of Science, Technology and Innovation (451-03-65/2024-03/200103). The research was partially conducted in the premises of the Palace of Science, Miodrag Kostić Endowment.

REFERENCES

[1] H. Zhang, *et al.*, Nature Communications 12, 457 (2021).
[2] Ye Tian, *et al.*, Advanced Photonics Research 4, 2300062 (2023).
[3] M. Banović, *et al.*, Optics Letters 48, 4165 (2023).
[4] D. Gvozdić, M. Krstić, and J. Crnjanski, Optics Letters 36, 4200 (2011).

ORCID: P.A. 0000-0001-7596-0266, K.J. 0009-0004-4674-5873, M.B. 0009-0001-1843-6326, J.C. 0000-0003-0685-4093, M.K. 0000-0001-5284-4959, D.G. 0000-0003-0917-5280

End-to-end deep learning reconstruction of simulated off-axis holograms

M. Marinković[1], P. Atanasijević[1], M. Badža Atanasijević[1,2], F. Krajinić[1,3], P. Mihailović[1]
[1]*University of Belgrade, School of Electrical Engineering, Belgrade, Serbia*
[2]*Innovation Center of the School of Electrical Engineering in Belgrade, Belgrade, Serbia*
[3]*University of Belgrade, Institute of Physics Belgrade, Belgrade, Serbia*
e-mail: marinkovic.d.marija@gmail.com

In recent years, hologram reconstruction using deep learning models has garnered significant attention due to its potential to accelerate and simplify the reconstruction process, and reduce its computational cost, making holographic imaging more accessible [1,2]. To this day, most reported studies on both simulated and experimental holograms focus on either near-field or in-line approaches, where the object can often be recovered even from low-resolution inputs [3-5]. The best-performing architectures, e.g., generative adversarial networks (GANs), are usually computationally heavy. On the other hand, typically reported U-net-like architectures are usually extended in complexity via the utilization of residual units, multi-path bottlenecks, or multi-branch decoders [3-5].

In this study, we investigate the feasibility of applying an end-to-end deep learning approach for reconstructing high-resolution, off-axis holograms at higher propagation distances using a dataset of simulated 1024x1024 holograms. The hologram simulation process was conducted using MNIST [6] images as amplitudes of the complex object field with the randomized phase and the wavelength of 532 nm. The field is further propagated to a distance of 95 cm, where it interferes with a spherical reference wave at an angle of ~3°, creating the final hologram. The zoomed portion of a representative simulated hologram is shown in Fig. 1 (a).

The proposed autoencoder model employs multiple attention mechanisms – convolutional block attention modules in the encoder, squeeze-and-excitation blocks in the decoder and bottleneck, and attention-gated skip connections - alongside multi-feature extraction layers, dropout, and input striding, resulting in 12 million parameters. The model was developed in Google Colab using PyTorch, and was trained, validated, and tested in a ratio 80%:10%:10% on 10,000 holograms using an A100 GPU. We tested the model's performance using the structural similarity index, and gained the result of 0.93±0.03, which is comparable to similar, in-line approaches [4,5]. Fig. 1 (b) and (c) show the ground truth and model prediction images, demonstrating the performance of the proposed approach.

The presented results promise that the proposed model will serve as a strong starting point in the future transition to experimental data, filling in the niche of deep learning off-axis hologram reconstruction at higher propagation distances.

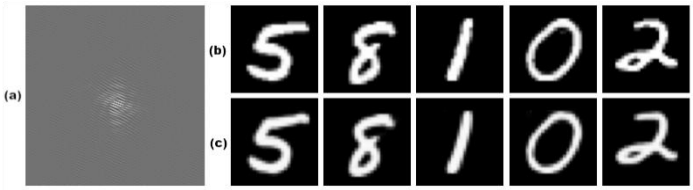

Figure 1. (a) The zoomed portion of a representative hologram, showing the interference fringes. (b) Ground truths and (c) model prediction images.

Acknowledgment: The research was supported by the Serbian Ministry of Science, Technology, and Innovation (grants 451-03-65/2024-03/200103 and 451-03-136/2025-03/200223). The research was partially conducted in the premises of the Palace of Science, Miodrag Kostić Endowment.

REFERENCES

[1] G. Situ, Light: Advanced Manufacturing 3, 278 (2022).
[2] T. Zeng, Y. Zhu, E.Y. Lam, Opt. Express 29, 40572 (2021).
[3] X. Sun, C. Xiong, Z. Ren, Opt. Express 33, 3414 (2025).
[4] A.S. Svistunov, D.A. Rymov, R.S. Starikov, Appl. Sci. 13, 6125 (2023).
[5] H. Wang, M. Lyu, G. Situ, Opt. Express 26, 22603 (2018).
[6] L. Deng, IEEE Signal Processing Magazine, 29(6), 141–142 (2012).

ORCID: M.M. 0009-0005-3091-6890, P.A. 0000-0001-7596-0266,
M.B.A. 0000-0002-5856-2626, F.K. 0009-0008-0284-9426, P.M. 0000-0002-9720-1102

12. Other topics in photonics

Optomechanics of nanoparticles in a hybrid anapole state

S.R. Rozental, D.A. Kislov, A.S. Shalin
Moscow Institute of Physics and Technology, Moscow, Russia
e-mail: rozental.sr@phystech.edu

Nowadays, anapole states [1], which are distinguished by the absence of the far-field radiation from one of the multipole channels excited in the particle, have become a subject of significant interest in nanophotonics. These states are able to efficiently store energy, which allows their further use, for example, for laser generation [2]. It has recently been demonstrated that it is possible to combine several anapole states at the same wavelength, which leads to a significant suppression of light scattering by a nanoparticle. This phenomenon is referred to as the hybrid anapole state (HAS) [3, 4]. The present work analyses the effect of the hybrid anapole state on the optical forces acting on a silicon cylindrical nanoparticle irradiated by a focused Gaussian beam – Figure 1.

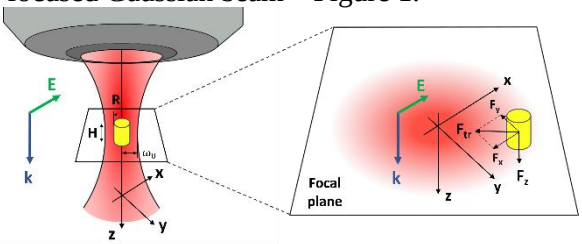

Figure 1. A cylindrical silicon nanoparticle placed in the focus of a linearly-polarized Gaussian beam. The inset shows the components of the optical force acting on the nanoparticle

It was found that near the HAS the system is highly sensitive to changes in the nanoparticle size. The Figure 2 compares transverse forces, acting on the HAS nanoparticle with the radius of 188 nm, and on the nanoparticle with normal scattering (R = 210 nm). Panels 1 and 3 show the distribution of the total transverse forces in the focal plane, and panels 2 and 4 show the trajectories of a nanocylinder subjected to these forces, which were obtained by solving the Langevin equation for some randomly selected 20 initial points in the focal plane.

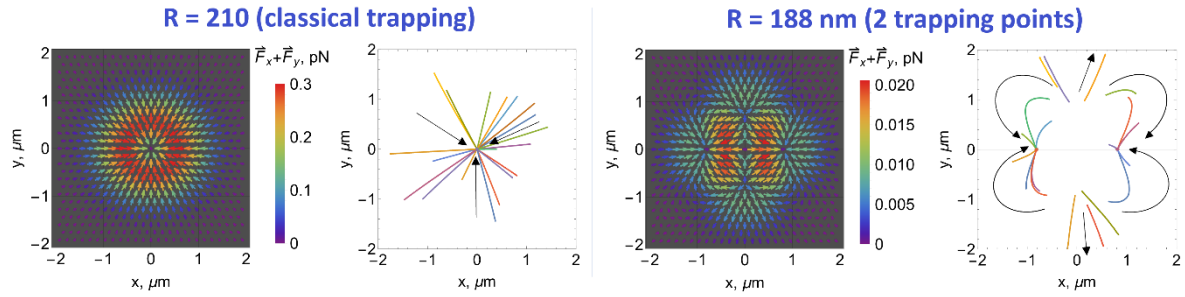

Figure 6. Distribution of the total transverse optical force acting on nanocylinders of different radii in the focal plane (left panels) and the trajectories of their movement under the influence of this force (right panels)

A fundamentally new phenomenon was identified, which is realized exclusively in the HAS: particle trapping at two points outside the optical axis. In contrast, within the non-anapole regime, a single trapping point is observed. The differences in the trapping scenarios can be leveraged for the purpose of optomechanical sorting of nanoparticles.

The author acknowledges the financial support from the Russian Science Foundation (Grant № 25-22-00266)).

REFERENCES

[1] E. A. Gurvitz, K. S. Ladutenko et al, Laser Photonics Rev. 13, 1–13 (2019)
[2] A. Tripathi et al, 21, Nano Letters, 1-7 (2021)
[3] B. Luk'yanchuk, R. Paniagua-Domínguez et al, Phys. Rev. A 95, 1–8 (2017)
[4] A. Canós Valero et al., Laser Photonics Rev. 15, 1–14 (2021)

ORCID: S.R. 0009-0008-3469-6866, D.K. 0000-0003-0478-1855

Electronic transport in semiconductors: from textbook knowledge to modern problems

N. Vukmirović
Institute of Physics Belgrade, University of Belgrade, Belgrade, Serbia
e-mail: nenad.vukmirovic@ipb.ac.rs

In this talk, I will start by giving a brief review of textbook knowledge on electronic transport in semiconductors, gained in the course of Solid State Physical Electronics by late Prof. Vitomir Milanović. Then, I will present the results of my first paper, resulting from diploma thesis work under Prof. Milanović. In that work [1], we analyzed the optical gain of a GaN quantum well as a potential active medium for an optically pumped terahertz laser. We showed that a three level design can yield significant population inversion between the upper and lower laser level.

I will then drift into modern problems on electronic transport in semiconductors and our recent results in this field. I will first talk about pieces of physics behind electron mobility in semiconducting materials [2]. The methodology for obtaining the electronic states, the phonon modes and the electron-phonon coupling constants within density functional theory will be reviewed. Particular focus will be given on physical considerations necessary to perform accurate interpolation of electron-phonon coupling constants to a dense momentum grid in the first Brillouin zone. The results for temperature dependence of mobility in II-VI semiconductors will be shown (see Fig. 1) and compared to experimental results from the literature.

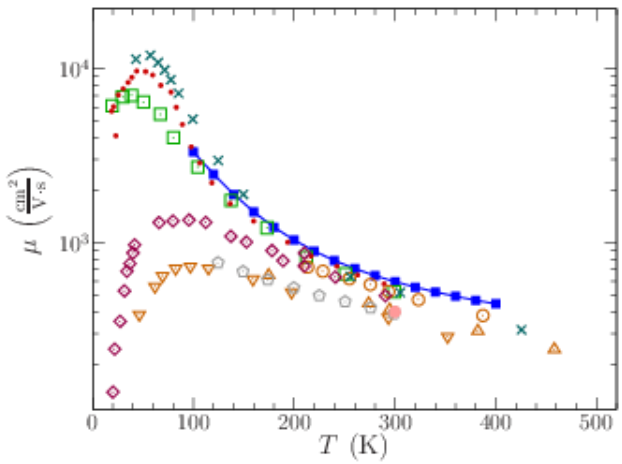

Figure 1. Temperature dependence of electronic mobility in ZnSe. Full line denotes the simulation results while other symbols denote various experimental results from the literature.

I will talk next about the methodology that we introduced to efficiently calculate electronic relaxation times and mobility in semiconducting materials [3]. The methodology will be illustrated by applying it in two cases: the Fröhlich model where analytic solutions exist and hence a comparison can be made, and the real semiconducting material ZnTe. The presentation will be concluded by showing the cases where the conventional Bloch-Boltzmann picture of electronic transport in semiconductors fails calling for novel approaches.

This research was supported by the Science Fund of the Republic of Serbia, Grant No. 5468, Polaron Mobility in Model Systems and Real Materials–PolMoReMa.

REFERENCES

[1] N. Vukmirović, V. D. Jovanović, D. Indjin, Z. Ikonić, P. Harrison, V. Milanović, J. Appl. Phys. 97, 103106 (2005).
[2] N. Vukmirović, Phys. Rev. B 104, 085203 (2021).
[3] N. Vukmirović, Comput. Phys. Commun. 312, 109583 (2025).

ORCID: N.V. 0000-0002-4101-1713

Nanophotonic light control for omnidirectional broadband absorption of the solar radiation for thin film solar cells

N. Vashistha[1], E. Golan[2], N. Aharon[2], G. Shalev[1,2]
[1]*School of Electrical Engineering, Ben-Gurion University of the Negev, 8410501, POB 653, Beer-Sheva, Israel*
[2]*The Ilse-Katz Institute for Nanoscale Science and Technology, Ben-Gurion University of the Negev, 8410501, POB 653, Beer-Sheva, Israel*
e-mail: nipunvashistha27@gmail.com

Thin films (TFs) are promising candidates for efficient low-cost solar cells (SC). However, the reduced thickness poses a challenge for efficient optical absorption [1,2]. This work demonstrates omnidirectional broadband absorption of polysilicon (p-Si) TFs decorated with light cone (LC) arrays composed of inverted cones decorated with sidewall subwavelength structures and top dielectric nanolenses. The study compares the optical absorption of p-Si samples: TF, TF with anti-reflection coating (ARC), TF decorated with optimized array of nanopillars (NP) each with SiO_2 nanolens (NL), and TF decorated with a LC array. The height of the p-Si is 1.2 μm on top of a glass substrate. Specular, diffused and specular-diffused far-field spectroscopy are employed. The specular-diffused spectroscopy indicates that the broadband transmission and reflection of the LC array is 19.3% and 56.3%, respectively, lower than that of the NP array. Three-dimensional numerical calculations suggest that LC array provides an efficient mechanism for refracting the incoming photons into the array lateral directions combined with enhanced coupling of the incoming photons to the p-Si dielectrics. The performance of SCs based on LC arrays is numerically evaluated with a significant efficiency enhancement. The LC array paradigm paves the way for low-cost and efficient TF SCs.

REFERENCES

[1] P. K. Nayak, S. Mahesh, H. J. Snaith, D. Cahen, Nat Rev Mater, 4, 269 (2019).
[2] J. Ramanujam, D. M. Bishop, T. K. Todorov, O. Gunawan, J. Rath, R. Nekovei, E. Artegiani, A. Romeo, Progress in Materials Science, 110, 100619 (2020).

ORCID: N.V. 0000-0002-5423-6364, G.S. 0000-0002-6893-1720.

Topologically Protected Modes in Diamond-like Photonic Ribbons

M. Nedić[1], M. G. Stojanović[1], G. Gligorić[1], J. Petrović[1] and A. Maluckov[1]
[1]*COHERENCE, Vinca Institute of Nuclear Sciences, University of Belgrade, National Institute of the Republic of Serbia*
e-mail: milica.brankovic@vin.bg.ac.rs

The discovery of topologically protected modes has marked a major milestone in photonics, enabling robust light transport immune to disorder, backscattering, and fabrication imperfections. These modes have opened new possibilities in integrated photonic circuits, quantum information processing, and topological lasers. Recently, compact topological edge modes have been demonstrated experimentally in a quasi-one-dimensional ribbon structure with a hexagonal unit cell [1]. These modes combine the robustness of topological edge states with the spatial confinement of compact modes, offering dual-layer protection that makes them highly promising for applications.

Here, we investigate the necessary conditions for the emergence of such modes in ribbon lattices composed of diamond-like unit cells. We design two different geometries in which an energy spectrum can be engineered through femtosecond (fs) laser writing of S- and P-type waveguides [2]. The specific ordering of couplings in the lattice induces an effective π-flux, which plays a key role in the band flattening mechanism.

By continuously tuning this artificial flux, we theoretically demonstrate transitions between trivial and nontrivial topological phases. At $\Phi = \pi$, all bands become flat, and compact localized states emerge. Using projector-based topological invariants and the mean chiral displacement method [3], we characterize the bulk-boundary correspondence and confirm the topological nature of the gapped bands and the associated edge modes.

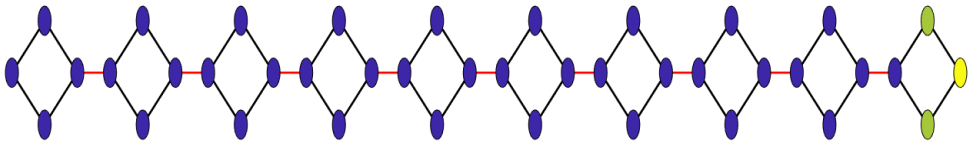

Figure 1. Topological edge state in diamond-like ribbon.

REFERENCES

[1] G. Cáceres-Aravena, M. Nedić, P. Vildoso, G. Gligorić, J. Petrovic, A. Maluckov, and R. A. Vicencio, Phys. Rev. Lett. 133, 116304 (2024).
[2] A. Szameit, D. Blömer, J. Burghoff, T. Schreiber, T. Pertsch, S. Nolte, A. Tünnermann, and F. Lederer, Opt. Express 13, 10552 (2005).
[3] F. Cardano, A. D'Errico, A. Dauphin, et al., Nat. Comm. 8, 15516 (2017).

ORCID: M.N. 0000-0001-8909-7360, M.S. 0000-0002-4376-7610, J.P. 0000-0002-1002-241X, G.G. 0000-0003-1890-7324, A.M. 0000-0002-6474-360X

Morphological changes and cell viability of GL261 and SMA-560 mouse glioma cells affected by direct infrared light illumination

I. A. Popović[1], J. Žakula[2], V. Ž. Ralić[1], I. S. Popović[3], N. A. Vukićević[3], T. D. Milinković[4], Đ. T. Todorović[5], A. K. Dimčić[5], M. D. Nešić[1], L. Korićanac[2], A. Régnier-Vigouroux[6], S. Gieß[6], M. Ž. Petković[1] and M. Stepić[1]

[1] *COHERENCE Centre, Department of Atomic Physics, VINČA Institute of Nuclear Sciences, National Institute of the Republic of Serbia, University of Belgrade, Belgrade, Serbia*

[2]*Department of Molecular Biology and Endocrinology, VINČA Institute of Nuclear Sciences, National Institute of the Republic of Serbia, University of Belgrade, Belgrade, Serbia*

[3]*Faculty of Chemistry, University of Belgrade, Belgrade, Serbia*

[4]*Faculty of Technology and Metallurgy, University of Belgrade, Belgrade, Serbia*

[5] *Faculty of Sciences, University of Novi Sad, Novi Sad, Serbia*

[6]*Institute of Developmental Biology and Neurobiology, Johannes Gutenberg University Mainz, Mainz, Germany*

e-mail: ivavukicevic@vin.bg.ac.rs

Glioma is a type of primary, malignant brain tumor [1]. This is a highly lethal tumor, which can cause headaches, vomiting, vision and memory loss, seizures, speech difficulties and complex visual hallucinations. Prevailing glioma treatment options include chemotherapy, surgical removal, and radiation therapy, which can cause severe side effects. On the other hand, light-based therapies, such as direct light therapy [2], photothermal [3], and photodynamic therapy [4], are minimally invasive, non-cumulative, and non-toxic treatment modalities, offering an effective and less damaging alternative to more invasive anti-cancer treatments.

We have experimentally examined the in vitro photokilling potential of continuous-wave infrared laser light on murine GL261 and SMA-560 glioma cancer cells. Cell viability was measured as a function of laser beam intensity and compared to a control, which was kept in the dark for 30 minutes. The laser wavelength was centered at 831 nm, and the beam diameter was approximately 6 mm. Glioma cells in each microtiter well were illuminated for 10 minutes at room temperature, ≈ 20˚C, with a total dose of ≈492 J/cm² and ≈ 313 J/cm^2 for SMA 560 and GL261 cells, respectively. The SRB assay, which measures the absorbance of sulforhodamine B dye at 550 nm, was performed 48 h after the treatment. The obtained results showed that the minimal achieved viability was slightly below 60% for the SMA-560, whereas for the GL261 cell line, this value was ≈ 69%.

Monitoring the morphological changes in illuminated cells is often used to elucidate the influence of light on cancer cells [5]. In GL261 cells, after illumination, a large number of round cells grouped in clusters can be observed. In SMA-560, after the light treatment, there is a significant decrease in the number of living cells, accompanied by a change in shape: cells lose their characteristic elongated profile and become round and shrunken. These morphological changes are typically observed in dying cells and suggest a cytotoxic effect of the light on the glioma cell lines.

These results demonstrate the effect that direct light therapy has on glioma cells and emphasize the potential of this approach in combating cancer.

REFERENCES

[1] L. C. Fontana et al., Photodiag. Photodyn.Therapy 37, 102669 (2021).
[2] V. Dremin et al., IEEE J. Sel. Topics Quant. Electron. 29, 7200911 (2023).
[3] Z. Chen et al., ACS Nano 10, 10049 (2016).
[4] M. E. Wieder et al., Photochem. Photobio.Sci. 5, 727 (2006).
[5] A. Castilho-Fernandes et al., Photodiag. Photodyn. Therapy 19, 221 (2017).

ORCID: I.A.P. 0000-0003-1120-8985, J.Ž. 0000-0001-7280-3273, V.R. 0000-0002-3206-1831, M.D.N. 0000-0002-9167-6553, L.K. 0000-0001-5497-284X, A.R.V. 0000-0002-8407-4300, M.Ž.P. 0000-0002-8354-995X, M.S. 0000-0002-0623-5113

Efficacy of Multiple-Antenna Microwave Ablation in the Treatment of Liver Tumors

N. Bošković, B. Radjenović and M. Radmilović-Radjenović[1]
[1]*Institute of Physics, University of Belgrade, Belgrade, Serbia*
e-mail: marija@ipb.ac.rs

Microwave ablation (MWA) is a minimally invasive thermal ablation technique used to treat various tumors, particularly in the liver. Both single-antenna and multi-antenna MWA are similarly effective for local tumor treatment; however, synchronous multi-antenna MWA offers improved local tumor progression-free survival, especially for larger tumors [1].

In addition to clinical studies, computational models have significantly contributed to predicting MWA outcomes, particularly three-dimensional (3D) models of an antenna and targeted tissue without assumptions of homogeneity [2]. This study aimed to determine optimal parameters for treating a large tumor (from a database [3]) using two identical 10-slot coaxial antennas.

Figure 1 illustrates the results from a single probe (above) and three probes arranged in a triangular formation (below), operating at a) 15 W and b) 16 W per probe. At 15 W, the overlapping ablation zones from simultaneous activation significantly enhance the overall ablation size, covering almost the entire tumor. The total ablation volume is 57% larger than three times the volume of a single 15 W probe. Since only small tumor areas remain outside the ablation zone, a slight increase in power would likely suffice. At 16 W per probe, complete tumor destruction is achieved, with the ablation volume being 43% larger than three times the volume of a single 16 W probe and 10% larger than with three probes at 15 W.

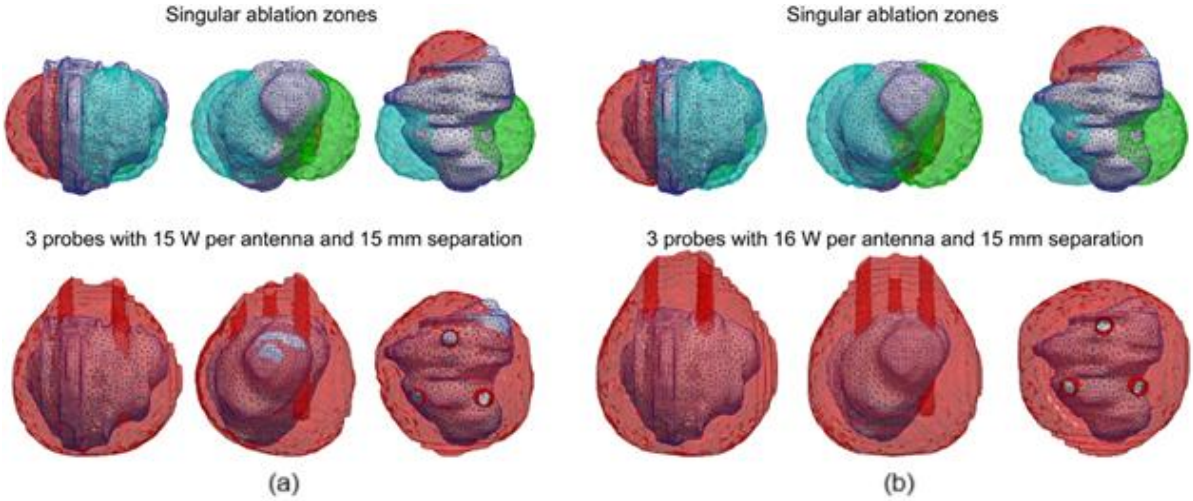

Figure 1. Ablation zones corresponding to a single antenna (above) and three antennas (below) with a separation of 15 mm and input power of: (a) 15 W per antenna, (b) 16 W per antenna.

REFERENCES

[1] N. Bošković, S. Nikolić, B. Radjenović, M. Radmilović-Radjenović, Bioengineering 11, 1133 (2024).
[2] N. Bošković, B. Radjenović, S. Nikolić, M. Radmilović-Radjenović, Open Phys. 22, 20240079 (2024).
[3] https://www.ircad.fr/research/data-sets/liver-segmentation-3d-ircadb-01/

ORCID: B.R. 0000-0002-8756-1008, M.R.R. 0000-0001-8931-859X

The comparative analysis of electromagnetic shielding efficiency of graphene oxide composites with different silver nanostructures

S. Dorontić[1], D. Kepić[1], M. Yasir[2], K. Haddadi[3], B. Nardin[4], S. Jovanović[1]
[1]*Vinča Institute of Nuclear Sciences - National Institute of the Republic of Serbia, University of Belgrade, Mihajla Petrovića Alasa 12-14, 11351 Belgrade, Serbia*
[2]*Department of Computing Science, University of Oldenburg, D-26129 Oldenburg, Germany*
[3]*Univ. Lille, CNRS, Centrale Lille, Univ. Polytechnique Hauts-de-France, UMR 8520 - IEMN - Institut d'Electronique de Microélectronique et de Nanotechnologie - Lille, 59650 Villeneuve-d'Ascq, France*
[4]*Faculty of Polymer Technology, Ozare 19, 2380 Slovenj Gradec, Slovenia*
e-mail: sladjana.dorontic@vin.bg.ac.rs

The electronic devices and gadgets that emit electromagnetic waves are omnipresent in modern society. They are causing the saturation of the environment with electromagnetic waves that might jeopardize human health [1], emphasizing the need to seek effective electromagnetic shielding materials [2,3]. This study provides a comparative analysis of the electromagnetic interference shielding effectiveness (EMI SE) of graphene oxide (GO) composites with two distinct silver nanostructures: AgNWs and AgNPs. AgNWs were synthesized using the "polyol" method and combined with GO, while AgNPs were directly formed on GO through low-dose gamma irradiation. By applying different microscopy and spectroscopy characterization techniques, the morphological and structural properties of the prepared composites were examined. The EMI SE measurement revealed a superior EMI SE of GO-AgNW composites compared to GO-AgNPs. Composites with higher concentrations of AgNWs exhibit increased total shielding effectiveness and reflective shielding effectiveness (SE_T values of 0.9, 1.4, and 4.0, and SE_R values of 0.4, 0.8, and 2 dB for GO-AgNWs 5:5, GO-AgNWs 3:7, and GO-AgNWs 1:9, respectively) (Figure 1.). As the amount of AgNWs in the composites increases, there is a slight rise in the measured SE_A values, which increase from 0.4 dB to 1.9 dB concerning the AgNWs content. This difference may be attributed to the structural differences between the Ag nanostructures.

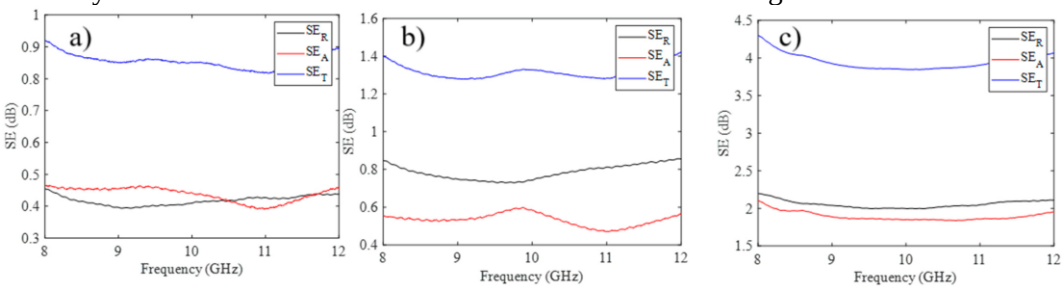

Figure 1. SE_T, SE_A, and SE_R values for GO-AgNWs 5:5 (a), GO-AgNWs 3:7 (b), and GO-AgNWs 1:9 (c), measured in the frequency range of 8-12 GHz. Reproduced with permission [4]. Copyright: Int. J. Mol. Sci. 2024.

Acknowledgments: This work was supported by the Horizon Europe program Coordination and Support Action, project ''Twinning for new graphene-based composites in electromagnetic interference shielding'' - GrInShield [No. 101079151] and by the Ministry of Science, Technological Development and Innovation of the Republic of Serbia [grant number 451-03-136/2025-03/200017].

REFERENCES

[1] M. Bagheri Hosseinabadi, N. Khanjani, M. H. Ebrahimi, B. Haji and M. Abdolahfard, Electromagn Biol Med, 38, 96-101, (2019).
[2] Y.-J. Wan, P.-L. Zhu, S.-H. Yu, R. Sun, C.-P. Wong and W.-H. Liao, Carbon, 122, 74-81, (2017).
[3] F. M. Oliveira, J. Luxa, D. Bouša, Z. Sofer and R. Gusmão, ACS Appl. Nano Mater. 5 (5) 6792-6800, (2022).
[4] M. Milenković, W. Saeed, M. Yasir, D. Sredojević, M. Budimir, A. Stefanović, D. Bajuk-Bogdanović and S. Jovanović, Int. J. Mol. Sci. (25) 24, 13401, (2024).

ORCID: S.D. 0000-0002-9838-8917, D.K. 0000-0003-2777-6864, S.J. 0000-0003-3577-5060

The impact of SRH recombination on the current-voltage characteristic of organic and perovskite solar cells

N. Arbutina, J. Gojanović, P. Matavulj
School of Electrical Engineering,
University of Belgrade, Serbia
email: an243193m@student.etf.bg.ac.rs

Nowadays, extremely important emerging technologies of solar cells are organic (OSC) and perovskite solar cells (PSC). Being cheap, lightweight, flexible, scalable and with good efficiency these solar cells are subject of further development, especially investigation of physical processes undergoing the solar cells operation, because of need for reaching their full potential. It is especially important to understand the influence of recombination as it is fundamental mechanism of losses both in OSCs and in PSCs.

In this paper we have used one dimensional drift-diffusion model for describing processes inside of the OSCs and PSCs, such as generation, transport and recombination of carriers [1]. Generation was calculated using transfer matrix method. We have assumed constant values for electron and hole mobility. For solving the drift-diffusion equations Dirichlet boundary conditions were applied. We used Shockley-Read-Hall (SRH) and Langevin recombination, where recombination rate was controlled by introducing variable coefficients: K_L and K_{SRH}, where the first correspond to change in reduction coefficient of Langevin recombination and the second correspond to change in trap states concentration (N_t). Drift-diffusion equations are then solved numerically. Discretization of equations was done using finite difference method with Scharfetter-Gummel approach. System of discretized equations was solved using Newton method [2].

Changes in the current density-voltage (J-V) characteristic of OSCs and PSCs with the change of K_L and K_{SRH} were analyzed. Changes in open-circuit voltage (V_{OC}), short-circuit current (J_{SC}), fill factor (FF) and power conversion efficiency (PCE) were observed and monitored. Our analysis has concluded that Langevin recombination has strong influence on OSCs performance, while its influence on PSCs is negligible. Increase in SRH recombination rate has negative impact on both OSC and PSC, whereat in OSCs its dominant impact is on declining J_{SC}, while in PSCs the V_{OC} is dominantly decreased. This indicates different operating mechanisms between OSCs and PSCs. In the case of OSCs stronger influence of SRH recombination begins with $N_t = 10^{15} cm^{-3}$ and total degradation of the device starts at $N_t = 2 \cdot 10^{17} cm^{-3}$, while in the case of PSCs stronger influence of SRH recombination begins at $N_t = 10^{17} cm^{-3}$ and total degradation of the device starts at $N_t = 10^{19} cm^{-3}$. The model was validated by successfully reproducing a PSCs J-V curve taken from the literature.

Acknowledgement: This work was financially supported by the Ministry of Science, Technological Development and Innovation of the Republic of Serbia under contract number: 451-03-137/2025-03/200103.

REFERENCES:

[1] D. Li, L. Song, et al, Adv. Sci. 7, (2019)
[2] A. Khalf, J. Gojanović, N. Ćirović, et al, IEEE J. Photovol. 10, 514, (2020)

ORCID: J.G. 0000-0002-4893-1926, P. M. 0000-0001-6635-5152

Structural characterization of Nb_2CT_z MXene for energy storage application

I. Pešić[1], V. Vojnović[1], A. Gavran[1], K. Tošić[1], M. Spasenović[1], M. Pergal[1]
[1]*Institute of Chemistry Technology and Metallurgy, University of Belgrade, Njegoševa 12, Belgrade, Serbia*
e-mail: marija.pergal@ihtm.bg.ac.rs, ivan.pesic@ihtm.bg.ac.rs

Niobium carbide (Nb_2CT_z) MXene is a promising material for energy storage applications due to its metal-like electrical conductivity, hydrophilic surface chemistry, and efficient ion transport pathways. In this work, we employed a 'MILD' etching method to selectively remove aluminum and partially exfoliate Nb_2CT_z MXene, resulting in few-layer nanosheets suitable for electrode fabrication. To tailor interfacial properties and improve electrochemical performance, Nb_2CT_z flakes were functionalized with three silane coupling agents: PEG-silane, acrylate silane, and amino-silane, prior to their transformation into freestanding, binder-free films via vacuum filtration. Structural characterization was conducted using Fourier-transform infrared spectroscopy (FTIR), X-ray diffraction (XRD), and X-ray photoelectron spectroscopy (XPS). The presence of functional groups on Nb-based MXenes was confirmed by FTIR, while XRD patterns revealed an increase in interlayer spacing following silane modification, indicating successful intercalation and surface grafting. XPS spectra further confirmed the presence of silicon originating from the silane molecules, supporting the occurrence of covalent functionalization. Based on previous findings in MXene research [1], it was hypothesized that silane functionalization would enhance electrochemical properties such as capacitance and rate capability by improving ion accessibility between layers. The effects of different types of organosilanes on the electrochemical performance of Nb_2CT_z electrodes were quantitatively evaluated through cyclic voltammetry, galvanostatic charge–discharge, and electrochemical impedance spectroscopy. A scalable preparation method facilitates the use of such materials as electrodes for supercapacitors in energy storage systems.

*This research was supported by the University of Belgrade - Institute of Chemistry, Technology and Metallurgy through the "Seed Research Grant" for young scientists ("*Surface Functionalized Niobium-Based MXene Electrodes for Enhanced Capacitance and Energy Storage Performance (SurfMEX)*"), financed by Serbia Accelerating Innovation and Entrepreneurship Project (SAIGE).*

REFERENCES

[1] Pešić, I., Pergal, M. V., Vasiljević-Radović, D., Popović, M., Uskoković, P., Petrović, M., & Radojević, V. (2024). Capacitance breakthroughs in free-standing electrodes through MXene functionalization. *Science of Sintering,* (00), 28-28.

ORCID: I.P. 0000-0002-2124-7139, V.V. 0009-0005-2304-0958, A.G. 0009-0004-7465-3087, K.T. 0000-0003-1141-4340, M.S. 0000-0002-2173-0972, M.P. 0000-0001-6078-2006

Self-consistent approach to quantum dynamics of photoinduced electronic excitations in molecular aggregates

V. Jankovic[1] and T. Mancal[2]
[1]*Institute of Physics Belgrade, University of Belgrade, Serbia*
[2]*Faculty of Mathematics and Physics, Charles University, Prague, Czechia*
e-mail: veljko.jankovic@ipb.ac.rs

Further progress in fundamental understanding of the initial steps of solar-energy conversion in both natural and artificial systems requires computationally inexpensive yet reasonably accurate methods for quantum dynamics of photoinduced electronic excitations in molecular aggregates immersed in structured bosonic environments.

Starting from the memory kernel in Born approximation, and recognizing the quantum master equation as the Dyson equation of Green's functions theory, we formulate the self-consistent Born approximation (SCBA) to resum the memory-kernel perturbation series in powers of the exciton–environment interaction [1]. Our SCBA is formulated in the Liouville space and frequency domain, and it handles arbitrary spectral densities of the interaction.

In a molecular dimer coupled to an overdamped oscillator environment, we find that the SCBA reproduces the true dynamics of excitons generated by an ultrashort laser pulse very well even in the most challenging regimes of strong interactions, slow environments, and low temperatures. While the SCBA is good (poor) at describing energy transfer modulated by an underdamped vibration resonant (off-resonant) with the exciton energy gap, we find it reasonably describes light-triggered exciton dynamics in the seven-site model of the Fenna–Matthews–Olson complex in a realistic environment comprising both an overdamped continuum and underdamped vibrations.

REFERENCES

[1] V. Jankovic and T. Mancal, J. Chem. Phys. 161, 204108 (2024).

ORCID: V.J. 0000-0002-0297-2167, T.M. 0000-0003-1736-3054

Single Shot Two-Dimensional Polarization Mapping of Birefringent Elements and Devices

M. Mincheva[1], A. Stefanov[2,3], I. Stefanov[1,4], L. Stoyanov[1,4], A. Dreischuh[1,4,5]
[1]*Department of Quantum Electronics, Faculty of Physics,*
Sofia University "St. Kliment Ohridski", Sofia, Bulgaria
[2]*Department of Mechatronics, Robotics and Mechanics, Faculty of Mathematics and Informatics,*
Sofia University "St. Kliment Ohridski", Sofia, Bulgaria
[3]*Institute of Mathematics and Informatics, Bulgarian Academy of Sciences, Sofia, Bulgaria*
[4]*National Centre of Excellence Mechatronics and Clean Technologies, 8 bul. Kliment Ohridski, Sofia, Bulgaria*
[5]*Bulgarian Academy of Sciences, Sofia, Bulgaria*
e-mail: mariatm@uni-sofia.bg

Light beam passing through different anisotropic elements undergoes a change in its polarization state. If one wants to analyze a more complex polarization structuring (e.g. radial, azimuthal or more sophisticated [1-3]), a suitable method for measuring the polarization in two transverse dimensions could be exploited. An intuitive example of where one can use the polarization mapping is the structured light in the form of polarization vortices. Here we present one such mapping method denoted as two-dimensional polarization mapping.

Conventionally, one records transmitted intensities through combinations of rotating polarizers, wave plates and imaging detectors under different analyzer settings. From these measurements full Stokes parameter maps or local polarization ellipses are reconstructed across the beam profile.

In this work, we implemented an innovative single-shot polarization mapping technique for birefringent devices, which employs a 9×9 array of probe sub-beams to capture spatially resolved polarization information in a single measurement. This means that the two-dimensional polarization distribution is reconstructed in only one step of data acquisition. The measurement time is reduced while the high spatial resolution remains preserved. We first performed a test measurement with commercially-available polarizing vortex plates converting the linearly polarized light to radially/azimuthally polarized light. To demonstrate the robustness of the technique, we applied the same approach to quantify the polarization transfer function of reflective phase-only liquid crystal on silicon spatial light modulator. The results show that the reported method is particularly useful for fast polarization monitoring and control in advanced photonics applications.

We acknowledge funding of the Bulgarian National Science Fund (project КП-06-Н78/6). The work was also supported by the Bulgarian Ministry of Education and Science as a part of National Roadmap for Research Infrastructure, project ELI ERIC BG. M.M., L.S. and A.D. were also supported by the European Union NextGenerationEU through the "National Recovery and Resilience Plan of the Republic of Bulgaria, project BG-RRP-2.004-0008-C01". Research equipment of the project № BG16RFPR002-1.014-0006 "National Centre of Excellence Mechatronics and Clean Technologies" was used for experimental work financially supported by European Regional Development Fund under "Research Innovation and Digitization for Smart Transformation" program 2021-2027.

REFERENCES

[1] X.Wang, F. Yang, J. Yin, "Mapping the polarization distribution of arbitrary vector polarization beam", Optik, 144, 124-131, (2017).
[2] B. Schaefer, E. Collett, R. Smyth, D. Barrett, B. Fraher, "Measuring the Stokes polarization parameters" Am. J. Phys.75 (2), 163–168 (2007)
[3] J. Yang, D. Lin, D. Bao, S.Tao, "Pixel level control of amplitude, phase, and polarization of an arbitrary vector beam" Appl. Phys. Lett., 121 (19), (2022).

Polaron properties within the Peierls model using unitary-transform approach

I. Vasić and N. Vukmirović
Institute of Physics Belgrade, University of Belgrade, Serbia
e-mail: ivana.vasic@ipb.ac.rs

Polaron properties play a crucial role in determining various physical properties and processes in materials. We develop an approximate method based on a suitable unitary transform for the calculation of polaron properties within the Peierls model, the simplest model with non-local electron-phonon interaction. The transform is chosen in such a way to allow for the perturbative treatment of the transformed model [1]. Recently, the approach has been successfully applied to the Holstein model [2]. As a next step, here we study the Peierls model and investigate the transformation proposed in [3] in more detail. We implement it in a numerically rigorous way and use it to calculate the electronic spectral function of the Peierls model. We resolve some important technical issues of the approach and crosscheck validity of our method by comparison with numerically exact path-integral Monte Carlo calculations.

This research was supported by the Science Fund of the Republic of Serbia, Grant No. 5468, Polaron Mobility in Model Systems and Real Materials–PolMoReMa.

REFERENCES

[1] Y. Luo, B. K. Chang, M. Bernardi, Phys. Rev. B 105 155132 (2022).
[2] N. Prodanović and N. Vukmirović, Phys. Rev. B 99, 104304 (2019).
[3] R. Silbey and R. W. Munn, J. Chem. Phys. 83, 1843 (1985).

ORCID: I.V. 0000-0002-1101-8877, N.V. 0000-0002-4101-1713

Index

Abu el Rub Anamarija, 83
Aharon N., 160
Aissa B., 150
Akar S., 103
Al-Ateqi A., 97
Aleksandrov L., 66
Aleksandrovich T. A., 122
Alekseevich T. A., 111, 122
Aleksić Jelisaveta, 118
Altan H., 141
Amendola V., 28
Andjus Pavle, 48, 91
Angelova L., 33, 133
Apostolakis A., 97
Apostolova T., 128
Aras K., 99, 100
Arbutina Nikola, 165
Arsoski Vladimir V., 112
Atanasijević Petar, 45, 93, 118, 149, 154, 155, 156
Atanasoski Vladimir, 92
Atanasova V., 65, 66
Aumiller M., 35
Aygun G., 102, 105
Aygün G., 141
Bąbińska J., 123, 124
Babińska M., 81, 123, 124
Badža Atanasijević Milica, 156
Bajić S. Jovan, 113
Bajuk-Bogdanović Danica, 134
Balaž Antun, 56
Balcı S., 141
Bald I., 142
Baloban M., 46
Bañares L., 21
Banović Mladen, 118, 149, 154, 155
Barendregt M., 43
Basal S. N., 100
Belča Ivan, 119
Belić Milivoj R., 59, 63, 64
Beličev P. Petra, 60, 92
Beric Sladjana, 53
Bijelić Dunja, 48
Birn H., 27
Bizzarri R., 20
Bobrinetskiy I., 96
Bojović Petar, 43
Bordoni L., 27
Bošković Marko, 134, 144
Bošković Nikola, 163
Božanić K. Dušan, 83, 142
Bozic Dušan, 139
Božinović Nevena, 104
Brantov A.V., 130
Bratić Nikolina, 149
Brunner D., 147
Brzezińska W., 81, 90
Bugarski Kolja, 110
Bugay A. N., 84
Bukumira Marta, 94
Bychenkov V. Yu., 130
Calamai M., 91
Cantas A., 70, 102, 105
Canteli D., 104
Cap J., 82
Capitini C., 91
Car T., 33
Cardenas-Razo L., 147
Catanzaro L., 131
Catarzi M., 91
Cavalieri S., 38
Chabanov A., 38
Chalopin T., 43
Chatzianagnostou E., 25
Chatzitheocharis D., 25
Chen G., 22
Chrisostomidis T., 25
Cierpiak K., 152
Compagnini G. R., 131
Corrales Urena Y. R., 48
Credi C., 91
Crnjanski Jasna, 118, 149, 154, 155
Ćurčić Milica, 72, 137
Ćurčić M. Marija, 53, 85
Cuzminschi M., 135, 136
Czyszanowski T., 147
D'Urso L., 131
Dąbrowska A., 123, 124
Dakić Andjela, 154
Dakić Borivoje, 37
Dallari C., 91
Damakoudi L., 25
Danilović Danijela, 83, 142
Daskalova A., 33, 133
De Giacomo A., 131
Delibašić Marković Hristina, 132
Demirbas S., 103
Demirhan Y., 100, 141
Demler E., 14
Denk P., 82

di Silvio L., 33
Dimčić K. Anastasija, 162
Dinić Ivana, 86
Djoković Vladimir, 83
Djurdjic Mijin Sanja, 52
Dmitrievich A. Y., 111, 122
Dobrowolski W.D., 137
Dojčilović Radovan, 142
Donato S., 91
Đorđević Tijana, 145
Dorontić Sladjana, 164
Dramićanin Miroslav, 113
Dreischuh A., 127, 168
Dremin V., 46
Drvenica Ivana T., 40
Dvorak J., 82
Ekmekcioglu M., 99, 103
Elkabetz S., 22
Enger R., 27
Erbas F., 103
Erdogan N., 103
Eroğlu S., 99, 100
Esen N., 102, 105
Farsari M., 15
Fashtami L. A., 79
Fernández-Garrido S., 69
Filipov E., 133
Filipović Lenka, 73
Finaeva U., 82
Firez I., 53
Gačević Žarko, 69
Galbacs G., 125
Galiakhmetova D., 46
Gaudiuso C., 131
Gaudiuso R., 131
Gavran Andjela, 106, 166
Gebski M., 147
Gennadievich K. V., 111, 122
Genova Ts., 88, 89
Georgijević Jelena P., 145
Gieß S., 162
Giorgini S., 18
Gligorić Goran, 60, 161
Gojanović Jovana, 165
Golan E., 160
Gómez V. J., 69
Gorodetsky A., 46
Gric T., 68
Gromova Yu., 101
Guzmán Á., 69
Gvozdić Dejan, 118, 149, 154, 155
Haboub A., 150
Haddadi K., 164
Hadžić Branka, 72, 137
Hadzievski Ljupčo, 92
Hansen A., 75
Hermann C. A., 29
Hilker T., 43
Hudomal Ana, 51
Ignjatović Milan, 109
Ilić Andjelija Ž., 72, 117, 119
Ilić Iskra., 63
Ilić Milan M., 117
Ilić Stefan, 106
Ilić Vesna Lj., 40
Ishihara R., 98
Israeli E., 22
Italyantsev A., 153
Ivanovic Marija, 92
Ivask A., 33
Jakóbczyk P., 80
Jakovac Josip, 47, 145
Jakovljević Ana, 48, 91
Jakovljević Dusan Z., 112
Jakšić Olga, 144
Jankovic Veljko, 167
Jelenković Brana, 53, 85, 91
Johansson M., 60
Jordovic Pavlovic Miroslava, 151
Jovanović Sonja, 164
Jovanović Vladimir P., 61
Jović Kristina, 155
Jović Savić Dragana M., 61, 62
Joža Ana, 113
Jugovic Dragana, 76
Kalinić Ana, 143, 145
Kapon E., 16
Karadeniz N., 102, 103, 105
Karatodorov S., 65, 66
Karbunar Lazar, 143
Karpuz S., 102, 105
Kasalica Bećko, 119
Kaschewski N., 54
Kaur H., 33
Kepić Dejan, 164
Kerdjoudj H., 133
Khasiyeva A., 73
Khelif A., 150
Kidmose H., 27
Kislov D.A., 158
Kolarž Predrag, 72
Korićanac Lela, 84, 162
Kosiel K., 102, 105
Kosowska M., 71
Kostadinov I., 114, 115
Kovačević Milan, 113
Kovacevic Slavica M., 151
Koviarov A., 46
Krajinić Filip, 53, 85, 156

Kristensen A. M., 27
Krmpot Aleksandar J., 40, 41, 42, 94
Krogstrup N. V., 27
Krstić Marko, 118, 149, 154, 155
Krstulovic Nikša, 125
Kudriavtseva A.S., 96
Kuratov A.S., 130
Kuryliszyn-Kudelska I., 137
Kymakis E., 19
Lalić Katarina, 40
Lazarević Miloš, 86
Lazarević Zorica, 72
Lazic Milos, 53
Lazić Snezana, 52
Lazovic Aleksandar, 92
Lekić Marina, 53, 85
Lemaire F., 133
Likhachev M., 101
Lobachevsky P., 84
Lobok M.G, 130
Lott J. A., 147
Loza-Alvarez P., 34
Maestri F., 38
Makarov M., 153
Maletić Dejan, 72
Maluckov Aleksandra, 60, 92, 108, 110, 161
Mancal T., 167
Mancic Lidija, 86
Marakhin A., 153
Marciniak M., 147
Marinin N., 148
Marinković Marija, 156
Marković Ognjen, 36
Markushev Dragan D., 151
Markushev Dragana K., 151
Matavulj Petar, 120, 165
Meglinski I., 26
Mei Y. L., 107
Mezzapesa F. P., 131
Mićić Milena, 45, 118
Mihailović Pedja, 45, 93, 118, 156
Miladinović Marko, 55
Milenović Stefan, 55
Miletić Marjan, 108
Milinković D. Teodora, 162
Miljković Nemanja, 120
Milosavljević Aleksandar R., 142
Milošević Milena, 42
Milovanović Aleksandar, 42
Mincheva M., 168
Mincheva R., 65
Minić Ana, 93
Minnullin R., 153
Miranda A., 98
Mišeljić Tijana, 83
Mišković Zoran, 75
Mišković Zoran L., 143
Mitić Damir V., 62
Mohajerani E., 79
Molpecres C., 104
Momcilovic Miloš, 125
Monge Bartolomé L., 69
Mujo Denis, 56
Munoz Garcia C., 104
Muric Branka, 77
Nahvifard E., 79
Nardin B., 164
Nedić Milica, 161
Nedyalkov N., 66
Neil S., 33
Nekrasov N.P., 96
Nemcova S., 82
Nešić Maja D., 84, 162
Nielsen M. B., 27
Nikolić Stanko N., 59, 94
Nocentini S., 38, 91
Novakovic Mirjana, 76
Nur S., 98
Nyga J., 123, 124
Obermeyer J., 43
Obradov Marko, 144
Obradović Jovana, 69
Obreshkov B., 128
Ozdemir M., 99, 100, 102, 105
Ozyuzer L., 31, 99, 100, 102, 105, 141
Pace M. L., 131
Pajić Tanja, 41, 42, 85, 91, 94
Pajović Jelena, 83
Pantelić Dejan, 45, 87, 93
Pašti Igor, 134
Paulus G. G., 127
Pavlović Danica, 45, 87, 93
Pavlović Vladan, 55
Pelster A., 32, 54
Pereira M.F., 97
Pereira Reyes R., 48
Pergal M. V., 106, 134, 166
Perić Milica, 55
Pešić Ivan, 106, 166
Pešić Jelena, 73, 74
Petakov Ana, 40
Petković Marijana Ž., 84, 162
Petričević Slobodan, 118
Petrov T., 138
Petrović Jovana, 92, 108, 110, 161
Petrović Milan, 63, 64
Petrović Nikola, 58, 64
Petrović Suzana, 104
Petrović Violeta, 132
Piljević Miljana, 86

Ponticelli L., 91
Popović Iva A., 84, 162
Popović S. Ivana, 162
Popovic Maja, 76
Popovic Marica N., 151
Potocnik Jelena, 77
Quiros-Corella F., 48
Rabanal M. E., 86
Rabasović Mihailo D., 40, 41, 42, 86, 94
Raczak-Gutknecht J., 81, 90
Radenović Lidija, 48
Radjenović Branislav, 163
Radmilović Mihajlo D., 40
Radmilović-Radjenović Marija, 163
Radovanović Jelena, 109
Radović Ivan, 143
Radulović Katarina, 144
Rafailov E. U., 30, 46, 68
Rafayelyan M., 148
Rafeeka R. S., 22
Rajić Vladimir, 104
Ralić Vanja Ž., 84, 162
Rašljić-Rafajilović Milena, 106
Régnier-Vigouroux A., 162
Reitzenstein S., 147
Renzoni F., 24
Riboli F., 38
Ristic Arsen, 92
Ristić Biljana, 83
Rojas Rodríguez M., 91
Romcevic Maja, 137
Romcevic Nebojsa, 137
Rozental S.R., 158
Rühm A., 35
Ruzic Jovana, 139
Rychert K., 152
Sa de Melo C., 54
Salatić Branislav, 45, 87, 93
Salvini L., 38
Sanjeev A., 22
Santagata A., 131
Sapegin A., 153
Sardella D., 27
Savić Slobodan V., 117, 119
Savic-Sevic Svetlana, 77
Scarano S., 91
Schiessl I. M., 27
Schürmann R., 142
Seregin E., 101
Shalaan A., 33
Shalev G., 160
Shalin A.S., 158
Shcherbakova D., 46
Shehadi M., 138
Shigapov A., 101
Shipman K. E., 27
Shirkavand A., 79
Shorakaie A., 79
Shumanov K., 65, 66
Sikiric Maja, 33
Simic Marko, 139
Skalli A., 147
Slaveeva S., 114, 115
Słowiński K., 123, 124
Smiljanić Pavle, 118
Socha R., 102, 105
Sokolovski S., 46
Sokołowski P., 81, 90
Šolajić Andrijana, 73, 74
Spasenović Marko, 106, 134, 166
Spasopoulos D., 25
Srećković Vladimir, 132
Sroka R., 35
Stajčić Ivana, 72
Stamboulis A., 33
Stanojević Novak, 109
Stasic Jelena, 139
Stefanov A., 168
Stefanov I., 168
Stefanov R., 65, 66
Stefanović Ognjen, 55
Stepić Milutin, 60, 84, 162
Stepp H., 35
Stevanović Katarina, 41, 42, 94
Stevanović Ljiljana, 55
Stojanović Danka B., 108
Stojanović Mirjana G., 44, 92, 110, 161
Stoliarov D., 46
Størling J., 27
Stoyanov L. I., 127, 168
Stoychev L., 115, 138
Strinić Aleksandra, 63, 64
Suplewski M., 80
Surucu S., 103
Szczerska M., 80, 81, 90, 123, 124, 152
Szerling A., 102, 105
Tadić Milan Ž., 112
Tadic Predrag, 92
Tell D., 43
Temelkov K., 114, 115
Tertemiz N. A., 141
Thon N., 35
Timotijević Dejan V., 61, 62
Tinoco M., 69
Tiosavljevic Masa, 92
Todorović T. Đorđe, 162
Todorović Nataša V., 41, 42, 94
Tomić Milos, 86
Tommasi F., 38
Tommasi I. C., 131

Tomović Aleksandar Ž., 61
Torres-Pardo A., 69
Torrini F., 91
Tosic Dragana, 76
Tošić Katarina, 106, 134, 166
Trajković Jelena Z., 117, 119
Tsankov D., 138
Tuchin V.V, 12
Unal U., 102, 105
Urošević Mira A., 72
Vaks V., 97
Valerievich Z. I., 111
Vashistha N., 160
Vasić Ivana, 169
Vasiljević Jadranka M., 62
Vasiljević-Radović Dana, 144
Vega Baudrit J. R., 48
Verkhusha V. V., 46
Vicencio R. A., 60
Vićentić Teodora, 106
Vinić Milica, 131
Vinogradova O. O., 84
Vinogradova V. S., 84
Vlaović Mitić Isidora J., 61
Vojnović Vanja, 106, 166
Vucetic Branislava, 139
Vukcevic Vladan, 92
Vukićević A. Nina, 162
Vukmirović Nenad, 159, 169
Vuković Marina, 86
Vuković Nikola, 109
Vyacheslavovich K. P., 111, 122
Vyrsokinos K., 25
Wang Chao, 107
Wang D. N., 107
Wang Qiaoben, 107
Wang S., 43
Wiersma D. S., 38
Wityk P., 81, 90
Władziński A., 123, 124
Yankov G., 65, 66, 114
Yankov G. P., 115
Yasir M., 164
Yordanova E., 65, 66
Zafar H., 97
Žakula Jelena, 84, 162
Zalevsky Z., 22
Zdoupas P., 25
Zekic Andrijana, 139
Zhang Y., 127
Zhang Z., 33
Zhelyazkova A., 88, 89
Zibar D., 13
Živanović Miloš, 84
Živić Miroslav, 41, 42, 94
Živković Milutin, 55
Zivkovic Sanja, 125
Zubarev A., 135, 136